Changing perspectives – from ecology to cellular biology in the bathymodioline symbiosis

Dissertation

zur Erlangung des Grades eines

Doktors der Naturwissenschaften

– Dr. rer. nat. –

dem Fachbereich Biologie / Chemie

der Universität Bremen

vorgelegt von

Maximilian Alexander Franke

Bremen

Oktober 2021

Die vorliegende Doktorarbeit wurde von Juni 2017 bis Oktober 2021 in der Abteilung Symbiose am Max-Planck-Institut für Marine Mikrobiologie unter der Leitung von Prof. Dr. Nicole Dubilier und direkter Betreuung von Dr. Nikolaus Leisch angefertigt.

The research presented in this thesis was performed from June 2017 until October 2021 at the Max Planck Institute for Marine Microbiology in the Department of Symbiosis under leadership of Prof. Dr. Nicole Dubilier and direct supervision of Dr. Nikolaus Leisch.

Gutachter*innen | reviewers

Prof. Dr. Nicole Dubilier

Prof. Dr. Peter R. Girguis

Dr. Frank Melzner

Tag des Promotionskolloquiums | date of doctoral defense

16. Dezember 2021

“Science cannot solve the ultimate mystery of nature. And that is because, in the last analysis, we ourselves are a part of the mystery that we are trying to solve.”

Max Plank

Table of content

Summary

Symbiotic associations are found in all domains of life. The associations between eukaryotic hosts and their bacterial symbionts have particularly contributed to the diversity of life. In many symbioses, where the symbionts are transmitted horizontally, the host must acquire the symbionts each generation anew. To do so many hosts adapt their development or morphology of individual organs, tissues, or cells. Thereby, they ensure that a stable association between host and symbiont can be established and maintained over the lifecycle of the holobiont. How the aposymbiotic life stages survive, how the symbiosis is initiated and how it is maintained over the lifecycle of the holobiont is only known for some model organisms.

In the context of this thesis I studied these questions in the bathymodioline symbiosis. Bathymodioline mussels successfully live at hydrothermal vents, cold seeps and organic falls worldwide. Despite the relatively good knowledge of this system their symbiont-host association on an ultrastructural level, their early development, the symbiont acquisition as well as aposymbiotic life is still mostly unknown.

In chapter II, I applied a three-dimensional ultrastructural imaging approach, namely focused ion beam scanning electron microscopy to resolve the symbiont localization in bathymodioline mussels on a sub-cellular resolution. Hereby, I detected a unique association form where the symbionts are located extracellularly in a membrane invagination which is connected to the outside via a channel system.

In chapter III, I focused on the symbiont colonization and associated developmental changes in the host. Based on phylogenetic data, previous studies assumed that bathymodioline mussels transmit their symbionts horizontally. However, it so far remained elusive when and how the symbiont acquisition proceeds. By using a correlative imaging approach combining µCT, light and electron microscopy as well as fluorescence in situ hybridization I resolved when the symbionts colonize the host and revealed morphological changes of the mussels that followed symbiont acquisition. These morphological changes ranged from cellular changes like microvilli effacement to the reduction of entire organs such as the digestive system.

In chapter IV, I investigated how the aposymbiotic life stages of bathymodioline mussels survive in the deep sea. This aposymbiotic phase is critical in every horizontally transmitted symbiotic system, but especially in hosts developing in nutrient depleted environments, such as the deep sea. I used a morphological based stable isotope approach by using secondary ion mass spectrometry and showed that the aposymbiotic life stages of bathymodioline mussels fed on phototrophic carbon and nitrogen. From these results I hypothesized a vertical larvae migration in bathymodioline mussels.

Despite being studied for more than 40 years, only now with the identification of aposymbiotic life stages and the technological advances over the last years I was able to answer fundamental question regarding the ecology, early development, and cellular biology of this symbiotic system in the context of this PhD thesis.

Zusammenfassung

Symbiotische Lebensgemeinschaften sind in allen Bereichen des Lebens zu finden. Besonders die Verbindungen zwischen eukaryotischen Wirten und ihren bakteriellen Symbionten haben zur Vielfalt des Lebens beigetragen. Bei vielen Symbiosen werden die Symbionten horizontal übertragen, so dass der Wirt die Symbionten in jeder Generation neu erwerben muss. Um ihre Symbionten aufzunehmen, passen viele Eukaryoten ihre Entwicklung sowie ihre Morphologie einzelner Organe, Gewebe oder Zellen an. Auf diese Weise stellen sie sicher, dass eine stabile Verbindung zwischen Wirt und Symbiont hergestellt und über den Lebenszyklus des Holobionten aufrechterhalten werden kann. Wie die aposymbiotischen Lebensstadien überleben, wie die Symbiose initiiert wird und wie sie über den Lebenszyklus des Holobionten aufrechterhalten wird, ist nur für einige Modellorganismen bekannt.

Im Rahmen dieser Arbeit habe ich diese Fragen an bathymodiolinen Muscheln und ihren chemosynthetischen Symbionten untersucht. Diese Muscheln leben weltweit erfolgreich an Hydrothermalquellen, kalten Quellen und organischen Ablagerungen. Trotz der relativ guten Kenntnis dieses Systems ist ihre Symbionten-Wirt-Assoziation auf ultrastruktureller Ebene, ihre frühe Entwicklung, der Symbiontenerwerb sowie das aposymbiotische Leben noch weitgehend unbekannt.

In Kapitel II habe ich einen dreidimensionalen ultrastrukturellen Bildgebungsansatz angewendet, nämlich die fokussierte Ionenstrahl-Rasterelektronenmikroskopie, um die Symbiontenlokalisation in bathymodiolinen Muscheln auf subzellulärer Ebene zu untersuchen. Dabei konnte ich eine einzigartige Assoziationsform nachweisen, bei der sich die Symbionten extrazellulär in einer Membraninvagination befinden, die über ein Kanalsystem mit der Außenwelt verbunden ist.

In Kapitel III habe ich mich auf die Besiedlung der Symbionten und die damit verbundenen Entwicklungsveränderungen im Wirt konzentriert. Auf der Grundlage phylogenetischer Daten wurde in früheren Studien angenommen, dass bathymodiolinen Muscheln ihre Symbionten horizontal übertragen. Bisher war jedoch nicht klar, wann und wie die Symbiontenakquisition abläuft. Mit Hilfe eines korrelativen bildgebenden Ansatzes, der µCT, Licht- und Elektronenmikroskopie sowie Fluoreszenz-in-situ-Hybridisierung kombiniert, konnte ich klären, wann die Symbionten den Wirt besiedeln und welche morphologische Veränderungen der Muscheln mit der Symbiontenaufnahme einhergehen. Diese morphologischen Veränderungen reichen von zellulären Veränderungen, wie dem Abbau von Mikrovilli, bis hin zur Verkleinerung ganzer Organe wie des Verdauungssystems.

In Kapitel IV habe ich untersucht, wie die aposymbiotischen Lebensstadien der bathymodiolinen Muscheln in der Tiefsee überleben. Diese aposymbiotische Phase ist in jedem System, in dem Symbionten horizontal übertragen werden, von entscheidender Bedeutung, besonders aber in Wirten, die sich in nährstoffarmen Umgebungen wie der Tiefsee entwickeln. Ich habe einen Morphologie -basierten stabilen Isotopen Ansatz unter Verwendung der Sekundärionen-Massenspektrometrie

verwendet und konnte zeigen, dass sich die aposymbiotischen Lebensstadien der bathymodiolinen Muscheln von phototrophen Kohlenstoff und Stickstoff ernähren. Aus diesen Ergebnissen habe ich geschlussfolgert, dass bathymodiolinen Muscheln eine vertikale Larvenmigration haben.

Obwohl sie seit mehr als 40 Jahren erforscht werden, konnte ich erst jetzt mit der Identifizierung der aposymbiotischen Lebensstadien und den technologischen Fortschritten der letzten Jahre grundlegende Fragen zur Ökologie, frühen Entwicklung und Zellbiologie dieses symbiotischen Systems im Rahmen dieser Doktorarbeit beantworten.

Chapter I | Introduction

1.1 Symbiosis

1.1.1 General concept

In the course of their lives, organisms interact with a large number of different living beings [1]. These interactions and the coexistence of different organisms is called symbiosis. Albert Bernhard Frank combined the Greek terms syn (“together”) and biosis (“living”) to define this relationship between two organisms living together [2]. In 1878, the definition by Frank was further specified by Heinrich Anton de Bary. Frank did not consider benefits or disadvantages which could result from an association of two partners. The term symbiosis was described by De Bary [3] as a living together of two different species which have close physical contact. Today symbiosis research divides into three forms of interaction: mutualism (both partners gain benefits from the association), commensalism (one partner gains benefits while the other remains unaffected), and parasitism (the symbiont gains benefits while the host is harmed) [4]. In the literature the term symbiosis is often used in the context of mutualism [5, 6], although De Bary did not initially limit the concept of symbiosis to any of these three types. It is still not clearly defined how long two organisms have to be associated to be considered a symbiotic system. The vague accepted time frame is that the two partners need to be associated for a significant proportion of their lifetime [5]. The great diversity of symbiotic associations with different forms of contact, different lengths of cohabitation, and the continuous increase of symbiotic associations in nature still pose a challenge for symbiosis research to clearly define these symbiotic associations. In this study, the term symbiosis is used interchangeably with mutualism, in which both partners gain benefits from the association.

1.1.2 Evolution of symbiotic systems

Today, the basic assumption is that symbiotic interactions between organisms are a central driver of evolution and this is evident throughout the tree of life [1]. Associations between bacterial endosymbionts that interact with hosts such as insects and provide them with essential nutrients have led to the species diversity we know today. Some of the most productive ecosystems on this planet, such as hydrothermal vents and coral reefs, are based on symbiotic interactions between microbes and their multicellular hosts [1].

In evolutionary terms, it is assumed that symbiotic systems became more and more specific over time and developed from extracellular to intracellular associations [7]. Today, the eukaryotic domain would not exist in its present diversity without these specific associations between eukaryotes and bacterial symbionts. In particular, the transformation of bacterial endosymbionts into mitochondria and chloroplasts has led to the rapid evolution of multicellular life forms [8-10]. The vast majority of these multicellular eukaryotes are today thought to be associated in some way with bacterial symbionts. The formation of a symbiotic system provides both partners with new properties, such as access to new metabolic and functional capabilities, protection from antagonists, or enhanced motility [5]. Over evolutionary time, many different associations with varying complexities have formed between eukaryotes and their symbiotic bacteria. In the following sections, I will describe different examples of the variability of symbiotic associations and introduce basic concepts of symbiosis research using these examples.

1.1.2.1 Obligate vs facultative symbiotic systems

A symbiotic association can be considered an obligate or facultative symbiosis. In obligate systems, both partners entirely depend on the association with their counterpart. A prime example is the symbiosis between aphids and their *Buchnera* symbionts [11]. It is a nutritional symbiosis in which the symbionts supply the host with essential amino acids [11]. In facultative systems, both partners in an association can also survive without each other. This type of symbiosis is found, among others, in the fly *Drosophila melanogaster* and its symbiont *Lactobacillus plantarum* [12, 13]. *L. plantarum* affects the growth of juvenile *Drosophila* flies by promoting the expression of peptidases in the larval gut, and thereby increasing its host digestion [14]. Furthermore, a symbiotic association may be considered optional for one partner and obligate for the other, as in the symbiotic association between aphids and their secondary symbiont the pea aphid (PASS) [15]. In the absence of the *Buchnera* symbiont (primary symbiont), the aphids rely on the facultative PASS symbiont, with the symbiosis being obligate for the aphids and facultative for the symbionts.

1.1.2.2 Different types of symbiont-host associations

As described above, the general concept that symbionts have evolved over evolution from ectosymbionts to intracellular endosymbionts is widely accepted [7]. The symbionts of the nematode *Laxus oneistus* are associated extracellular on the cuticle of the nematode (Figure 1 a, e and l; [16]) and the *Buchnera aphidicola* symbionts from the pea aphid *Acyrthosiphon pisum* as well as the symbionts from tubeworms are associated intracellular in vacuoles (Figure 1 c, d, g, h, k, and l; [17, 18]). However, evolution has shown that not only these two types of symbiont-host association exists. Besides ectosymbionts, and intracellular endosymbionts, a variety

of intermediate forms have evolved. Symbionts can be associated extracellularly but inside of a closed lumen of the host (e.g. symbionts of the nematode *Astomonema southwardorum*; [19]), the symbiont can be located underneath the cuticle but above the epidermis cells (e.g. symbionts of the oligochaete worm *Olavius algarvensis*, Figure 1 b, f and j; [20]), or they can transmit between an extracellular and intracellular association during different life stages of the host (e.g. Ca. *Erwinia dacicola* the symbionts of the olive fly *Bactrocera aleae*; [21]).

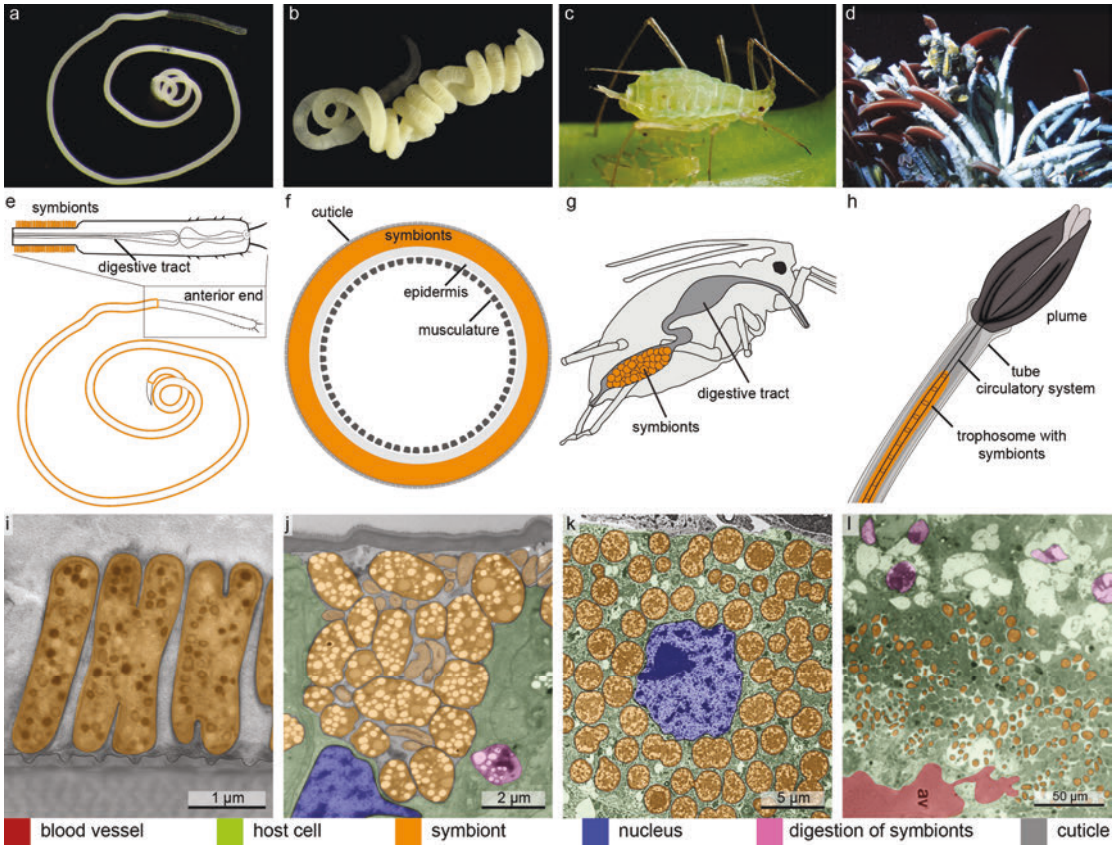

Figure 1 Overview of different symbiont-host associations in mutualistic systems. From left to right: the symbionts are associated extracellular on the host surface of the stilbonematine nematode *Laxus oneistus* (a, e and i) extracellular between the cuticle and epidermis cells of the marine oligochaete *Olavius algarvensis* (b, f and j) and intracellular in vacuoles of the aphid XXX (c, d and g) and tubeworm *Riftia pachyptila* (h, k and l). From top to bottom: an overview image of the host (a – d), schematic drawing of the host with symbiont location highlighted (e – h) and a false-colored transmission electron micrographs highlighting the symbionts in orange (i – l). The figure was adapted after Sogin *et al.* [22]. Usage of the figure was licensed under the license 5166950665658. Image credits: (a) U. Dirks, (b) A. Gruhl, (c) Shipher Wu (photograph) and Gee-way Lin (aphid provision), National Taiwan University, CC BY 2.5 https://creativecommons.org/licenses/by/2.5 (d) M. Bright, (g) inspired by [23] (k) taken from Hoff [17] photograph by J. White and N. Moran, University of Arizona (l) modified from Bright and Sorgo [18].

1.1.2.3 Symbiont specificity

The specificity of a symbiotic system is defined as the taxonomic range of the symbionts. Between different symbiotic associations it can vary from only a few different symbiont types per host, as seen in the tubeworm, squid as well as aphid symbiosis [11, 24-29], to symbiotic systems which are associated with several hundred different symbiont types forming a complex microbiome, e.g. the human gut microbiome [30, 31].

1.1.2.4 Symbiont transmission

A critical step in all symbiotic systems is the transmission of symbionts from one generation to the next. Over their evolution, different symbiotic systems have developed different strategies to transmit their symbionts. Symbionts can be transmitted vertically, horizontally, or in a mixed mode in which both transmission modes are involved [32].

Vertical symbiont transmission is the direct transfer of symbionts from the parental organism to the offspring. Direct transmission of symbionts from parents to offspring ensures that the symbionts are associated with the host throughout the entire life cycle [32]. In many of these systems, symbionts are transmitted via the maternal germ line e.g. the symbionts of the rice weevil *Sitophilus oryzae* [33, 34].

Next to the vertical transmission of symbionts, symbionts can also be recruited each generation anew from the environment. This so called horizontal symbiont transmission requires the finding and recognition of the initially aposymbiotic host and its free living symbionts. Furthermore, it implies that both partners are able to survive initially alone before symbiosis is established [32]. Examples of such a horizontal transmission mode are commonly found in many marine symbiotic

systems [35], like the symbionts (*Vibrio fischeri*) of the Hawaiian bobtail squid (*Euprymna scolopes*) [26, 27].

In several symbiotic systems where transmission was thought to be vertical, horizontal transmission events have also been reported. This enabled those hosts to supplement their symbiont population with symbionts from the environment or other hosts. Mixed modes of transmission have recently been shown in two bivalve species (solemyid and vesicomyid bivalves) previously thought to have only vertically transmitted symbionts [36, 37]. According to Bright and Bulgheresi [32] a strict vertical transmission with the complete absence of horizontally transmitted symbionts might be rare.

By comparing the phylogeny between host and symbiont, the effects of the transmission mode on the evolution of the symbiotic partners become very clear. Vertically transmitted symbionts show congruent phylogenies with their host. Such a close phylogeny between symbiont and host has been demonstrated, for example, in *Paracatenula* flatworms from shallow water sediments [38]. The phylogeny also indicates when vertical transmitted symbionts have been horizontally transmitted or have undergone host switching events during evolution [37]. In contrast to vertically transmitted symbionts, the phylogeny between horizontally transmitted symbionts and their hosts, such as in bathymodioline mussels, is not as close and shows little concordance [32, 39].

1.1.2.5 How the host adapts to the symbiotic association

Regardless of the type of symbiont transfer, both partners must fundamentally adapt to the symbiotic association. To do this, the host often needs to change its developmental program [26, 32]. However, there are important differences between

vertically and horizontally transferred symbionts. In vertical transmission, because symbionts are associated with the host throughout the life cycle, mechanisms are not required to allow specific colonization of symbionts in each generation [26]. In these systems it is essential that the host develops mechanisms that allow the symbionts to be passed on to the offspring. In many symbiotic systems this is done via the maternal germ line [32]. Once the bacteria are passed on, they often colonize other organs/tissues where they remain for the duration of the association.

In horizontal symbiont transfer, the host comes into contact not only with the appropriate free-living symbiont, but also with hundreds of other bacteria living in its environment. This requires specific recognition mechanisms between host and symbiont so that the symbiosis can be formed with the exclusion of intruders [26]. To accommodate the bacterial symbionts, many eukaryotes undergo drastic morphological and developmental changes [32]. These morphological changes are specific to each symbiotic system, e.g., the crypts of *Euprymna scolopes* undergo tissue restructuring to accommodate *Vibrio fischeri* [26], and the hydrothermal vent tubeworms (*Vestimentifera*, *Siboglinidae*) develop an entirely new organ, the trophosome, to accommodate their symbionts [24, 25]. No matter if the symbionts are transmitted horizontally or vertically certain mechanisms must be anchored in the developmental “blueprint” of the host so that the new host generation can establish a stable symbiotic association [26, 40].

1.1.2.6 How the symbiont adapts to the symbiotic association

During the course of coexistence, not only will the host adapt to the symbionts, but also the symbionts to the host. In general, vertically transmitted symbionts are much more adapted to the host than horizontally transmitted symbionts [41]. This is particularly evident in the observation that many obligate bacterial symbionts have

reduced genomes [35, 41]. This is due to decreased homologous recombination and inefficient selection in these systems [35]. This loss of gene function has been demonstrated for many obligate insect symbioses [42], including the symbionts of aphids *Buchnera aphidicola* [11, 42]. However, this genome reduction also has negative effects. In particular, vertical transfer of symbionts from long-term relationships can lead to evolutionary bottlenecks in the bacterial genome. Extreme genome-wide reductions due to deletions lead to the loss of symbiotically important genes [43-45]. For example, extreme reductions in symbiont genome size can limit the ecological range of the host species and increase the risk of extinction [45].

In marine environments numerous symbiotic associations contradict these patterns of extreme genome reduction. This is most likely due to continuous horizontal gene flow, which causes even the most reduced marine endosymbionts to have much larger genomes than their terrestrial insect symbiont counterparts. Efficient natural selection is therefore enabled by horizontal transfers and recombination, resulting in intermediate symbiont genome sizes and substantial functional genetic variation [35].

1.2 Nutritional symbiosis

Association with bacterial symbionts confers new capabilities to eukaryotes such as protection from predators/antagonists, expanded dispersal and mobility, and access to new metabolic pathways. In particular, these nutritional symbiosis, which are mainly known from microbiome research, are spread through many different animal phyla ranging from the human gut [30, 31] over insects [11, 46] to marine symbiotic systems such as fish [47], mussels of the family bathymodiolinae [48] or tubeworms [24]. Some systems form obligate nutritional symbiosis, where the host is not able to survive without their symbionts, such as aphids and their *Buchnera* symbionts [11]

and others form facultative nutritional symbiosis, where the host benefits from the association but can also survive alone, such as the fly *Drosophila melanogaster* and its symbiont *Lactobacillus plantaruim* [12, 13, 41]. Furthermore, nutritional symbioses can be very specific and the symbiotic partner is only responsible for the provision of a few to a single vitamins/amino acids [49-51]. A very well-known example of a nutritional symbiosis from the marine environment are photosynthetic symbioses between cyanobacteria or algae and cnidarians, flatworms and sponges [52]. The photosynthetic symbionts use light energy to supply the host with organic carbon.

By hosting mutualistic symbionts that provide the host with its nutrition, eukaryotes colonize unique habitats that would not be colonize able without a symbiotic association [48, 53, 54]. One prime example for such a system are chemosynthetic environments. These systems were discovered about 40 years ago and since then a variety of different nutritional symbiosis have been reported [22, 48, 55].

1.2.1 Chemosynthetic symbiosis

In 1981 Cavanaugh *et al.* [56] and Felbeck [57] described the first marine chemosynthetic symbiotic association in the deep sea tubeworm *Riftia pachyptila.* Today we know that symbiotic associations between chemosynthetic bacteria and eukaryotes can be found not only in the deep sea at hydrothermal vents, cold seeps and organic falls but also in shallow water systems such as seagrass beds and coral reef sediments (Figure 2; [22, 48, 55]).

From the deep sea to shallow water systems these symbiotic associations are considered to be among the most successful inhabitants of their different habitats. The habitats can be quite diverse but share the same basic characteristics: the presence of reduced chemical compounds that serve as energy sources and

presence of oxidants such as oxygen and nitrate [58, 59]. Oxygen is not only used by the chemosynthetic bacteria to oxidize the reduced chemical compounds but also for respiration by the eukaryotic hosts. Therefore, the oxygen concentrations need to be high enough to sustain dense animal populations. In shallow water habitats, the enrichment of sulfide formed by the biodegradation of organic material and the associated oxygen depletion allows a variety of chemosynthetic systems such as *Olavius* oligochaetes, nematodes, solemya clams, *Paracatenula* flatworms, and ciliates to thrive in these systems (Figure 2; [22, 48]). Chemosynthetic symbioses from the deep sea environment are the main focus of this thesis so I will introduce these environments in more detail in a separate section (see 1.3.1).

The process of chemosynthetic primary production requires chemical energy, instead of light (photosynthetic primary production), to fix inorganic carbon (or methane) into biomass [48, 59, 60]. Methane and sulfur-oxidizing bacteria have been found associated to many marine invertebrates inhabiting habitats that are rich in inorganic compounds [38, 55, 61-64]. The methane-oxidizing bacteria (MOX) are chemoorganoheterotrophs that use methane as a source of carbon and energy [62, 65, 66]. The sulfur-oxidizing bacteria (SOX) are chemolithoautotophs that oxidize reduced sulfur compounds as well as hydrogen to fix carbon [67, 68]. Since these bacteria use chemical energy to fix carbon, they can survive in light depleted environments. Thus, not only the chemosynthetic bacteria but also their associated eukaryotic hosts can survive in these light depleted habitats. Under non-symbiotic living conditions many of these eukaryotes would not be able to survive in these habitats, as they rely on phototrophic primary production.

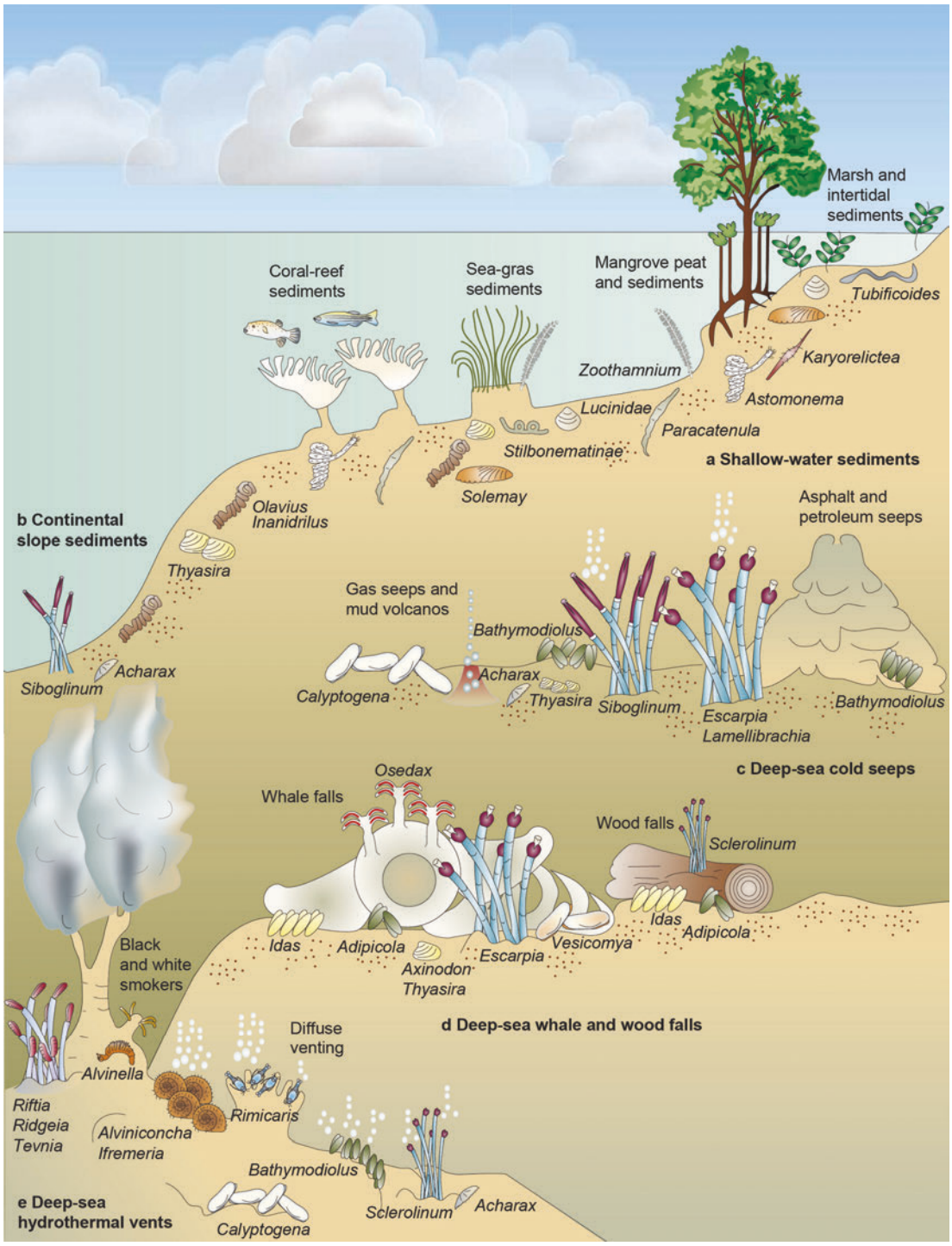

Figure 2 Different marine habitats are inhabited by a diverse set of chemosynthetic symbiotic systems. Chemosynthetic symbiosis can be found from shallow-water habitats such as shallow-water sediments (a) and continental slope sediments (b), to the deep-sea environment at cold seeps (c), whale and wood falls (d), and hydrothermal vents (e). This figure is taken from Dubilier *et al.* [48]. Usage of the figure was licensed under the license 5166950137627.

Chemosynthetic nutritional symbioses are one of the most successful and widespread symbioses in marine systems and are found in a variety of animal phyla such as flatworms, nematodes, annelids and bivalves [22, 48, 55]. Their associated symbionts often belong to the *Gammaproteobacteria* [55, 69], but also representatives of *Epsilonproteobacteria* and *Alphaproteobacteria* have been found [38, 70]. To host their different symbionts, many hosts have developed drastic strategies and often undergo morphological changes, compared to their non-symbiotic shallow water relatives. A well-known example are bathymodioline mussels. These deep-sea mytilids harbor chemosynthetic bacteria in specialized gill cells called bacteriocytes [48, 63, 71]. Due to the nutritional symbiosis with chemosynthetic symbionts, most bathymodioline species have a reduced digestive system compared to their shallow water relatives [72-74]. As bathymodioline mussels are the main study organism of this thesis, I will introduce this symbiotic system below (see 1.4).

1.3 The deep sea ecosystem

The deep sea represents the largest ecosystem on Earth. It is thought to comprise 95 percent of Earth's living space and is characterized by high pressure, permanent darkness (below 200 m all light is gone), cold temperatures, and nutrient limitation [75]. Most of the oceans sea-floor is dependent on phototrophic organic matter from the sea surface, but only about 1 – 3 % of this organic matter, which sinks into the deep sea in form of marine snow and particulate organic matter (POM), reaches the see-floor [60, 76]. Nevertheless, the deep sea harbors a great diversity of organisms [77]. This biodiversity is surprising, given the harsh and unfavorable living conditions. While individual deep-sea habitats and organisms are by now relatively well understood, the overall complexity of this environment is still largely unknown. This is

mainly because research in this habitat is difficult and requires sophisticated technology such as underwater robots and research submarines.

The complexity of this ecosystem is still mostly unknown, therefore, it is hard to believe that mankind has been exploiting this ecosystem for several years in the form of deep-sea fishing, deep-sea mining and hydrocarbon extraction [78-80]. The damage caused by this exploitation can have an impact on the entire ecosystem, such as extinction of deep-sea animals and the destruction of deep-sea habitats [80]. Therefore, basic research in this ecosystem is very important and should focus on the questions how and where animal populations live, how they disperse to colonize new habitats, how their larvae survive, and how all of this influences the integrity of this special ecosystem.

1.3.1 Chemosynthetic deep-sea environments

While most life on the sea-floor is dependent on the organic matter sinking into the deep-sea, chemosynthetic environments are independent of this. These environments are dominated by chemosynthetic primary production and are therefore home for a diverse community of bacteria as well as symbiotic invertebrates [60]. In the following sections, I will describe the three important types of chemosynthetic deep-sea environments covered in my thesis: organic (wood and whale) falls, hydrothermal vents, and cold seeps (Figure 2). In all of these habitats, dense populations of invertebrates that live in a chemosynthetic symbiosis with either MOX or SOX symbionts or both are found.

1.3.1.1 Organic falls

Wood and whale falls are restricted temporary environments; they provide a habitat for a variety of organisms but until they are fully decomposed. When whale

carcasses sink to the sea floor, they get colonized by a variety of bacteria, which begin to decompose the organic material, creating a sulfide-rich environment. These local hot spots have higher concentrations of reductants and oxidants than the open sea floor, and therefore form temporary oases in the deep sea. These ecosystems are quickly colonized by a variety of chemosynthetic symbiotic systems such as: tubeworms (*Osedax* species), clams , mussels (*Idas* species) and polychaetes [81, 82]. This process is very similar for wood falls. Here, the degradation of wood leads to sulphide-rich environments, which also attract chemosynthetic symbioses such as mussels (*Idas* species, *Adipicola* species) and wood-boring shipworms [83, 84]. These locally and temporally restricted oases were called “stepping stones” as they were thought to be important evolutionary steps for the colonization of chemosynthetic systems in the deep sea [85].

1.3.1.2 Hydrothermal vents

Hydrothermal vents occur worldwide in all oceans and release hot, chemical rich, seawater into the water column. Furthermore, they are mostly found at sea-floor spreading zones along the edges of tectonic plates like the Mid-Atlantic ridge [86]. In these geographic settings, seawater flows through the porous seafloor, is heated by magma chambers, and becomes enriched with dissolved gases (e.g. CO_2, H_2S, H_2, CH_4) and metals (e.g. Mn and Fe) [87]. As the heated seawater emerges from the seafloor and meets the colder deep-sea water, minerals that were previously dissolved in the vent fluids are released. Furthermore, precipitates can appear that look like black smoke and give the hydrothermal vents their distinctive name "black smokers". The dissolved chemicals in the vent fluids fuel the chemosynthetic symbiosis [59]. But, their concentration can change over time and hydrothermal systems can become inactive, resulting in the death of many organisms living in

these habitats [88-90]. The spreading velocities of the different spreading centers influence how stable hydrothermal systems are overtime. If a spreading zone has a high velocity, it is mostly influenced by volcanic activities, while slow spreading centers are more stable over time [91, 92]. So depending on the environment chemosynthetic organisms live in, they are under a constant threat that their nutritional source will come to an end.

1.3.1.3 Cold seeps

A third type of chemosynthetic deep-sea environment are so called cold seeps. In these systems relatively cold pore-water seeps out of the see floor and is enriched in hydrocarbons and dissolved gases (e.g. CH_4 and H_2S). These dissolved chemicals fuel the chemosynthetic organisms that are inhabiting these systems. Cold seeps are dominantly found at active and passive continental margins such as the Gulf of Mexico [93]. Tectonic activities and the disintegration of gas hydrates are responsible for pushing the water through the deep seafloor [94].

1.4 The bathymodioline symbiosis

Symbiotic deep-sea mussels belonging to the subfamily Bathymodiolinae (family Mytilidae) inhabit hydrothermal vents (Figure 3 a), cold seeps, and organic falls throughout the world's oceans [48, 55, 95]. They form large mussel beds and often dominate communities in these reduced habitats in terms of biomass [95]. In doing so, they serve as an ideal settlement substrate for other organisms and are therefore important foundation species for their habitat [82, 96]. Bathymodioline mussels evolved from shallow-water mytilids such as the blue mussel *Mytilus edulis* and probably colonized the deep sea via "stepping stones" (wood and whale falls) about 89 million years ago [85, 97-99].

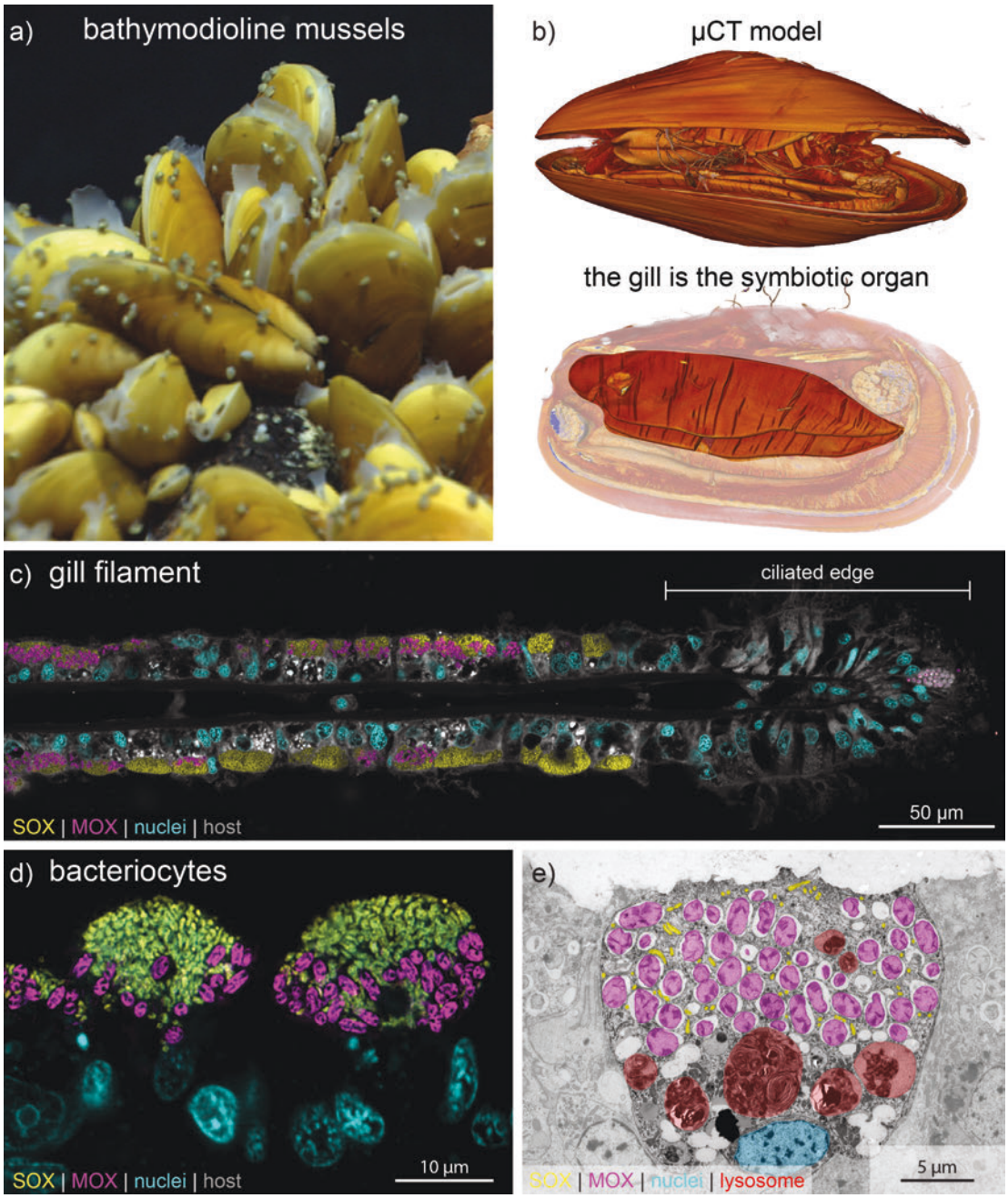

Figure 3 Overview of the bathymodioline symbiosis. a) Bathymodioline mussels in their natural habitat. Image credits MARUM. **b)** µCT model of an adult bathymodioline mussel. The gill is the most prominent organ once the mussel is cut open. The gill is the symbiotic organ. **c)** Fluorescence in situ hybridization (FISH) overview image of a gill filament. The gill epithelia cells harbor SOX and MOX symbionts and the filaments are separated into an aposymbiotic ciliated edge region and a symbiotic region. **d)** High resolution FISH image of two bacteriocytes harboring SOX and MOX symbionts. **e)** False-colored transmission electron micrograph showing the intracellular symbionts and the lysosomal digestion.

The phylogeny of these mussels is still controversially discussed but 10 different genera were currently suggested by Jang *et al.* [100] and Xu *et al.* [101]:

Bathymodiolus, *"Bathymodiolus", Benthomodiolus*, *Gigantidas, Idas*, *Lignomodiolus*, *Nypamodiolus, Tamu*, *Terua,* and *Vulcanidas*. Over time, some species have been reassigned to a new genus based on molecular data. One example are *G. childressi* mussels, which were originally described as *"B". childressi* mussels [102]. Based on morphological and molecular characteristics, about 30 species of the genus *Bathymodiolus* have been described to date [103]. Some of these 30 species are extinct fossil species such as *B. inuei* [104] and *B. miomediterraneus* [105].

1.4.1 Symbiont association

To survive in the deep-sea, bathymodioline mussels acquired chemosynthetic Gammaproteobacteria (Figure 3 b – e; [48, 55, 69]). Depending on the species they are either associated with SOX symbionts [63, 106], MOX symbionts [66, 71, 107, 108] or both [109, 110]. The SOX symbionts are more widespread in the different bathymodioline species than the MOX symbionts. The MOX symbionts are mainly found in the *G. childressi* clade and in some *Bathymodiolus* species such as *B. azoricus* and *B. puteoserpentis* that host both symbiont types [98]. This mutualistic nutritional symbiosis is necessary because many bathymodioline species have reduced digestive systems and live in a nutrient depleted habitat [72, 73], with limited access to phototrophic organic material that mytilids would feed on by filtration. Bathymodioline mussels are thought to obtain their nutrition by intracellular digestion of symbionts and "milking" of symbionts via a direct transfer of nutrients from the symbionts to the host [111-113]. Although most bathymodioline species rely on the energy provided by their symbionts they can still supplement their nutrition via filter-feeding. Some species such as *V. insolatus* are hypothesized to be much more successful in filter feeding than others because their digestive system is not as reduced as in most other bathymodioline species [114]. Apart from the nutritional

benefits the symbionts might also be responsible for sulfide detoxification [115], amino acid supply [116] or pathogen defense [117]. .

Depending on the species, but especially on the habitat in which the mussels live, the symbionts are associated intracellularly in vacuoles (Figure 3 e) or extracellularly as ectosymbionts on the apical cell membrane [118, 119]. Adult bathymodioline species inhabiting hydrothermal vents and cold seeps harbor their endosymbionts intracellular in vacuoles in specialized gill cells called bacteriocytes (Figure 3 d – e; [65, 110, 112]). These epithelial cells lost their microvilli and show a hypertrophic habitus upon colonization (Figure 3 e). In juvenile mussels it was shown that the budding zone (meristem-like cells which form new gill filaments) as well as the first seven gill filaments were always free of symbionts [120]. Furthermore, all other growth zones, such as the ventral ends of the gill filaments as well as the dorsal ends of the descending and ascending lamellae, were identified to be symbiont free (Figure 3 c; [120]). In bathymodioline species living at organic falls, such as wood and whale falls, mostly ectosymbiotic SOX symbionts were found [118, 119]. Also in these species the symbionts were found associated with the gill epithelial cells. The SOX symbionts were located between microvilli and in close contact with the apical cell membrane [83]. Recently, an intermediate symbiont-host association was shown for *B. septemdierum* mussels. These mussels harbored their symbionts in vacuoles which were connected to the outside [121]. Ikuta *et al.* [121] also mentioned that it needs further research to test whether this form of symbiont-host association is more common in bathymodioline mussels.

In addition to the two main SOX and MOX symbionts, associations with other mutualistic symbionts were also described in bathymodioline mussels,

gammaproteobacterial *Cycloclasticus* symbionts were found in *B. heckerae* mussels [122] and extracellular epsilonproteobacterial symbionts were found in *G. childressi*, *B. azoricus*, *B. mauritanicus* and *"B". manusensis* mussels [70]. Mutualistic associations have been well documented in bathymodioline mussels but this is not the only symbiotic relationship; parasitic associations have also been described in these hosts. In the nucleus of non-colonized gill epithelia cells parasitic bacteria called "*Candidatus* Endonucleobacter bathymodioli" were identified [123]. Single rod-shaped bacteria infect the nucleus of the mussels and begin to multiply until the infected nucleus is 50 times larger than a non-infected nucleus. The infected nucleus will eventually burst, releasing the parasites, and allowing for their cycle of infection to continue

1.4.2 What is known about the early development of these mussels and the symbiont acquisition?

1.4.2.1 Larval development and dispersal

Detailed larval development in bathymodioline mussels has so far only been described for some *Idas* species living at organic falls [124, 125]; larval development of hydrothermal vent and cold seeps species is largely unknown. A few studies have addressed early developmental stages of *Bathymodiolus* mussels: studying parameters including egg sizes of different species, the relative size of larval shells, as well as the different cleavage stages during early development. All of these studies have agreed that bathymodioline mussels live as planktotrophs [126-128] and have a larvae duration between 9 and 13 months [126]. Larval duration was estimated indirectly from the size distribution of recruits sampled in the deep sea and by comparison with known spawning times. As bathymodioline mussels have a

planktotrophic larva that must actively feed, they have a distinct planktonic larval life style. During this time, larvae are dispersed with ocean currents to colonize new habitats. Over time this planktonic larvae dispersal has led to the geographic distribution we know today. Many factors such as larval predators, water temperatures, nutrition, water currents, and time of dispersal can influence the larval dispersal [129, 130]. How bathymodioline larvae disperse in the water column is still mostly unknown. Breusing *et al.* [131] have modeled the median maximum dispersal distance of bathymodioline mussels from the Mid-Atlantic ridge, resulting in a distance of ~ 150 km. How far bathymodioline mussels really disperse is hard to estimate as it depends on many more factors than Breusing *et al.* [131] included in their model. For example, Arellano *et al.* [132] presented evidence that *G. childressi* mussels migrate vertically in the water column. If this behavioral trait is included in the dispersal models, the model predicts that bathymodioline larvae can disperse up to 1000 km [133, 134].

It is believed that the life cycle of bathymodioline mussels is very similar to that of shallow water mytilids [95, 135]. Since our understanding of the specific life cycle of bathymodioline mussels is still incomplete, I will describe the general life cycle of mytilids. Where there is information about the deep-sea mussels, I will make a note at the respective life cycle step. In the past, different life stages have been named differently throughout the literature; especially when comparing deep-sea mytilids with shallow-water mytilids, one can identify differences in the terminology between different stages. Throughout my thesis I will stick to the following definitions:

The life cycle of shallow water mytilids and bathymodioline mussels begins with the spawning and fertilization in the water column near the settling habitat of the parental

organisms (Figure 4 a). Within ~ 40 h after fertilization the 64 cell (blastula, Figure 4 b) stage is formed in bathymodioline mussels [126]. As soon as the throchophora larvae is formed, mytilid larvae are capable of active swimming (cilia movement) and feeding (Figure 4 c). From this point on, the early larvae enter the planktonic dispersal phase. The secretion of the first larvae shell, the prodissochon I, initiates the D-veliger stage (Figure 4 d). During this developmental stage, the velum (the larvae feeding and swimming organ) develops and all of the yolk from the parental organisms is used. This means the larvae need to actively feed to survive. The formation of the second larvae shell, the prodissoconch II, initiates the pediveliger stage (Figure 4 e). The pediveliger stage is the last developmental stage before the metamorphosis and the majority of the mature anatomy has already developed, such as the alimentary, excretory, and central nervous systems [135], the stomach, the digestive diverticula forming the digestive gland, and the first gill filaments. During the pediveliger stage, shallow-water larvae build up large amounts of energy storages in form of lipid vesicles, which serve as an energy storage during the metamorphosis [135-137].

Once settled on the seafloor, the animal initiates its metamorphosis from a planktonic to a benthic lifestyle (Figure 4 f). The exact settling cues are still unknown in bathymodioline mussels. In shallow-water relatives, chemosensory recognition of morphogenic and regulatory molecules in the environment [138] play a major role in initiating settlement and thus metamorphosis. Certain bacterial biofilms as well as algae can influence settlement [139-142]. Furthermore, it was shown that non-symbiotic as well as chemosymbiotic shallow-water species are capable of delaying metamorphosis due to missing substrata [143] or suppression of metabolism due to low temperatures [144], which results in a longer larvae life.

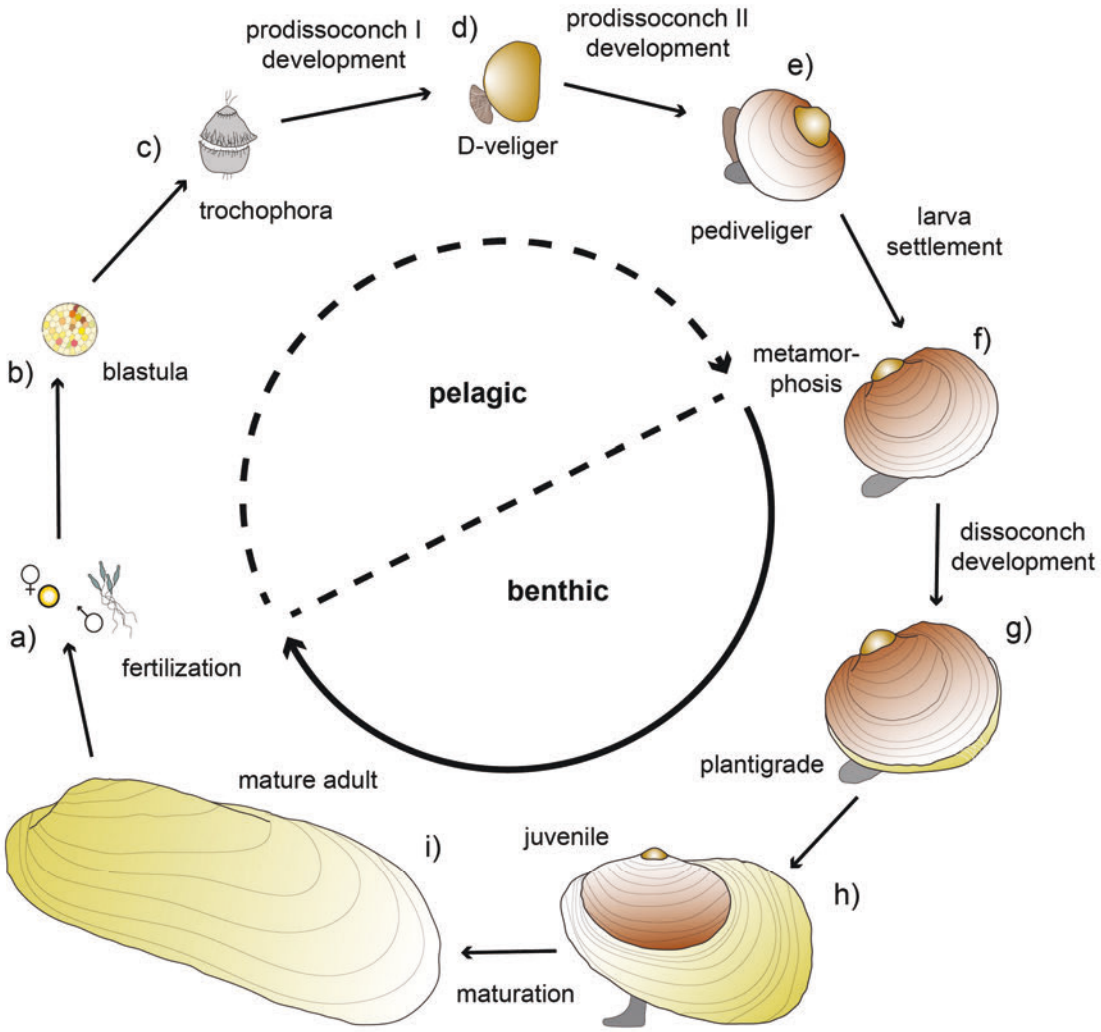

Figure 4 Potential life cycle of bathymodioline mussels. The early development of shallow water mytilids and bathymodioline mussels is thought to be comparable, therefore this lifecycle is based on the broad knowledge from shallow-water mytilids as well as the scare knowledge about bathymodioline development. The figure was modified from Franke *et al.* [145].

In mytilids, the first step in metamorphosis is the degradation of the velum and once the adult shell, the dissoconch, is secreted, the mussels enter the plantigrade developmental stage (Figure 4 g; [146]). In this stage, all tissue rearrangements of the metamorphosis are completed. The mussel grows into a juvenile mussel as soon as the ventral groove, which transports food particles to the labial palps of the gill, is formed (Figure 4 h; [147]). As soon as the gonads are fully developed the mussels are considered as adults (Figure 4 i; [135]).

1.4.2.2 Symbiont acquisition

Information on symbiont uptake in bathymodioline mussels is very limited, similar to other deep-sea symbioses. Based on data from phylogenetic studies, which have shown a lack of co-speciation between hosts and symbionts [35, 39, 148, 149], and morphological studies, which have found no evidence of symbionts in the reproductive tissues of mussels [150], it is assumed that symbionts are transmitted horizontally. However, very little is known about the developmental stage at which the symbionts are acquired and how the acquisition of the symbionts affects the development and morphology of the mussels [95]. The currently available information on symbiont acquisition consists of data on mussels of the genus *Idas*, which live at organic falls and have ectosymbionts. It was shown that the larvae of these mussels are still aposymbiotic and that the symbiont colonization starts after the metamorphosis [124, 125]. In the past, it was hypothesized that the initial symbiont colonization in bathymodioline mussels takes place in mantel cells rather than gill cells because these tissues develop before the gills [151]. This implies some benefit to from the symbiotic association already in developmental stages in which the gills were not completely developed [113]. Wentrup et al. (2013) could show that the intracellular endosymbionts of the Mid-Atlantic ridge species *B. azoricus* and *B. puteoserpentis* were widespread through all epithelial tissues of the mantle cavity in juvenile stages and restricted to the gill filaments in adult mussels. A similar trend was also observed in *Idas* species that host their symbionts extracellularly [95, 124, 125].

Data indicates that bathymodioline mussels acquire their symbionts horizontally, but when this happens is still unclear. The timing of this acquisition step is critical to these mussels. The uptake of locally adapted microorganisms, at a later life stage,

ensures that the mussels are best adapted to the differences in vent fluids between the settling habitat and the spawning habitat [152].

1.5 How to study symbiotic interactions: the challenge of understanding the ecological meaning down to subcellular resolution of individual bacterial cells

“Owing to recent methodological breakthroughs, symbiosis research is undergoing a revolution” [1]. Until recently, the genetic as well as metabolic characterization of symbiotic systems was a major challenge. Most hosts, as well as symbionts, are still difficult or impossible to enrich / culture [48, 153]. Obligate symbiotic systems as well as symbioses from extreme environments pose even greater challenges, as they can usually only be cultivated together or the environmental conditions cannot be easily reproduced in the lab [1]. To overcome these difficulties, many studies in symbiosis research have focused on model organisms, such as zebrafish *Danio rerio*, bobtail squid *Eupyrmna scolopes*, nematode *Caenorhaditis elegans*, fruit fly *Drosophila melanogaster,* aphids and their *Buchnera* symbiont and leech *Hirudo verbana* [11, 26, 46, 154]. However, it is becoming clearer that many of these model organisms, on which many basic principles of biology have been discovered and described, are not representative of their close relatives [155] and therefore are not as meaningful as once thought.

Advances in genomic and metabolic methods [156-158] as well as improvements in sample collection, sample fixation, and sample preparation [159, 160] have allowed us to overcome the challenges of studying non-model organisms. Especially the improvements in experimental techniques such as single cell imaging [161, 162], microfluidics [163], in situ hybridization [164], and secondary ion mass spectrometry

(SIMS), which allows intracellular measurement of metabolic fluxes [165], have led to the ability to overcome culture dependent methods. Thus, the field of symbiosis research has increased over the last years with more than 2500 publications in 2016 alone [1]. With the improved methodology current symbiotic research ranges from the ecological study of the diversity of microbial communities in hosts to the study of what long-term effects symbiotic associations have on the cell organization and genome evolution of both partners [1].

A key problem in studying symbiosis research are the different size ranges of both partners: The symbionts are orders of magnitude smaller than their multicellular eukaryotic host, making it for example very difficult to image both partners as a whole. In microscopy, either macroscopic datasets can be acquired to get an overview of whole animals, or high resolution datasets can be acquired to visualize details and the subcellular structure. There are two ways to combine the benefits of both acquisition methods, by either (I) using a high-resolution imaging technique with a small imaging volume that is rasterized through the entire specimen in 3D, or (II) using a correlative approach by first taking the macroscopic images and then generating detail images in certain areas that are later merged during the analysis [166].

However, both methods are currently very time consuming and therefore, many previous studies focused only on the symbiotic organ or tissue. To overcome these limitations, correlative methods were developed more recently, which are linking different techniques such as imaging, chemical imaging, genomics, and transcriptomics to resolve the interplay between the two symbiotic partners as a whole [158, 167-172]. These correlative imaging techniques often include (I)

macroscopic imaging methods such as µCT or light sheet microscopy, techniques resolving individual host cells such as confocal imaging or light microscopy of histological sections, as well as (II) high resolution techniques to resolve the subcellular structures of host cells and to resolve individual symbionts such as focused ion beam scanning electron microscopy (FIB-SEM), transmission electron microscopy (TEM) or in situ hybridization coupled with high resolution imaging techniques to resolve individual symbiont cells. Due to technical improvements over the last years, many of these methods have become culture independent, which makes them available for the research on non-model systems. Thus, it was possible to study a number of non-model organisms in more detail and to better understand the interaction of the two symbiotic partners.

1.6 Aims of this thesis

The goal of this thesis is to understand the symbiont-host association between chemosynthetic bacteria and bathymodioline mussels from the initial colonization to the adult form. This includes (I) understanding both how the symbiont free developmental stages can survive in the deep sea and (II) how the host responds to the symbiont colonization by adapting its development and morphology in the early developmental life stages and in adult mussels.

For the study of symbiotic systems, it is important to understand when and how symbionts establish themselves on or within their host and how they persist throughout the life of their host. Once these basic ecological questions are answered, investigation of the underlying molecular mechanisms of symbiont recognition, acquisition and maintenance can follow. These questions will allow researchers to

better understand the dialogue between bacteria and eukaryotes, and to identify essential mechanisms in host-microbe interactions.

Associations with horizontally transmitted symbionts are particularly exciting to investigate, as the host must adapt to the symbiotic association anew from generation to generation. It is assumed that the morphological changes that often occur in such systems during the initial uptake of the symbionts are anchored in the developmental “blueprint” of the host [26]. In some systems, it has been shown that the host is even dependent on receiving signals from its symbionts at certain stages of development in order to continue its development [40]. Understanding when and how symbionts colonize the host will also allow to study the host's aposymbiotic life forms and free-living bacteria. This allows us to understand the different life strategies of symbiotic and aposymbiotic life forms. In nutritional symbiosis from extreme habitats, where the host is dependent on the energy of the symbionts, it is essential to study the survival strategies of the aposymbiotic life forms to understand the whole system. For example, tubeworm (*Vestimentifera*) larvae are aposymbiotic and possess a functional mouth and digestive system. They actively feed to survive in the deep sea. However once settled on the sea floor they get colonized by their symbionts and the digestive system gets reduced and is completely absence in adult tubeworms [24, 25]. This illustrates how remarkable morphological and developmental changes are that relate to symbiont acquisition and persistence.

So far, the understanding of symbiont colonization is mostly limited to a few model organisms including *Euprymna scolopes* squid, legumes, and intracellular rhizobia in root nodules of the soybean *Glycine max*, *Bradyrhizobium spp.* [26, 32, 173]; this information is very scarce for symbiotic systems from extreme environmental

conditions, such as the deep sea [95]. The fact that these topics in deep-sea symbioses have not been studied in detail is mainly due to the fact that it is very difficult to collect early developmental life stages of these symbiotic animals in the deep sea. Therefore, research in the last 40 years has more or less focused on adult and juvenile animals.

Throughout this work, I have used a combination of different imaging techniques and stable isotope analyses to address the aforementioned problems in studying bathymodioline mussels. To study the symbiont acquisition and persistence of these uncultivable systems requires a different approach than when working with cultivable organisms. Since deep sea samples are mostly fixed, I could not perform live cell imaging or other molecular techniques such as knock out mutants to follow uptake strategies. Therefore, I used a series of different developmental stages (from larvae to adults) of these mussels and performed detailed analyses on the (I) overall host morphology, (II) stable isotope signatures, and as well as (III) ultrastructure analysis of individual host as well as symbiont cells. This approach allowed me to analyze both the symbiont-host association from initial colonization to adult form and also to analyze ecological questions related to the different lifestyles between aposymbiotic and symbiotic mussels.

1.6.1 Which type how symbiont-host association do we find in different bathymodioline species?

Understanding the symbiont-host association is essential in symbiosis research. It is the first step to understand how the two partners are interwoven. Multiple other processes depend on the form of association. For example, the intracellular digestion of ectosymbionts needs to be differently controlled than that of intracellular

endosymbionts. Until now, the symbiont-host association in adult bathymodioline mussels was thought to correlate to the habitat these mussels live in [118]. Mussels from hydrothermal vents and cold seeps were thought to house intracellular symbionts while mussels from organic falls were thought to house ectosymbionts. Recently, it was shown that the symbionts of *B. septemdierum* were associated to the host as extracellular endosymbionts [121]. In chapter II, I investigated if this intermediate symbiont-host association is a general pattern in bathymodioline mussels or if the prediction based on the habitat is still valid. To do this we used a three-dimensional ultrastructural imaging approach to investigate the ultrastructure of entire bathymodioline host cells.

1.6.2 When do the symbionts colonize bathymodioline mussels and how does the host react to the symbiont colonization?

The mode of symbiont transmission has so far only been indirectly predicted from phylogenetic and morphological studies, which focused on the phylogeny of host and symbiont and analyzed the symbiont presence in the reproductive tissues of adult bathymodioline mussels from hydrothermal vents and cold seeps [35, 39, 148-150]. These studies assumed that symbionts are transmitted horizontally in bathymodioline mussels. Information on when, how, and where the bathymodioline mussels from hydrothermal vents and seeps get colonized was missing so far. In Chapter III, I analyzed the symbiont colonization status in different developmental stages from three bathymodioline species, *B. azoricus* and *B. puteoserpentis* from hydrothermal vents and *G. childressi* from cold seeps. By using a correlative imaging approach we were able to study entire animals and resolve morphological changes that occurred during the symbiont colonization; we could also focus on the subcellular structure and identify symbionts that were in the process of colonizing the host cell.

1.6.3 How can bathymodioline larvae survive without their symbionts in the deep sea?

How bathymodioline larvae can survive in the deep sea without their symbionts, and therefore without the energy provided, is so far not clear. In the past, it was shown that adult bathymodioline mussels can supplement their nutrition via filter-feeding [174]. However, it was still uncertain if bathymodioline larvae can survive in the deep sea by only filter-feeding was not clear [95]. In chapter IV, I resolved how the aposymbiotic life stages of bathymodioline mussels might survive in the deep sea. As these larvae are too small to be monitored in the water column, we used a stable isotope approach to investigate their trophic relationships and their potential food sources. I analyzed the stable isotope composition of pediveligers to adult mussels of three bathymodioline species (*B. azoricus* and *B. puteoserpentis* from hydrothermal vents and *G. childressi* from cold seeps). A morphologically informed stable isotope approach was chosen to not only look at the stable isotope ratios of entire specimens but also from individual organs.

List of publications

Manuscripts included in this thesis:

1. **How to live with, on and in eukaryotic cells? The different forms of symbiont-host associations in bathymodioline mussels**

   Maximilian Franke, Julian Hennies, Nicole L. Schieber, Yannick Schwab, Nicole Dubilier, and Nikolaus Leisch

   Manuscript in preparation

2. **Coming together—symbiont acquisition and early development in deep-sea bathymodioline mussels**

   Maximilian Franke, Benedikt Geier, Jörg U. Hammel, Nicole Dubilier, and Nikolaus Leisch

   Manuscript published in Proceedings of the Royal Society B (2021-08-18 available under: https://doi.org/10.1098/rspb.2021.1044)

3. **How to make a living without symbionts? The vertical migration of planktotrophic deep-sea mussels**

   Maximilian Franke, Merle Ücker, Nicole Dubilier, and Nikolaus Leisch

   Manuscript in preparation

Contributions to manuscripts not included in this thesis:

1. **Intra-host symbiont diversity in eastern Pacific cold seep tubeworms identified by the 16S-V6 region, but undetected by the 16S-V4 region**

   Corinna Breusing, **Maximilian Franke**, and Curtis Robert Young

   Manuscript published in PLOS ONE (2020-01-15 available under: https://doi.org/10.1371/journal.pone.0227053)

2. **Correlative 3D anatomy and spatial chemistry in animal-microbe symbioses: developing sample preparation for phase-contrast synchrotron radiation based micro-computed tomography and mass spectrometry imaging**

   Benedikt Geier, **Maximilian Franke**, Bernhard Ruthensteiner, Miguel Ángel González Porras, Alexander Gruhl, Lars Wörmer, Julian Moosmann, Jörg U. Hammel, Nicole Dubilier, Nikolaus Leisch, and Manuel Liebeke

   Manuscript published in Proc. SPIE (2019-09-10 available under: https://doi.org/10.1117/12.2530652)

3. **Mitonuclear discordance suggests long-distance migration and mitochondrial introgression of deep-sea mussels along the Mid-Atlantic Ridge**

   Merle Ücker, Yui Sato, Rebecca Ansorge, Anne Kupczok, **Maximilian Franke**, Harald Gruber-Vodicka, and Nicole Dubilier

Manuscript in preparation

4. **Adaptive feeding in chemosynthetic symbioses – from self-cannibalism to symbiont transmission**

   Benedikt Geier, **Maximilian Franke**, Alexander Gruhl, Bernhard Ruthensteiner, Jörg U. Hammel, Nicole Dubilier, Nikolaus Leisch, and Manuel Liebeke

   Manuscript in preparation

5. **Lysosomal symbiont digestion shapes innate immunity and fuels the metabolism of bacteriocytes in a deep-sea mussel host.**

   Målin Tietjen, Nikolaus Leisch, **Maximilian Franke**, Claas Hiebenthal, Frank Melzner, Thorsten Reusch, Nicole Dubilier, and Harald R. Gruber-Vodicka

   Manuscript in preparation

References

[1] Raina, J.-B., Eme, L., Pollock, F.J., Spang, A., Archibald, J.M. & Williams, T.A. 2018 Symbiosis in the microbial world: from ecology to genome evolution. *Biology Open* **7**. (doi:10.1242/bio.032524).
[2] Frank, A.B. 1877 Über die biologischen Verhältnisse des Thallus einiger Krustenflechten. *Biologie der Pflanzen* **2**, 123-200.
[3] De Bary, A. 1878 Über Symbiose. In *Versammlung der Deutschen Naturforscher und Ärzte* (Kassel.
[4] Leung, T. & Poulin, R. 2008 Parasitism, commensalism, and mutualism: exploring the many shades of symbioses. *Vie Milieu* **58**, 107-115.
[5] Douglas, A.E. 2010 *The Symbiotic Habit*, Princeton University Press.
[6] Martin, D.M. & Schwab, E. 2013 Current Usage of Symbiosis and Associated Terminology. *International Journal of Biology* **5**. (doi:10.5539/ijb.v5n1p32).
[7] Smith, D.C. 1979 From Extracellular to Intracellular: The Establishment of a Symbiosis. *Proc. R. Soc. B* **204**, 115-130.
[8] Margulis, L. 1970 *Origin of eukaryotic cells: Evidence and research implications for a theory of the origin and evolution of microbial, plant and animal cells on the precambrian Earth*, Yale University Press.
[9] Gray, M.W. 2017 Lynn Margulis and the endosymbiont hypothesis: 50 years later. *Molecular Biology of the Cell* **28**, 1285-1287. (doi:10.1091/mbc.e16-07-0509).
[10] Margulis, L. & Fester, R. 1991 Bellagio conference and book. Symbiosis as Source of Evolutionary Innovation: Speciation and Morphogenesis. Conference--June 25-30, 1989, Bellagio Conference Center, Italy. *Symbiosis* **11**, 93-101.
[11] Douglas, A.E. 1998 Nutritional Interactions in Insect-Microbial Symbioses: Aphids and Their Symbiotic Bacteria *Buchnera*. *Annu. Rev. Entomol.* **43**, 17-37. (doi:10.1146/annurev.ento.43.1.17).
[12] Douglas, A.E. 2011 Lessons from studying insect symbioses. *Cell host & microbe* **10**, 359-367.
[13] Martino, M.E., Joncour, P., Leenay, R., Gervais, H., Shah, M., Hughes, S., Gillet, B., Beisel, C. & Leulier, F. 2018 Bacterial Adaptation to the Host's Diet Is a Key Evolutionary Force Shaping Drosophila-Lactobacillus Symbiosis. *Cell Host & Microbe* **24**, 109-119.e106. (doi:10.1016/j.chom.2018.06.001).
[14] Matos, R.C., Schwarzer, M., Gervais, H., Courtin, P., Joncour, P., Gillet, B., Ma, D., Bulteau, A., Martino, M.E. & Hughes, S. 2017 D-Alanylation of teichoic acids contributes to *Lactobacillus plantarum*-mediated Drosophila growth during chronic undernutrition. *Nat. Microbiol* **2**, 1635-1647. (doi:10.1038/s41564-017-0038-x).
[15] Koga, R., Tsuchida, T. & Fukatsu, T. 2003 Changing partners in an obligate symbiosis: a facultative endosymbiont can compensate for loss of the essential endosymbiont *Buchnera* in an aphid. *Proc Biol Sci* **270**, 2543-2550. (doi:10.1098/rspb.2003.2537).
[16] Polz, M., Distel, D., Zarda, B., Amann, R., Felbeck, H., Ott, J. & Cavanaugh, C. 1995 Phylogenetic analysis of a highly specific association between ectosymbiotic, sulfur-oxidizing bacteria and a marine nematode. *Appl. Environ. Microbiol.* **60**, 4461-4467. (doi:10.1128/AEM.60.12.4461-4467.1994).
[17] Hoff, M. 2007 When Bacteria Lose a Single DNA Base, Aphids Suffer. *PLoS Biol.* **5**, e126. (doi:10.1371/journal.pbio.0050126).
[18] Bright, M. & Sorgo, A. 2005 Ultrastructural reinvestigation of the trophosome in adults of *Riftia pachyptila* (Annelida, Siboglinidae). *Invertebr. Biol.* **122**, 347-368. (doi:10.1111/j.1744-7410.2003.tb00099.x).
[19] Giere, O., Windoffer, R. & Southward, E.C. 1995 The Bacterial Endosymbiosis of the Gutless Nematode, *Astomonema Southwardorum*: Ultrastructural Aspects. *J. Mar. Biol. Assoc. U.K.* **75**, 153-164. (doi:10.1017/S0025315400015265).
[20] Dubilier, N., Mülders, C., Ferdelman, T., de Beer, D., Pernthaler, A., Klein, M., Wagner, M., Erséus, C., Thiermann, F., Krieger, J., et al. 2001 Endosymbiotic sulphate-reducing and

sulphide-oxidizing bacteria in an oligochaete worm. *Nature* **411**, 298-302. (doi:10.1038/35077067).
[21] Estes, A.M., Hearn, D.J., Bronstein, J.L. & Pierson, E.A. 2009 The Olive Fly Endosymbiont, "*Candidatus* Erwinia dacicola," Switches from an Intracellular Existence to an Extracellular Existence during Host Insect Development. *Appl. Environ. Microbiol.* **75**, 7097-7106. (doi:10.1128/AEM.00778-09).
[22] Sogin, E.M., Leisch, N. & Dubilier, N. 2020 Chemosynthetic symbioses. *Curr. Biol.* **30**, R1137-R1142. (doi:10.1016/j.cub.2020.07.050).
[23] Thompson, M.C., Feng, H., Wuchty, S. & Wilson, A.C.C. 2019 The green peach aphid gut contains host plant microRNAs identified by comprehensive annotation of Brassica oleracea small RNA data. *Sci. Rep.* **9**, 18904. (doi:10.1038/s41598-019-54488-1).
[24] Bright, M., Klose, J. & Nussbaumer, A.D. 2013 Giant tubeworms. *Curr. Biol.* **23**, R224-R225. (doi:10.1016/j.cub.2013.01.039).
[25] Nussbaumer, A.D., Fisher, C.R. & Bright, M. 2006 Horizontal endosymbiont transmission in hydrothermal vent tubeworms. *Nature* **441**, 345-348. (doi:10.1038/nature04793).
[26] McFall-Ngai, M.J. 2014 The importance of microbes in animal development: lessons from the squid-vibrio symbiosis. *Annu. Rev. Microbiol.* **68**, 177-194. (doi:10.1146/annurev-micro-091313-103654).
[27] Nyholm, S.V., Stewart, J.J., Ruby, E.G. & McFall-Ngai, M.J. 2009 Recognition between symbiotic *Vibrio fischeri* and the haemocytes of *Euprymna scolopes*. *Environ. Microbiol.* **11**, 483-493. (doi:10.1111/j.1462-2920.2008.01788.x).
[28] Moran, N.A. & Dunbar, H.E. 2006 Sexual acquisition of beneficial symbionts in aphids. *Proceedings of the National Academy of Sciences* **103**, 12803. (doi:10.1073/pnas.0605772103).
[29] van Ham, R.C.H.J., Kamerbeek, J., Palacios, C., Rausell, C., Abascal, F., Bastolla, U., Fernández, J.M., Jiménez, L., Postigo, M., Silva, F.J., et al. 2003 Reductive genome evolution in <em>Buchnera aphidicola</em&gt. *Proceedings of the National Academy of Sciences* **100**, 581. (doi:10.1073/pnas.0235981100).
[30] Turnbaugh, P.J., Ley, R.E., Hamady, M., Fraser-Liggett, C.M., Knight, R. & Gordon, J.I. 2007 The Human Microbiome Project. *Nature* **449**, 804-810. (doi:10.1038/nature06244).
[31] Gomaa, E.Z. 2020 Human gut microbiota/microbiome in health and diseases: a review. *Antonie Van Leeuwenhoek* **113**, 2019-2040. (doi:10.1007/s10482-020-01474-7).
[32] Bright, M. & Bulgheresi, S. 2010 A complex journey: transmission of microbial symbionts. *Nature Reviews Microbiology* **8**, 218-230. (doi:10.1038/nrmicro2262).
[33] Heddi, A. & Nardon, P. 2005 *Sitophilus oryzae L.*: a model for intracellular symbiosis in the Dryophthoridae weevils (Coleoptera). *Symbiosis*.
[34] Nardon, P. 1971 Contribution à l'étude des symbiotes ovariens de Sitophilus sasakii: localisation, histochimie et ultrastructure chez la femelle adulte. *CR Acad. Sci. Paris* **272**, 2975-2978.
[35] Russell, S.L., Pepper-Tunick, E., Svedberg, J., Byrne, A., Ruelas Castillo, J., Vollmers, C., Beinart, R.A. & Corbett-Detig, R. 2020 Horizontal transmission and recombination maintain forever young bacterial symbiont genomes. *PLoS Genet.* **16**, e1008935. (doi:10.1371/journal.pgen.1008935).
[36] Russell, S.L., Corbett-Detig, R.B. & Cavanaugh, C.M. 2017 Mixed transmission modes and dynamic genome evolution in an obligate animal–bacterial symbiosis. *ISME J* **11**, 1359-1371. (doi:10.1038/ismej.2017.10).
[37] Ozawa, G., Shimamura, S., Takaki, Y., Takishita, K., Ikuta, T., Barry, J.P., Maruyama, T., Fujikura, K. & Yoshida, T. 2017 Ancient Occasional Host Switching of Maternally Transmitted Bacterial Symbionts of Chemosynthetic Vesicomyid Clams. *Genome Biol Evol* **9**, 2226-2236. (doi:10.1093/gbe/evx166).
[38] Gruber-Vodicka, H.R., Dirks, U., Leisch, N., Baranyi, C., Stoecker, K., Bulgheresi, S., Heindl, N.R., Horn, M., Lott, C., Loy, A., et al. 2011 An ancient symbiosis between thiotrophic Alphaproteobacteria and catenulid flatworms. *Proceedings of the National Academy of Sciences* **108**, 12078. (doi:10.1073/pnas.1105347108).

[39] Won, Y.J., Jones, W.J. & Vrijenhoek, R.C. 2008 Absence of cospeciation between deep-sea mytilids and their thiotrophic endosymbionts. *J. Shellfish Res.* **27**, 129-138. (doi:10.2983/0730-8000(2008)27[129:AOCBDM]2.0.CO;2).
[40] McFall-Ngai, M., Hadfield, M.G., Bosch, T.C.G., Carey, H.V., Domazet-Lošo, T., Douglas, A.E., Dubilier, N., Eberl, G., Fukami, T., Gilbert, S.F., et al. 2013 Animals in a bacterial world, a new imperative for the life sciences. *Proc. Natl. Acad. Sci. USA* **110**, 3229-3236. (doi:10.1073/pnas.1218525110).
[41] Fisher, R.M., Henry, L.M., Cornwallis, C.K., Kiers, E.T. & West, S.A. 2017 The evolution of host-symbiont dependence. *Nature Communications* **8**, 15973. (doi:10.1038/ncomms15973).
[42] Moran, N.A. & Bennett, G.M. 2014 The Tiniest Tiny Genomes. *Annu. Rev. Microbiol.* **68**, 195-215. (doi:10.1146/annurev-micro-091213-112901).
[43] Kuwahara, H., Yoshida, T., Takaki, Y., Shimamura, S., Nishi, S., Harada, M., Matsuyama, K., Takishita, K., Kawato, M. & Uematsu, K. 2007 Reduced genome of the thioautotrophic intracellular symbiont in a deep-sea clam, *Calyptogena okutanii*. *Curr. Biol.* **17**, 881-886. (doi:10.1016/j.cub.2007.04.039).
[44] Peek, A.S., Vrijenhoek, R.C. & Gaut, B.S. 1998 Accelerated evolutionary rate in sulfur-oxidizing endosymbiotic bacteria associated with the mode of symbiont transmission. *Mol. Biol. Evol.* **15**, 1514-1523. (doi:10.1093/oxfordjournals.molbev.a025879).
[45] Bennett, G.M. & Moran, N.A. 2015 Heritable symbiosis: The advantages and perils of an evolutionary rabbit hole. *Proceedings of the National Academy of Sciences* **112**, 10169. (doi:10.1073/pnas.1421388112).
[46] Douglas, A.E. 2019 Simple animal models for microbiome research. *Nature Reviews Microbiology*. (doi:10.1038/s41579-019-0242-1).
[47] Ghanbari, M., Konrad, J.D. & Wolfgang, K. 2015 A new view of the fish gut microbiome: Advances from next-generation sequencing. *Aquaculture (Amsterdam, Netherlands)* **448**, 464-475. (doi:10.1016/j.aquaculture.2015.06.033).
[48] Dubilier, N., Bergin, C. & Lott, C. 2008 Symbiotic diversity in marine animals: the art of harnessing chemosynthesis. *Nature Reviews Microbiology* **6**, 725-740. (doi:10.1038/nrmicro1992).
[49] Douglas, A.E. 1989 Mycetocyte Symbiosis in insects. *Biological Reviews* **64**, 409-434. (doi:10.1111/j.1469-185X.1989.tb00682.x).
[50] McCutcheon, J.P., McDonald, B.R. & Moran, N.A. 2009 Convergent evolution of metabolic roles in bacterial co-symbionts of insects. *Proceedings of the National Academy of Sciences* **106**, 15394. (doi:10.1073/pnas.0906424106).
[51] Baumann, P. 2005 Biology of bacteriocyte-associated endosymbionts of plant SAP-sucking insects. *Annu. Rev. Microbiol.* **59**, 155-189. (doi:10.1146/annurev.micro.59.030804.121041).
[52] Venn, A.A., Loram, J.E. & Douglas, A.E. 2008 Photosynthetic symbioses in animals. *J. Exp. Bot.* **59**, 1069-1080. (doi:10.1093/jxb/erm328).
[53] Little, A.E.F. 2010 Parasitism is a Strong Force Shaping the Fungus-Growing Ant–Microbe Symbiosis. In *Symbiosis and Stress* (eds. J. Seckbach & M. Grube), pp. 245-264, Springer
[54] Moran, N.A. & Telang, A. 1998 Bacteriocyte-Associated Symbionts of Insects: A variety of insect groups harbor ancient prokaryotic endosymbionts. *Bioscience* **48**, 295-304. (doi:10.2307/1313356).
[55] Sogin, E.M., Kleiner, M., Borowski, C., Gruber-Vodicka, H.R. & Dubilier, N. 2021 Life in the Dark: Phylogenetic and Physiological Diversity of Chemosynthetic Symbioses. *Annu. Rev. Microbiol.* (doi:10.1146/annurev-micro-051021-123130).
[56] Cavanaugh, C.M., Gardiner, S.L., Jones, M.L., Jannasch, H.W. & Waterbury, J.B. 1981 Prokaryotic cells in the hydrothermal vent tube worm Riftia pachyptila Jones: possible chemoautotrophic symbionts. *Science* **213**, 340-342.

[57] Felbeck, H. 1981 Chemoautotrophic potential of the hydrothermal vent tube worm, *Riftia pachyptila Jones* (Vestimentifera). *Science* **213**, 336-338. (doi:10.1126/science.213.4505.336).
[58] Smith, C. 2012 Chemosynthesis in the deep-sea: life without the sun. *Biogeosciences Discuss.* **2012**, 17037-17052. (doi:10.5194/bgd-9-17037-2012).
[59] Jannasch, H.W. & Mottl, M.J. 1985 Geomicrobiology of Deep-Sea Hydrothermal Vents. *Science* **229**, 717-725. (doi:10.1126/science.229.4715.717).
[60] Jannasch, H.W. 1985 Review Lecture - The chemosynthetic support of life and the microbial diversity at deep-sea hydrothermal vents. *Proceedings of the Royal Society of London. Series B. Biological Sciences* **225**, 277-297. (doi:10.1098/rspb.1985.0062).
[61] Cary, S.C., Fisher, C.R. & Felbeck, H. 1988 Mussel growth supported by methane as sole carbon and energy source *Science* **240**, 78-79. (doi:10.1126/science.240.4848.78).
[62] Childress, J.J., Fisher, C.R., Brooks, J.M., Kennicutt, M.C., Bidigare, R.R. & Anderson, A.E. 1986 A methanotrophic marine molluscan (bivalvia, mytilidae) symbiosis: mussels fueld by gas. *Science* **233**, 1306-1308. (doi:10.1126/science.233.4770.1306).
[63] Fisher, C.R., Childress, J.J., Oremland, R.S. & Bidigare, R.R. 1987 The importance of methane and thiosulfate in the metabolism of the bacterial symbionts of two deep-sea mussels. *Mar. Biol.* **96**, 59-71. (doi:10.1007/BF00394838).
[64] Zimmermann, J., Wentrup, C., Sadowski, M., Blazejak, A., Gruber-Vodicka, H.R., Kleiner, M., Ott, J.A., Cronholm, B., De Wit, P., Erséus, C., et al. 2016 Closely coupled evolutionary history of ecto- and endosymbionts from two distantly related animal phyla. *Mol. Ecol.* **25**, 3203-3223. (doi:doi.org/10.1111/mec.13554).
[65] Cavanaugh, C. 1993 Methanotroph-invertebrate symbioses in the marine environment: ultrastructural, biochemical and molecular studies. *Microbial growth on C* **1**, 315-328.
[66] Cavanaugh, C.M., Levering, P.R., Maki, J.S., Mitchell, R. & Lidstrom, M.E. 1987 Symbiosis of methylotrophic bacteria and deep-sea mussels. *Nature* **325**, 346-348. (doi:10.1038/325346a0).
[67] Petersen, J.M., Zielinski, F.U., Pape, T., Seifert, R., Moraru, C., Amann, R., Hourdez, S., Girguis, P.R., Wankel, S.D., Barbe, V., et al. 2011 Hydrogen is an energy source for hydrothermal vent symbioses. *Nature* **476**, 176-180. (doi:10.1038/nature10325).
[68] Cavanaugh, C.M. 1983 Symbiotic chemoautotrophic bacteria in marine invertebrates from sulphide-rich habitats. *Nature* **302**, 58-61. (doi:10.1038/302058a0).
[69] Cavanaugh, C.M., McKiness, Z.P., Newton, I.L.G. & Stewart, F.J. 2006 Marine Chemosynthetic Symbioses. In *The Prokaryotes: Volume 1: Symbiotic associations, Biotechnology, Applied Microbiology* (eds. M. Dworkin, S. Falkow, E. Rosenberg, K.-H. Schleifer & E. Stackebrandt), pp. 475-507. New York, NY, Springer New York.
[70] Assié, A., Borowski, C., van der Heijden, K., Raggi, L., Geier, B., Leisch, N., Schimak, M.P., Dubilier, N. & Petersen, J.M. 2016 A specific and widespread association between deep-sea *Bathymodiolus* mussels and a novel family of Epsilonproteobacteria. *Environmental Microbiology Reports* **8**, 805-813. (doi:10.1111/1758-2229.12442).
[71] Cavanaugh, C.M., Wirsen, C.O. & Jannasch, H.W. 1992 Evidence for Methylotrophic Symbionts in a Hydrothermal Vent Mussel (Bivalvia: *Mytilidae*) from the Mid-Atlantic Ridge. *Appl. Environ. Microbiol.* **58**, 5. (doi:10.1128/aem.58.12.3799-3803.1992).
[72] Le Pennec, M., Benninger, P.G. & Herry, A. 1995 Feeding and digestive adaptations of bivalve molluscs to sulphide-rich habitats. *Comparative Biochemistry and Physiology* **111**, 183-189. (doi:10.1016/0300-9629(94)00211-B).
[73] Le Pennec, M., Donval, A. & Herry, A. 1990 Nutritionl strategies of the hydrothermal ecosystem bivalves. *Prog. Oceanogr.* **24**. (doi:10.1016/0079-6611(90)90020-3).
[74] Fiala-Medioni, A. & Le Pennec, M. 1987 Trophic structural adaptations in relation to the bacterial association of bivalve molluscs from hydrothermal vents and subduction zones. In *Symposium on marine symbioses. 1 (1987)* (pp. 63-74, Balaban, Philadelphia, .
[75] Nybakken, J.W. & Bertness, M.D. 2005 *Marine biology: an ecological approach*. sixth ed. San Francisco, Pearson/Benjamin Cummings.

[76] Riou, V., Colaco, A., Bouillon, S., Khripounoff, A., Dando, P., Mangion, P., Chevalier, E., Korntheuer, M., Santos, R.S. & Dehairs, F. 2010 Mixotrophy in the deep sea: a dual endosymbiotic hydrothermal mytilid assimilates dissolved and particulate organic matter. *Marine Ecology-progress Series* **405**, 187-201. (doi:10.3354/meps08515).
[77] Ramírez-Llodra, E. & Billett, D.S.M. 2006 Deep-Sea Ecosystems: Pristine Biodiversity Reservoir and Technological Challenge. (pp. 63 - 92.
[78] Clark, M.R., Durden, J.M. & Christiansen, S. 2020 Environmental Impact Assessments for deep-sea mining: Can we improve their future effectiveness? *Mar. Policy* **114**. (doi:10.1016/j.marpol.2018.11.026).
[79] Clark, M.R., Althaus, F., Schlacher, T.A., Williams, A., Bowden, D.A. & Rowden, A.A. 2016 The impacts of deep-sea fisheries on benthic communities: a review. *ICES J. Mar. Sci.* **73**, i51-i69. (doi:10.1093/icesjms/fsv123).
[80] Ramirez-Llodra, E., Tyler, P.A., Baker, M.C., Bergstad, O.A., Clark, M.R., Escobar, E., Levin, L.A., Menot, L., Rowden, A.A., Smith, C.R., et al. 2011 Man and the Last Great Wilderness: Human Impact on the Deep Sea. *PLOS ONE* **6**, e22588. (doi:10.1371/journal.pone.0022588).
[81] Smith, C.R., Glover, A.G., Treude, T., Higgs, N.D. & Amon, D.J. 2015 Whale-Fall Ecosystems: Recent Insights into Ecology, Paleoecology, and Evolution. *Annual Review of Marine Science* **7**, 571-596. (doi:10.1146/annurev-marine-010213-135144).
[82] Vrijenhoek, R. 2010 Genetics and Evolution of Deep-Sea Chemosynthetic Bacteria and Their Invertebrate Hosts. (pp. 15-49.
[83] Thubaut, J., Corbari, L., Gros, O., Duperron, S., Couloux, A. & Samadi, S. 2013 Integrative Biology of Idas iwaotakii (Habe, 1958), a 'Model Species' Associated with Sunken Organic Substrates. *PLOS ONE* **8**, e69680. (doi:10.1371/journal.pone.0069680).
[84] Velásquez, M. & Shipway, J.R. 2018 A new genus and species of deep-sea wood-boring shipworm (Bivalvia: Teredinidae) *Nivanteredo coronata n. sp.* from the Southwest Pacific. *Mar. Biol. Res.* **14**, 806-815. (doi:10.1080/17451000.2018.1544421).
[85] Distel, D.L., Baco, A.R., Chuang, E., Morrill, W., Cavanaugh, C. & Smith, C.R. 2000 Do mussels take wooden steps to deep-sea vents? *Nature* **403**, 725-726. (doi:10.1038/35001667).
[86] Beaulieu, S.E., Baker, E.T. & German, C.R. 2015 Where are the undiscovered hydrothermal vents on oceanic spreading ridges? *Deep Sea Research Part II: Topical Studies in Oceanography* **121**, 202-212. (doi:10.1016/j.dsr2.2015.05.001).
[87] Martin, W., Baross, J.A., Kelley, D.S. & Russell, M.J. 2008 Hydrothermal vents and the origin of life. *Nature Reviews Microbiology* **6**, 805-814. (doi:10.1038/nrmicro1991).
[88] Van Dover, C.L. 2000 *The Ecology of Deep-Sea Hydrothermal Vents*. Princeton, Princeton University Press.
[89] Lalou, C., Thompson, G., Arnold, M., Brichet, E., Druffel, E. & Rona, P.A. 1990 Geochronology of TAG and Snakepit hydrothermal fields, Mid-Atlantic Ridge: Witness to a long and complex hydrothermal history. *Earth and Planetary Science Letters* **97**, 113-128. (doi:10.1016/0012-821X(90)90103-5).
[90] Lalou, C. & Brichet, E. 1982 Ages and implications of East Pacific Rise sulphide deposits at 21 °N. *Nature* **300**, 169-171. (doi:10.1038/300169a0).
[91] Snow, J.E. & Edmonds, H.N. 2007 Ultraslow-Spreading Ridges Rapid Paradigm Changes. *Oceanography* **20**, 90-101. (doi:10.5670/oceanog.2007.83).
[92] Kelley, D.S., Baross, J.A. & Delaney, J.R. 2002 Volcanoes, Fluids, and Life at Mid-Ocean Ridge Spreading Centers. *Annual Review of Earth and Planetary Sciences* **30**, 385-491. (doi:10.1146/annurev.earth.30.091201.141331).
[93] Kennicutt, M.C., Brooks, J.M., Bidigare, R.R., Fay, R.R., Wade, T.L. & McDonald, T.J. 1985 Vent-type taxa in a hydrocarbon seep region on the Louisiana slope. *Nature* **317**, 351-353. (doi:10.1038/317351a0).
[94] Cordes, E.E., Cunha, M.R., Galéron, J., Camilo, M., Olu, K., Sibuet, M., Saskia, V., Ann, V. & Levin, A. 2010 The influence of biogenic habitat heterogeneity on seep diversity. *Marine Ecology-an Evolutionary Perspective* **31**, 51-65. (doi:10.1111/j.1439-0485.2009.00334.x).

[95] Laming, S.R., Gaudron, S.M. & Duperron, S. 2018 Lifecycle Ecology of Deep-Sea Chemosymbiotic Mussels: A Review. *Front. Mar. Sci.* **5**. (doi:10.3389/fmars.2018.00282).
[96] Govenar, B. 2010 Shaping Vent and Seep Communities: Habitat Provision and Modification by Foundation Species. In *The Vent and Seep Biota: Aspects from Microbes to Ecosystems* (ed. S. Kiel), pp. 403-432. Dordrecht, Springer Netherlands.
[97] Liu, J., Liu, H. & Zhang, H. 2018 Phylogeny and evolutionary radiation of the marine mussels (Bivalvia: *Mytilidae*) based on mitochondrial and nuclear genes. *Mol Phylogenet Evol* **126**, 233-240. (doi:10.1016/j.ympev.2018.04.019).
[98] Lorion, J., Kiel, S., Faure, B., Kawato, M., Ho, S.Y., Marshall, B., Tsuchida, S., Miyazaki, J. & Fujiwara, Y. 2013 Adaptive radiation of chemosymbiotic deep-sea mussels. *Proc Biol Sci* **280**, 20131243. (doi:10.1098/rspb.2013.1243).
[99] Samadi, S., Quéméré, E., Lorion, J., Tillier, A., von Cosel, R., Lopez, P., Cruaud, C., Couloux, A. & Boisselier-Dubayle, M.C. 2007 Molecular phylogeny in mytilids supports the wooden steps to deep-sea vents hypothesis. *C R Biol* **330**, 446-456. (doi:10.1016/j.crvi.2007.04.001).
[100] Jang, S., Ho, P., Jun, S., Kim, D. & Won, Y.J. 2020 A newly discovered *Gigantidas* bivalve mussel from the Onnuri Vent Field in the northern Central Indian Ridge. *Deep Sea Research Part I: Oceanographic Research Papers* **161**, 103299. (doi:10.1016/j.dsr.2020.103299).
[101] Xu, T., Feng, D., Tao, J. & Qiu, J. 2019 A new species of deep-sea mussel (Bivalvia: Mytilidae: *Gigantidas*) from the South China Sea: Morphology, phylogenetic position, and gill-associated microbes.
[102] Gustafson, R.G., Turner, R.D., Lutz, R.A. & Vrijenhoek, R.C. 1998 A new genus and five new species of mussels (Bivalvia, Mytilidae) from deep-sea sulfide/hydrocarbon seeps in the Gulf of Mexico. *Malacologia* **40**, 63-112.
[103] 2021 MolluscaBase. 2021. https://www.molluscabase.org (accessed September 14, 2021)
[104] Amano, K. & Jenkins, R.G. 2011 New fossil *Bathymodiolus* (sensu lato) (Bivalvia: Mytilidae) from Oligocene seep-carbonates in eastern Hokkaido, Japan, with remarks on the evolution of the genus. *The Nautilus* **125**, 29-35.
[105] Kiel, S. & Taviani, M. 2017 Chemosymbiotic bivalves from Miocene methane-seep carbonates in Italy. *J. Paleontol.* **91**, 444-466. (doi:10.1017/jpa.2016.154).
[106] Duperron, S., Lorion, J., Samadi, S., Gros, O. & Gaill, F. 2009 Symbioses between deep-sea mussels (Mytilidae : *Bathymodiolinae*) and chemosynthetic bacteria : diversity, function and evolution. *C. R. Biol.* **332**, 298-310. (doi:10.1016/j.crvi.2008.08.003).
[107] Fisher, C.R. 1990 Chemoautotrophic and methanotrophic symbioses in marine invertebrates. *Reviews In Aquatic Sciences* **2**, 399-436.
[108] DeChaine, E. & Cavanaugh, C.M. 2005 Symbioses of methanotrophs and deep-sea mussels (*Mytilidae*: *Bathymodiolinae*). *Prog Mol Subcell Biol.* **41**, 227-249. (doi:10.1007/3-540-28221-1_11).
[109] Duperron, S., Bergin, C., Zielinski, F.U., Blazejak, A., Pernthaler, A., McKiness, Z.P., DeChaine, E., Cavanaugh, C.M. & Dubilier, N. 2006 A dual symbiosis shared by two mussel species, *Bathymodiolus azoricus* and *Bathymodiolus puteoserpentis* (Bivalvia: Mytilidae), from hydrothermal vents along the northern Mid-Atlantic Ridge. *Environ. Microbiol.* **8**, 1441-1447. (doi:10.1111/j.1462-2920.2006.01038.x).
[110] Distel, D.L., Lee, H.K.-W. & Cavanaugh, C.M. 1995 Intracellular coecistence of methano- and thioautorophic bacteria in a hydrothermal vent mussel. *Microbiology* **92**.
[111] Kádár, E., Davis, S.A. & Lobo-da-Cunha, A. 2008 Cytoenzymatic investigation of intracellular digestion in the symbiont-bearing hydrothermal bivalve *Bathymodiolus azoricus*. *Mar. Biol.* **153**, 995-1004. (doi:10.1007/s00227-007-0872-0).
[112] Fiala-Médioni, A., McKiness, Z., Dando, P., Boulegue, J., Mariotti, A., Alayse-Danet, A., Robinson, J. & Cavanaugh, C. 2002 Ultrastructural, biochemical, and immunological characterization of two populations of the mytilid mussel *Bathymodiolus azoricus* from the

Mid-Atlantic Ridge evidence for a dual symbiosis. *Mar. Biol.* **141**, 1035-1043. (doi:10.1007/s00227-002-0903-9).
[113] Streams, M.E., Fisher, C.R. & Fiala-Médioni, A. 1997 Methanotrophic symbiont location and fate of carbon incorporated from methne in a hydrocabon seep mussel. *Mar. Biol.* **129**, 465-476. (doi:10.1007/s002270050187).
[114] Von Cosel, R. & Marshall, B.A. 2010 A new genus and species of large mussel (Mollusca: Bivalvia: *Mytilidae*) from the Kermadec Ridge. *Records of the Musuem of New Zealand Te Papa* **21**, 15.
[115] Powell, M.A. & Somero, G.N. 1986 Adaptations to Sulfide by Hydrothermal Vent Animals: Sites and Mechanisms of Detoxification and Metabolism. *Biol. Bull,* **171**, 274-290. (doi:10.2307/1541923).
[116] Ponnudurai, R., Kleiner, M., Sayavedra, L., Petersen, J.M., Moche, M., Otto, A., Becher, D., Takeuchi, T., Satoh, N., Dubilier, N., et al. 2017 Metabolic and physiological interdependencies in the Bathymodiolus azoricus symbiosis. *ISME J* **11**, 463-477. (doi:10.1038/ismej.2016.124).
[117] Sayavedra, L., Kleiner, M., Ponnudurai, R., Wetzel, S., Pelletier, E., Barbe, V., Satoh, N., Shoguchi, E., Fink, D., Breusing, C., et al. 2015 Abundant toxin-related genes in the genomes of beneficial symbionts from deep-sea hydrothermal vent mussels *eLife* **4**. (doi:10.7554/eLife.07966).
[118] Fujiwara, Y., Kawato, M., Noda, C., Kinoshita, G., Yamanaka, T., Fujita, Y., Uematsu, K. & Miyazaki, J. 2010 Extracellular and Mixotrophic Symbiosis in the Whale-Fall Mussel *Adipicola pacifica*: A Trend in Evolution from Extra- to Intracellular Symbiosis. *PLOS ONE* **5**, e11808. (doi:10.1371/journal.pone.0011808).
[119] Duperron, S. 2010 The diversity of deep-sea mussels and their bacterial symbioses. In *The vent and seep biota* (ed. S. Kiel), pp. 137-167. Netherlands, Springer.
[120] Wentrup, C., Wendeberg, A., Schimak, M., Borowski, C. & Dubilier, N. 2014 Forever competent: deep-sea bivalves are colonized by their chemosynthetic symbionts throughout their lifetime. *Environ. Microbiol.* **16**, 3699-3713. (doi:10.1111/1462-2920.12597).
[121] Ikuta, T., Amari, Y., Tame, A., Takaki, Y., Tsuda, M., Iizuka, R., Funatsu, T. & Yoshida, T. 2021 Inside or out? Clonal thiotrophic symbiont populations occupy deep-sea mussel bacteriocytes with pathways connecting to the external environment. *ISME Communications* **1**, 38. (doi:10.1038/s43705-021-00043-x).
[122] Rubin-Blum, M., Paul Antony, C., Borowski, C., Sayavedra, L., Pape, T., Sahling, H., Bohrmann, G., Kleiner, M., Redmond, M.C., Valentine, D.L., et al. 2017 Short-chain alkanes fuel mussel and sponge *Cycloclasticus* symbionts from deep-sea gas and oil seeps. *Nat. Microbiol* **2**, 11. (doi:10.1038/nmicrobiol.2017.93).
[123] Zielinski, F.U., Pernthaler, A., Duperron, S., Raggi, L., Giere, O., Borowski, C. & Dubilier, N. 2009 Widespread occurrence of an intranuclear bacterial parasite in vent and seep bathymodiolin mussels. *Environ. Microbiol.* **11**, 1150-1167. (doi:10.1111/j.1462-2920.2008.01847.x).
[124] Laming, S.R., Duperron, S., Gaudron, S.M., Hilario, A. & Cunha, M.R. 2015 Adapted to change: The rapid development of symbiosis in newly settled, fast-maturing chemosymbiotic mussels in the deep sea. *Mar. Environ. Res.* **112**, 100-112. (doi:10.1016/j.marenvres.2015.07.014).
[125] Laming, S.R., Duperron, S., Cunha, M.R. & Gaudron, S.M. 2014 Settled, symbiotic, then sexually mature: adaptive developmental anatomy in the deep-sea, chemosymbiotic mussel *Idas modiolaeformis*. *Mar. Biol.* **161**, 1319-1333. (doi:10.1007/s00227-014-2421-y).
[126] Arellano, S.M. & Young, C.M. 2009 Spawning, development, and the duration of larval life in a deep-sea cold-seep mussel. *Biol. Bull,* **216**, 149-162. (doi:10.1086/BBLv216n2p149).
[127] Tyler, P.A. & Young, C.M. 1999 Reproduction and dispersal at vents and cold seeps. *J. Mar. Biol. Assoc. U.K.* **79**, 193-208. (doi:10.1017/S0025315499000235).
[128] Gustafson, R.G. 1994 Molluscan life history traits at deep-sea hydrothermal vents and cold methane/sulfide seeps. *Reproduction, Larval Biology and Recruitment of the Deep-sea Bethos*.

[129] Hilário, A., Metaxas, A., Gaudron, S.M., Howell, K.L., Mercier, A., Mestre, N.C., Ross, R.E., Thurnherr, A.M. & Young, C.M. 2015 Estimating dispersal distance in the deep sea: challenges and applications to marine reserves. *Front. Mar. Sci.* **2**, 6. (doi:10.3389/fmars.2015.00006).
[130] Young, C.M., Arellano, S.M., Hamel, J.F. & Mercier, A. 2018 Ecology and evolution of larval dispersal in the deep sea. In *Evolutionary ecology of marine invertebrate larvae* (eds. T.J. Carrier, A.M. Reitzel & A. Heyland). Oxford, Oxford University Press.
[131] Breusing, C., Biastoch, A., Drews, A., Metaxas, A., Jollivet, D., Vrijenhoek, R.C., Bayer, T., Melzner, F., Sayavedra, L., Petersen, J.M., et al. 2016 Biophysical and Population Genetic Models Predict the Presence of "Phantom" Stepping Stones Connecting Mid-Atlantic Ridge Vent Ecosystems. *Curr. Biol.* **26**, 2257-2267. (doi:10.1016/j.cub.2016.06.062).
[132] Arellano, S.M., Van Gaest, A.L., Johnson, S.B., Vrijenhoek, R.C. & Young, C.M. 2014 Larvae from deep-sea methane seeps disperse in surface waters. *Proc Biol Sci* **281**, 20133276. (doi:10.1098/rspb.2013.3276).
[133] McVeigh, D.M., Eggleston, D.B., Todd, A.C., Young, C.M. & He, R. 2017 The influence of larval migration and dispersal depth on potential larval trajectories of a deep-sea bivalve. *Deep Sea Research Part I: Oceanographic Research Papers*. (doi:10.1016/j.dsr.2017.08.002).
[134] Young, C.M., He, R., Emlet, R.B., Li, Y., Qian, H., Arellano, S.M., Van Gaest, A., Bennett, K.C., Wolf, M., Smart, T.I., et al. 2012 Dispersal of deep-sea larvae from the intra-American seas: simulations of trajectories using ocean models. *Integr. Comp. Biol.* **52**, 483-496. (doi:10.1093/icb/ics090).
[135] Bayne, B.L. 1971 Some morphological changes that occur at the metamorphosis of the larvae of *Mytilus edulis*. In *The Fourth European Marine Biology Symposium* (pp. 259-280.
[136] Gallager, S.M., Mann, R. & Sasaki, G.C. 1986 Lipid as an index of growth and viability in three species of bivalve larvae. *Aquaculture* **56**, 81-103. (doi:10.1016/0044-8486(86)90020-7).
[137] Bayne, B.L. 1965 Growth and the delay of metamorphosis of the larvae of M*ytilus edulis* (L.). *Ophelia* **2**, 1-47. (doi:10.1080/00785326.1965.10409596).
[138] Morse, D.E. 1990 Recent progress in larval settlement and metamorphosis: closing the gaps between molecular biology and ecology. *Bull. Mar. Sci.* **46**, 465-483.
[139] Ganesan, A.M., Alfaro, A.C., Brooks, J.D. & Higgins, C.M. 2010 The role of bacterial biofilms and exudates on the settlement of mussel (*Perna canaliculus*) larvae. *Aquaculture* **306**, 388-392. (doi:10.1016/j.aquaculture.2010.05.007).
[140] Wang, C., Bao, W.Y., Gu, Z.Q., Li, Y.F., Liang, X., Ling, Y., Cai, S., Shen, H. & Yang, J. 2012 Larval settlement and metamorphosis of the mussel *Mytilus coruscus* in response to natural biofilms. *Biofouling* **28**, 249-256. (doi:10.1080/08927014.2012.671303).
[141] Alfaro, A.C., Copp, B.R., Appleton, D.R., Kelly, S. & Jeffs, A.G. 2006 Chemical cues promote settlement in larvae of the green-lipped mussel, *Perna canaliculus*. *Aquacult. Int.* **14**, 405-412. (doi:10.1007/s10499-005-9041-y).
[142] Dobretsov, S.V. 1999 Effects of macroalgae and biofilm on settlement of blue mussel (*Mytilus edulis L.*) larvae. *Biofouling* **14**, 153-165. (doi:10.1080/08927019909378406).
[143] Gros, O., Frenkiel, L. & Moueza, M. 1997 Embryonic, larval, and post-larval development in the symbiotic clam *Codakia orbicularis* (Bivalvia: Lucinidae). *Invertebr. Biol.*, 86-101. (doi:10.2307/3226973).
[144] Marshall, D.J. & Keough, M.J. 2003 Variation in the dispersal potential of non-feeding invertebrate larvae: the desperate larva hypothesis and larval size. *Mar. Ecol. Prog. Ser.* **255**, 145-153. (doi:10.3354/meps255145).
[145] Franke, M., Geier, B., Hammel, J.U., Dubilier, N. & Leisch, N. 2021 Coming together - symbiont acquisition and early development in deep-sea bathymodioline mussels. *Proceedings of the Royal Society B: Biological Sciences* **288**, 20211044. (doi:doi:10.1098/rspb.2021.1044).

[146] Baker, P. & Mann, R. 1997 The postlarval phase of bivalve mollusks: a review of functional ecology and new records of postlarval drifting of Chesapeake Bay bivalves. *Bull. Mar. Sci.* **61**, 409-430.
[147] Cannuel, R., Beninger, P.G., Mc Combie, H. & Boudry, P. 2009 Gill Development and Its Functional and Evolutionary Implications in the Blue Mussel *Mytilus edulis*. *Biol. Bull,* **217**, 173-188. (doi:10.1086/BBLv217n2p173).
[148] Fontanez, K.M. & Cavanaugh, C.M. 2014 Evidence for horizontal transmission from multilocus phylogeny of deep-sea mussel (*Mytilidae*) symbionts. *Environ. Microbiol.* **16**, 3608-3621. (doi:10.1111/1462-2920.12379).
[149] Won, Y.J., Hallam, S.J., O'Mullan, G.D., Pan, I.L., Buck, K.R. & Vrijenhoek, R.C. 2003 Environmental Acquisition of Thiotrophic Endosymbionts by Deep-Sea Mussels of the Genus *Bathymodiolus*. *Appl. Environ. Microbiol.* **69**, 6785-6792. (doi:10.1128/aem.69.11.6785-6792.2003).
[150] Gaudron, S.M., Demoyencourt, E. & Duperron, S. 2012 Reproductive Traits of the Cold-Seep Symbiotic Mussel Idas modiolaeformis: Gametogenesis and Larval Biology. *Biol. Bull,* **222**, 6-16. (doi:10.1086/bblv222n1p6).
[151] Raven, C.P. 1958 *Morphogenesis: the analysis of molluscan development*. New York, Pergamon Press.
[152] Trask, J.L. & Van Dover, C.L. 1999 Site-specific and ontogenetic variations in nutrition of mussels (*Bathymodiolus* sp.) from the Lucky Strike hydrothermal vent field, Mid-Atlantic Ridge. *Limnology Oceanography* **44**, 334-343. (doi:10.4319/lo.1999.44.2.0334).
[153] Alain, K. & Querellou, J. 2009 Cultivating the uncultured: limits, advances and future challenges. *Extremophiles* **13**, 583-594. (doi:10.1007/s00792-009-0261-3).
[154] Koch, E.J. & McFall-Ngai, M. 2018 Model systems for the study of how symbiotic associations between animals and extracellular bacterial partners are established and maintained. *Drug Discovery Today: Disease Models* **28**, 3-12. (doi:10.1016/j.ddmod.2019.08.005).
[155] Alfred, J. & Baldwin, I.T. 2015 New opportunities at the wild frontier. *eLife* **4**, e06956. (doi:10.7554/eLife.06956).
[156] Siegl, A., Kamke, J., Hochmuth, T., Piel, J., Richter, M., Liang, C., Dandekar, T. & Hentschel, U. 2011 Single-cell genomics reveals the lifestyle of Poribacteria, a candidate phylum symbiotically associated with marine sponges. *ISME J* **5**, 61-70. (doi:10.1038/ismej.2010.95).
[157] Woyke, T., Teeling, H., Ivanova, N.N., Huntemann, M., Richter, M., Gloeckner, F.O., Boffelli, D., Anderson, I.J., Barry, K.W., Shapiro, H.J., et al. 2006 Symbiosis insights through metagenomic analysis of a microbial consortium. *Nature* **443**, 950-955. (doi:10.1038/nature05192).
[158] Geier, B., Sogin, E.M., Michellod, D., Janda, M., Kompauer, M., Spengler, B., Dubilier, N. & Liebeke, M. 2020 Spatial metabolomics of in situ host–microbe interactions at the micrometre scale. *Nat. Microbiol*. (doi:10.1038/s41564-019-0664-6).
[159] Geier, B., Franke, M., Ruthensteiner, B., González Porras, M., Gruhl, A., Wörmer, L., Moosmann, J., Hammel, J.U., Dubilier, N., Leisch, N., et al. 2019 Correlative 3D anatomy and spatial chemistry in animal-microbe symbioses: developing sample preparation for phase-contrast synchrotron radiation based micro-computed tomography and mass spectrometry imaging. In *SPIE Optical Engineering + Applications* (eds. B. Müller & G. Wang), SPIE.
[160] Montanaro, J., Gruber, D. & Leisch, N. 2016 Improved ultrastructure of marine invertebrates using non-toxic buffers. *PeerJ* **4**, e1860. (doi:10.7717/peerj.1860).
[161] Sigal, Y.M., Zhou, R. & Zhuang, X. 2018 Visualizing and discovering cellular structures with super-resolution microscopy. *Science* **361**, 880-887. (doi:10.1126/science.aau1044).
[162] Wu, Y. & Shroff, H. 2018 Faster, sharper, and deeper: structured illumination microscopy for biological imaging. *Nat. Methods* **15**, 1011-1019. (doi:10.1038/s41592-018-0211-z).

[163] Lambert, B.S., Raina, J.-B., Fernandez, V.I., Rinke, C., Siboni, N., Rubino, F., Hugenholtz, P., Tyson, G.W., Seymour, J.R. & Stocker, R. 2017 A microfluidics-based in situ chemotaxis assay to study the behaviour of aquatic microbial communities. *Nat. Microbiol* **2**, 1344-1349. (doi:10.1038/s41564-017-0010-9).
[164] Stoecker, K., Dorninger, C., Daims, H. & Wagner, M. 2010 Double labeling of oligonucleotide probes for fluorescence in situ hybridization (DOPE-FISH) improves signal intensity and increases rRNA accessibility. *Appl. Environ. Microbiol.* **76**, 922-926. (doi:10.1128/AEM.02456-09).
[165] Thompson, A.W., Foster, R.A., Krupke, A., Carter, B.J., Musat, N., Vaulot, D., Kuypers, M.M. & Zehr, J.P. 2012 Unicellular Cyanobacterium Symbiotic with a Single-Celled Eukaryotic Alga. *Science* **337**, 1546-1550. (doi:10.1126/science.1222700).
[166] Perkel, J.M. 2019 The microscope makers putting ever-larger biological samples under the spotlight. *Nature* **575**, 715-718.
[167] Geier, B., Oetjen, J., Ruthensteiner, B., Polikarpov, M., Gruber-Vodicka, H.R. & Liebeke, M. 2021 Connecting structure and function from organisms to molecules in small-animal symbioses through chemo-histo-tomography. *Proceedings of the National Academy of Sciences* **118**, e2023773118. (doi:10.1073/pnas.2023773118).
[168] Chaston, J. & Douglas, A.E. 2012 Making the most of "omics" for symbiosis research. *The Biological bulletin* **223**, 21-29. (doi:10.1086/BBLv223n1p21).
[169] Loussert-Fonta, C., Toullec, G., Paraecattil, A., Jeangros, Q., Krueger, T., Escrig, S. & Meibom, A. 2020 Correlation of fluorescence microscopy, electron microscopy, and NanoSIMS stable isotope imaging on a single tissue section. *Communications Biology* **3**, 362. (doi:10.1038/s42003-020-1095-x).
[170] Airs, P.M., Vaccaro, K., Gallo, K.J., Dinguirard, N., Heimark, Z.W., Wheeler, N.J., He, J., Weiss, K.R., Schroeder, N.E., Huisken, J., et al. 2021 Spatial transcriptomics reveals antiparasitic targets associated with essential behaviors in the human parasite *Brugia malayi*. *bioRxiv*, 2021.2008.2024.456436. (doi:10.1101/2021.08.24.456436).
[171] Jiang, H., Kilburn, M.R., Decelle, J. & Musat, N. 2016 NanoSIMS chemical imaging combined with correlative microscopy for biological sample analysis. *Curr. Opin. Biotechnol.* **41**, 130-135. (doi:10.1016/j.copbio.2016.06.006).
[172] Vergara, H.M., Pape, C., Meechan, K.I., Zinchenko, V., Genoud, C., Wanner, A.A., Mutemi, K.N., Titze, B., Templin, R.M., Bertucci, P.Y., et al. 2021 Whole-body integration of gene expression and single-cell morphology. *Cell* **184**, 4819-4837.e4822. (doi:10.1016/j.cell.2021.07.017).
[173] Gage, D.J. 2004 Infection and Invasion of Roots by Symbiotic, Nitrogen-Fixing Rhizobia during Nodulation of Temperate Legumes. *Microbiol. Mol. Biol. Rev.* **68**, 280-300. (doi:10.1128/mmbr.68.2.280-300.2004).
[174] Martins, I., Colaço, A., Dando, P.R., Martins, I., Desbruyères, D., Sarradin, P.-M., Marques, J.C. & Serrão-Santos, R. 2008 Size-dependent variations on the nutritional pathway of *Bathymodiolus azoricus* demonstrated by a C-flux model. *Ecol. Model.* **217**, 59-71. (doi:10.1016/j.ecolmodel.2008.05.008).

Chapter II

This manuscript is in preparation and has not been reviewed by all authors.

How to live with, on or in eukaryotic cells? The different forms of symbiont-host associations in bathymodioline mussels

Maximilian Franke[1,4], Julian Hennies[2], Nicole L. Schieber[2], Yannick Schwab[2,3], Nicole Dubilier[1,4*] and Nikolaus Leisch[1*]

[1] Max Planck Institute for Marine Microbiology, Celsiusstr. 1, 28359 Bremen, Germany

[2] Cell Biology and Biophysics Unit, European Molecular Biology Laboratory, Heidelberg, Germany.

[3] Electron Microscopy Core Facility, European Molecular Biology Laboratory, Heidelberg, Germany

[4] MARUM—Zentrum für Marine Umweltwissenschaften, University of Bremen, Leobener Str. 2, 28359 Bremen, Germany

*Corresponding authors

Nikolaus Leisch, e-mail: nleisch@mpi-bremen.de

Nicole Dubilier, e-mail: ndubilie@mpi-bremen.de

Max-Planck-Institute for Marine Microbiology

Celsiusstr.1, D-28359 Bremen, Germany

Phone: 0049 (0)421 2028

Fax: 0049 (0)421 2028 760

Keywords: symbiosis, cellular morphology, 3D, host microbe interactions, invertebrate, bivalve, ultrastructure, FIB-SEM

Abstract

Symbiotic associations between bacteria and eukaryotes have shaped the biodiversity we know today. Almost all multicellular eukaryotes are associated with bacteria, and in the course of evolution, have formed a variety of associations with bacteria that fundamentally differ in morphology. Evolutionarily, a general trend from extra- to intracellular association is assumed in many symbiotic systems, including bathymodioline mussels. These deep-sea mussels live worldwide at hydrothermal vents, cold seeps and organic falls in a symbiosis with chemosynthetic bacteria that supply the bivalves with carbon. In this study, we used three-dimensional, sub-organelle resolution imaging analysis - focused ion beam scanning electron microscopy - to resolve the ultrastructure of the symbiotic organ at the subcellular level. Our state-of-the-art 3D analyses allowed us to demonstrate that mussels of the *Bathymodiolus* and *Gigantidas* clade do not harbor intracellular endosymbionts as assumed for decades, but predominantly extracellular endosymbionts housed in a complex membrane invagination connected to the outside via a complex channel system. For the first time, we compared ultrastructure-based cell morphology across bathymodioline species and symbiont types revealing unique cellular phenotypes in terms of association. Our key finding shows that once a SOX symbiont is present the complex channel system is open to the outside or the symbionts fully attach to the outside. Conversely, the bacteria-carrying vacuoles of mussels that only harbor MOX symbionts are closed from the surrounding fluids yet connected via a channel system. Our findings give rise to the question of the molecular machinery associated with these complex cytological features and the link between these physiological adaptations and the evolutionary history of the bathymodioline symbiosis itself.

Introduction

The way bacteria associate on, with, or in eukaryotes is of fundamental interest to understand their pathogenic and mutualistic associations. One hypothesis in evolution is that most symbiotic associations have transitioned from an extracellular to an intracellular association [1]. This gradient from extra to intracellular host-microbe associations has given rise to the diversity of interactions ranging from extracellular symbioses to intracellular associations and even organelles [2, 3]. Over the course of evolution, this means that both partners become extremely adapted to each other in terms of genome streamlining to achieve metabolic streamlining and anatomic integration of the symbionts [4]. For example the intracellular symbiont *Buchnera aphidicola* from the aphid *Baizongia pistacea* has drastically reduced its genome to a size of 618kb [5, 6]. The synchronous diversification of *Buchnera* and its host nicely illustrates how metabolically and functionally dependent both partners have become on each other after forming a mutualistic symbiosis ~ 200 million years ago [5, 7]. The eukaryotic domain would not be so diverse today, if some of these very specific associations between bacteria and eukaryotes had not evolved. Today, symbiotic associations are found in almost all multicellular eukaryotes and the associations can vary from ectosymbionts, such as the symbionts of nematodes of the family desmodoridae [8, 9], to endosymbionts, such as the symbionts of *Vesicomyidae* clams [10] or the *Buchnera* symbionts from aphids [7]. While ectosymbionts are associated extracellular on the surface of the host endosymbionts are mostly associated intracellular in vacuoles or in the host's cytoplasm.

Many mutualistic symbioses have evolved evolutionary-stable intermediate symbiont-host associations. For example the endosymbionts of the gutless Nematode *Astomonema southwardorum* [11] are located extracellularly but inside the host in a

closed lumen and the endosymbionts of the gutless phallodriline annelids are located below the cuticle and above the epidermal cells [12]. In some symbiotic systems like the olive fly *Bactrocera aleae* the symbionts (*Ca.* Erwinia dacicola) transition between an extracellular and intracellular lifestyle throughout host development [13]. Morphologically, symbiont-host associations are very diverse [1] and rely on different molecular processes allowing the microorganisms to colonize and persist within the animals' tissues. The molecular machinery behind these processes involves recognition, attachment, uptake of the bacteria, as well as tissue rearrangements in the host that are highly regulated and depend on a tight communication between bacteria and eukaryotes [14, 15]. Today most of these processes are only well-understood for a hand full of model organisms like the squid vibrio symbiosis [15], insects like aphids hosting *Buchnera* symbionts [7], or in pathogens such as *Salmonella* [16]. For the majority of host-microbe systems and in particular non-model symbioses these mechanisms have remained unresolved.

One prime example of a non-model system are bathymodioline mussels. These mussels inhabit hydrothermal vents, cold seeps, and organic falls in the deep sea across the world. To survive in deep-sea environments lacking phototrophic primary production these mussels have depend on a nutritional symbiosis with chemosynthetic bacteria. The symbionts use the reduced compounds in the vent and seep fluids to fix carbon [17, 18]. Different mussel species harbor different set of symbionts, which mainly are a sulfur-oxidizing (SOX) symbiont, a methane-oxidizing (MOX) symbiont or both [19-21]. Depending on the species, the symbionts are either located intracellularly in gill epithelial cells called bacteriocytes [22] or extracellular on the cell membrane of these gill cells [23]. The bacteriocytes have lost their microvilli and developed a hypertrophic habitus [24]. To gain most of their nutrition the mussels

perform an intracellular lysosomal digestion of the symbionts [22, 25-28]. The symbionts are transmitted horizontally from the environment to each new generation, which means they have to be able to enter and potentially exit the host cell environment [24, 29, 30].

In the past it was suggested that the location of the symbionts is habitat-dependent. Mussels living near hydrothermal vents and seeps harbor intracellular symbionts in vacuoles [22, 24, 25, 30-34], while mussels thriving at organic falls have extracellular symbionts sitting on the apical membrane of their gill epithelia [23, 35-37]. Furthermore, the intracellular symbiont-host association has been described independently of the symbiont type, for bathymodioline mussels harboring either only SOX / MOX symbionts or both symbiont types [22, 24, 25, 30-34]. However the evolutionary stability and level of cellular integration of these mussels has never been assessed in the light of cell-cell organization.

Despite first evidence for an intermediate form of symbiont-host association in bathymodioline mussels [22, 30, 38, 39] it is unclear how mussel hosts and their symbionts associate on a cellular level across species. In bathymodioline mussels that host intracellular symbionts it was described that some bacterial vacuoles were open to the outside. Those observations were never elucidated further. For a single species it was recently shown that the SOX symbionts of *B. septemdierum* have to be redefined as extracellular endosymbionts located in a network of vacuoles connected to each other and to the environment [40]. Whether this is a general form of symbiont-host association in bathymodioline mussels is impossible to deduce from this proof-of-principle study.

In this study, we for the first time compared the symbiont-host association in eight bathymodioline species (Table 1) from hydrothermal vents and cold seeps across the Atlantic and Pacific Ocean. We used a three dimensional (3D) ultrastructural imaging approach to investigate the symbiont-host association in *B. puteoserpentis* at so far unprecedented resolutions. To resolve even the minutest 3D changes in membrane morphology, we used focused ion beam milling combined with Scanning Electron Microscopy (FIB-SEM) to analyze whole gill cells. Once we identified and defined ultrastructural features with 3D imaging we used 2D transmission electron microscopy (TEM) to screen the seven other species for their type of association. This allowed us to extrapolate from the symbiont-host association of *B. puteoserpentis* to the seven other mussel species.

Methods

Sampling and fixation

All deep-sea mussels were collected with remotely operated vehicles from the sea floor. In total, eight deep-sea mussels species from the Mid-Atlantic-Ridge (*Bathymodiolus puteoserpentis* and *B. azoricus*), Gulf of Mexico (*B. brooksi, B. heckerae* and *Gigantidas childressi* originally described as *"B". childressi* [41]) and Pacific (*"B". manusensis*, G. gladius and *Vulcanidas insulatus*) were included into this study (Table 1). Upon recovery, specimens were fixed in 2.5% glutaraldehyde (GA) and stored in PHEM buffer (piperazine-N, N′-bis , 4-(2-hydroxyethyl)-1-piperazineethanesulfonic acid, ethylene glycol-bis(β-aminoethyl ether and $MgCl_2$; Montanaro *et al.* [42]) or Trump`s solution.

Table 1 Specimen information

species	sampling location	latitude	longitude	sampling depth (m)	sampling year	fixation	storage buffer	symbionts
B. puteoserpentis	Semenov -2	13.51 N	-44.96 W	2446.60	2016	2.5% GA	PHEM	SOX and MOX
B. azoricus	Montsegur	37.29	-32.28 W	1700	2013	2.5% GA	Trump's solution	SOX and MOX
B. brooksi	MC 853	28.12 N	-89.14 W	1073.00	2015	2.5% GA	PHEM	SOX and MOX
B. heckerae	Chapopote	21.89 N	-93.44 W	2925.00	2015	2.5% GA	PHEM	SOX and MOX
G. childressi	MC 853	28.12 N	-89.14 W	1071.00	2015	2.5% GA	PHEM	MOX
"B". manusensis	Haungaroa	-32.62 S	-179.62 W	673.40	2017	2.5% GA	PHEM	SOX
G. gladius	Macauley cone	-30.21 S	-178.45 W	291.14	2016	2.5% GA	PHEM	SOX
V. insulatus	Macauley cone	-30.21 S	-178.45 W	290.20	2016	2.5% GA	PHEM	SOX

Sample preparation for transmission electron microscopy and focused ion beam milling combined with scanning electron microscopy

For transmission electron microscopy (TEM) individual gill filaments were cut in pieces and high-pressure frozen with a Leica EM ICE (Leica Microsystem) in 3 mm Cu/Au sample holders. A quick freeze-substitution method was used to transfer the samples into acetone containing 1 – 2% osmium tetroxide (OsO_4) [43]. Samples were washed three times with 100% acetone after reaching room temperature.

For Focused Ion Beam milling combined with Scanning Electron Microscopy (FIB-SEM) analyses individual GA fixed gill filaments were washed two times for 5 min in their corresponding buffer sodium cacodylate buffer (CaCO; Sigma-Aldrich, USA) at room temperature. Of all available samples, *B. puteroserpentis* specimens were chosen for the 3D FIB-SEM microscopy as they were the best preserved. Afterwards samples were first stained with 1% OsO_4in buffer at 4°C followed by an incubation

with 0.8% potassium ferricyanide in buffer at 4°C for 2 h. After staining, the samples were washed three times with MilliQ. For a better contrast samples were additionally stained with a solution of 0.5% aqueous uranyl acetate (UA) for 30 min at 4°C and washed three times with MilliQ. Gill filaments were high-pressure frozen with a Leica EM ICE (Leica Microsystem) in 3 mm Cu/Au sample holders for a better sample preservation. A quick freeze-substitution method was used to transfer the samples into 2 ml acetone containing 1% $OsO_4$and 0.5% UA. Samples were brought to room temperature over a time period of 90 min. Before washing and embedding samples were rested at room temperature for 60 min.

For TEM and FIB-SEM, infiltration was done with a few modifications after McDonald [44]. Individual gill filaments were sequentially centrifuged for 30 s with a benchtop centrifuge (Heathrow Scientific) at 2,000x*g* in 2 ml tubes filled with 25%, 50%, 75% and 2 × 100% Agar Low Viscosity Resin (Agar Scientific) or Epoxy resin (Agar Scientific) for TEM or with Epon Hard plus resin 812 (Agar Scientific) for FIB-SEM. After the second infiltration with100% resin the samples were stored in 100% resin at room temperature overnight. The next day the samples were transferred into freshly prepared resin, embedded and polymerized at 60 °C for 24 to 48 h in embedding molds.

For TEM, embedded samples were sectioned with an Ultracut UC7 (Leica Microsystem) ultra-microtome. Ultrathin sections (70 nm) were mounted on formvar-coated slot grids (Agar Scientific), which were contrasted with 1 – 2% aqueous UA (Science Services) for 20 min and with 2% Reynold's lead citrate for 8 min.

For FIB-SEM the polymerized blocks were trimmed and polished with an Ultracut UC7 (Leica Microsystem) ultra-microtome. The sample was trimmed with a 90°

diamond knife (Diatome) to expose the sample at two surfaces (the imaging surface and the surface perpendicular to the focused ion beam, FIB) in order to optimize the acquisition [45]. After trimming, the sample was mounted onto the edge of an SEM stub (Agar Scientific) using silver conductive epoxy (CircuitWorks) with the trimmed surfaces facing up and towards the edge of the stub. Afterwards, the sample was gold sputter-coated (Quorum Q150RS; 180s at 30mA).

Ruthenium red staining for determining membrane porosity

Before the Ruthenium red (RR) staining procedure *B. puteoserpentis* gill filaments were washed three times for 10 min in 0.1M CaCO buffer. Samples were stained in 0.1M CaCO buffer containing 2% OsO_4 and 0.5% RR. The staining was performed under light protected conditions at 4°C with agitation for 3 h. The staining procedure was followed by three washing steps, each 10 min, in 0.1M CaCO buffer. After the samples were stained with RR and washed they were dehydrated and embedded as described above for the normal TEM samples. The only difference was that the prepared sections from this experiment were not counter-stained with UA and lead citrate, as the RR stain is otherwise hard to identify.

Microscopy

For TEM analyses ultra-thin sections were either imaged at 20–30 kV with a Quanta FEG 250 scanning electron microscope (FEI Company, USA) equipped with a STEM detector using the xT microscope control software (ver. 6.2.6.3123) or at 80 – 120 kV with a Jeol JEM-2100PLUS transmission electron microscope (Jeol, Japan) equipped with a Emsis XAROSA 20 megapixel CMOS-camera (EMSIS GmbH, Germany) using the Radius software (EMSIS GmbH, Germany).

The FIB-SEM acquisition was done with a Crossbeam 550 (Carl Zeiss Microscopy GmbH). Once the ROI was located in the sample, Atlas3D software (Fibics Inc. and Carl Zeiss Microscopy GmbH) was used to perform sample preparation and 3D acquisition. First a 1 µm platinum protective coat of (50 µm x 50 µm) was deposited with 3nA FIB current. The rough trench was then milled to expose the imaging cross-section with 15nA FIB current, followed by a polishing step at 7nA. The 3D acquisition milling was done with 1.5nA or 3nA FIB current. For SEM imaging the beam was operated at 1.5kV/700pA in analytic mode using the EsB detector (1.1kV collector voltage) at a dwell time from 9-11 µs with no line averaging. Datasets were acquired with 5 or 8 nm isotropic voxel size (Table 2).

Table 2 FIB-SEM data sets

species	sample	resolution	slices	imaged symbionts	acquisition area	3D reconstruction
B. puteoserpentis	M893	8 nm	660	SOX only	part of cell	no
B. puteoserpentis	M983	8 nm	3411	SOX only	large whole cell	no
B. puteoserpentis	M983	5 nm	2074	SOX only	apical part of cell	yes
B. puteoserpentis	M812	8 nm	2683	SOX and MOX	small whole cell	yes
B. puteoserpentis	M812	8 nm	4254	SOX and MOX	part of cell	no

Image processing and 3D visualization

Histograms of 2D-TEM images were adjusted using Fiji (ver. 2.1.0/1.53c) [46]. Figure panels were composed using Adobe Illustrator 2021 (Adobe Systems Software, Ireland Ltd.).

Prior to the 3D reconstructions, FIB-SEM datasets were aligned using the AMST alignment [47]. Additionally, a membrane prediction algorithm was applied to the aligned FIB-SEM datasets to ease image segmentation. Before inference, the raw

data was normalized to cover the full 8bit-depth range and scaled to 5 nm isotropic resolution. For the automated membrane prediction a modified convolutional neuronal network after [47] was used. The model was implemented in PyTorch [48] with a 3D U-Net architecture [49]. A tophat filter was applied to the membrane predictions prior to the distance transform which was performed after [50]. The result of the membrane prediction and the distance transform were averaged and used for further processing.

Prior to image segmentation the FIB-SEM datasets and averaged membrane predictions were split into multiple sub-stacks as they were too large to be handled as a whole. Semi-automated segmentation, which means a manually curated machine learning approach, was done based on the membrane predictions of the FIB-SEM datasets by using the graphcut-based watershed algorithm in MIB (ver. 2.702) [51]. For segmentation we first semi-automatically segmented the channel system and membrane invaginations, followed by the symbiont labels and other organelles. As a last label we generated the cytosol. The semi-automated segmentation was manually corrected in MIB and Amira 2020.2 (ThermoFisher Scientific). After all sub-stacks were segmented and labels were corrected they were stitched into one large dataset using Fiji.

3D surface reconstructions were performed in Amira 2020.2 (ThermoFisher Scientific). Individual labels were rendered into a 3D surface model using the following steps: *create surface*, *reduce faces*, *remesh surface* and *smooth surface*. The number of *Faces* were reduced down between values of 50,000 – 100,000 per label. Surfaces were remeshed and the percentage value in the ‘Desired Size’ port

was kept at 50%. All surface meshes were visualized with the *Direct Normals* shading mode under *Surface View*.

SOX symbionts analyses

We analyzed the SOX symbionts in regards of their volume and length distribution. To do so we used the SOX symbiont label from the high resolution data set (5 nm voxel size, Table 2), which we generated in Amira. In a first step we applied the *separate objects* function to separate all individual SOX symbionts. To remove all SOX symbionts which touched the image boundaries we used the *selective border kill* function. Afterwards we applied the *label analysis* function and selected *basic* under the *measurement* port to extract the volume and length information of each SOX symbiont. To analyze individual size fractions we applied the *sieve analysis* and the *analysis filter* function. The mean volume and length, the standard deviation, the maximum and the minimum were calculated in Excel.

COI Tree

Full length COI sequences were downloaded from NCBI as indicated by their accession numbers. For *G. gladius* and *V. insolatus*, a metagenomics assembly was loaded into Bandage [52], and using the inbuilt Blast function and previously deposited COI sequences as bait, the mitochondrial genome was interactively retrieved. The mitochondrial genome of the host was annotated with the MITOS2 [53] webserver and the full length COI sequence extracted. All sequences were aligned using MAFFT (v7.480) [54] with the LINSI mode and the tree was calculated using IQ-TREE (v2.1.4) [55] with ModelFinder [56] choosing TN+F+I+G4 as the most appropriate model and the Ultrafast Bootstrap Approximation UFBoot [57] (1000

bootstraps). The tree was annotated in iTOL [58] and the figure generated with Adobe Illustrator 2021 (Adobe Systems Software, Ireland Ltd.).

Results

To analyze the symbiont-host association of bathymodioline mussels we used 3D FIB-SEM to resolve whole cells of *B. puteoserpentis* gill tissue on a nanometer scale. Informed by this three dimensional dataset we investigated seven other bathymodioline species using 2D TEM. Mussels from eight different bathymodioline species originating from hydrothermal vents and cold seeps across the Atlantic and Pacific Ocean were included for this study (Table 1). Among the samples analyzed, we observed three types of symbiont-host associations: 1. an ectosymbiotic association of the SOX of *"B". manusensis* (Figure 1 and Figure S1), 2. an extracellular endosymbiont association of the SOX and MOX symbionts of *B. puteoserpentis, B. azoricus, B. brooksi, B. heckerae, G. gladius and V. insolatus* (Figure 1 and Figure S2 – S5), , and 3. an intracellular association of the MOX of *G. childressi* (Figure 1 and Figure S7). Furthermore, we observed intracellular lysosomal digestion of symbionts in all analyzed species (Figure 2, Figure S1, S2, S5 and S7 – S8), even in those bathymodioline species in which the symbionts were associated extracellularly.

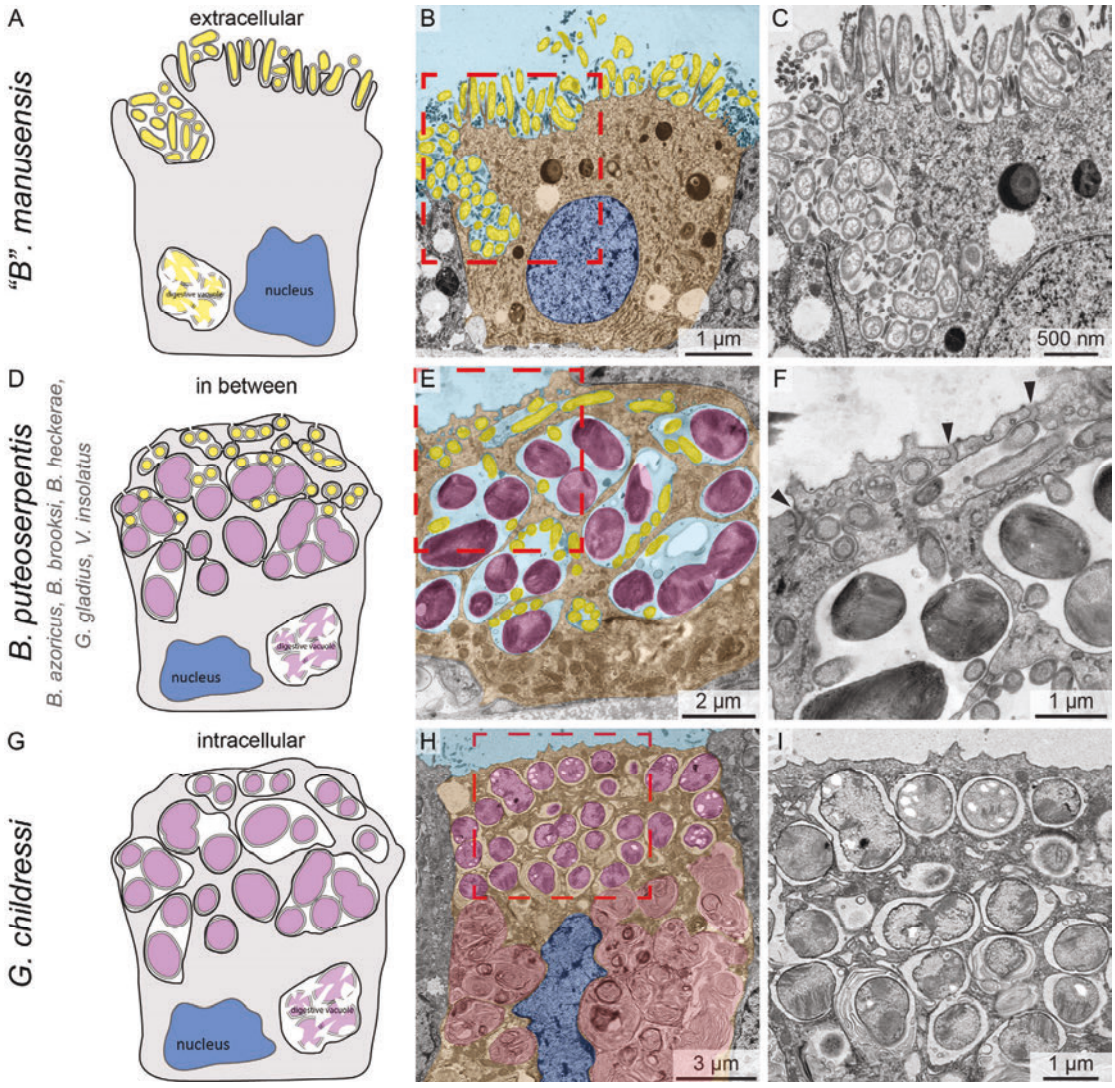

Figure 1 The three types of symbiont association in bathymodioline mussels. A) Schematic drawing of *"B". manusensis* gill epithelial cell. **B)** Overview image of a gill epithelial cell colonized by SOX ectosymbionts. **C)** Zoom in image of **B** showing SOX ectosymbionts. Some are located on the apical cell surface and others in a large membrane invagination. **D)** Schematic drawing of *B. puteoserpentis* gill epithelial cell. **E)** Overview image of a *B. puteoserpentis* gill epithelial cell, which is colonized by SOX and MOX symbionts. These symbionts are hosted in a channel system which is open to the outside. **F)** Zoom in image of **E** showing extracellular endosymbionts (SOX and MOX). **G)** Schematic drawing of *G. childressi* gill epithelial cell. **H)** Overview image of a *G. childressi* gill epithelial cell, which is colonized by intracellular MOX symbionts. **I)** Zoom in image of **H** showing intracellular MOX symbionts. light blue: outside, dark blue: nucleus, orange: cytosol, red: lysosomes, magenta: MOX and yellow: SOX.

Bathymodiolus puteoserpentis harbors extracellular endosymbionts

The 3D analyses of the *B. puteoserpentis* gill bacteriocytes revealed that the SOX and MOX symbionts in *B. puteoserpentis* are extracellular endosymbionts. We first checked the symbiont location and connectivity in a whole cell (Figure 2 A-C and Video S1). *B. puteoserpentis* mussels harbor their symbionts in one large, interconnected membrane invagination of the host apical cytoplasmic membrane open to the environment. This invagination of the host cytoplasmic membrane transitioned into larger compartments containing one to multiple symbiont cells and that we termed “bacterial compartments”. The analysis of the 3D datasets showed that SOX and MOX symbionts shared the same bacterial compartments. These bacterial compartments were connected to the extracellular space via a round tubular morphology which we termed “channels” here (Figure 2 B, C, and F – H, Video S1). The channels had a mean diameter of 120.9 nm (±33.75, n = 52), which makes them 2.5 times smaller than diameter of an average SOX symbiont (~ 303 nm, ±51.69, n = 21) and about 8.8 times smaller than the mean MOX symbiont diameter (~ 1063 nm, ±92.37, n = 20). The channels did not only connect the bacterial compartments to the extracellular medium but also connected all bacterial compartments with each other (Figure 2 E – H, Video S1). This means, all symbionts of one bacteriocyte were in one large, but highly compartmentalized membrane invagination. The channel system was most pronounced underneath the apical host membrane were one channel often displayed multiple branches (Figure 2 E) connecting multiple bacterial compartments with each other, or a single compartment via multiple channels to the outside.

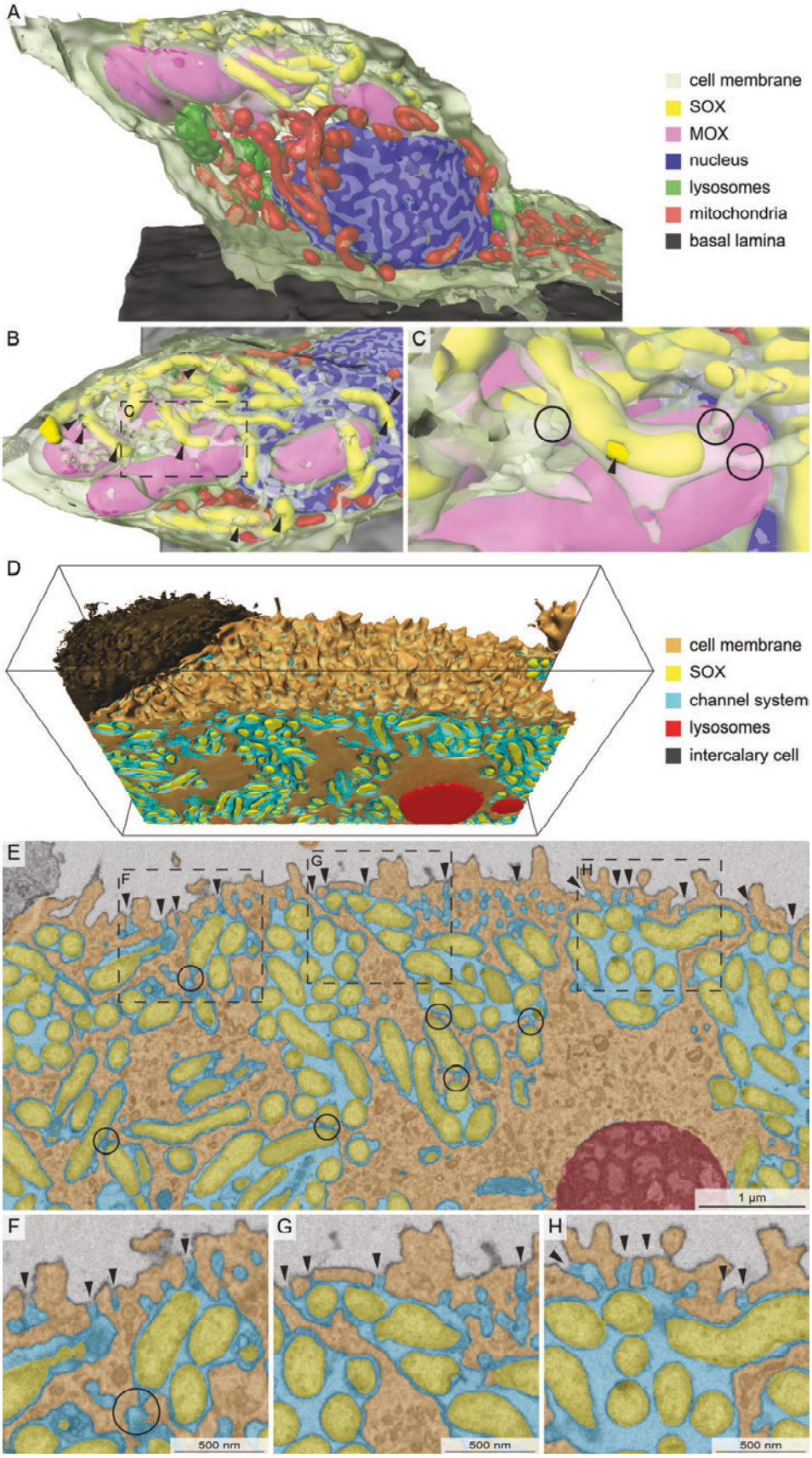
A
cell membrane
SOX
MOX
nucleus
lysosomes
mitochondria
basal lamina
B
C
D
cell membrane
SOX
channel system
lysosomes
intercalary cell
E
F
G
H
1 µm
F
G
H
500 nm
500 nm
500 nm

Figure 2 *B. puteoserpentis* symbionts are extracellular endosymbionts which are connected to the outside via a complex channel system. A) 3D segmentation of a FIB-SEM scan (8 nm voxel size) of a whole *B. puteoserpentis* bacteriocyte. The bacteriocyte harbored SOX and MOX symbionts. **B)** Top view of the segmented bacteriocyte shows the channels (indicated by black arrow heads). **C)** Zoom in of **B** shows the connections between bacterial compartments (black circle) and one channel which connects a SOX symbiont to the outside (black arrow head). **D)** The 3D segmentation of the high-res dataset (5nm voxel size) of the apical part of a *B. puteoserpentis* gill epithelial cell shows the channels in the host cell membrane. **E)** Overview image of the apical part of a *B. puteoserpentis* gill epithelial cell. The channel system (blue) is connected at several points (black circles) with each other so that all symbionts are connected to the outside (indicated by black arrow heads). **F-H)** Zoom-ins of the host cell membrane shows the openings to the outside (arrow heads).

To analyze the apical cell interface and the channel system in higher detail, we recorded a high resolution dataset (5 nm voxel size; Figure 2 D – H) and could identify 48 channels on a cell surface area of 4 μm^2. Extrapolating the frequency of channels per μm^2 onto the surface of an average bacteriocyte cell surface (~ 20 μm^2), we calculated that a single bacteriocyte of an adult *B. puteoserpentis* gill would have ~ 4800 channels. Interestingly, most channels connected to the apical surface, but we could trace a few that terminated to the side of the cells (Figure S9). In the close proximity of these laterally branching channels towards the neighboring cells, new channels started and entered from the adjacent cell. Here it is tempting to speculate if these lateral channels are connecting the symbiont population of the neighboring cells and if this allows for nutrient as well as symbiont exchange between the two host cells.

With the high-res dataset we could also calculate the apical cell surface enlargement that resulted from the membrane invagination and the channel system. We used the segmented cell surface from a *B. puteoserpentis* gill cell (high resolution data set) and virtually removed all channels (Figure S10 A). This modified cell surface reflects the cell surface of a bacteriocyte that harbors intracellular endosymbionts that are not connected to the extracellular space. By comparing this modified cell surface (Figure S10 A) with the segmented cell surface (Figure S10 B), we could identify a cell surface enlargement of 3.5 times.

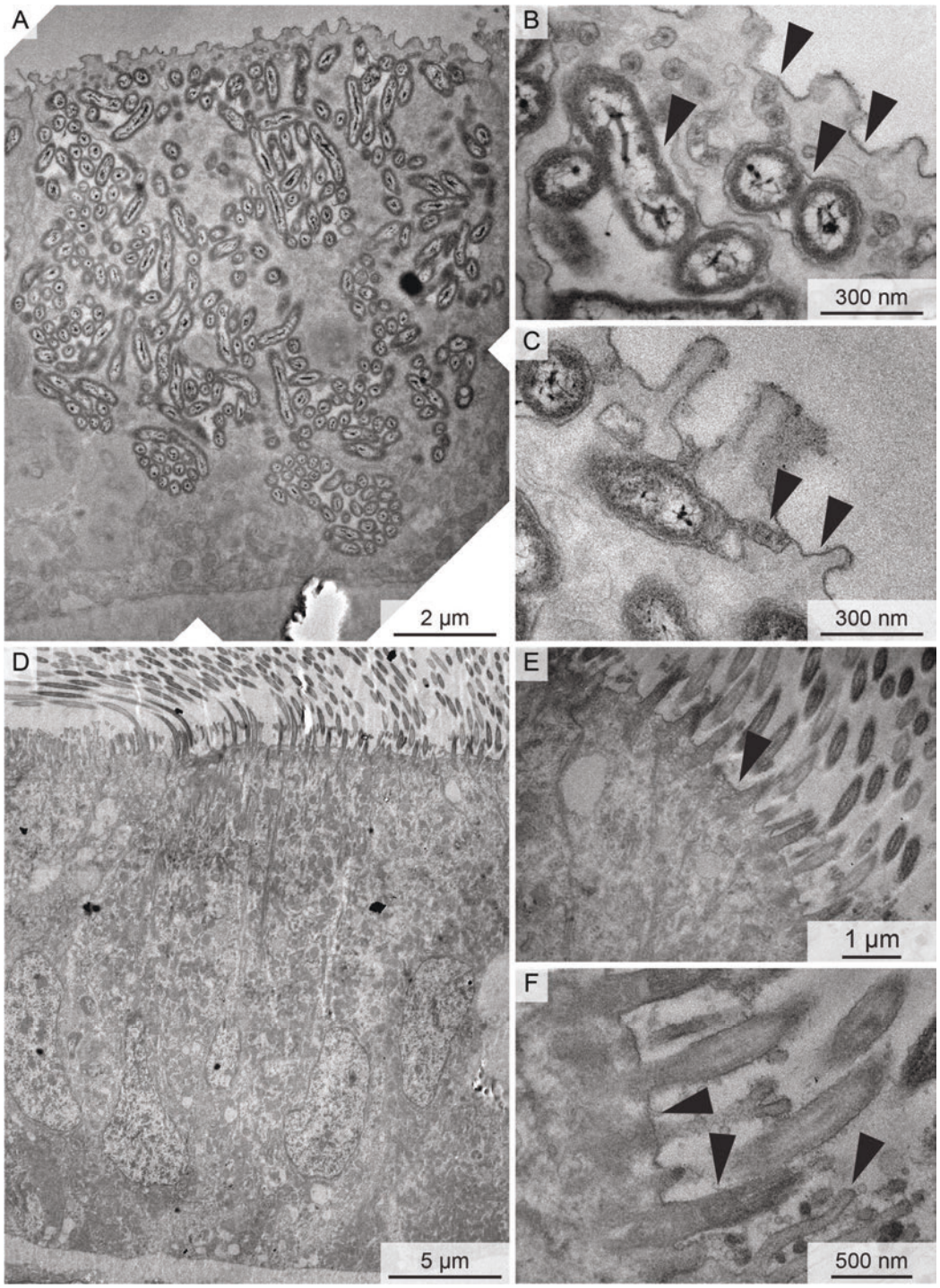

Figure 3 The channel system is open to the outside revealed by ruthenium red staining based electron microscopy. A) Overview image of *B. puteoserpentis* gill epithelial cell showing that the apical cell membrane as well as the symbionts and channel system is stained by ruthenium red. **B-C)** Black arrow heads indicate the ruthenium red stain on the symbionts, in the channel system and on the apical cell membrane. **D)** Overview image of *B. puteoserpentis* ciliated edge cell shows that only the apical cell membrane, the cilia and the microvilli are stained by ruthenium red, while no stain penetrates into the cytoplasm. **E-F)** Black arrow heads indicate the ruthenium red stain on the apical cell membrane and microvilli. Results of the ruthenium red negative controls can be found in the Figure S11.

As the high-res dataset does not reflect a whole cell but only the apical part, the cell surface enlargement of a whole cell is much larger. Based on an average cell size of ~ 4000 µm³ we estimated that the cell surface of an average *B. puteoserpentis* gill bacteriocyte would be at least 6.5 times larger compared to a gill cell harboring intracellular endosymbionts.

The ruthenium red staining revealed that the bacterial compartments are connected to the outside medium via the channel system in *B. puteoserpentis* gill epithelia and closed towards the cell's cytosol (Figure 3 A-C). Ruthenium red is a highly charged stain unable to penetrate through fixed cell membranes. It accumulates at the cell membranes and results in an electron dense signal. In *B. puteoserpentis* bacteriocytes the ruthenium red stain accumulated not only on the apical host cell membrane but also inside of the bacterial compartments surrounding the bacteria and on the bacterial outer membrane (Figure 3 A-C). Serving as an internal control, neighboring non-symbiotic cells, which did not show comparable membrane invaginations, only showed a ruthenium red staining on the apical cell membrane, microvilli and cilia (Figure 3 D-F). The ruthenium red stain indicates that the bacterial compartments are open to the outside via the channel system in *B. puteoserpentis.*

B. puteoserpentis **gills harbor bacteriocytes that are only colonized by SOX symbionts**

The bathymodioline SOX symbionts itself contains extreme fine-scale genetic heterogeneity [59] and we thus wanted to see if we could use morphometric measurements of the symbiont population to deduce aspects of the bacterial physiology, such as cell division rates. To analyze the SOX symbionts in more detail we extracted the SOX symbiont segmentation from the high-res dataset (Figure 4 A).

B. puteoserpentis mussels harbor SOX and MOX symbionts in their gill epithelial cells. So far it has been described that in cells, which host both symbiont types, a clear symbiont stratification can be observed [19]. The SOX symbionts were reported to reside closer to the apical cell membrane, whereas the MOX symbionts closer to the basal part of the cell [19]. We observed a similar symbiont stratification in *B. puteoserpentis* bacteriocytes (Figure 1 D – F).

While most *B. puteoserpentis* bacteriocytes harbored both symbiont types, we identified bacteriocytes that only harbored SOX symbionts. These cells were less abundant compared to host cells harboring both symbiont types and showed the same host cell morphology, including hypertrophy and microvilli loss, compared to bacteriocytes colonized by both symbiont types. The SOX symbionts were located in a membrane invagination in individual bacterial compartments, which were all connected to the extracellular medium by the channel system. In these SOX only host cells no clear symbiont stratification regarding size or division state between individual SOX symbionts could be observed. In terms of size small and large cells were randomly distributed within bacterial compartments of the host cell (Figure 4 B). The average SOX cell length was 1.38 µm (±0.41, n = 414) and the average SOX cell volume was 1.26 μm^3 (±0.38, n = 414; Figure 4 C). In total 314 of the 414 analyzed SOX symbionts clustered within 1σ difference to the mean volume (Figure 3 C). Only 38 cells were significantly smaller and 62 significantly larger. Assuming that all significantly enlarged SOX symbionts are indicative of cell division would result in a ~15% fraction of dividing SOX.

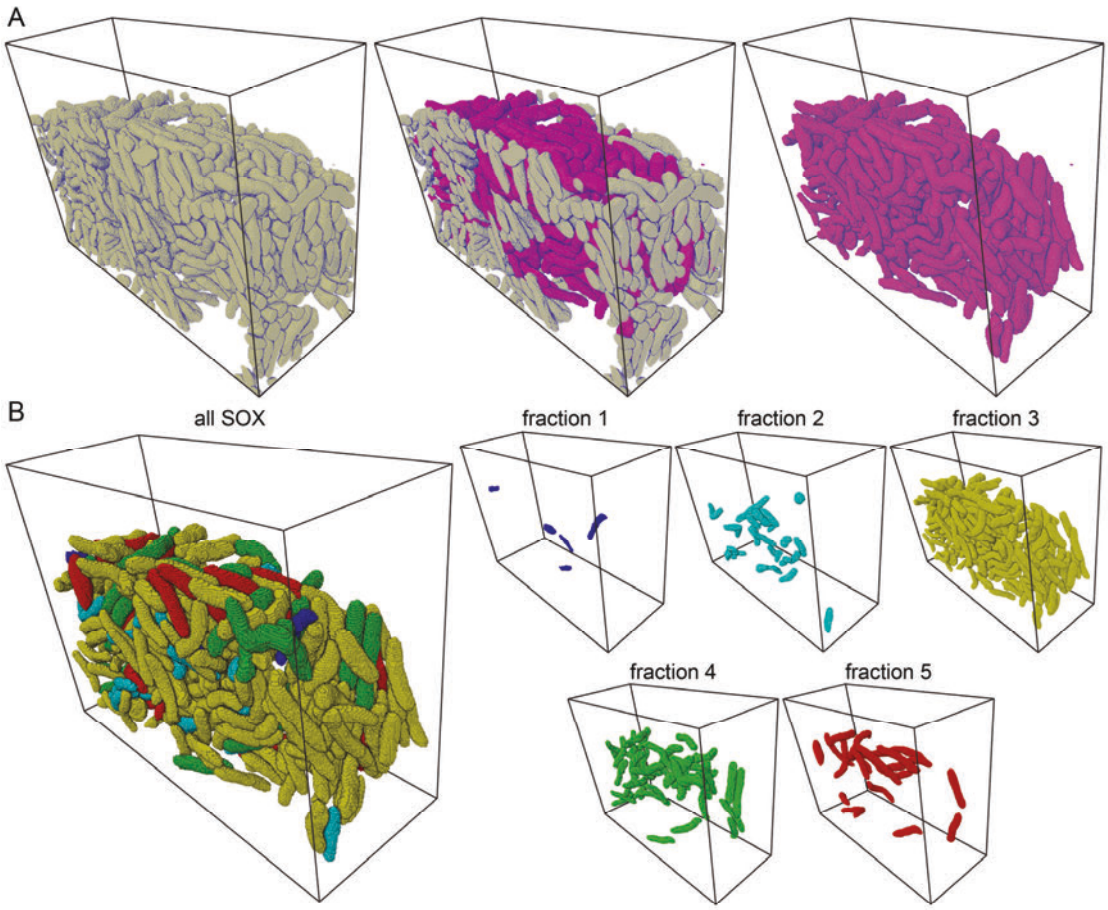

C

	all SOX	fraction 1	fraction 2	fraction 3	fraction 4	fraction 5
mean volume:	1.26 µm³ (± 0.38)	0.39 µm³ (± 0.08)	0.79 µm³ (± 0.09)	1.19 µm³ (± 0.19)	1.79 µm³ (± 0.09)	2.31 µm³ (± 0.37)
min volume:	0.25 µm³	0.24 µm³	0.58 µm³	0.89 µm³	1.65 µm³	2.02 µm³
max volume:	3.58 µm³	0.48 µm³	0.88 µm³	1.62 µm³	1.98 µm³	3.58 µm³
mean length:	1.38 µm (± 0.41)	0.43 µm (± 0.09)	0.86 µm (± 0.10)	1.30 µm (± 0.21)	1.95 µm (± 0.09)	2.51 µm (± 0.40)
min length:	0.27 µm	0.27 µm	0.63 µm	0.96 µm	1.79 µm	2.20 µm
max length:	3.89 µm	0.53 µm	0.96 µm	1.76 µm	2.15 µm	3.89 µm
no. of SOX:	414	6	32	314	44	18

Figure 4 Different size fractions of *B. puteoserpentis* SOX symbionts are distributed equally throughout the gill epithelial cell. A) To only analyze whole SOX symbionts we identified those cells (magenta) that were not touching the image boundaries and discarded all other SOX (grey) cells from the analysis. The black bounding box indicates the dimensions of the original image stack. **B)** All magenta SOX symbionts of **A** were grouped regarding their volume into five size fractions. The individual size fractions are displayed in a bounding box showing the distribution of the individual SOX symbionts within the 3D data. The individual size fractions are displayed next to the overview image. **C)** The statistical analysis of all size fractions indicates that most SOX symbionts cluster in fraction 3 which clusters around the overall mean of all SOX symbionts.

B. puteoserpentis symbionts were intracellular digested although they are associated extracellular

We observed intracellular lysosomal digestion of symbionts (Figure 2 C) in *B. puteoserpentis* gill epithelial cells. The morphology of these lysosomes was different in host cells harboring SOX and MOX symbionts compared to host cell harboring only SOX symbionts. While the lysosomes in cells that harbored SOX and MOX symbionts had a round morphology and densely membranous structures inside (Figure S8), the lysosomes of bacteriocytes harboring only SOX symbionts were homogenous and electron dense (Figure S8). Due to the difference in lysosome morphology, symbiont content can easily be predicted using a 2D TEM approach once lysosomes are identified. That *B. puteoserpentis* mussels digest their symbionts intracellularly is in agreement with the existing literature [24, 60]. However, this was under the assumption that all symbionts are housed intracellularly and raises the question of how this digestion is regulated when the symbionts are housed extracellular.

Different bathymodioline species show different symbiont-host associations

Informed by the 3D-analyses of *B. puteoserpentis* gill epithelial cells we were able to identify characteristics which we then used to screen 2D TEM data of several other bathymodioline species such as: membrane openings, circular membrane structures underneath the apical cell membrane, and connections between bacterial compartments.

In five of the seven analyzed species (*B. azoricus, B. brooksi, B. heckerae, G. gladius* and *V. insolatus*) a similar symbiont-host association as in *B. puteoserpentis*

could be observed (Figure S2 – S6). The symbionts were not intracellular but in membrane invaginations which had openings to the outside. The morphology of the membrane invaginations and the channel system was very similar to the observed structures from *B. puteoserpentis*. The only differences we could observe, between the different species, was the amount of channels between the apical cell membrane and the bacterial compartments. As the channels were randomly distributed over the apical cell surface we could estimate the amount of channels on a 2D level. We compared the amount of channels across multiple TEM sections of five different host cells and counted channels in an area of 5 μm^2. In *B. puteoserpentis* (n = ~ 20), *B. brooksi* (n = ~ 16), and *B. heckerae* (n = ~ 23) similar amounts of channels were visible, while in *G. gladius* (n = ~ 9) and *V. insolatus* (n = ~ 7) the channels were less abundant and shorter (Figure 2, Figure S2 – S6).

***"B". manusensis* has ectosymbionts**

We observed that *"B". manusensis* mussels had a different symbiont-host association compared to *B. puteoserpentis.* The majority of the SOX symbionts of *"B". manusensis* were located extracellularly on the apical cell membrane (Figure 1 and Figure S1). Less SOX symbionts were located within large membrane invaginations and seemed as if in some locations the apical cell membrane extruded to enlarge the surface (Figure S1). The morphology of these invaginations was different from the membrane invagination of *B. puteoserpentis*. The membrane invaginations of *"B". manusensis* were larger and the opening of these invaginations was not comparable to the channel system of *B. puteoserpentis*. The entire apical region of the invagination was open to the outer medium and not closed and only opened by a channel system as in *B. puteoserpentis* (Figure 1 and Figure S1 A – C). Independent of the location of the SOX bacteria, one pole of the rod shaped bacteria was touching

the host cell membrane (Figure 1 and Figure S1 F). In a few cases we observed that the SOX symbionts appeared to be connected to the host cell membrane with a tubular extension of their outer membrane (Figure S1 F – I, indicated by the red arrow). In *"B". manusensis* gill epithelial cells we could observe intracellular lysosomal digestion of symbionts (Figure S1 A, B and D). As described for *B. puteoserpentis* these lysosomes had the typical SOX only morphology. They had a roundish morphology, were homogenous and very electron dense. These findings suggest that the SOX symbionts of *"B". manusensis* are ectosymbionts, which are hosted on the apical cell membrane of *"B". manusensis* gill cells and only get internalized for the intracellular lysosomal symbiont digestion.

***G. childressi* has intracellular endosymbionts**

Additionally, to the ectosymbionts and the extracellular endosymbionts we observed a third type of symbiont-host association in bathymodioline mussels that only host MOX symbionts. The MOX symbionts of *G. childressi* were found in intracellular vacuoles within the cytosol of gill epithelial cells (Figure 1 and Figure S7). This morphology was already described in multiple studies [21, 42, 61]. We observed intracellular digestion of symbionts in form of lysosomes, which were located at the basal side of the host cell. These lysosomes had a similar morphology as the lysosomes of *B. puteoserpentis* gill bacteriocytes that harbored SOX and MOX symbionts (Figure S7 A and S8). We concluded that the MOX symbionts of *G. childressi* were intracellular endosymbionts, which were completely engulfed in a vacuole within the mussel's cytoplasm.

Mussels that host MOX symbionts harbor them intracellularly

Next to analyzing different bathymodioline species via FIB-SEM and TEM we also did a literature research to investigate the diversity of symbiont-host associations in bathymodioline mussels. The results of this research are based on visual identification of characteristics such as ectosymbionts, intracellular endosymbionts, a channel system, and membrane invaginations from published TEM data. We have identified the channel system with its characteristics, which we already observed in *B. puteoserpentis,* also in *B. brevior, B. septemdierum* and *B. thermophilus* (Table 3). These bathymodiolin mussels only host SOX symbionts. So far the symbiont-host association was described as intracellular endosymbionts in these species. But based on the published TEM data and the knowledge we gained from analyzing multiple bathymodioline species we speculate that these three species host their symbionts also extracellularly in membrane invaginations which are open to the outside via a channel system. From the literature research we also noticed that all mussel species which host either exclusively SOX or MOX and SOX symbionts harbor their symbionts extracellularly. Only bathymodioline mussels that host MOX symbionts harbor their symbionts intracellularly in vacuoles (Table 3 and Figure 5).

Table 3 Bathymodioline species included into the literature research

species	symbiont-host association	symbiont type	literature
G. cypta	ectosymbionts / intracellular endosymbionts	SOX	[62, 63]
G. japonicus	intracellular endosymbionts	MOX	[40, 64]
G. platifrons	intracellular endosymbionts	MOX	[64, 65]
A. longissima	ectosymbionts	SOX	[66]
T. arcuatilis	ectosymbionts	SOX	[35]
T. pacifica	ectosymbionts	SOX	[62]
B. thermophilus	extracellular endosymbionts	SOX	[67, 68]
B. brevior	extracellular endosymbionts	SOX	[38, 39]
B. septemdierum	extracellular endosymbionts	SOX	[40, 64]
I. washingtonius	ectosymbionts	SOX	[35]
I. iwaotaki	ectosymbionts	SOX	[23]

The type of association is dependent on the associated symbiont

We analyzed the symbiont-host association in multiple bathymodioline mussels from hydrothermal vents and cold seeps and compared it to the habitat these mussels lived in as well as the host phylogeny and associated symbiont type (Figure 5). The host phylogeny was calculated based on the full length COI sequence and clustered in 4 clades: the *Bathymodiolus* clade, the *"Bathymodiolus"* clade (recently also named as *Nipponiomodiolus* [69]), the *Gigantidas* clade and the *Vulcanidas* clade. Both habitat and host phylogeny showed no clear trend in the type of symbiont-host association. Only the symbiont type was a good indicator for the symbiont-host association (Figure 5 B). Whenever SOX symbionts were present, all symbionts were associated extracellularly, either as ectosymbionts (*"B". manusensis*) or as extracellular endosymbionts (*B. puteoserpentis, B. azoricus, B. brooksi, B. heckerae, G. gladius* and *V. insolatus*). Only mussels which hosted only MOX symbionts, like *G. childressi, G. japonicus,* and *G. platifrons*, had intracellular symbionts in vacuoles.

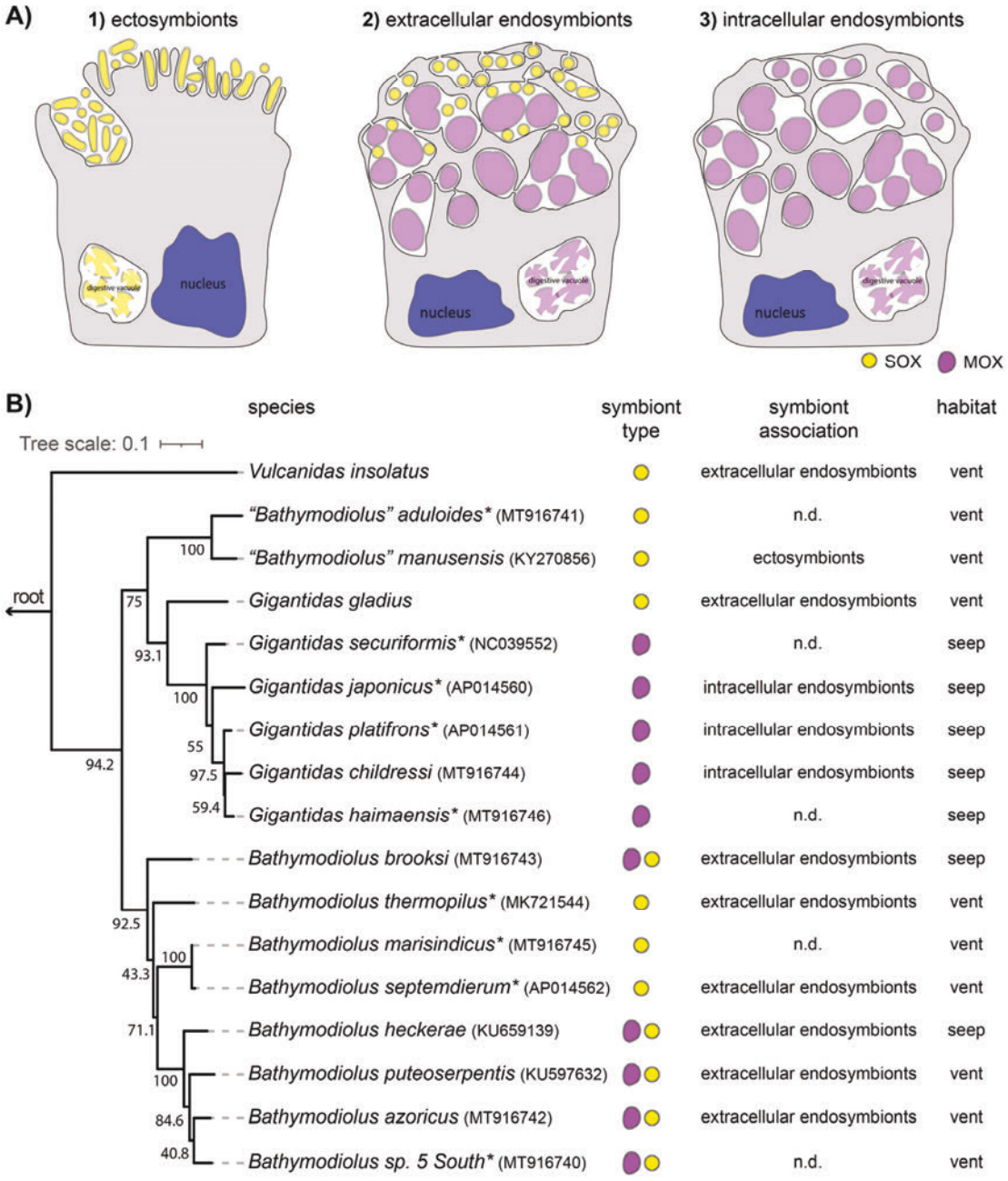

Figure 5 Symbiont-host association in bathymodioline mussels depends on the symbiont type.
A) Schematic drawings of the three forms of symbiont-host association we observed in bathymodioline mussels. SOX symbionts are illustrated in yellow and MOX symbionts in magenta. **B)** The phylogenetic tree is based on the full length COI sequence. As an outgroup *Modiolus modiolus* was used. The bootstrap values are indicated next to the branches of the host tree. **A**. Species indicated with an "*" were not analyzed during this study and information is based on literature data, which is summarized in table 3.

Discussion

Here, we reveal a so far hidden ultrastructural phenotypic heterogeneity across symbiont-host associations with drastic implications for the physiology of these global key-symbioses of deep-sea ecosystems. We show that the location of the symbionts in seven bathymodioline mussels is different to what has been previously described. So far all bathymodioline mussels living at hydrothermal vents and cold seeps were assumed to host intracellular endosymbionts [21, 22, 24, 25, 30-34]. We only observed this pattern in *G. childressi*, a mussel species hosting solely MOX symbionts. However, we could show that in six species the mussels host their symbionts extracellularly in membrane invaginations which are connected to the extracellular medium via a channel system (*B. puteoserpentis, B. azoricus, B. brooksi, B. heckerae, G. gladius,* and *V. insolatus*). In *"B". manusensis* the symbionts are located extracellular on the apical cell surface forming an ectosymbiotic association. To test whether we could detect a pattern in the symbiont-host association of bathymodioline mussels, we included published TEM results from additional bathymodioline species as well as the host phylogeny, symbiont composition, and the habitat of these mussels into our analysis. The habitat as well as the host phylogeny had no influence on the symbiont-host association. Only the symbiont phylotype, more specifically the presence of the SOX symbionts seemed to determine the location of the symbionts. As soon as a SOX symbiont was present all mutualistic symbionts were associated extracellular (Figure 5 B). Furthermore, we could show for the first time that a *"Bathymodiolus"* mussel from hydrothermal vents has ectosymbionts (*"B". manusensis*) and thereby shows the typical symbiont-host association of mussels living at organic falls like *Idas* species [23].

Evolutionary symbiotic systems evolve from ectosymbiotic associations over intracellular associations to organelles

In symbiosis research, the evolutionary trend from extra- to intracellular associations between host and symbionts is an important theory [1, 70]. However, the highest level of integration in terms of becoming an organelle is not reached in every system. Different intermediate forms of successful symbiont-host associations developed in mutualistic and pathogenic systems and have reached stability over evolutionary time. The symbionts can be located extracellularly on the outside of the host's body [8, 9], extracellular but in a closed lumen inside the host [12], they transition between extracellular and intracellular associations during the hosts development [13], or are associated intracellular in vacuoles [71]. The adaptations of both symbiotic partners are often not as drastic in horizontally transmitted symbiosis. For example the genomes of the symbionts are often not as reduced as compared to vertically transmitted symbionts [72], which could be because host and symbionts are less metabolically dependent on each other. For instance, horizontally transmitted symbioses allow apo-symbiotic stages of the host and free-living forms of the bacteria [24, 71].

In the past, first evidence was presented that intermediate forms between extra- and intracellular symbiont-host associations exist in deep-sea symbiotic systems. In the symbiotic bivalve *Maorithyas hadalis* of the family *Thyasiridae* and in the symbiotic snails *Ifremeria nautilei* and *Alviniconcha hessleri*, apically located bacterial vacuoles have been described to be open to the external medium [70, 73-75]. This morphology has been suggested to be an intermediate symbiont-host association between extracellular and intracellular symbiosis [70]. Such a morphology was also observed in some bathymodioline species, but it was never further investigated [22, 30, 38, 39].

Ikuta *et al.* [40] recently highlighted that the symbionts of *B. septemdierum* are all interconnected and the bacterial compartments are open to the outside. However, a broader assessment of the distribution of this symbiont-host association in bathymodioline mussels was missing. We could show that the symbionts of six bathymodioline species were associated extracellular in a complex membrane invagination and literature data points into the direction that this association form might be a general pattern in most bathymodioline species from hydrothermal vents and cold seeps hosting SOX symbionts.

The symbiont association in bathymodioline mussels does not follow the general accepted evolutionary trend from an extra- to an intracellular association

In a recent study an evolutionary model was presented explaining how different forms of symbiont-host associations in bathymodioline mussels evolved [62]. The authors followed the common assumption that bathymodioline mussels evolved from shallow water Mytilids and colonized the deep-sea by “wooden steps” [62, 76]. As chemosynthetic deep-sea mussels from wood falls have ectosymbionts, which is thought to be a primary form of symbiotic association [1], Fujiwara *et al.* [62] assumed that all further symbiont-host associations in chemosynthetic deep-sea mussels have evolved from these ectosymbiotic associations. According to their evolutionary model this resulted in extra- and intracellular associations at whale falls and intracellular endosymbionts in vent and seep mussels.

However, our morphological results on the symbiont-host association in bathymodioline mussels from vents and seeps indicates that the model presented by Fujiwara *et al.* [62] does not apply to all bathymodioline species. We demonstrated

that bathymodioline bivalves from hydrothermal vents and cold seeps are not only associated with intracellular endosymbionts, but also with extracellular endosymbionts and ectosymbionts. Fujiwara *et al.* [62] presented their model, assuming that bathymodioline mussels from hydrothermal vents and cold seeps only harbor intracellular endosymbionts. This reflects the significance of our data and the gap it closes in terms of understanding the cellular diversity of symbiotic associations across the same clade. Nevertheless, the basic idea of Fujiwara *et al.* [62] can still be applied to this system even under consideration of our data. We cannot exclude the hypothesis that bathymodioline mussels colonized the deep sea using organic falls as stepping stones to move into depth, comparable to the colonization patterns of hydrothermal vents along the Mid-Atlantic ridge [77].

Considering the physiology of the bathymodioline symbiosis integrating the symbiotic bacteria appears highly favorable. For instance, the bacteria are consistently flushed with hydrothermal vent fluids by residing in the filtrating respiratory organ of the host animal [17, 21, 78, 79]. Consequently, it is tempting to speculate that the cellular integration of symbiotic bacteria of bathymodioline mussels occurred along their colonization of hydrothermal vents and seeps, after organic falls enabled them to enter the deep sea. Furthermore, by colonizing vents and seeps that have more consistent and higher levels of reduced chemicals [80-82], which fuel chemosynthesis, a larger population of symbionts could be sustained by the host compared to the organic fall populations. However, hosting more symbionts requires a strategy of how to host them. One solution would be to host intracellular symbionts, a second strategy would be to enlarge the apical cell membrane in a way that more symbionts can be stored. Indeed we could show that some bathymodioline mussels hosted intracellular symbionts and some developed a complex system formed by

membrane invaginations shaping symbiont compartments and channels connecting them to the outside. The advantage of the extracellular endosymbiotic symbiont-host association is that the symbionts would have direct access to vent fluids and the host would benefit as the symbionts are not hosted intracellularly. Considering the physiological benefits of hosting more symbiotic bacteria while ensuring their access to the hydrothermal fluids, we hypothesize that the association type of 'extracellular endosymbionts' is favorable in terms of selective pressure for the symbiosis of bathymodioline mussels and might therefore be a general pattern across multiple species.

Symbiont type vs. host phylogeny – what defines the form of symbiont-host association in bathymodioline mussels?

We could show that the form of symbiont-host association does not correlate with the host phylogeny nor the habitat as recently assumed for bathymodioline mussels [62, 83]. The symbiont phylotype is the only factor influencing the localization of the symbionts. In the presence of SOX symbionts, all mutualistic symbionts were associated extracellularly. Only in mussels which hosted only MOX symbionts (*G. childressi*), the symbionts were found intracellularly in vacuoles. Our data support the hypotheses raised by Ikuta *et al.* [40], that mussels hosting only MOX have intracellular symbionts. It also raises the question of whether the SOX symbionts, that first colonize the host cell [84], can prevent other microorganisms from an intracellular colonization of the host cell. This for example has been shown for the probiotic strain *Lactobacillus salivarius* in the human intestine [85]. Furthermore, the MOX symbionts, between the different bathymodioline species with different symbiont-host associations, could be so fundamentally different that they are associated differently with the host tissue.

To answer the question why the SOX symbionts of bathymodioline mussels are associated extracellularly on the apical cell surface (*"B". manusensis, Idas* species) or enclosed in open membrane invaginations (*B. puteoserpentis, B. azoricus, B. brooksi, B. heckerea, V. insolatus* and *G. gladius*) one could compare them to other intracellular sulfur-oxidizing symbionts from other chemosynthetic systems, such as to the sulfur-oxidizing symbionts from lucinid clams [86] or to the sulfur-oxidizing symbionts from other deep-sea invertebrates such as vesicomyid clams and tubeworms [10, 71, 87-89]. A genomic as well as transcriptomic comparison between these different sulfur-oxidizing symbionts could reveal why some are associated intracellularly while others are extracellularly associated. Molecular mechanisms that could give rise to the observed symbiont-host associations could be linked to the recognition and acquisition mechanism of the symbiotic bacteria. However, it should be noted that not all chemosynthetic systems, such as vesicomyid clams and tubeworms, have been studied in such great detail that one can fully exclude the presence of similar cytological feature that can only be found in a 3D ultrastructural analysis. Therefore, the analysis genomic as well as transcriptomic of the different sulfur-oxidizing symbionts should be coupled with a 3D ultrastructural analysis, such as we have performed, to ensure that the genomic and transcriptomic data can be interpreted correctly.

Morphological adaptations of the host cell membrane shape the extracellular endosymbiotic association

Biology is a 3D phenomenon and therefore requires 3D imaging techniques to comprehensively study processes [90]. This also includes processes that happen on a cellular to sub-cellular level. On a cellular level the extracellular endosymbiotic association in bathymodioline mussels presents a unique morphology. A 3D

ultrastructural approach enables us to understand the complex system of membrane invaginations, symbiont compartments and the channel system. The morphology of the channel system was on a 2D level very similar to the morphology of membrane vacuoles and thereby the symbiont-host association was misinterpreted in previous studies, in the past. Only after characterizing these structures in 3D we were able to correctly interpret them also on a 2D TEM level.

Extracellular endosymbiotic associations lead to a cell surface enlargement and increase demand for lipid production in bathymodioline mussels

The membrane invaginations coupled with the channel system are a sophisticated system which is capable of hosting more symbionts compared to mussels that host ectosymbionts like *“B”. manusensis* (this study) and *Idas* species [36, 37, 91]. The apical cell surface area is increased by more than 3.5-fold and thus provides more space for symbionts. Such an enlargement of the apical cell membrane requires the production and formation of new cell membrane material. In a typical epithelial cell, the membrane needed for the phagocytotic uptake of particles or even bacterial cells originates from intracellular membranes, such as membranes from the endoplasmic reticulum, recycled endosomes, late endosomes and lysosomes [92, 93]. In the epithelial cells observed in bathymodioline mussels, the demand for membrane material is much higher and therefore the typically used pathways of membrane synthesis are most likely insufficient, unless the rate of lipid synthesis is increased. The access to the large amounts and constant nutrient supply in these environments enables a large symbiont population to thrive in the membrane invaginations of the gill cells. The energy gained through the intracellular digestion of these symbionts most likely fuels the eukaryotic membrane synthesis.

The eukaryotic membrane needs to be restructured

To generate such a complex cell membrane morphology the cytoplasmic membrane is not only enlarged but heavily restructured, which involves tight control of membrane curvature and the host's cytoskeleton. If the host or the symbionts mediate this morphological change of the cytoplasmic membrane is still unknown.

The host could remodel its membrane using BAR domain proteins

If the host regulates the formation of the membrane invagination proteins of the cytoskeleton must be involved. In eukaryotic cells multiple proteins can be involved in membrane curvature [94]. On a macroscopic scale these modifications are mediated by the cytoskeleton. The cytoskeleton imposes macroscopic shapes by providing an underlying scaffold which is connected to the cytoplasmic membrane in regular intervals [94]. Through membrane pulling or pushing, proteins like kinesin, dynein and myosin induce considerable changes in the membrane reorganization [95, 96].

One protein domain responsible for tubule formation in eukaryotic cells is the bin-amphiphysin-rvs (BAR) domain [97]. These proteins are involved in membrane shaping during cell trafficking and endocytotic processes, such as shaping the membrane during membrane fission at the end of the clathrin mediated endocytosis [98]. BAR domains self-assemble around the neck of the endocytotic vesicle and thereby shape the membrane into very stable tubules [97, 99, 100]. These invaginations that are formed by BAR domains have a similar form and diameter compared to the channels we observed in bathymodioline gill epithelial cells. Therefore, BAR domain proteins could be one of the structural proteins involved in bending the cytoplasmic membrane in bathymodioline mussels and thereby form the channel system.

To test whether BAR domains are involved in the formation of the channels in bathymodioline mussels, one could check the proteome and transcriptome whether these proteins are higher expressed compared to mussels that host there symbionts intracellularly. To test whether the channels co-localize with the channel system specific antibodies need to be generated. A combined cryo-fluorescence light microscopy with cryo-electron tomography, by using a cryo-FIB lift-out method [101], could visualize the distribution of the BAR domains but also resolve their atomic structure [102]. Thereby one could see if the BAR domains are involved in shaping the channel structure. A differential gene expression analysis between mussels hosting intracellular and mussels hosting extracellular endosymbionts could reveal further target proteins involved in the formation of the complex membrane structure.

Could the symbionts interfere with the host cytoskeleton to remodel the hots cell membrane?

Remodeling of the cytoplasmic membrane could also be induced by the symbionts. Pathogenic bacteria can directly interfere with the host cytoskeleton using specific uptake mechanisms. Most intracellular pathogens can be sorted into two groups based on their colonization strategy. Some use the "trigger" approach while others apply the "zipper" mechanism to colonize the host cells [103]. In brief, both mechanisms rely on the activation of a signaling cascade that leads to the reorganization of the actin cytoskeleton at the level of the host cytoplasmic membrane [103, 104]. In case of the “zipper” mechanism pathogens bind to proteins involved in cellular adhesion like cadherins or integrins, which then mediate a rearrangement of the cytoskeleton and eventually the uptake of the pathogens. In the case of bathymodioline mussels it was reported that the SOX symbionts, who colonize the host cell first [84], encode for a homologue of eukaryotic intergrins [105,

106]. Integrins are eukaryotic transmembrane receptors and are involved in processes like cell adhesion, migration and tissue organization [107]. They provide a direct transmembrane link from the environment to the host cytoskeleton, and thereby the eukaryotic cell can react to extracellular stimuli on the outside of the cell membrane [107]. Integrins are used by many pathogens as a receptor to directly interact with the host's cytoskeleton and thereby mediate cell-cell contact and uptake [108]. Previously, integrins were thought to be specific to eukaryotes, but there is growing evidence that they are also present in bacteria [109]. If the SOX symbionts of bathymodioline mussels encode for such functional integrin it would be a novel way for bacteria to directly interact with the host cytoskeleton without injecting effector proteins. Furthermore, it could explain why the SOX symbionts are always physically attached to the host cell membrane with at least one pole (Figure S1). To solve this question a correlative cryo-electron tomography and fluorescence antibody labeling workflow described above could be used to analyze the symbiont-host interface and resolve how the symbionts are physically connected to the host cell membrane. A detailed genomic and transcriptomic analyzes would support the visual dataset and show if the potential bacterial integrins are functional and expressed.

How does the intracellular digestion of extracellular symbionts work in bathymodioline mussels?

Regardless of the symbiont localization, the intracellular digestion of symbionts is a key process of the nutritional symbiosis between bathymodioline mussels and their symbionts [22, 27]. We observed intracellular digestion of symbionts in all analyzed bathymodioline species, even in mussels that harbored their symbionts extracellularly, e.g. *B. puteoserpentis* and *"B". manusensis*. In those mussels the digestion needs to be strictly controlled because the symbionts first must be

internalized, otherwise digestive enzymes would simply be diluted in the open lumen of the bacterial compartments likely to contain the surrounding sea water. One potential strategy to internalize the symbionts would be to pinch off a symbiont compartment by closing the channel system and thereby internalizing the symbionts in a vacuole. The uptake of the symbionts could also be mediated through endocytotic processes like phagocytosis or receptor mediated endocytosis.

Although the molecular uptake mechanisms might vary among the different bathymodioline species the intracellular digestion of the symbionts might have similar molecular mechanisms among the different species. The detailed molecular mechanisms of this digestion are still unknown, but lysosomal digestion of symbionts has been suggested for multiple bathymodioline species [22, 25-28]. In bacteriocytes of *G. childressi* a set of digestive enzymes and proteins involved in phagolysosomal digestion were higher expressed in wild type mussels compared to aposymbiotic mussels [110]. Similar results have been reported for *B. azoricus* mussels, here lysosomal proteases such as saposin B and cathepsin were higher expressed in the symbiotic gill compared to the aposymbiotic foot [111]. Recently transcriptomic evidence of a nutritional gain by *B. platifrons* through lysosomal digestion of symbionts was reported [28]. Furthermore, we observed lysosomes in all eight analyzed species. This indicates, as also previously suggested in the literature [25, 60, 112], that intracellular lysosomal symbiont digestion provides bathymodioline bivalves with their demanding energy. Besides the uptake of nutrition, the digestion of symbionts might also present a key-mechanism in symbiont control. Considering the fast turnover of the chemosynthetic environments and the high energy content, the mussel would need a mechanism to control the size of the symbiont population to be not overgrown by their own symbionts.

The escape – How bathymodioline symbionts avoid extinction

Bathymodioline mussels get first colonized by their symbionts during metamorphosis [84] and stay competent for symbiont acquisition throughout their lifespan [113]. There are two pools for symbiont uptake, free living symbionts from the environment or by self-infection of symbionts from neighboring host cells. Based on the results from Wentrup *et al.* [113] the second uptake hypothesis seems to be more likely. If symbiont-free host cells get colonized through self-infection, symbionts need to be able to leave colonized host cells. Furthermore, symbionts need to escape the mussel tissue once the host dies. The extracellular symbiont-host association could be advantageous in both scenarios because the symbionts are already in the extracellular medium and would not need to cross multiple membranes to escape the host cell, as seen in the symbionts of tubeworms [71, 114]. The intracellular symbionts of the tubeworms were shown to leave the host tissue within hours after the death of the animal host [114]. To leave the host cell, the symbionts would need to widen the channels connecting the bacterial compartments to the outside so that the symbionts would fit through. Therefore, the symbionts would most likely need to interfere with the host's cytoskeleton, more specifically with the proteins shaping the tubular structure. This open system could answer the long-standing question of how symbionts leave their host. Furthermore, it would also explain how new gill filaments are colonized. Once new gill filaments are formed they are aposymbiotic and after a certain growth period they are colonized by the symbionts [113]. Wentrup *et al.* [113] has shown that this most likely happens by self-infection of the own symbiont population. The extracellular association of the symbionts would ease this process. It would also allow symbionts to leave the animal host once it dies to prevent the bacterial population from extinction.

Summary and outlook

Our 3D ultrastructural image analyses revealed an unexpected symbiont-host association in six bathymodioline species. The symbionts were associated in a membrane invagination, which was connected to the outside by a channel system. Furthermore, we could show for the first time an ectosymbiotic symbiont-host association in bathymodioline mussels from hydrothermal vents (in *"B". manusensis*). Unlike other chemosynthetic symbiotic systems inhabiting similar environments and harboring similar symbiont phylotypes, bathymodioline symbioses have diverse symbiont-host associations. In tubeworms of the family *Siboglinidae* and clams of the family *Vesicomyidae* the sulfur-oxidizing symbionts are associated intracellular and closely related genera have the same type of symbiont-host association [10, 71, 87-89]. However, closely related genera of bathymodioline mussels have diverse symbiont-host associations ranging from ectosymbionts, over extracellular endosymbionts to intracellular endosymbionts.

Now that we have identified such diverse symbiont-host associations in closely related host species, discovering the molecular mechanisms that underlie these striking patterns by resolving how host or symbionts form these associations could fundamentally contribute to our understanding of how bacteria and epithelial cells interact. A wide range of experiments could be performed to resolve which mechanisms are involved in reshaping the host's cell membrane and which processes mediate symbiont uptake.

To elucidate the molecular processes involved in the formation of the channel system and the membrane invagination, one could perform a differential gene expression analysis of mussels harboring intracellular endosymbionts (*G. childressi*),

extracellular endosymbionts (*B. puteoserpentis*), and ectosymbionts (*"B". manusensis*). This analysis would show if, for example, certain cytoskeletal proteins are more expressed in the mussels with the extracellular endosymbiont association compared to the other mussels. Coupled with antibody staining of target proteins, identified by differential gene expression, and a high-resolution microscopy approach, the proteins involved in shaping the channel system could be determined and visualized.

Answering the question why some MOX symbionts are associated intracellular, such as in the case of *G. childressi*, while others are associated as extracellular endosymbionts, such as in the case of *B. brooksi* could reveal the different symbiont uptake strategies the two different mussel species have. Comparing the genomes and transcriptomes of *G. childressi* and *B. brooksi* mussels and their symbionts, which co-occur at the same habitat, potential proteins involved in the symbiont recognition and uptake of the different hosts could be identified.

Furthermore, it would be interesting to keep these mussels in aquaria and supply them only with methane to follow what happens in *B. brooksi* with the SOX symbionts. Do the SOX symbionts "escape" the host when they don't have any nutrition or do they get intracellularly degraded by the host? In this way, one could track what effect the loss of the SOX symbionts has on the MOX symbionts. Do the MOX symbionts become intracellular endosymbionts once the SOX are gone or do they remain extracellular endosymbionts? This experiment would address the question of whether the SOX symbionts drive the extracellular symbiont-host association in bathymodioline mussels and whether the host would be able to internalize the MOX symbionts once the SOX symbionts disappeared. Furthermore

the experiment would clarify, whether the two MOX symbionts of *G. childressi* and *B. brooksi* are so fundamentally different that one type of symbiont always remains extracellular while the other symbiont associates intracellularly.

Our 3D ultrastructural approach has revealed how important it is to have a second look at known symbiotic systems. Bathymodioline mussels have been studied for more than 40 years, but only now, thanks to advances in sample preservation and imaging techniques, we have been able to understand the structure of this symbiont-host association in great detail. Our findings raise new questions not only about the molecular processes responsible for the formation of these associations, but also about the evolution of these systems. At the cellular level, this system provides the ideal conditions to understand how epithelial cells communicate with bacterial symbionts and how they adapt to the coexistence. Evolutionarily and ecologically, it is highly interesting to understand the processes that have led bathymodioline mussels to form this variety of symbiont-host associations, even though the different bathymodioline species harbor closely related symbionts. Our findings, together with the technological advances, motivate and invites to extend these approaches to a broader range of symbiotic and pathogenic systems and reevaluate their type of host association.

Authors' contributions

M.F., **N.L., Y.S.** and **N.D.** conceived this study. **N.L.** performed the sample preparations and **N.S.** performed the FIB-SEM analysis. **M.F.** and **N.L.** did the 2D-TEM data acquisition. **J.H.** performed the FIB-SEM image alignment and calculated the membrane predictions, **M.F.** did the 3D segmentations, data analysis and wrote the manuscript. **N.L.** revised the manuscript.

Competing interests

We declare no competing interests.

Funding

Funding was provided by the Max Planck Society, the MARUM Cluster of Excellence 'The Ocean Floor' (Deutsche Forschungsgemeinschaft (German Research Foundation) under Germany's Excellence Strategy - EXC-2077 – 39074603), a Gordon and Betty Moore Foundation Marine Microbial Initiative Investigator Award (grant no. GBMF3811 to N.D.) and a European Research Council Advanced Grant (BathyBiome, Grant 340535 to N.D.).

Acknowledgements

We highly appreciate the work of the captains, crew members, and ROV pilots of the cruises M126, M82-3, and NA58. We want to thank Wiebke Ruschmaier and Miriam Sadowski for their held during the sample preparation and 3D segmentation.

Appendix

Supplementary Figures

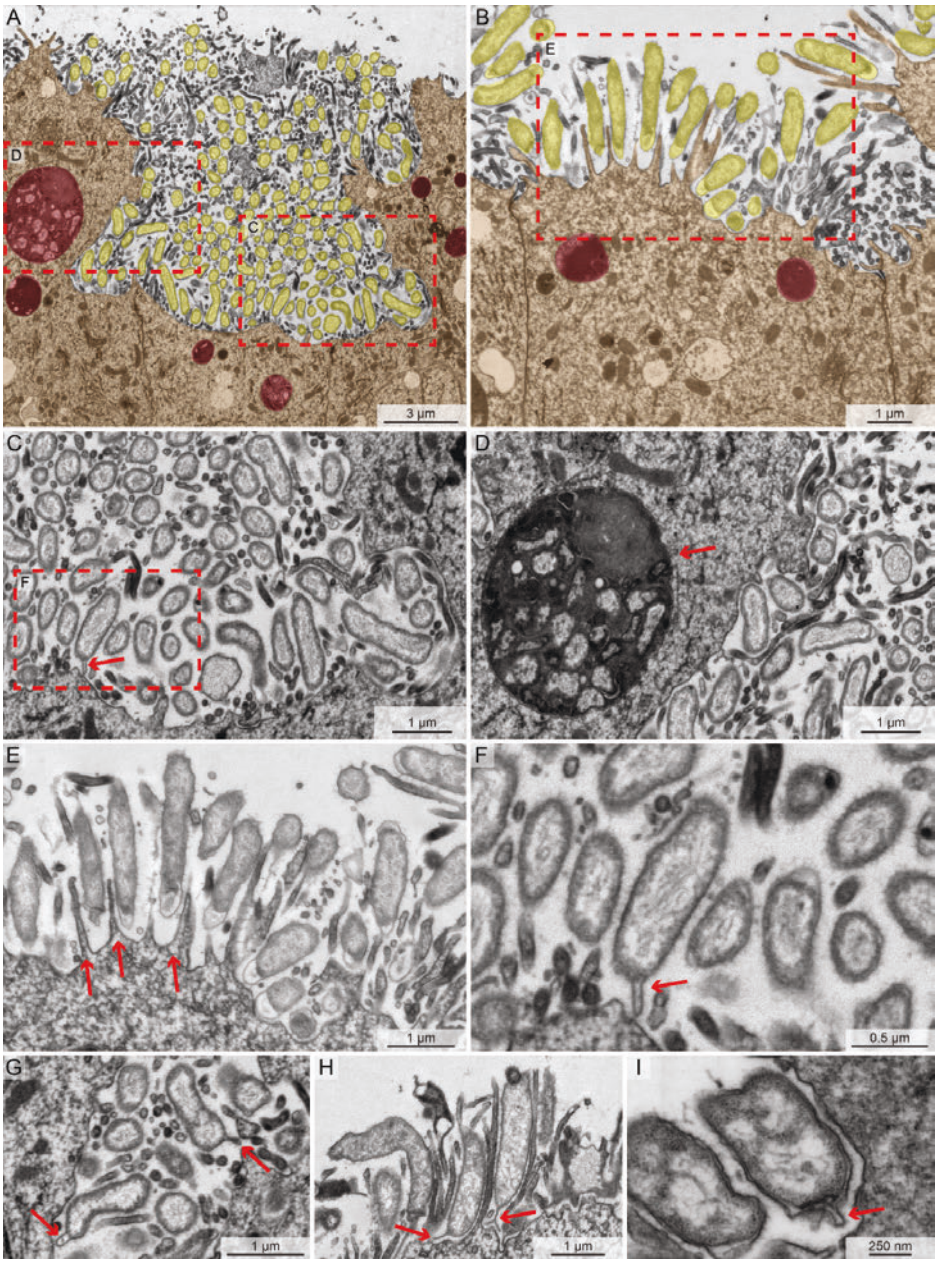

Figure S1 Symbiont of *"B". manusensis* are located extracellular on the apical cell membrane of the gill cells. A-B) The overview images of *"B". manusensis* gill epithelia cells (brown) indicate that the symbionts (yellow) are located on the apical cell membrane of gill cells. This suggests that these symbionts are ectosymbionts. Lysosomes are indicated by the red color overlay. The zoom-ins **C** and **D** show the ectosymbionts in more detail. Furthermore, lysosomal digestion of symbionts is indicated by the red arrow in **D**. **E)** The ectosymbionts of *"B". manusensis* are located in membrane ruffels of the host membrane (indicated by the red arrow). F – I) The red arrows show SOX symbiont that are connected to the host cell membrane with one pole. It seems that the outer bacterial membrane forms a tubular extension.

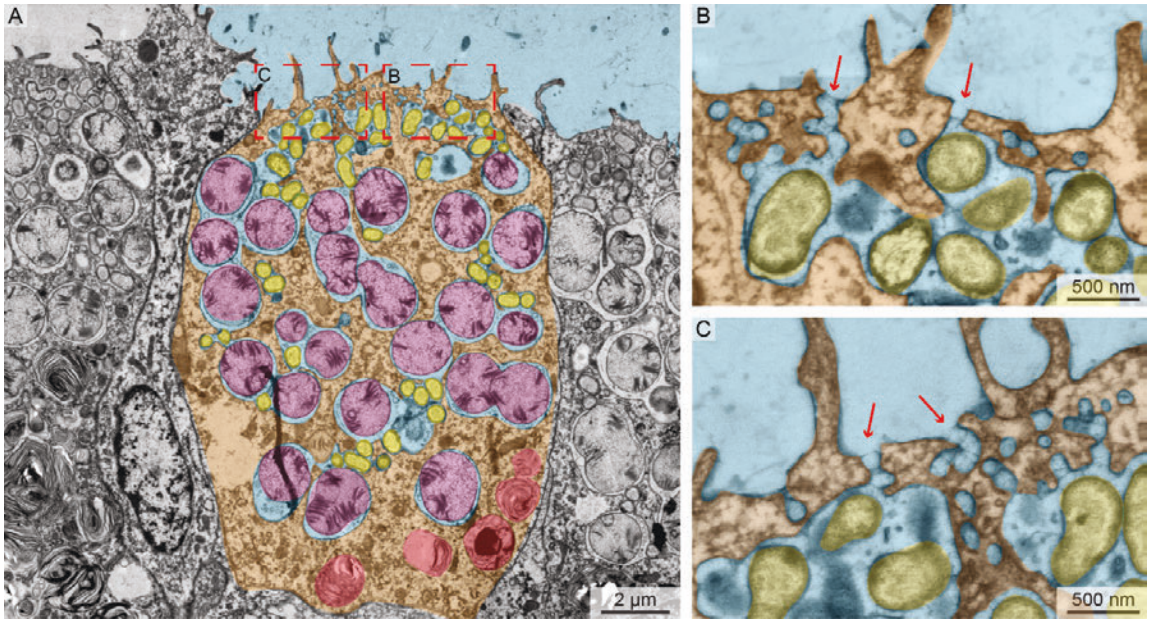

Figure S2 *B. brooksi* has extracellular endosymbionts A) *B. brooksi* harbors SOX and MOX in membrane invaginations which are connected to the outside by a channel system. The SOX (yellow) and MOX (magenta) symbionts are enclosed by the extracellular medium (blue) and not the host cytosol (brown). The lysosomes are indicated in red. Zoom-ins **B** and **C** show the channels to the outside indicated by the red arrows.

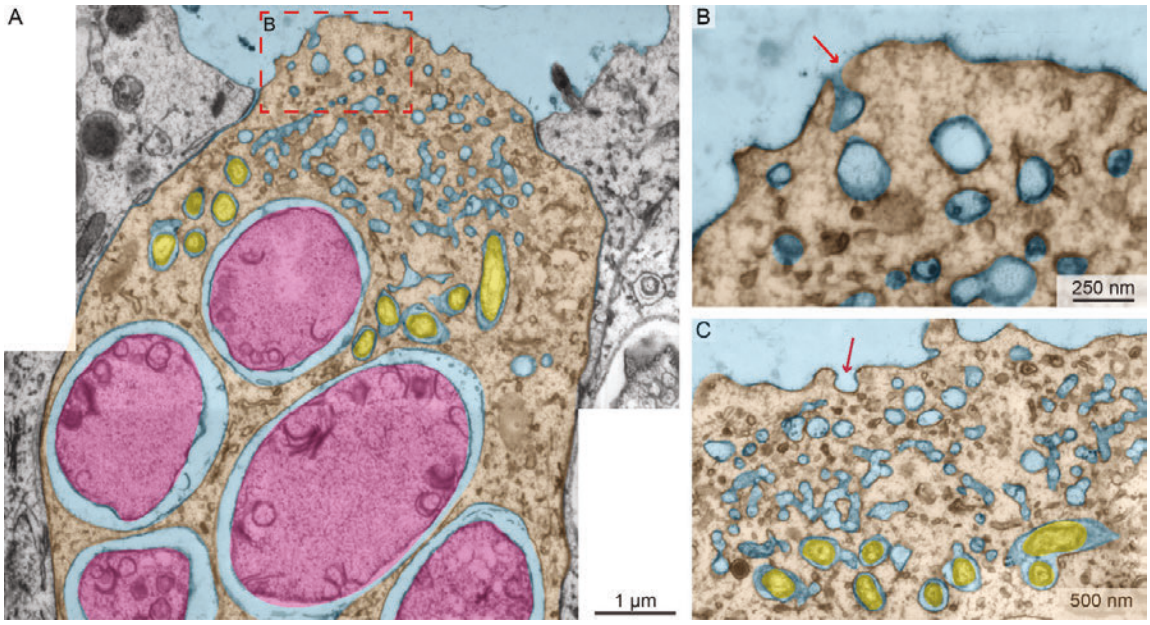

Figure S3 *B. heckerae* has extracellular endosymbionts A) *B. heckerae* harbors SOX (yellow) and MOX (magenta) symbionts in membrane invaginations which are connected to the outside (blue) by channels. The symbionts are not enclosed by the host cytosol (brown). Zoom-ins **B** and **C** show the channels to the outside indicated by the red arrows.

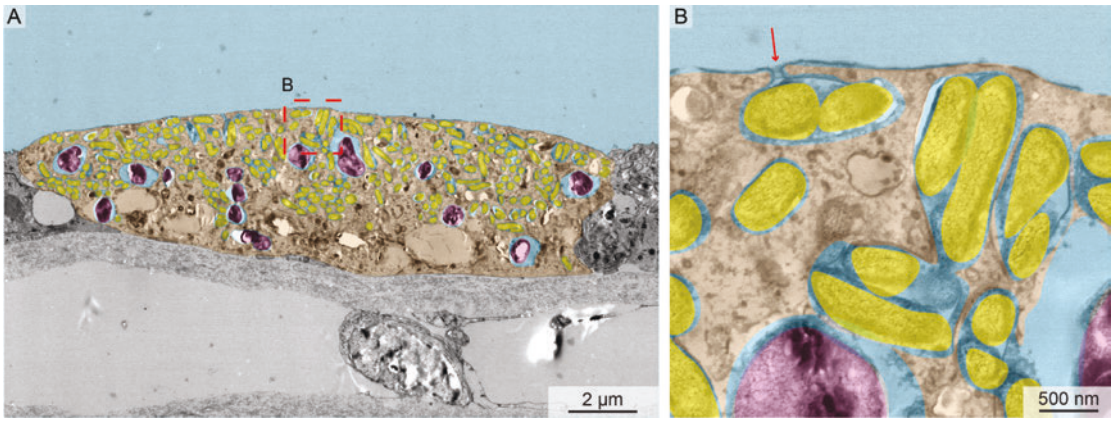

Figure S4 *B. azoricus* has extracellular endosymbionts A) *B. azoricus* harbors SOX (yellow) and MOX (magenta) symbionts in membrane invaginations which are connected to the outside (blue) by channels. The symbionts are not enclosed by the host cytosol (brown). Although, the preservation of *B. azoricus* mussels was not ideal, as they were fixed with trumps solution, the channel system was visible. Zoom-in **B** show the channels to the outside indicated by the red arrows.

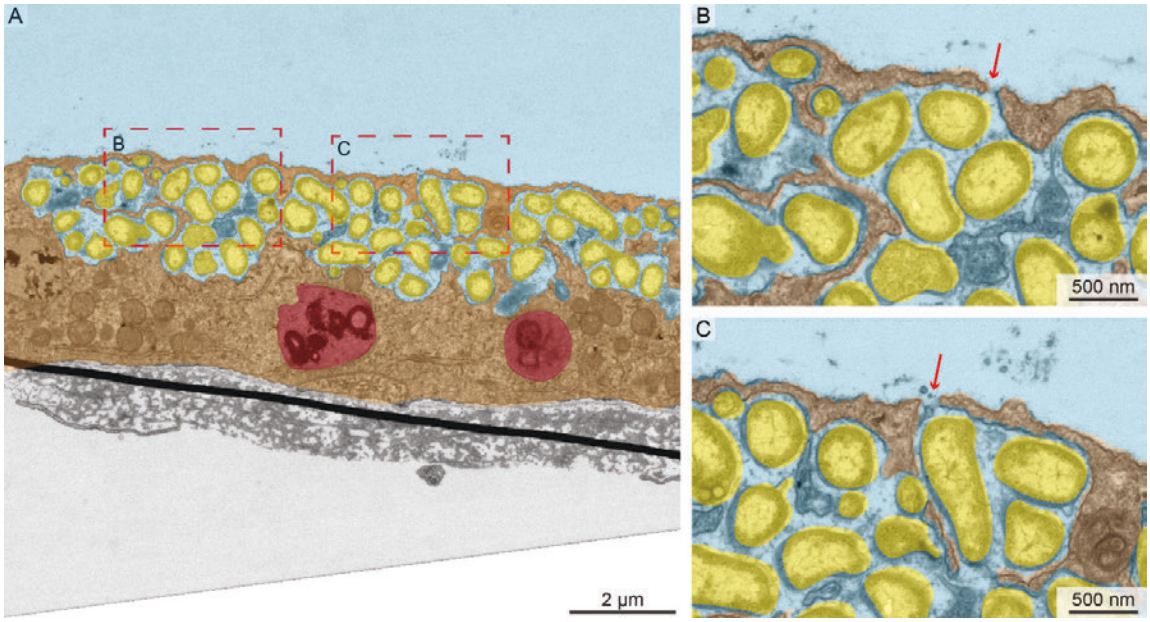

Figure S5 *G. gladius* has extracellular endosymbionts A) *G. gladius* harbors SOX (yellow) symbionts in membrane invaginations which are connected to the outside (blue) by channels. The host cytosol is shown in brown. The lysosomes are indicated in red. Zoom-ins **B** and **C** show the channels to the outside indicated by the red arrows.

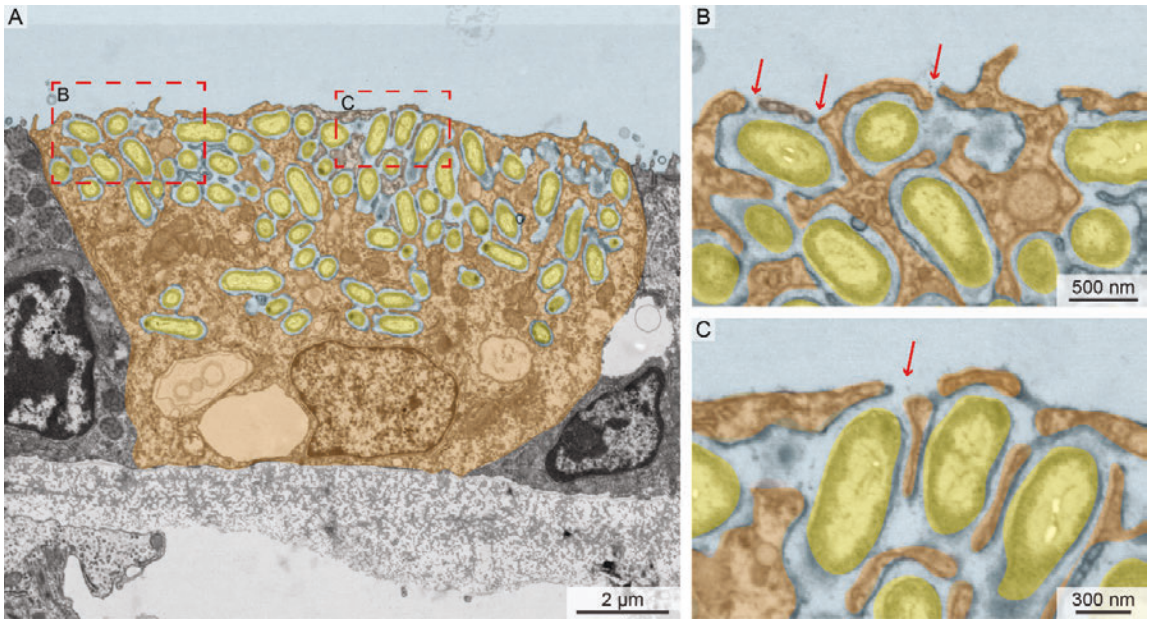

Figure S6 *V. insolatus* has extracellular endosymbionts A) *V. insolatus* harbors SOX (yellow) symbionts in membrane invaginations which are connected to the outside (blue) by channels. The host cytosol is shown in brown. Zoom-ins **B** and **C** show the channels to the outside indicated by the red arrows.

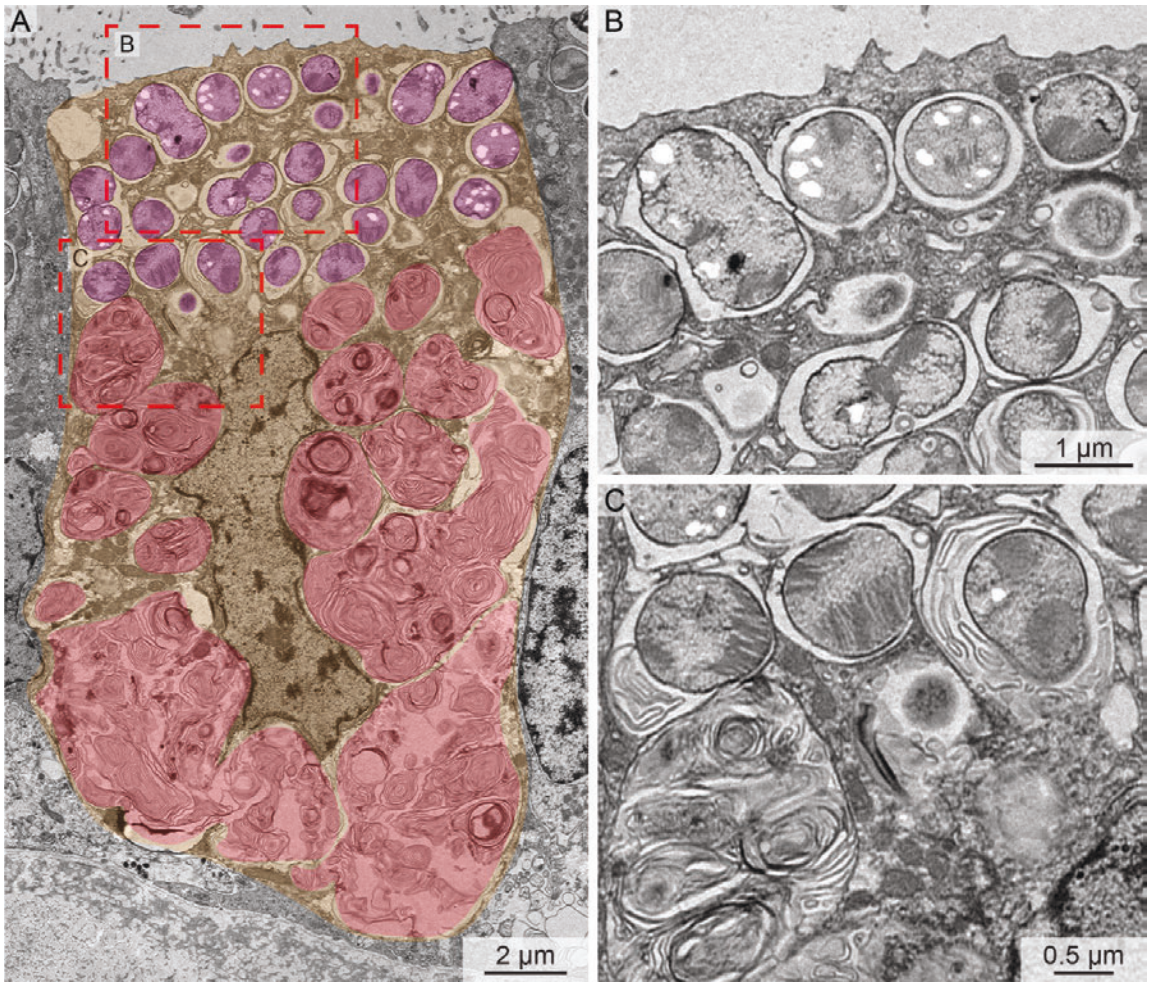

Figure S7 The MOX symbionts of *G. childressi* are intracellular symbionts. A) The overview image of shows that the MOX symbionts (magenta) are intracellular symbionts located in vacuoles inside the host cytoplasm (orange). The red color overlay indicates lysosomal digestion. The zoom-ins **B** and **C** show the intracellular symbionts and the lysosomal digestion in more detail.

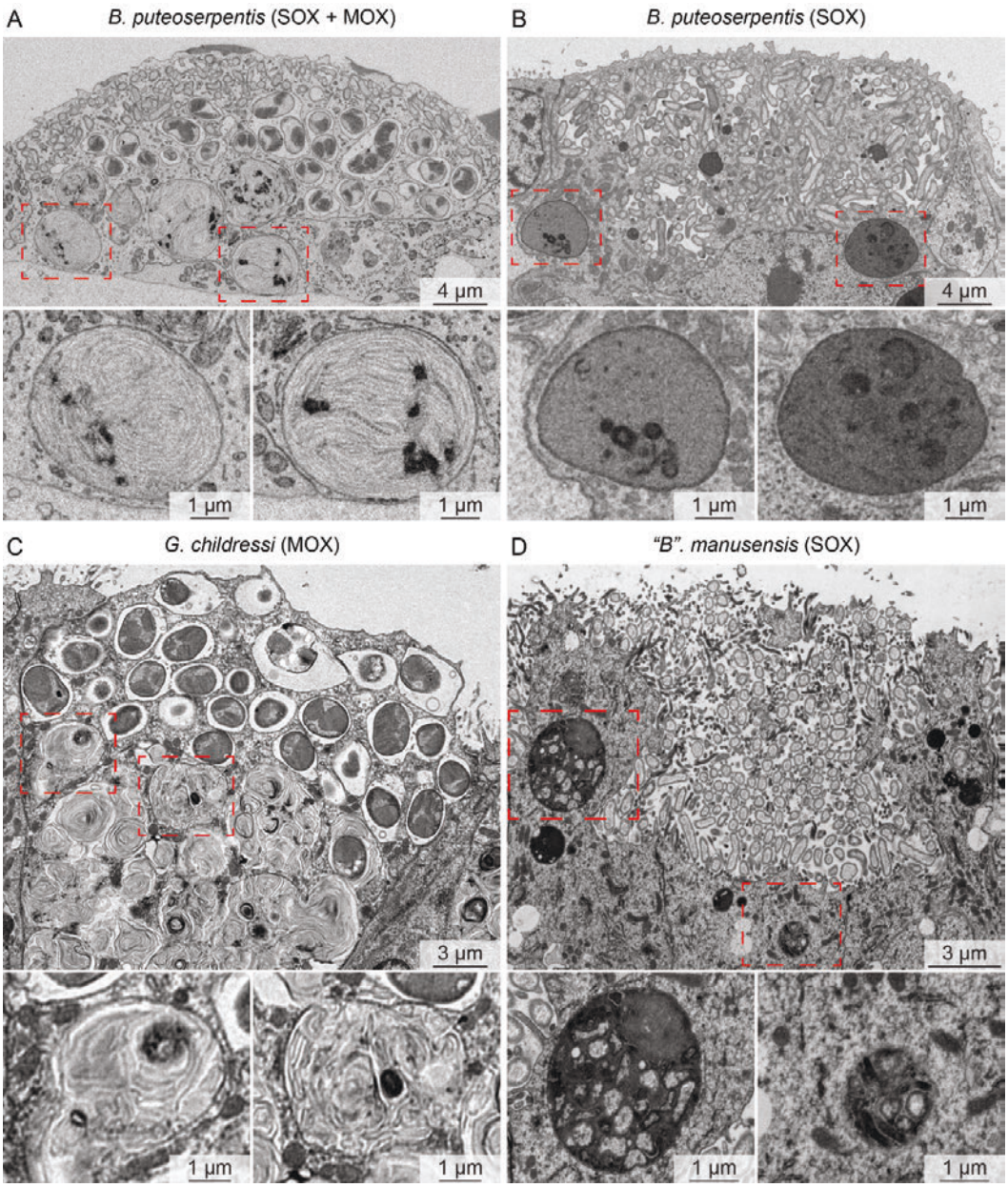

Figure S8 Comparison of lysosomes between bacteriocytes hosting SOX or MOX or both symbionts. A) Lysosomes of *B. puteoserpentis* bacteriocytes harboring SOX and MOX symbionts have a roundish morphology and membranous structures inside. **B)** Lysosomes of *B. puteoserpentis* bacteriocytes harboring only SOX symbionts have a roundish morphology and are very electron dense. **C)** Lysosomes of *G. childressi* bacteriocytes harboring only MOX symbiont have a similar morphology as the lysosomes of *B. puteoserpentis* bacteriocytes harboring SOX and MOX symbionts. The lysosomes are roundish and are filled with membranous structures. **D)** Lysosomes of *"B". manusensis* bacteriocytes harboring only SOX symbionts have a similar morphology as the lysosomes of *B. puteoserpentis* bacteriocytes harboring only SOX. The lysosomes are roundish and very electron dense.

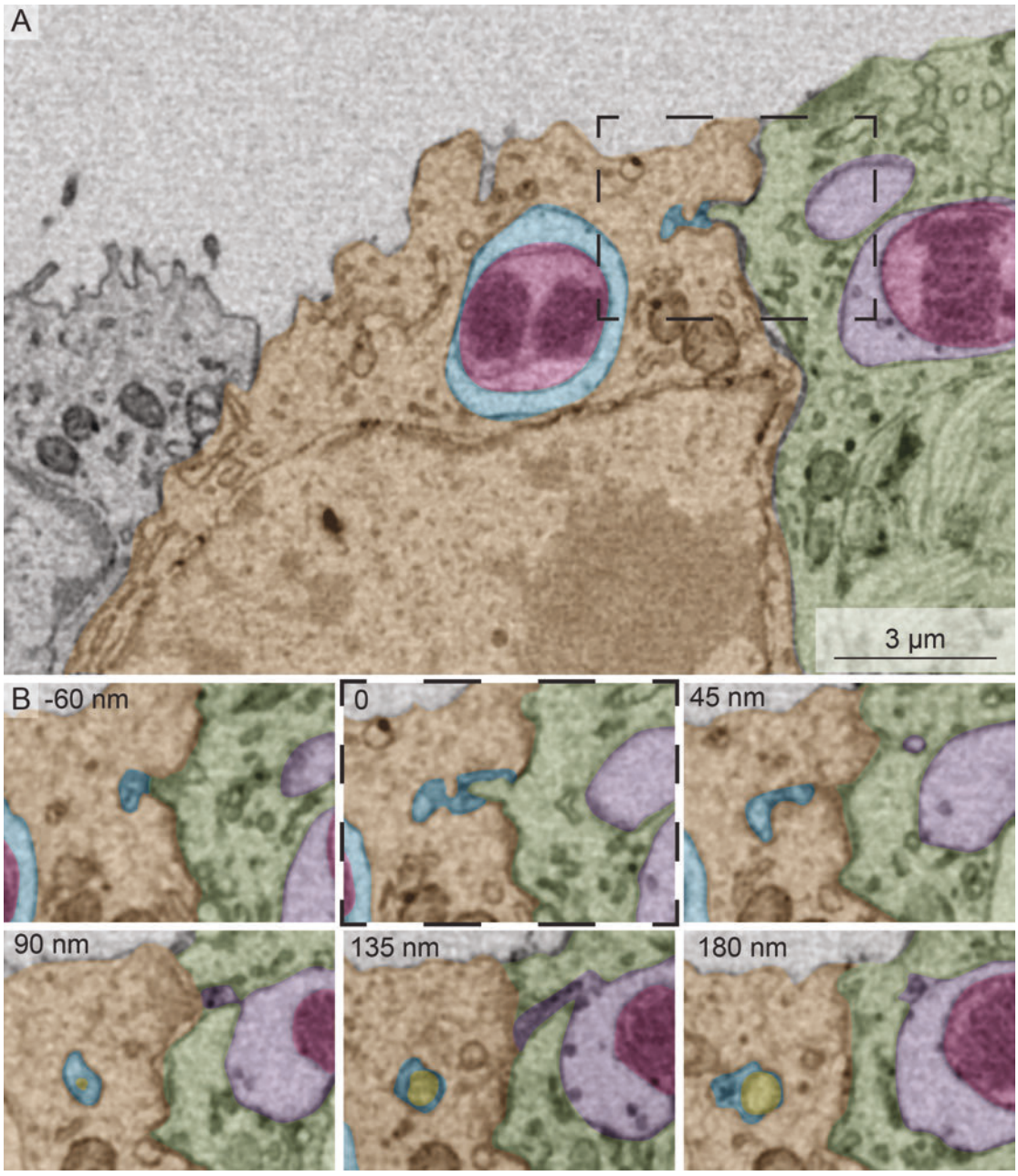

Figure S9 The channel system of *B. puteoserpentis* gill cells is not only connected to the apical cell surface but also to the side of the host cell. A) The black box shows the region were a channel is connected to the the side of the host cell. The colors indicate the channels (blue / purple), the MOX symbionts (magenta), SOX symbiont (yellow) and the two host cells (orange / green). **B)** The small Zoom-ins show how the channel is connected to the side of the host cell and how a new channel starts in the neighboring host cell in close proximity over a series of different Z-planes of the image stack. The Z-plane is indicated by the number in the top left corner.

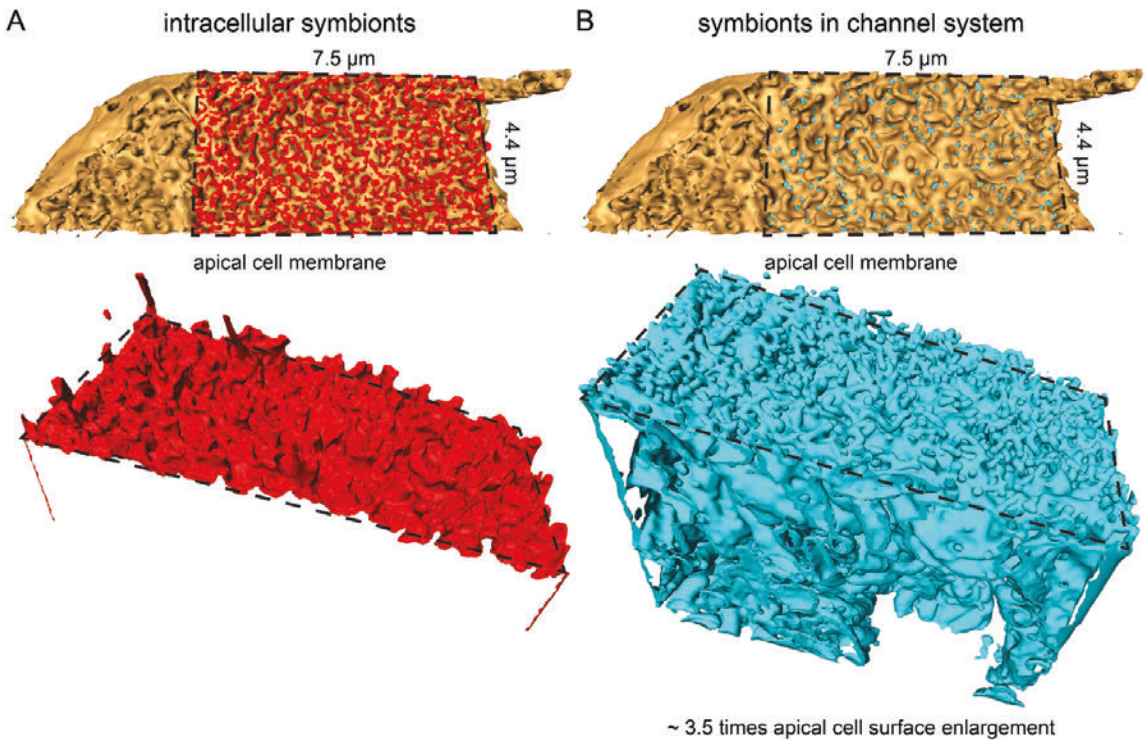

Figure S10 ***Bathymodiolus puteoserpentis*** **gill epithelia cells have an apical surface enlargement of ~6.5 compared to gill cells which harbor intracellular symbionts. A)** 3D modeling the apical cell membrane of a bacteriocyte containing intracellular symbionts. To generate this model we took a *B. puteoserpentis* gill cell and virtually closed the channel system. The resulting cell surface is displayed in red. **B)** 3D modeling of the apical cell membrane of a *B. puteoserpentis* gill cell. The membrane is ~3.5 times larger than compared to the cell surface shown in **A**.

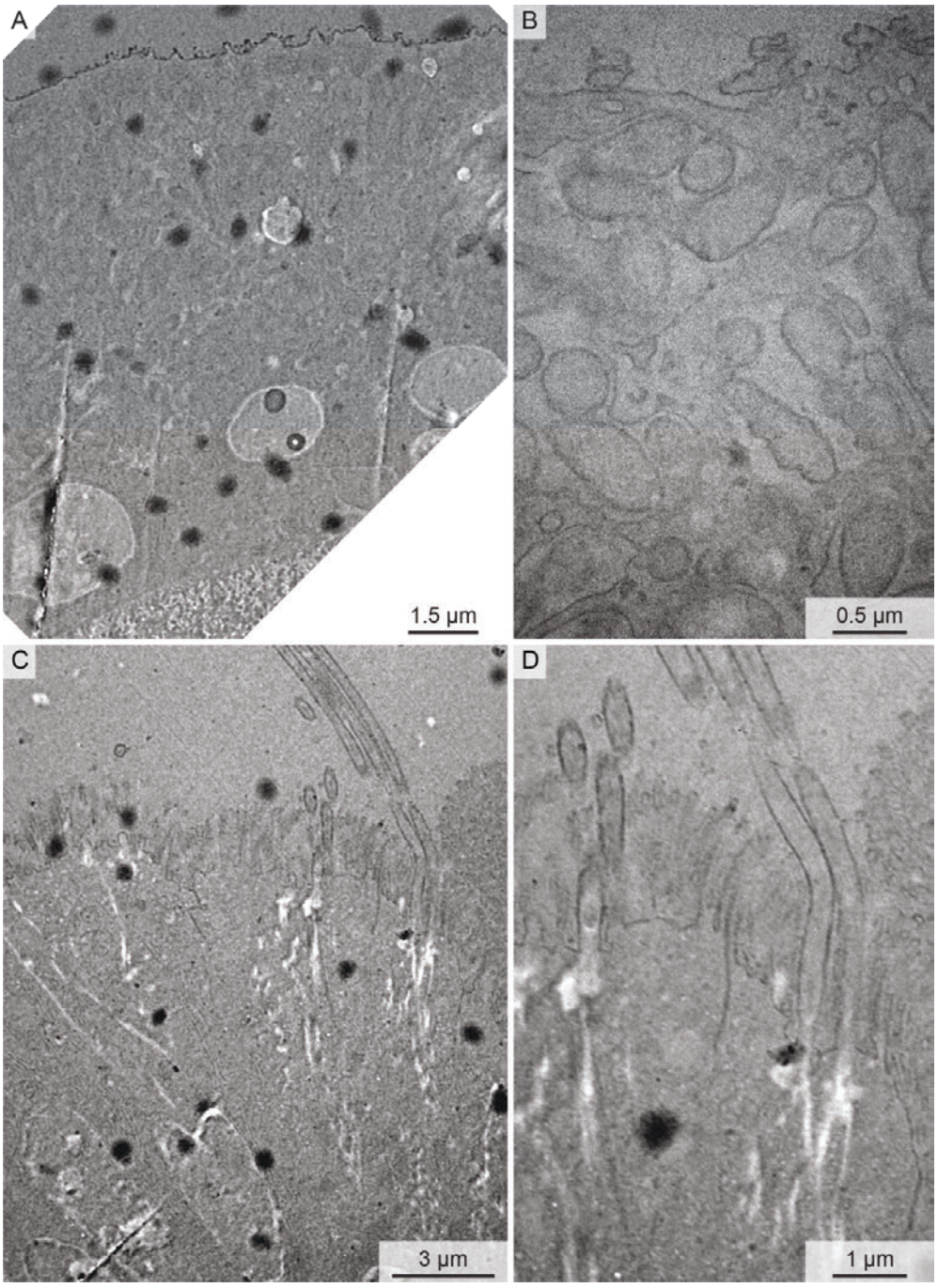

Figure S11 Ruthenium red control of unstained and uncontrasted *B. puteoserpentis* gill cells. A and **B)** The uncontracted and unstained TEM images of a *B. puteoserpentis* gill cell shows now signal coming from the cell surface or bacteria. The same can be observed in ciliated edge cells (**C** and **D**). This indicates that the ruthenium red stain (presented in Figure 3) is specific and shows that the channel system is open to the outside.

References

[1] Smith, D.C. 1979 From Extracellular to Intracellular: The Establishment of a Symbiosis. *Proc. R. Soc. B* **204**, 115-130.
[2] Gray, M.W. 2017 Lynn Margulis and the endosymbiont hypothesis: 50 years later. *Molecular Biology of the Cell* **28**, 1285-1287. (doi:10.1091/mbc.e16-07-0509).
[3] Margulis, L. 1970 *Origin of eukaryotic cells: Evidence and research implications for a theory of the origin and evolution of microbial, plant and animal cells on the precambrian Earth*, Yale University Press.
[4] McCutcheon, J.P., Boyd, B.M. & Dale, C. 2019 The Life of an Insect Endosymbiont from the Cradle to the Grave. *Curr. Biol.* **29**, R485-R495. (doi:10.1016/j.cub.2019.03.032).
[5] van Ham, R.C.H.J., Kamerbeek, J., Palacios, C., Rausell, C., Abascal, F., Bastolla, U., Fernández, J.M., Jiménez, L., Postigo, M., Silva, F.J., et al. 2003 Reductive genome evolution in *Buchnera aphidicola*. *Proceedings of the National Academy of Sciences* **100**, 581. (doi:10.1073/pnas.0235981100).
[6] McCutcheon, J.P. & Moran, N.A. 2012 Extreme genome reduction in symbiotic bacteria. *Nature Reviews Microbiology* **10**, 13-26. (doi:10.1038/nrmicro2670).
[7] Douglas, A.E. 1998 Nutritional Interactions in Insect-Microbial Symbioses: Aphids and Their Symbiotic Bacteria *Buchnera*. *Annu. Rev. Entomol.* **43**, 17-37. (doi:10.1146/annurev.ento.43.1.17).
[8] Zimmermann, J., Wentrup, C., Sadowski, M., Blazejak, A., Gruber-Vodicka, H.R., Kleiner, M., Ott, J.A., Cronholm, B., De Wit, P., Erséus, C., et al. 2016 Closely coupled evolutionary history of ecto- and endosymbionts from two distantly related animal phyla. *Mol. Ecol.* **25**, 3203-3223. (doi:10.1111/mec.13554).
[9] Ott, J., Bright, M. & Bulgheresi, S. 2004 Symbioses between marine nematodes and sulfur-oxidizing chemoautotrophic bacteria. *Symbiosis* **36**, 103-126.
[10] Endow, K. & Ohta, S. 1990 Occurrence of bacteria in the primary oocytes of vesicomyid clam *Calyptogena soyoae*. *Mar. Ecol. Prog. Ser.* **64**, 309-311.
[11] Giere, O., Windoffer, R. & Southward, E.C. 1995 The Bacterial Endosymbiosis of the Gutless Nematode, *Astomonema Southwardorum*: Ultrastructural Aspects. *J. Mar. Biol. Assoc. U.K.* **75**, 153-164. (doi:10.1017/S0025315400015265).
[12] Dubilier, N., Mülders, C., Ferdelman, T., de Beer, D., Pernthaler, A., Klein, M., Wagner, M., Erséus, C., Thiermann, F., Krieger, J., et al. 2001 Endosymbiotic sulphate-reducing and sulphide-oxidizing bacteria in an oligochaete worm. *Nature* **411**, 298-302. (doi:10.1038/35077067).
[13] Estes, A.M., Hearn, D.J., Bronstein, J.L. & Pierson, E.A. 2009 The Olive Fly Endosymbiont, "*Candidatus* Erwinia dacicola," Switches from an Intracellular Existence to an Extracellular Existence during Host Insect Development. *Appl. Environ. Microbiol.* **75**, 7097-7106. (doi:10.1128/AEM.00778-09).
[14] Bright, M. & Bulgheresi, S. 2010 A complex journey: transmission of microbial symbionts. *Nature Reviews Microbiology* **8**, 218-230. (doi:10.1038/nrmicro2262).
[15] McFall-Ngai, M.J. 2014 The importance of microbes in animal development: lessons from the squid-vibrio symbiosis. *Annu. Rev. Microbiol.* **68**, 177-194. (doi:10.1146/annurev-micro-091313-103654).
[16] Coburn, B., Grassl, G.A. & Finlay, B.B. 2007 *Salmonella*, the host and disease: a brief review. *Immunology & Cell Biology* **85**, 112-118. (doi:10.1038/sj.icb.7100007).
[17] Dubilier, N., Bergin, C. & Lott, C. 2008 Symbiotic diversity in marine animals: the art of harnessing chemosynthesis. *Nature Reviews Microbiology* **6**, 725-740. (doi:10.1038/nrmicro1992).
[18] Sogin, E.M., Kleiner, M., Borowski, C., Gruber-Vodicka, H.R. & Dubilier, N. 2021 Life in the Dark: Phylogenetic and Physiological Diversity of Chemosynthetic Symbioses. *Annu. Rev. Microbiol.* (doi:10.1146/annurev-micro-051021-123130).
[19] Duperron, S., Bergin, C., Zielinski, F.U., Blazejak, A., Pernthaler, A., McKiness, Z.P., DeChaine, E., Cavanaugh, C.M. & Dubilier, N. 2006 A dual symbiosis shared by two mussel

species, *Bathymodiolus azoricus* and *Bathymodiolus puteoserpentis* (Bivalvia: Mytilidae), from hydrothermal vents along the northern Mid-Atlantic Ridge. *Environ. Microbiol.* **8**, 1441-1447. (doi:10.1111/j.1462-2920.2006.01038.x).
[20] DeChaine, E. & Cavanaugh, C.M. 2005 Symbioses of methanotrophs and deep-sea mussels (*Mytilidae*: *Bathymodiolinae*). *Prog Mol Subcell Biol.* **41**, 227-249. (doi:10.1007/3-540-28221-1_11).
[21] Fisher, C.R., Childress, J.J., Oremland, R.S. & Bidigare, R.R. 1987 The importance of methane and thiosulfate in the metabolism of the bacterial symbionts of two deep-sea mussels. *Mar. Biol.* **96**, 59-71. (doi:10.1007/BF00394838).
[22] Fiala-Médioni, A., McKiness, Z., Dando, P., Boulegue, J., Mariotti, A., Alayse-Danet, A., Robinson, J. & Cavanaugh, C. 2002 Ultrastructural, biochemical, and immunological characterization of two populations of the mytilid mussel *Bathymodiolus azoricus* from the Mid-Atlantic Ridge evidence for a dual symbiosis. *Mar. Biol.* **141**, 1035-1043. (doi:10.1007/s00227-002-0903-9).
[23] Thubaut, J., Corbari, L., Gros, O., Duperron, S., Couloux, A. & Samadi, S. 2013 Integrative Biology of Idas iwaotakii (Habe, 1958), a 'Model Species' Associated with Sunken Organic Substrates. *PLOS ONE* **8**, e69680. (doi:10.1371/journal.pone.0069680).
[24] Franke, M., Geier, B., Hammel, J.U., Dubilier, N. & Leisch, N. 2021 Coming together - symbiont acquisition and early development in deep-sea bathymodioline mussels. *Proceedings of the Royal Society B: Biological Sciences* **288**, 20211044. (doi:doi:10.1098/rspb.2021.1044).
[25] Fiala-Médioni, A., Métivier, C., Herry, A. & Le Pennec, M. 1986 Ultrastructure of the gill of the hydrothermal-vent mytilid *Bathymodiolus sp. Mar. Biol.* **92**, 65-72. (doi:10.1007/BF00392747).
[26] Fiala-Medioni, A. & Le Pennec, M. 1987 Trophic structural adaptations in relation to the bacterial association of bivalve molluscs from hydrothermal vents and subduction zones. In *Symposium on marine symbioses. 1 (1987)* (pp. 63-74, Balaban, Philadelphia, .
[27] Kádár, E., Davis, S.A. & Lobo-da-Cunha, A. 2008 Cytoenzymatic investigation of intracellular digestion in the symbiont-bearing hydrothermal bivalve *Bathymodiolus azoricus*. *Mar. Biol.* **153**, 995-1004. (doi:10.1007/s00227-007-0872-0).
[28] Zheng, P., Wang, M., Li, C., Sun, X., Wang, X., Sun, Y. & Sun, S. 2017 Insights into deep-sea adaptations and host-symbiont interactions: a comparative transcriptome study on *Bathymodiolus* mussels and their coastal relatives. *Mol. Ecol.* (doi:10.1111/mec.14160).
[29] Fontanez, K.M. & Cavanaugh, C.M. 2014 Evidence for horizontal transmission from multilocus phylogeny of deep-sea mussel (*Mytilidae*) symbionts. *Environ. Microbiol.* **16**, 3608-3621. (doi:10.1111/1462-2920.12379).
[30] Won, Y.J., Hallam, S.J., O'Mullan, G.D., Pan, I.L., Buck, K.R. & Vrijenhoek, R.C. 2003 Environmental Acquisition of Thiotrophic Endosymbionts by Deep-Sea Mussels of the Genus *Bathymodiolus*. *Appl. Environ. Microbiol.* **69**, 6785-6792. (doi:10.1128/aem.69.11.6785-6792.2003).
[31] Kádár, E., Bettencourt, R., Costa, V., Santos, R.S., Lobo-da-Cunha, A. & Dando, P. 2005 Experimentally induced endosymbiont loss and re-acquirement in the hydrothermal vent bivalve *Bathymodiolus azoricus*. *J. Exp. Mar. Biol. Ecol.* **318**, 99-110. (doi:10.1016/j.jembe.2004.12.025).
[32] Salerno, J.L., Macko, S.A., Hallam, S.J., Bright, M., Won, Y.J., McKiness, Z. & Van Dover, C.L. 2005 Characterization of symbiont populations in life-history stages of mussels from chemosynthetic environments. *Biol. Bull,* **208**, 145-155. (doi:10.2307/3593123).
[33] Taylor, J.D. & Glover, E.A. 2010 Chemosymbiotic Bivalves. In *The Vent and Seep Biota: Aspects from Microbes to Ecosystems* (ed. S. Kiel), pp. 107-135. Dordrecht, Springer Netherlands.
[34] Nelson, D. & Fisher, C. 1995 Chemoautotrophic and methanotrophic endosymbiotic bacteria at deep-sea vents and seeps. *The Microbiology of Deep-Sea Hydrothermal Vents*, 125-167.

[35] Southward, E.C. 2008 The Morphology of Bacterial Symbioses in the Gills of Mussels of the Genera *Adipicola* (Bivalvia: *Mytilidae*). *J. Shellfish Res.* **27**, 139-146. (doi:10.2983/0730-8000(2008)27[139:TMOBSI]2.0.CO;2).
[36] Laming, S.R., Duperron, S., Cunha, M.R. & Gaudron, S.M. 2014 Settled, symbiotic, then sexually mature: adaptive developmental anatomy in the deep-sea, chemosymbiotic mussel *Idas modiolaeformis*. *Mar. Biol.* **161**, 1319-1333. (doi:10.1007/s00227-014-2421-y).
[37] Laming, S.R., Duperron, S., Gaudron, S.M., Hilario, A. & Cunha, M.R. 2015 Adapted to change: The rapid development of symbiosis in newly settled, fast-maturing chemosymbiotic mussels in the deep sea. *Mar. Environ. Res.* **112**, 100-112. (doi:10.1016/j.marenvres.2015.07.014).
[38] Dubilier, N., Windoffer, R. & Giere, O. 1998 Ultrastructure and stable carbon isotope composition of the hydrothermal vent mussels *Bathymodiolus brevior* and *B. sp. affinis brevior* from the North Fiji Basin, western Pacific. *Mar. Ecol. Prog. Ser.* **165**, 187-193.
[39] Pranal, V., Fiala-Médioni, A. & Colomines, J.C. 1995 Amino acid and related compound composition in two symbiotic mytilid species from hydrothermal vents. *Mar. Ecol. Prog. Ser.* **119**, 155-166.
[40] Ikuta, T., Amari, Y., Tame, A., Takaki, Y., Tsuda, M., Iizuka, R., Funatsu, T. & Yoshida, T. 2021 Inside or out? Clonal thiotrophic symbiont populations occupy deep-sea mussel bacteriocytes with pathways connecting to the external environment. *ISME Communications* **1**, 38. (doi:10.1038/s43705-021-00043-x).
[41] Gustafson, R.G., Turner, R.D., Lutz, R.A. & Vrijenhoek, R.C. 1998 A new genus and five new species of mussels (Bivalvia, Mytilidae) from deep-sea sulfide/hydrocarbon seeps in the Gulf of Mexico. *Malacologia* **40**, 63-112.
[42] Montanaro, J., Gruber, D. & Leisch, N. 2016 Improved ultrastructure of marine invertebrates using non-toxic buffers. *PeerJ* **4**, e1860. (doi:10.7717/peerj.1860).
[43] McDonald, K.L. & Webb, R.I. 2011 Freeze substitution in 3 hours or less. *Journal of Microscopy* **243**, 227-233. (doi:10.1111/j.1365-2818.2011.03526.x).
[44] McDonald, K.L. 2014 Rapid Embedding Methods into Epoxy and LR White Resins for Morphological and Immunological Analysis of Cryofixed Biological Specimens. *Microscopy and Microanalysis* **20**, 152-163. (doi:10.1017/S1431927613013846).
[45] Maco, B., Cantoni, M., Holtmaat, A., Kreshuk, A., Hamprecht, F.A. & Knott, G.W. 2014 Semiautomated correlative 3D electron microscopy of in vivo–imaged axons and dendrites. *Nat. Protoc.* **9**, 1354-1366. (doi:10.1038/nprot.2014.101).
[46] Schindelin, J., Arganda-Carreras, I., Frise, E., Kaynig, V., Longair, M., Pietzsch, T., Preibisch, S., Rueden, C., Saalfeld, S., Schmid, B., et al. 2012 Fiji: an open-source platform for biological-image analysis. *Nat. Methods* **9**, 676-682. (doi:10.1038/nmeth.2019).
[47] Hennies, J., Lleti, J.M.S., Schieber, N.L., Templin, R.M., Steyer, A.M. & Schwab, Y. 2020 AMST: Alignment to Median Smoothed Template for Focused Ion Beam Scanning Electron Microscopy Image Stacks. *Sci. Rep.* **10**, 2004. (doi:10.1038/s41598-020-58736-7).
[48] Paszke, A., Gross, S., Massa, F., Lerer, A., Bradbury, J., Chanan, G., Killeen, T., Lin, Z., Gimelshein, N., Antiga, L., et al. 2019 PyTorch: An Imperative Style, High-Performance Deep Learning Library. (p. arXiv:1912.01703.
[49] Çiçek, Ö., Abdulkadir, A., Lienkamp, S.S., Brox, T. & Ronneberger, O. 2016 3D U-Net: Learning Dense Volumetric Segmentation from Sparse Annotation. In *Medical Image Computing and Computer-Assisted Intervention – MICCAI 2016* (eds. S. Ourselin, L. Joskowicz, M.R. Sabuncu, G. Unal & W. Wells), pp. 424-432. Cham, Springer International Publishing.
[50] Beier, T., Pape, C., Rahaman, N., Prange, T., Berg, S., Bock, D.D., Cardona, A., Knott, G.W., Plaza, S.M., Scheffer, L.K., et al. 2017 Multicut brings automated neurite segmentation closer to human performance. *Nat. Methods* **14**, 101-102. (doi:10.1038/nmeth.4151).
[51] Belevich, I., Joensuu, M., Kumar, D., Vihinen, H. & Jokitalo, E. 2016 Microscopy Image Browser: A Platform for Segmentation and Analysis of Multidimensional Datasets. *PLoS Biol.* **14**, e1002340. (doi:10.1371/journal.pbio.1002340).

[52] Wick, R.R., Schultz, M.B., Zobel, J. & Holt, K.E. 2015 Bandage: interactive visualization of de novo genome assemblies. *Bioinformatics* **31**, 3350-3352. (doi:10.1093/bioinformatics/btv383).
[53] Donath, A., Jühling, F., Al-Arab, M., Bernhart, S.H., Reinhardt, F., Stadler, P.F., Middendorf, M. & Bernt, M. 2019 Improved annotation of protein-coding genes boundaries in metazoan mitochondrial genomes. *Nucleic Acids Res.* **47**, 10543-10552. (doi:10.1093/nar/gkz833).
[54] Katoh, K. & Standley, D.M. 2013 MAFFT Multiple Sequence Alignment Software Version 7: Improvements in Performance and Usability. *Mol. Biol. Evol.* **30**, 772-780. (doi:10.1093/molbev/mst010).
[55] Nguyen, L.-T., Schmidt, H.A., von Haeseler, A. & Minh, B.Q. 2015 IQ-TREE: A Fast and Effective Stochastic Algorithm for Estimating Maximum-Likelihood Phylogenies. *Mol. Biol. Evol.* **32**, 268-274. (doi:10.1093/molbev/msu300).
[56] Kalyaanamoorthy, S., Minh, B.Q., Wong, T.K.F., von Haeseler, A. & Jermiin, L.S. 2017 ModelFinder: fast model selection for accurate phylogenetic estimates. *Nat. Methods* **14**, 587-589. (doi:10.1038/nmeth.4285).
[57] Hoang, D.T., Chernomor, O., von Haeseler, A., Minh, B.Q. & Vinh, L.S. 2018 UFBoot2: Improving the Ultrafast Bootstrap Approximation. *Mol. Biol. Evol.* **35**, 518-522. (doi:10.1093/molbev/msx281).
[58] Letunic, I. & Bork, P. 2021 Interactive Tree Of Life (iTOL) v5: an online tool for phylogenetic tree display and annotation. *Nucleic Acids Res.* **49**, W293-W296. (doi:10.1093/nar/gkab301).
[59] Ansorge, R., Romano, S., Sayavedra, L., Porras, M.Á.G., Kupczok, A., Tegetmeyer, H.E., Dubilier, N. & Petersen, J. 2019 Functional diversity enables multiple symbiont strains to coexist in deep-sea mussels. *Nat. Microbiol* **4**, 2487-2497. (doi:10.1038/s41564-019-0572-9).
[60] Streams, M.E., Fisher, C.R. & Fiala-Médioni, A. 1997 Methanotrophic symbiont location and fate of carbon incorporated from methne in a hydrocabon seep mussel. *Mar. Biol.* **129**, 465-476. (doi:10.1007/s002270050187).
[61] Childress, J.J., Fisher, C.R., Brooks, J.M., Kennicutt, M.C., Bidigare, R.R. & Anderson, A.E. 1986 A methanotrophic marine molluscan (bivalvia, *mytilidae*) symbiosis: mussels fueld by gas. *Science* **233**, 1306-1308. (doi:10.1126/science.233.4770.1306).
[62] Fujiwara, Y., Kawato, M., Noda, C., Kinoshita, G., Yamanaka, T., Fujita, Y., Uematsu, K. & Miyazaki, J. 2010 Extracellular and Mixotrophic Symbiosis in the Whale-Fall Mussel *Adipicola pacifica*: A Trend in Evolution from Extra- to Intracellular Symbiosis. *PLOS ONE* **5**, e11808. (doi:10.1371/journal.pone.0011808).
[63] Lorion, J., Duperron, S., Gros, O., Cruaud, C. & Samadi, S. 2009 Several deep-sea mussels and their associated symbionts are able to live both on wood and on whale falls. *Proceedings of the Royal Society B: Biological Sciences* **276**, 177-185. (doi:10.1098/rspb.2008.1101).
[64] Fujiwara, Y., Takai, K., Uematsu, K., Tsuchida, S., Hunt, J.C. & Hashimoto, J. 2000 FPhylogenetic characterization of endosymbionts in three hydrothermal vent mussels: influence on host distributions. . *Marine Ecology-progress Series - MAR ECOL-PROGR SER* **208**, 147-155. (doi:10.3354/meps208147).
[65] Wang, H., Zhang, H., Zhong, Z., Sun, Y., Wang, M., Chen, H., Zhou, L., Cao, L., Lian, C. & Li, C. 2021 Molecular analyses of the gill symbiosis of the bathymodiolin mussel *Gigantidas platifrons*. *iScience* **24**, 101894. (doi:10.1016/j.isci.2020.101894).
[66] Duperron, S., Lorion, J., Samadi, S., Gros, O. & Gaill, F. 2009 Symbioses between deep-sea mussels (Mytilidae : *Bathymodiolinae*) and chemosynthetic bacteria : diversity, function and evolution. *C. R. Biol.* **332**, 298-310. (doi:10.1016/j.crvi.2008.08.003).
[67] Raulfs, E.C., Macko, S.A. & Van Dover, C.L. 2004 Tissue and symbiont condition of mussels (*Bathymodiolus thermophilus*) exposed to varying levels of hydrothermal activity. *J. Mar. Biol. Assoc. U.K.* **84**, 229-234. (doi:10.1017/S0025315404009087h).

[68] Le Pennec, M., Diouris, M. & Herry, A. 1988 Endocytosis and lysis of bacteria in gill epithelium of *Bathymodiolus thermophilus*, Thyasira flexuosa and Lucinella divaricata (Bivalve, Molluscs). *J. Shellfish Res.* **7**, 483-489.
[69] Thubaut, J., Puillandre, N., Faure, B., Cruaud, C. & Samadi, S. 2013 The contrasted evolutionary fates of deep-sea chemosynthetic mussels (Bivalvia, *Bathymodiolinae*). *Ecol Evol* **3**, 4748-4766. (doi:10.1002/ece3.749).
[70] Windoffer, R. & Giere, O. 1997 Symbiosis of the Hydrothermal Vent Gastropod *Ifremeria nautilei* (Provannidae) With Endobacteria-Structural Analyses and Ecological Considerations. *The Biological Bulletin* **193**, 381-392. (doi:10.2307/1542940).
[71] Nussbaumer, A.D., Fisher, C.R. & Bright, M. 2006 Horizontal endosymbiont transmission in hydrothermal vent tubeworms. *Nature* **441**, 345-348. (doi:10.1038/nature04793).
[72] Russell, S.L., Pepper-Tunick, E., Svedberg, J., Byrne, A., Ruelas Castillo, J., Vollmers, C., Beinart, R.A. & Corbett-Detig, R. 2020 Horizontal transmission and recombination maintain forever young bacterial symbiont genomes. *PLoS Genet.* **16**, e1008935. (doi:10.1371/journal.pgen.1008935).
[73] Endow, K. & Ohta, S. 1989 The Symbiotic Relationship between Bacteria and a Mesogastropod Snail, *Alviniconcha hessleri*, collected from Hydrothermal Vents of the Mariana Back-Arc Basin. *Bulletin of Japanese Society of Microbial Ecology* **3**, 73-82. (doi:10.1264/microbes1986.3.73).
[74] Fujiwara, Y., Kato, C., Masui, N., Fujikura, K. & Kojima, S. 2001 Dual symbiosis in the cold-seep thyasirid clam *Maorithyas hadalis* from the hadal zone in the Japan Trench, western Pacific. *Mar. Ecol. Prog. Ser.* **214**, 151-159. (doi:10.3354/meps214151).
[75] Dufour, S.C. 2005 Gill Anatomy and the Evolution of Symbiosis in the Bivalve Family *Thyasiridae*. *Biol. Bull,* **208**, 200-212. (doi:10.2307/3593152).
[76] Distel, D.L., Baco, A.R., Chuang, E., Morrill, W., Cavanaugh, C. & Smith, C.R. 2000 Do mussels take wooden steps to deep-sea vents? *Nature* **403**, 725-726. (doi:10.1038/35001667).
[77] Breusing, C., Biastoch, A., Drews, A., Metaxas, A., Jollivet, D., Vrijenhoek, R.C., Bayer, T., Melzner, F., Sayavedra, L., Petersen, J.M., et al. 2016 Biophysical and Population Genetic Models Predict the Presence of "Phantom" Stepping Stones Connecting Mid-Atlantic Ridge Vent Ecosystems. *Curr. Biol.* **26**, 2257-2267. (doi:10.1016/j.cub.2016.06.062).
[78] Cavanaugh, C.M., Wirsen, C.O. & Jannasch, H.W. 1992 Evidence for Methylotrophic Symbionts in a Hydrothermal Vent Mussel (Bivalvia: *Mytilidae*) from the Mid-Atlantic Ridge. *Appl. Environ. Microbiol.* **58**, 5. (doi:10.1128/aem.58.12.3799-3803.1992).
[79] Cavanaugh, C.M., Levering, P.R., Maki, J.S., Mitchell, R. & Lidstrom, M.E. 1987 Symbiosis of methylotrophic bacteria and deep-sea mussels. *Nature* **325**, 346-348. (doi:10.1038/325346a0).
[80] Jannasch, H.W. 1985 Review Lecture - The chemosynthetic support of life and the microbial diversity at deep-sea hydrothermal vents. *Proceedings of the Royal Society of London. Series B. Biological Sciences* **225**, 277-297. (doi:10.1098/rspb.1985.0062).
[81] Cavanaugh, C.M., McKiness, Z.P., Newton, I.L.G. & Stewart, F.J. 2006 Marine Chemosynthetic Symbioses. In *The Prokaryotes: Volume 1: Symbiotic associations, Biotechnology, Applied Microbiology* (eds. M. Dworkin, S. Falkow, E. Rosenberg, K.-H. Schleifer & E. Stackebrandt), pp. 475-507. New York, NY, Springer New York.
[82] Smith, C.R. & Baco, A.R. 2003 Ecology of whale falls at the deep-sea floor. In *Oceanography and Marine Biology, An Annual Review, Volume 41* (eds. R.N. Gibson & R.J.A. Atkinson), pp. 319-333, CRC Press.
[83] Miyazaki, J.-I., Martins, L.d.O., Fujita, Y., Matsumoto, H. & Fujiwara, Y. 2010 Evolutionary Process of Deep-Sea *Bathymodiolus* Mussels. *PLOS ONE* **5**, e10363. (doi:10.1371/journal.pone.0010363).
[84] Franke, M., Geier, B., Hammel, J.U., Dubilier, N. & Leisch, N. 2020 Becoming symbiotic – the symbiont acquisition and the early development of bathymodiolin mussels. *bioRxiv*, 2020.2010.2009.333211. (doi:10.1101/2020.10.09.333211).

[85] Corr, S.C., Li, Y., Riedel, C.U., Toole, P.W., Hill, C. & Gahan, C.G.M. 2007 Bacteriocin production as a mechanism for the antiinfective activity of *Lactobacillus salivarius*; UCC118. *Proceedings of the National Academy of Sciences* **104**, 7617. (doi:10.1073/pnas.0700440104).
[86] Duperron, S., Fiala-Médioni, A., Caprais, J.-C., Olu, K. & Sibuet, M. 2007 Evidence for chemoautotrophic symbiosis in a Mediterranean cold seep clam (Bivalvia: *Lucinidae*): comparative sequence analysis of bacterial 16S rRNA, APS reductase and RubisCO genes. *FEMS Microbiol. Ecol.* **59**, 64-70. (doi:10.1111/j.1574-6941.2006.00194.x).
[87] Bright, M., Klose, J. & Nussbaumer, A.D. 2013 Giant tubeworms. *Curr. Biol.* **23**, R224-R225. (doi:10.1016/j.cub.2013.01.039).
[88] Fisher, C.R. 1990 Chemoautotrophic and methanotrophic symbioses in marine invertebrates. *Reviews In Aquatic Sciences* **2**, 399-436.
[89] Cavanaugh, C.M. 1983 Symbiotic chemoautotrophic bacteria in marine invertebrates from sulphide-rich habitats. *Nature* **302**, 58-61. (doi:10.1038/302058a0).
[90] Geier, B. 2020 Correlative mass spectrometry imaging of animal–microbe symbioses, Universität Bremen FB02 Biologie/Chemie.
[91] Gaudron, S.M., Demoyencourt, E. & Duperron, S. 2012 Reproductive Traits of the Cold-Seep Symbiotic Mussel *Idas modiolaeformis*: Gametogenesis and Larval Biology. *Biol. Bull,* **222**, 6-16. (doi:10.1086/bblv222n1p6).
[92] Jutras, I. & Desjardins, M. 2005 Phagocytosis: At the Crossroads of Innate and Adaptive Immunity. *Annu. Rev. Cell. Dev. Biol.* **21**, 511-527. (doi:10.1146/annurev.cellbio.20.010403.102755).
[93] Huynh, K.K., Kay, J.G., Stow, J.L. & Grinstein, S. 2007 Fusion, Fission, and Secretion During Phagocytosis. *Physiology* **22**, 366-372. (doi:10.1152/physiol.00028.2007).
[94] McMahon, H.T. & Boucrot, E. 2015 Membrane curvature at a glance. *J. Cell Sci.* **128**, 1065-1070. (doi:10.1242/jcs.114454).
[95] Leduc, C., Campàs, O., Joanny, J.-F., Prost, J. & Bassereau, P. 2010 Mechanism of membrane nanotube formation by molecular motors. *Biochim. Biophys. Acta* **1798**, 1418-1426. (doi:10.1016/j.bbamem.2009.11.012).
[96] Doherty, G.J. & McMahon, H.T. 2008 Mediation, Modulation, and Consequences of Membrane-Cytoskeleton Interactions. *Annual Review of Biophysics* **37**, 65-95. (doi:10.1146/annurev.biophys.37.032807.125912).
[97] Frost, A., Perera, R., Roux, A., Spasov, K., Destaing, O., Egelman, E.H., De Camilli, P. & Unger, V.M. 2008 Structural Basis of Membrane Invagination by F-BAR Domains. *Cell* **132**, 807-817. (doi:10.1016/j.cell.2007.12.041).
[98] Daumke, O., Roux, A. & Haucke, V. 2014 BAR Domain Scaffolds in Dynamin-Mediated Membrane Fission. *Cell* **156**, 882-892. (doi:10.1016/j.cell.2014.02.017).
[99] Frost, A., Unger, V.M. & De Camilli, P. 2009 The BAR Domain Superfamily: Membrane-Molding Macromolecules. *Cell* **137**, 191-196. (doi:10.1016/j.cell.2009.04.010).
[100] Simunovic, M., Evergren, E., Callan-Jones, A. & Bassereau, P. 2019 Curving Cells Inside and Out: Roles of BAR Domain Proteins in Membrane Shaping and Its Cellular Implications. *Annu. Rev. Cell. Dev. Biol.* **35**, 111-129. (doi:10.1146/annurev-cellbio-100617-060558).
[101] Schaffer, M., Pfeffer, S., Mahamid, J., Kleindiek, S., Laugks, T., Albert, S., Engel, B.D., Rummel, A., Smith, A.J., Baumeister, W., et al. 2019 A cryo-FIB lift-out technique enables molecular-resolution cryo-ET within native *Caenorhabditis elegans* tissue. *Nat. Methods* **16**, 757-762. (doi:10.1038/s41592-019-0497-5).
[102] Beck, M. & Baumeister, W. 2016 Cryo-Electron Tomography: Can it Reveal the Molecular Sociology of Cells in Atomic Detail? *Trends Cell Biol.* **26**, 825-837. (doi:10.1016/j.tcb.2016.08.006).
[103] Ribet, D. & Cossart, P. 2015 How bacterial pathogens colonize their hosts and invade deeper tissues. *Microb. Infect.* **17**, 173-183. (doi:10.1016/j.micinf.2015.01.004).
[104] Cossart, P. & Roy, C.R. 2010 Manipulation of host membrane machinery by bacterial pathogens. *Curr. Opin. Cell Biol.* **22**, 547-554. (doi:10.1016/j.ceb.2010.05.006).

[105] Sayavedra, L., Ansorge, R., Rubin-Blum, M., Leisch, N., Dubilier, N. & Petersen, J.M. 2019 Horizontal acquisition followed by expansion and diversification of toxin-related genes in deep-sea bivalve symbionts. *bioRxiv*, 605386. (doi:10.1101/605386).
[106] Sayavedra, L., Kleiner, M., Ponnudurai, R., Wetzel, S., Pelletier, E., Barbe, V., Satoh, N., Shoguchi, E., Fink, D., Breusing, C., et al. 2015 Abundant toxin-related genes in the genomes of beneficial symbionts from deep-sea hydrothermal vent mussels *eLife* **4**. (doi:10.7554/eLife.07966).
[107] Moser, M., Legate, K.R., Zent, R. & Fässler, R. 2009 The Tail of Integrins, Talin, and Kindlins. *Science* **324**, 895. (doi:10.1126/science.1163865).
[108] Scibelli, A., Roperto, S., Manna, L., Pavone, L.M., Tafuri, S., Morte, R.D. & Staiano, N. 2007 Engagement of integrins as a cellular route of invasion by bacterial pathogens. *The Veterinary Journal* **173**, 482-491. (doi:10.1016/j.tvjl.2006.01.010).
[109] Chouhan, B., Denesyuk, A., Heino, J., Johnson, M.S. & Denessiouk, K. 2011 Conservation of the Human Integrin-Type Beta-Propeller Domain in Bacteria. *PLOS ONE* **6**, e25069. (doi:10.1371/journal.pone.0025069).
[110] Tietjen, M. 2020 Physiology and ecology of deep-sea Bathymodiolus symbioses, Universität Bremen.
[111] Ponnudurai, R., Kleiner, M., Sayavedra, L., Petersen, J.M., Moche, M., Otto, A., Becher, D., Takeuchi, T., Satoh, N., Dubilier, N., et al. 2017 Metabolic and physiological interdependencies in the *Bathymodiolus azoricus* symbiosis. *ISME J* **11**, 463-477. (doi:10.1038/ismej.2016.124).
[112] Zheng, P., Wang, M., Li, C., Sun, X., Wang, X., Sun, Y. & Sun, S. 2017 Insights into deep-sea adaptations and host–symbiont interactions: A comparative transcriptome study on *Bathymodiolus* mussels and their coastal relatives. *Mol. Ecol.* **26**, 5133-5148. (doi:10.1111/mec.14160).
[113] Wentrup, C., Wendeberg, A., Schimak, M., Borowski, C. & Dubilier, N. 2014 Forever competent: deep-sea bivalves are colonized by their chemosynthetic symbionts throughout their lifetime. *Environ. Microbiol.* **16**, 3699-3713. (doi:10.1111/1462-2920.12597).
[114] Klose, J., Polz, M.F., Wagner, M., Schimak, M.P., Gollner, S. & Bright, M. 2015 Endosymbionts escape dead hydrothermal vent tubeworms to enrich the free-living population. *Proceedings of the National Academy of Sciences* **112**, 11300. (doi:10.1073/pnas.1501160112).

Chapter III

This manuscript has been published in Proceedings of the Royal Society B

(2021-08-18 available under: https://doi.org/10.1098/rspb.2021.1044)

PROCEEDINGS B

royalsocietypublishing.org/journal/rspb

Research

Cite this article: Franke M, Geier B, Hammel JU, Dubilier N, Leisch N. 2021 Coming together—symbiont acquisition and early development in deep-sea bathymodioline mussels. *Proc. R. Soc. B* **288**: 20211044. https://doi.org/10.1098/rspb.2021.1044

Received: 4 May 2021
Accepted: 26 July 2021

Subject Category:
Development and physiology

Subject Areas:
developmental biology, microbiology

Keywords:
aposymbiotic, morphology, symbiosis, host–microbe interaction, bivalves, anatomy

Authors for correspondence:
Nicole Dubilier
e-mail: ndubilie@mpi-bremen.de
Nikolaus Leisch
e-mail: nleisch@mpi-bremen.de

Electronic supplementary material is available online at https://doi.org/10.6084/m9.figshare.c.5545388.

THE ROYAL SOCIETY PUBLISHING

Coming together—symbiont acquisition and early development in deep-sea bathymodioline mussels

Maximilian Franke[1,3], Benedikt Geier[1], Jörg U. Hammel[2], Nicole Dubilier[1,3] and Nikolaus Leisch[1]

[1]Max Planck Institute for Marine Microbiology, Celsiusstrasse 1, 28359 Bremen, Germany
[2]Helmholtz-Zentrum Hereon, Institute of Materials Physics, Max-Planck-Strasse 1, 21502 Geesthacht, Germany
[3]MARUM—Zentrum für Marine Umweltwissenschaften, University of Bremen, Leobener Strasse 2, 28359 Bremen, Germany

MF, 0000-0002-1930-1036; BG, 0000-0002-2942-2624; JUH, 0000-0002-6744-6811; ND, 0000-0002-9394-825X; NL, 0000-0001-7375-3749

How and when symbionts are acquired by their animal hosts has a profound impact on the ecology and evolution of the symbiosis. Understanding symbiont acquisition is particularly challenging in deep-sea organisms because early life stages are so rarely found. Here, we collected early developmental stages of three deep-sea bathymodioline species from different habitats to identify when these acquire their symbionts and how their body plan adapts to a symbiotic lifestyle. These mussels gain their nutrition from chemosynthetic bacteria, allowing them to thrive at deep-sea vents and seeps worldwide. Correlative imaging analyses using synchrotron-radiation based microtomography together with light, fluorescence and electron microscopy revealed that the pediveliger larvae were aposymbiotic. Symbiont colonization began during metamorphosis from a planktonic to a benthic lifestyle, with the symbionts rapidly colonizing first the gills, the symbiotic organ of adults, followed by all other epithelia of their hosts. Once symbiont densities in plantigrades reached those of adults, the host's intestine changed from the looped anatomy typical for bivalves to a straightened form. Within the Mytilidae, this morphological change appears to be specific to *Bathymodiolus* and *Gigantidas*, and is probably linked to the decrease in the importance of filter feeding when these mussels switch to gaining their nutrition largely from their symbionts.

1. Introduction

Mutualistic interactions between hosts and their microbiota play a fundamental role in the ecology and evolution of animal phyla. By associating with microbial symbionts, animals benefit from the metabolic capabilities of their symbionts and gain fitness advantages that allow them thrive in habitats they could not live in on their own [1]. Prime examples for such symbioses are bathymodioline mussels, which occur worldwide at cold seeps, hot vents, and whale and wood falls in the deep sea. Mussels of the genera *Bathymodiolus* and *Gigantidas* house chemosynthetic bacteria in their gills, in cells called bacteriocytes [2]. In these nutritional symbioses, the bacteria use reduced compounds in the vent and seep fluids as an energy source for carbon fixation, which in turn provides nutrition to their hosts. Two types of symbionts dominate bathymodioline mussels, sulfur-oxidizing (SOX) symbionts, whose main source of energy are reduced sulfur compounds, and methane-oxidizing symbionts (MOX), which gain their energy from oxidizing methane [3].

The transmission of symbionts from one generation to the next plays a central role in the ecology and evolution of mutualistic associations [4]. Symbionts

can be transmitted vertically from parent to offspring, intimately tying them to the reproduction and development of their host [4], as known from vesicomyid clams [5]. Alternatively, in horizontal transmission, symbionts are recruited each generation anew from the environment, and the symbiotic partners are physically separate from each other before the symbiosis is established [4]. In many hosts that rely on horizontal transmission, the acquisition of symbionts triggers morphological and developmental changes in the host. These can range from tissue rearrangements, known to be symbiont-induced in the *Euprymna* squid–*Vibrio* symbiosis [6], to largescale modifications of host organs, typically through hypertrophy [7], or the development of a novel symbiont-housing organ, like the trophosome of the tubeworm *Riftia pachyptila* [8]. As most of these symbioses are uncultivable, it is still unclear if these developmental changes are mediated by the host, actively induced by the symbiont or a mix of both.

Although bathymodioline mussels have been studied for over 40 years, very little is known about how their symbionts are transmitted, at which developmental stage the symbionts colonize the mussels, and how symbiont acquisition affects the development and body plan of the mussels [9]. It is assumed the symbionts are transmitted horizontally, based on phylogenetic studies that showed a lack of cospeciation between hosts and symbionts, as well as morphological studies that found no evidence for symbionts in the mussels' reproductive tissues [10–14]. In bathymodiolins of the genus *Idas*, commonly found at organic falls as well as seeps, the larvae remained aposymbiotic until they settled and developed the dissoconch shell, indicating a heterotrophic lifestyle in the larval dispersal phase, and horizontal acquisition of symbionts during or after metamorphosis [7,15].

Given the high abundance of *Bathymodiolus* and *Gigantidas* at vents and seeps worldwide, it is surprising that definitive evidence of an aposymbiotic early life stage of these mussels is lacking. The earliest life stages described so far had undergone metamorphosis and were already colonized by symbionts, with a well-developed symbiotic habitus that was indistinguishable from adult mussels [16]. As the early life stages of aposymbiotic *Bathymodiolus* and *Gigantidas* mussels have not yet been described, fundamental questions in the acquisition of symbionts in these bathymodioline genera have remained unanswered, including at which developmental stage the mussels acquire their symbionts, whether the SOX and MOX symbionts colonize their hosts at the same time, and which developmental changes occur in the mussels at the onset of symbiont colonization.

In this study, we were fortuitous in discovering very early, aposymbiotic life stages of three bathymodioline species, two from hydrothermal vents on the Mid-Atlantic Ridge (MAR), *Bathymodiolus puteoserpentis* and *B. azoricus*, and one from cold seeps in the Gulf of Mexico, *Gigantidas childressi* (originally described as '*B*'. *childressi* [17]). We used a correlative imaging approach by combining synchrotron-radiation based micro-computed tomography (SRμCT), correlative light (LM) and transmission electron microscopy (TEM), and complemented it with fluorescence *in situ* hybridization (FISH) to analyse the early life stages and compare them to their shallow water relative *Mytilus edulis* [18]. This approach allowed an integrative analysis of symbiont colonization and its effects on the host body plan, from the whole animal down to single host and symbiont cells.

2. Methods

(a) Sampling, fixation and sample preparation

Deep-sea mussels were collected from the sea floor with remotely operated vehicles (electronic supplementary material, table S1). *Mytilus edulis* were collected in the Baltic Sea at a site close to Kiel, Germany (electronic supplementary material, table S1). Samples were preserved for morphological, FISH and TEM analysis (electronic supplementary material, Methods a). All specimens were photographed and shell dimensions and shell margin limits were recorded as shown in electronic supplementary material, figure S1b–d (see also electronic supplementary material, Methods b, table S2). For histological analysis, all samples were post-fixed, embedded, serial sectioned and stained with a toluidine blue and sodium tetraborate solution. For TEM, semi-thin sections were re-sectioned according to [19] (electronic supplementary material, Methods c). Paraformaldehyde fixed samples were decalcified and DOPE-FISH was performed on embedded and sectioned samples using general and specific probes (electronic supplementary material, table S3, Methods d and e) [20]. Details of the light, fluorescence and electron microscopes used are found in electronic supplementary material, Methods f.

(b) SRμCT measurements

SRμCT datasets were recorded at the DESY using the P05 beamline of PETRA III, operated by the Helmholtz-Zentrum Hereon (Geesthacht, Germany [21]). The X-ray microtomography setup at 15–30 keV and 5× to 40× magnification was used to scan resin-embedded samples with attenuation contrast and uncontrasted samples in PBS-filled capillaries [22] with propagation-based phase contrast. Scan parameters are summarized in electronic supplementary material, table S4. The tomography data were processed with custom scripts implemented in the ASTRA toolbox [23–25] (electronic supplementary material, Methods g).

(c) Correlative workflow for SRμCT, light and electron microscopy, and FISH

Section series were screened by eye to identify individual host cells and predict symbiont colonization state based on three morphological characteristics: hypertrophy, loss of microvilli and loss of cilia (table 1, electronic supplementary material, Methods i). The location and symbiont colonization state of the analysed host cells was marked using Cell Counter in Fiji [26]. The analysed sections were re-sectioned and the same fields of view were recorded with TEM (electronic supplementary material, figure S2). To validate the LM-based predictions, symbionts were identified in TEM images based on their morphology (electronic supplementary material, video S5).

(d) Image processing and three-dimensional visualization

Microscopy images were adjusted and figures composed using Fiji, Adobe Photoshop and Adobe Illustrator 2021. LM-images were stitched and aligned with TrackEM2 [27] in Fiji. Amira 2020.2 (ThermoFisher Scientific) was used to generate three-dimensional models from LM and μCT datasets. Co-registration between μCT, LM and TEM datasets was carried out after [19] (electronic supplementary material, Methods j).

3. Results

We analysed developmental stages of *B. puteoserpentis*, *B. azoricus* and *G. childressi* ranging from aposymbiotic pediveligers to symbiotic adults, to determine at which stage the

Table 1. Overview of number of individuals analysed for each species, developmental stage, and imaging method. The numbers correspond from left to right to *B. puteoserpentis* (black), *B. azoricus* (dark yellow) and *B. childressi* (blue).

method	pediveliger			metamorphosis			plantigrade			juvenile			adult		
SRμCT/μCT	–	–	–	–	–	–	–	–	–	1	2	–	–	2	1
SRμCT + serial sectioning + LM	1	–	–	1	–	–	2	1	–	1	–	–	–	–	–
SRμCT + serial sectioning + LM +TEM	–	–	1	–	–	–	–	–	–	–	–	–	–	–	–
serial sectioning + LM	2	1	–	2	1	2	–	1	2	–	–	–	–	–	–
serial sectioning + LM + TEM	2	1	–	2	–	–	3	–	–	–	–	–	–	–	–
FISH	2	–	–	1	–	–	3	–	–	1	–	–	–	–	–
total	**7**	**2**	**1**	**6**	**1**	**2**	**8**	**2**	**2**	**3**	**2**	**–**	**–**	**2**	**1**

symbionts colonize their hosts, and the developmental modifications that these mussels have evolved to adapt to their symbiotic lifestyle (figure 1; electronic supplementary material, figures S3 and S4). Because the names for larval stages of bivalves have not always been used consistently, we define them as follows. The earliest life stages in our study were at the last planktonic larval stage—the pediveliger. Once settled on the seafloor, the animal initiates its metamorphosis from a planktonic to a benthic lifestyle, and we refer to this stage as being in metamorphosis. While metamorphosing, the mussel degrades its velum, the larval feeding and swimming organ, and develops into a plantigrade [28]. During the plantigrade stage, the mussel secretes the adult shell and once the ventral groove of the gills, which transports particles to the labial palps, is formed, it enters the juvenile stage [29]. When the gonads are developed, the mussel is considered an adult [18].

(a) Identification of developmental stages

We measured the shell lengths of 259 specimens: 129 *B. puteoserpentis*, 124 *B. azoricus* and 6 *G. childressi* individuals. We assume that these had already settled or were in the process of settling, as we collected them from mussel beds on the sea floor. The specimens ranged from 370 µm to 4556 µm shell length (electronic supplementary material, tables S2 and S5). The earliest developmental stages were pediveligers, with shell lengths of 366–465 µm. Developmental stages could only be identified through detailed analyses of the mussels' soft body anatomy (electronic supplementary material, figure S1a,b). These analyses revealed that the shell sizes of 58 pediveligers and mussels in metamorphosis overlapped with those of the smallest plantigrade stages (electronic supplementary material, figure S1f).

(b) Morphological characterization of *Bathymodiolus* and *Gigantidas* developmental stages

For our morphological analyses, we analysed 39 individuals (table 1). *Bathymodiolus puteoserpentis* specimens were best preserved and covered the widest range of developmental stages. We therefore focussed our detailed morphological analyses on *B. puteoserpentis*, and compared these with selected *B. azoricus* and *G. childressi* stages (electronic supplementary material, figures S3 and S4). In the following, we describe the shared morphological features of all three species unless specified otherwise.

The pediveliger larvae were characterized by the presence of a velum, a fully developed digestive system, a foot with two pairs of retractor muscles and two gill baskets (figure 1*a*; electronic supplementary material, table S6, figure S5a,d and video S1). The digestive system consisted of the mouth, oral labial palps, oesophagus, stomach, two digestive glands, gastric shield, the style sac with crystalline style, mid gut, s-shaped looped intestine and anal papillae (figure 1*a*; electronic supplementary material, figure S6). The diverticula of the digestive glands and the epithelia of the stomach contained membrane-bound lipid vesicles (figure 1; electronic supplementary material, figures S6 and S7). The gill baskets on each side of the foot (figure 1*a*; electronic supplementary material, figure S6) consisted of three to four single gill filaments in *B. puteoserpentis* and five in *B. azoricus* and *G. childressi* (electronic supplementary material, figure S3b,*c*). These filaments form the descending lamella of the inner demibranch in later life stages. For further details, see electronic supplementary material, Note 1.

In mussels undergoing metamorphosis, the first steps from a planktonic to a benthic lifestyle were visible in the degradation of the velum (electronic supplementary material, figure S5) and the appearance of byssus threads (electronic supplementary material, figure S8). Rearrangements of all organs occurred in this stage, for example, the alignment of the growth axis of the gill 'basket' with the length axis of the mussel (figure 1*a–c*; electronic supplementary material, figure S9 and video S2). The number of gill filaments increased by one in all species (electronic supplementary material, figure S6). Furthermore, gill filaments separated from each other, increasing the gaps between them from 47 µm to 120 µm (figure 1*c*). In the digestive gland and stomach epithelia, the number and volume of lipid vesicles decreased from 12.8% of the soft body volume in pediveligers, to 3.9% in metamorphosing mussels, 1.5% in plantigrades, and were no longer present in juveniles and adults (figure 1*a–d*; electronic supplementary material, table S6). The organs involved in filter feeding also changed. In pediveligers, the main feeding organ was the velum, which collects particles from the seawater and transports them to the oral labial palps and mouth. After the degradation of the velum, particle sorting was taken over by the highly ciliated foot (electronic supplementary material, figures S5, S8 and S9) in metamorphosing mussels, and by the gills in late plantigrades and juveniles. The plantigrade stage began once the mussels secreted the dissoconch and completed metamorphosis (electronic supplementary material, figures S1 and S10). As the mussels transitioned from the plantigrade to the juvenile stage, the digestive system straightened (figure 1*c,d*; electronic supplementary material, figure S11 and videos S3 and S4). This morphological change was most prominent in the intestine,

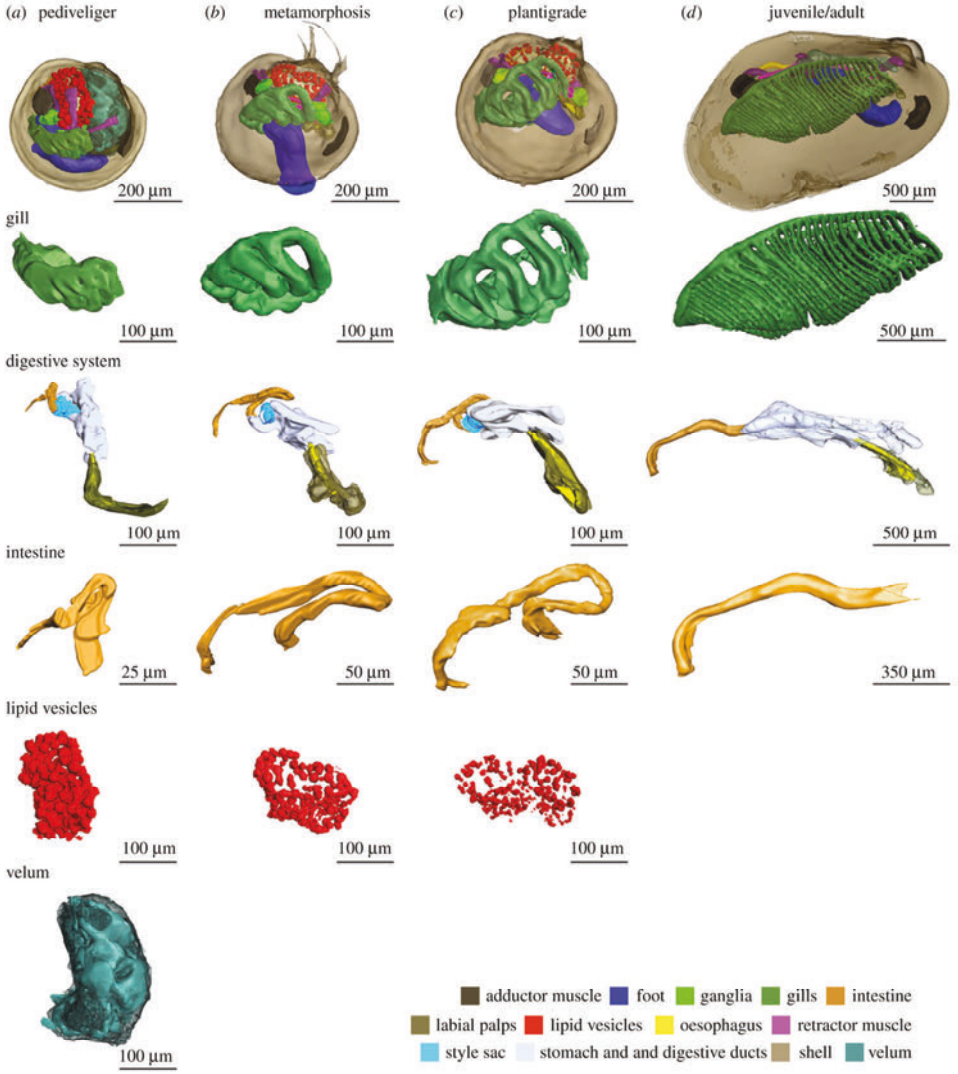

Figure 1. Three-dimensional visualization of section series and SRµCT measurements of *B. puteoserpentis* developmental stages based on analyses of four individuals for each stage. Note the different scale bars.

which went from a looped to a straight shape and remained straight in all later developmental stages (figure 1*c,d*; electronic supplementary material, figure S11). For further details see electronic supplementary material, Note 2.

(c) Establishment of the symbiosis

Central to an accurate assessment of symbiont colonization and symbiont-mediated morphological changes was our correlative approach, which combined SRµCT, light and electron microscopy (electronic supplementary material, video S5 and figure S2) and was complemented with FISH. This allowed us to rapidly screen whole animals, yet achieve the resolution needed to identify the colonization of single eukaryotic cells by symbiotic bacteria. We first searched for a morphological characteristic that was visible using light microscopy and reliably revealed the presence of symbionts in host cells. Previous studies [30,31] showed that in juvenile and adult *Bathymodiolus* mussels, the morphology of epithelial cells colonized by symbionts is fundamentally altered: (i) the microvilli that cover all epithelial cells are lost (known as microvillar effacement) and (ii) epithelial cells become hypertrophic (swollen) compared to aposymbiotic cells. We identified a third characteristic change in epithelial cells colonized by symbionts that has not received much attention, namely the loss of cilia (figure 2*c, f,i*). We tested if these three morphological characteristics had predictive power for symbiont colonization by analysing 1965 epithelial cells from a subset of seven *B. puteoserpentis*

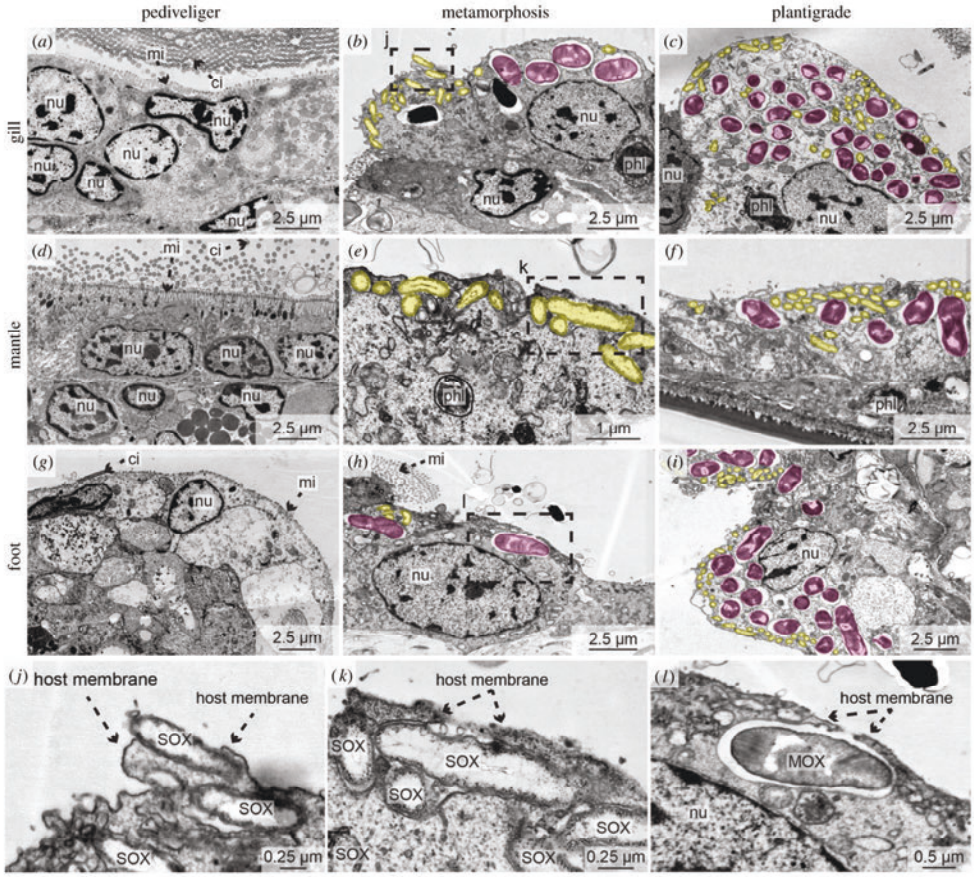

Figure 2. Symbionts first colonize *Bathymodiolus puteoserpentis* during metamorphosis. TEM micrographs of gills (*a–c*), mantle (*d–f*) and foot (*g–i*) epithelial tissues of pediveligers (*a,d,g*), metamorphosing mussels (*b,e,h*) and plantigrades (*c,f,i*). SOX (yellow) and MOX symbionts (magenta) are highlighted with colour overlays for visibility reasons (*a–i*). All epithelial tissues of pediveligers were aposymbiotic (*a,d,g*). Colonization by the SOX and MOX symbionts was first observed during metamorphosis (*b,e,h*). In plantigrades, all epithelial tissues were colonized by both symbiont types (*c,f,i*). Dashed boxes indicate regions in which symbionts were in the process of colonizing epithelial tissue (shown magnified in *j–l*). ci, cilia; mi, microvilli; MOX, methane-oxidizing symbiont; nu, nucleus; phl, phagolysosome; SOX, sulfur-oxidizing symbiont. For raw image data see electronic supplementary material, figure S14.

individuals (table 1) and comparing LM images of these cells with their correlated TEM images. Our analyses revealed that all cells predicted to have symbionts in the LM dataset were indeed colonized in the TEM dataset, and likewise, all cells predicted to be aposymbiotic were free of symbionts (electronic supplementary material, figure S2). Our approach allowed us to identify host cells that were colonized by only a few SOX symbionts based on the absence of microvilli and cilia, indicating that these are lost immediately after the first symbionts colonize host cells (figure 2*e*). We next used our verified morphological characters to reveal the onset of symbiont colonization in *B. puteoserpentis* in this subset of seven mussels. All pediveliger cells were free of symbionts ($n = 797$ host cells in two pediveliger). In the metamorphosing mussels examined with our correlative approach 1–15% ($n = 488$ host cells in two metamorphosing mussels) and in plantigrades 21–26% ($n = 680$ host cells in three plantigrades) of all analysed gill, mantle, foot and retractor muscle epithelia cells were colonized by symbionts.

We then expanded our analyses to LM on another 10 *B. puteoserpentis* individuals (table 1). These analyses confirmed our results from the correlative dataset: All additional pediveligers ($n = 3$) and metamorphosing mussels were aposymbiotic ($n = 3$), all additional plantigrades ($n = 2$) and juveniles ($n = 2$) were colonized by symbionts. Finally, we performed FISH on another seven *B. puteoserpentis* individuals (table 1). These analyses corroborated our LM data on the timing of symbiont colonization, with all pediveliger aposymbiotic and symbiont colonization beginning at metamorphosis (figure 3; electronic supplementary material, figures S12 and S13).

Our correlative workflow revealed that pediveliger were aposymbiotic in all three mussel species (figure 2*a,d,g*; electronic supplementary material, figure S15a,c). Interestingly, two of the aposymbiotic *B. puteoserpentis* pediveligers had bacterial morphotypes similar to the SOX and MOX symbionts attached to the outside of their shell (electronic supplementary material, figure S16). Mussels that were undergoing

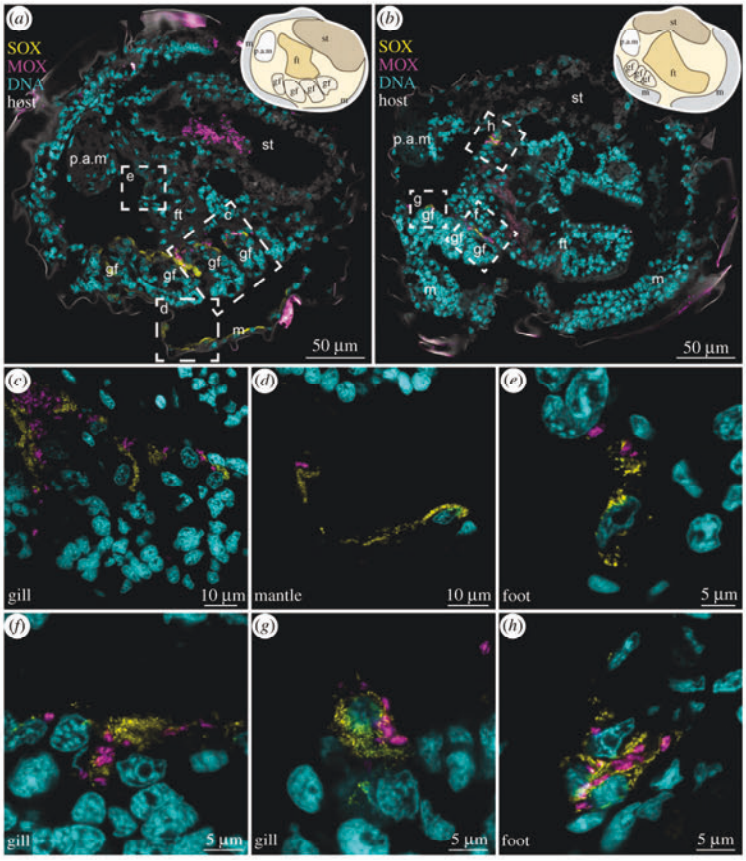

Figure 3. SOX and MOX symbionts colonize all epithelial tissues in *Bathymodiolus puteoserpentis* plantigrades. False-coloured FISH images show probes specific for SOX (yellow, BMARt-193) and MOX symbionts (magenta, BMARm-845) and host nuclei stained with DAPI (cyan). Sagittal cross-sections of two individuals (*a*,*b*) show SOX and MOX symbionts in the gill, foot and mantle epithelia. Schematic drawings of the anatomy are provided in the top right corners. To visualize host tissue autofluorescence is shown in grey in (*a*) and (*b*). Dashed boxes indicate magnified regions of the colonized gill, mantle and foot region shown in (*c*–*h*). ft, foot; m, mantle; gf, gill filament; p.a.m, posterior adductor muscle; st, stomach.

metamorphosis were the earliest developmental stage in which we found symbionts in all three host species, with a shell length of 432 µm in the smallest *B. puteoserpentis* individual, 510 µm in *B. azoricus*, and 383 µm in *G. childressi*. In these metamorphosing mussels, we observed symbionts in epithelial cells of the gill filaments, mantle, foot and retractor muscle (figure 2*b*,*e*,*h*, *j*–*l*; electronic supplementary material, figure S15). Once symbiont colonization began, gill tissue morphology was similar to that of adult mussels [30–32]: the majority of gill cells were symbiont-containing bacteriocytes without microvilli or cilia, whereas the only gill cells without symbionts were those at the ventral ends of the gill filaments and at the frontal-to-lateral zones along the length of the filaments, as well as the intercalary cells (electronic supplementary material, figures S6, S9 and S10). In addition to the gills, the epithelial tissues of the mantle, foot and retractor muscles also had symbionts in all three host species (figure 2*c*,*f*,*i*; electronic supplementary material, figure S15). We never observed other bacteria besides the two symbionts in any of the developmental stages, including the intranuclear parasite that infects these mussels, based on FISH analyses with symbiont-specific and eubacterial probes of *B. puteoserpentis*, and TEM analyses of symbiont morphology of *B. puteoserpentis*, *B. azoricus* and *G. childressi* specimen (figures 2 and 3; electronic supplementary material, figures S12, S13 and S15).

The superior preservation of *B. puteoserpentis* specimens allowed us to analyse the process of symbiont colonization in this species in more detail. We first found evidence of symbiont colonization in metamorphosing mussels that had only a few bacteria in gill, mantle and foot epithelial (figure 2*b*,*e*,*h*,*j*–*l*). Bacterial density per gill cell was the lowest in metamorphosing mussels with 13.7% (±6.3) of the host cell area occupied by symbionts, and steadily increased in later developmental stages, reaching up to 29.0% (±5.0) in plantigrades and 32.1% (±6.1) in adult mussels (electronic supplementary material, table S7). With the onset of symbiont colonization, we observed phagolysosomal digestion of the symbionts in all epithelial cells, even those with only very few symbionts

(figure 2*b*,*c*,*e*,*f*). The process of symbiont colonization appeared to be extremely rapid. Nearly all metamorphosing mussels had either no symbionts at all, or all of their epithelial tissues were colonized. In only two out of six individuals, we occasionally observed SOX and MOX symbionts that were not completely engulfed by the host's apical cell membrane, which we interpreted as ongoing colonization (figure 2*j–l*). These first steps in colonization were particularly common in mantle epithelial cells, while in the same specimen the gill epithelial cells were already fully colonized (figure 2*b*,*e*,*f*). Furthermore, in host cells where colonization was ongoing, we observed that these were colonized only by SOX (figure 2*e*), or by both SOX and MOX (figure 2*h*), but we never observed host cells only colonized by MOX symbionts.

4. Discussion

(a) Post-metamorphosis development in *Bathymodiolus* and *Gigantidas* deviates from the mytilid blueprint

Our study shows that the use of shell characteristics alone to determine developmental stages of deep-sea mussels is not reliable (e.g. [16]), particularly for shell lengths of settling pediveligers and early plantigrades. Our analyses of shell lengths in developmental stages of the three mussel species revealed an overlap in size of 50 µm between pediveligers and plantigrades. This inconsistency in shell lengths between developmental stages indicates that metamorphosis begin is not dependent on size, and provides further evidence for the ability of mussels to delay metamorphosis while continuing to grow, as previously suggested for *G. childressi* [33]. Such a delay could be due to a lack of settlement cues or limited nutrition, similar to what is known from *M. edulis* [34]. Delaying metamorphosis would favour dispersal, potentially leading to an increase in geographical distribution and the colonization of new and remote habitats [35].

The pre-metamorphosis development of *Bathymodiolus* and *Gigantidas* mussels is similar to that of their close relatives from the genus *Idas* [7,15] and shallow water mytilids such as *M. edulis* [18,29,36]. The pediveligers of *Bathymodiolus*, *Gigantidas*, *Idas* and *Mytilus* have a large velum, foot, mantle epithelium, digestive system, central nerve system and two preliminary gill baskets consisting of three to five gill buds [7,15,18]. During metamorphosis, the velum is degraded, organs within the mantle cavity are rearranged and the lipid vesicles in the digestive diverticula and stomach are reduced. In early developmental stages of mussels from the *Mytilidae*, lipid vesicles serve as storage compounds to fuel the energy-demanding process of metamorphosis [18] and they probably have a similar function in *Bathymodiolus* and *Gigantidas*. Furthermore, these lipid vesicles could provide energy for movement of the pediveligers during their searches for sites to settle [37,38].

Although early development appears to be conserved across *Bathymodiolus*, *Gigantidas*, *Idas* and their shallow water relatives, marked differences occur as soon as symbiont colonization begins in the deep-sea mytilids. All colonized epithelial cells lost not only their microvilli but also their cilia, and developed a hypertrophic habitus, as previously shown for gill bacteriocytes [7,30,31]. If the symbionts of *Bathymodiolus* and *Gigantidas* actively induce these cellular changes or if these are a response by the host to symbiont colonization remains unresolved, but our data shows that these processes were tightly linked spatially and temporally. Furthermore, our correlative analyses demonstrate that these cell surface modifications serve as reliable markers for the state of symbiont colonization. Observations of effacement of cilia and microvilli have been reported for a wide range of bacteria that invade epithelia, particularly pathogens, and for these it also remains to be shown if the bacteria or the host drive these processes [39–41].

Although it has been known for several decades that the symbionts of *Bathymodiolus* and *Gigantidas* mussels supply their host with nutrition, and that adults possess only a rudimentary gut, nothing was known about the development of the digestive system in these mussels. We observed a straightening of the digestive system after completion of metamorphosis in all three species (figure 4). The stomach and the intestine straightened and the digestive system changed from the complex looped type found in *Mytilus* to the straight type seen in adults of bathymodioline mussels (electronic supplementary material, table S8). This transformation is striking, as in mytilids like *M. edulis*, such drastic morphological changes after metamorphosis are not known [42]. In *Bathymodiolus* and *Gigantidas*, the straightening of the digestive system did not coincide with the first stages of symbiont colonization or metamorphosis, but rather occurred during the transition from the plantigrade to the juvenile stage, well after metamorphosis and only when these hosts had become fully colonized by their symbionts (figure 4).

In general, the morphology of an animal's gastrointestinal tract reflects its food sources. Animals that digest complex foods possess enlarged compartments and lengthened gastrointestinal structures to slow down the flow of digested material and increase the breakdown of complex molecules [43]. We hypothesize that the straightening of the digestive system in the vent and seep mussels we analysed here was induced by their shift from filter feeding to gaining nutrition from their symbionts. The straightening of the digestive tract could be an evolutionary adaptation to minimize the energy needed for maintaining the digestive tract once the majority of nutrition is gained through intracellular digestion of symbionts in the bacteriocytes.

Not all bathymodiolins have a straightened digestive system. *Idas* intestines are complex with one or more loops [7,15,44]. These small mussels are commonly found at organic falls, which typically have higher inputs of organic matter than vents and seeps. Also, symbiont abundances are lower in *Idas* than in the large vent and seep bathymodiolins, indicating that *Idas* mussels may depend more on filter feeding than their larger relatives. Intriguingly, the relatively large adults of the bathymodioline genus *Vulcanidas* have a pronounced looped intestine despite high symbiont abundances [45]. *Vulcanidas* inhabits relatively shallow hydrothermal vents close to the photic zone (140 m compared to 1000–2500 m depth for the mussels in our study) where more organic material from the photic zone is available for their nutrition. It is thus likely that filter feeding plays a greater role in the nutrition of *Idas* and *Vulcanidas* than in the three species analysed in this study. These findings raise the question whether the straightening of the digestive tract is a conserved developmental trait in only some genera, or if the environment and availability of organic matter and other non-symbiotic food sources drives the morphology of the digestive tract in bathymodioline mussels.

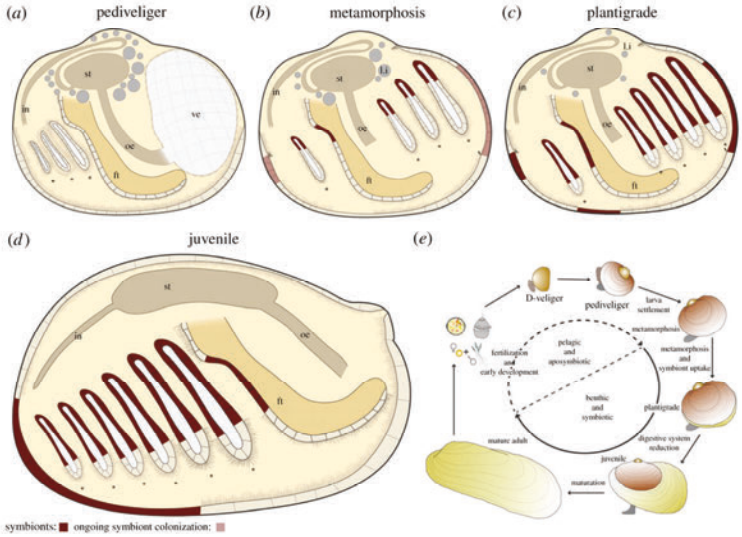

Figure 4. Summary of symbiont colonization and development of *Bathymodiolus* and *Gigantidas* mussels. Pediveliger are aposymbiotic (*a*), and symbiont colonization begins in metamorphosing mussels (*b*). By the plantigrade (*c*) and juvenile (*d*) stages, all epithelial tissues are fully colonized by symbionts. The digestive system is reduced between the plantigrade and juvenile stages, changing from a looped to a straight morphology. (*e*) Schematic of the hypothetical life cycle of bathymodioline mussels indicating the aposymbiotic pelagic developmental stages and the symbiotic benthic developmental stages. ft, foot; gf, gill filament; in, intestine; l.i, lipid inclusion; oe, oesophagus.

(b) Symbiont colonization begins during the plantigrade stage as soon as the velum is degraded

As recently highlighted, how and when *Bathymodiolus* and *Gigantidas* mussels acquire their symbionts has remained, as yet, unclear [9]. Here, we used correlative imaging analyses to reveal that the early developmental stages of two *Bathymodiolus* and one *Gigantidas* species were aposymbiotic, and narrowed the window of symbiont acquisition to mussels undergoing metamorphosis (figure 4). Our analyses revealed that the symbionts colonize the gills only after the velum is lost. As long as the velum is present and active, particles from the surrounding seawater are either transported directly into the digestive system or expelled from the mussel. In *M. edulis*, once the velum is degraded the gill filaments separate further from each other and take over the task of sorting food particles and generating a water current [18,29]. Beginning in the late plantigrade stage of *Bathymodiolus*, we identified a similar increase of space between the gill filaments. Given that the developmental changes in the morphology of the bathymodiolin gills are so similar to those of *M. edulis* [7,15,18,29], it is likely that the functional roles of the gills in *Bathymodiolus* change in a similar manner as in *M. edulis*: The pediveligers' gills of *Bathymodiolus* are used for respiration only, and then become responsible for water current generation in late metamorphosing mussels, and the sorting of particles in plantigrades and juveniles. We hypothesize that this functional shift of the gills plays an important role in enabling the symbionts to adhere to the gill epithelium and initiate symbiont colonization.

The initial colonization of the host by its symbionts appears to be rapid, based on our observation that 22 out of 24 *B. puteoserpentis* individuals were either completely aposymbiotic or fully colonized, and the first stages of symbiont colonization were only visible in two metamorphosing mussels. As we were working with preserved samples that represent a snapshot of development, the chance of observing a process depends on how often it occurs and how long it takes. The less frequent or the faster a process happens, the smaller the chance of observing it. We therefore conclude that symbiont colonization occurs rapidly in *B. puteoserpentis*, given the small percentage of individuals in which we observed the first steps of colonization. Symbiont colonization seems to be even more rapid than in *I. simpsoni* and *I. modiolaeformis* [7,15]. This could reflect the importance for *Bathymodiolus* mussels to quickly acquire symbionts once they have nearly consumed their internal energy reserves and settled in an environment that lacks energy-rich planktonic nutrition [46].

We found symbionts in epithelial cells of the gills, mantle, foot and retractor muscle in the plantigrades and juveniles of all three bathymodioline species, similar to previous studies [16,47,48]. Previous work suggested that the symbionts first colonize the mantle epithelia, and from there colonize gill cells, as the first gill filaments are formed from mantle tissues [47]. Our data contradicts this assumption, as the gills had already begun to develop in pediveligers before the onset of symbiont colonization. Furthermore, in two *B. puteoserpentis* specimens we detected fully colonized gills, while the mantle tissue was still in the process of being colonized. Our findings indicate that symbionts first colonize gill cells before colonizing other epithelial tissues, and that the SOX symbionts colonize individual host cells first, before the MOX.

Our analyses revealed that *B. puteoserpentis*, *B. azoricus* and *G. childressi* larvae are aposymbiotic during their planktonic phase and first acquire their symbionts when they transition to a benthic lifestyle. The timing of symbiont acquisition and major developmental changes was similar in all three species, and, with the exception of the digestive system, corresponds to observations of early life stages of *Idas* [7,9,15]. These similarities in developmental biology and symbiont acquisition suggest that these traits are conserved in bathymodiolins. The acquisition of symbionts after settlement allows these mussels to recruit locally adapted symbionts. As the geochemistry of vent and seep environments varies strongly across spatial scales [49], recruiting locally adapted symbiont populations would confer a strong fitness advantage to these hosts. Indeed, recent studies have revealed that *Bathymodiolus* mussels host multiple strains of symbionts that vary in key functions, such as the use of energy and nutrient sources, electron acceptors and viral defence mechanisms [50,51]. By acquiring their symbionts from the sites where they settle, bathymodioline mussels can establish symbioses with those strains that are best adapted to the local environment.

5. Conclusion and outlook

Our correlative imaging workflow revealed the intricate developmental processes from the subcellular to the whole animal scale that are thought to be triggered when deep-sea mussels acquire their symbionts. Furthermore, we identified the narrow window in which symbiont acquisition begins and showed the morphological changes of the digestive system following symbiont uptake. Given that we never observed bacterial morpho- or phylotypes other than the known SOX and MOX symbionts, even in the earliest larval life stages, strong recognition mechanisms must ensure this high specificity. Now that we have identified when and how symbiont colonization occurs in *Bathymodiolus* and *Gigantidas*, a spatial and temporal transcriptomic approach could shed light on the underlying molecular mechanisms of symbiont recognition, acquisition and maintenance, and further our understanding of the entwined dialogue between animal hosts and their microbial symbionts.

Data accessibility. LM data, µCT-data and videos are available on figshare [52].

Authors' contributions. M.F.: conceptualization, data curation, formal analysis, investigation, methodology, visualization, writing—original draft, writing—review and editing; B.G.: data curation, formal analysis, visualization, writing—review and editing; J.U.H.: data curation, formal analysis, resources, writing—review and editing; N.D.: conceptualization, funding acquisition, resources, supervision, writing—review and editing; N.L.: conceptualization, data curation, formal analysis, investigation, methodology, project administration, supervision, visualization, writing—original draft, writing—review and editing.

All authors gave final approval for publication and agreed to be held accountable for the work performed therein.

Competing interests. We declare we have no competing interests.

Funding. Funding was provided by the Max Planck Society, the MARUM Cluster of Excellence 'The Ocean Floor' (Deutsche Forschungsgemeinschaft (German Research Foundation) under Germany's Excellence Strategy—EXC-2077-39074603), a Gordon and Betty Moore Foundation Marine Microbial Initiative Investigator Award (grant no. GBMF3811 to N.D.) and a European Research Council Advanced Grant (BathyBiome, grant no. 340535 to N.D.). µCT measurements were performed at the DESY under the proposal IDs: 20170337 and 20180295.

Acknowledgements. We thank the captains, crew members and ROV pilots of the cruises M126, M82-3 and NA58. We are grateful to Christian Borowski and Stéphane Hourdez for their valuable contributions to collecting mussel larvae and Wiebke Ruschmeier for her help in the laboratory. We thank all involved in supporting us at the DESY at the P05 beamline of PETRA III (Helmholtz-Zentrum Hereon, Geesthacht, Germany). We also thank Benjamin Cooper (Max-Planck Institute for Experimental Medicine, Göttingen) for preliminary sample preparation, and Bernhard Ruthensteiner (Zoologische Staatsammlung München) and Frank Melzner (GEOMAR, Kiel) for fruitful discussions.

References

1. McFall-Ngai M *et al.* 2013 Animals in a bacterial world, a new imperative for the life sciences. *Proc. Natl Acad. Sci. USA* **110**, 3229–3236. (doi:10.1073/pnas.1218525110)
2. Dubilier N, Bergin C, Lott C. 2008 Symbiotic diversity in marine animals: the art of harnessing chemosynthesis. *Nat. Rev. Microbiol.* **6**, 725–740. (doi:10.1038/nrmicro1992)
3. DeChaine E, Cavanaugh CM. 2005 Symbioses of methanotrophs and deep-sea mussels (*Mytilidae*: *Bathymodiolinae*). *Prog. Mol. Subcell. Biol.* **41**, 227–249. (doi:10.1007/3-540-28221-1_11)
4. Bright M, Bulgheresi S. 2010 A complex journey: transmission of microbial symbionts. *Nat. Rev. Microbiol.* **8**, 218–230. (doi:10.1038/nrmicro2262)
5. Endow K, Ohta S. 1990 Occurrence of bacteria in the primary oocytes of vesicomyid clam *Calptogena soyoae*. *Mar. Ecol. Prog. Ser.* **64**, 309–311. (doi:10.3354/meps064309)
6. Montgomery MK, McFall-Ngai M. 1994 Bacterial symbionts induce host organ morphogenesis during early postembryonic development of the squid *Euprymna* scolopes. *Development* **120**, 1719–1729. (doi:10.1242/dev.120.7.1719)
7. Laming SR, Duperron S, Cunha MR, Gaudron SM. 2014 Settled, symbiotic, then sexually mature: adaptive developmental anatomy in the deep-sea, chemosymbiotic mussel *Idas modiolaeformis*. *Mar. Biol.* **161**, 1319–1333. (doi:10.1007/s00227-014-2421-y)
8. Nussbaumer AD, Fisher CR, Bright M. 2006 Horizontal endosymbiont transmission in hydrothermal vent tubeworms. *Nature* **441**, 345–348. (doi:10.1038/nature04793)
9. Laming SR, Gaudron SM, Duperron S. 2018 Lifecycle ecology of deep-sea chemosymbiotic mussels: a review. *Front. Mar. Sci.* **5**, 282. (doi:10.3389/fmars.2018.00282)
10. Fontanez KM, Cavanaugh CM. 2014 Evidence for horizontal transmission from multilocus phylogeny of deep-sea mussel (*Mytilidae*) symbionts. *Environ. Microbiol.* **16**, 3608–3621. (doi:10.1111/1462-2920.12379)
11. Won YJ, Hallam SJ, O'Mullan GD, Pan IL, Buck KR, Vrijenhoek RC. 2003 Environmental acquisition of thiotrophic endosymbionts by deep-sea mussels of the genus *Bathymodiolus*. *Appl. Environ. Microbiol.* **69**, 6785–6792. (doi:10.1128/aem.69.11.6785-6792.2003)
12. Won YJ, Jones WJ, Vrijenhoek RC. 2008 Absence of cospeciation between deep-sea mytilids and their thiotrophic endosymbionts. *J. Shellfish Res.* **27**, 129–138. (doi:10.2983/0730-8000(2008)27[129:AOCBDM]2.0.CO;2)
13. Russell SL, Pepper-Tunick E, Svedberg J, Byrne A, Ruelas Castillo J, Vollmers C, Beinart RA, Corbett-Detig R. 2020 Horizontal transmission and recombination maintain forever young bacterial symbiont genomes. *PLoS Genet.* **16**, e1008935. (doi:10.1371/journal.pgen.1008935)

14. Gaudron SM, Demoyencourt E, Duperron S. 2012 Reproductive traits of the cold-seep symbiotic mussel *Idas modiolaeformis*: gametogenesis and larval biology. *Biol. Bull.* **222**, 6–16. (doi:10.1086/bblv222n1p6)
15. Laming SR, Duperron S, Gaudron SM, Hilario A, Cunha MR. 2015 Adapted to change: the rapid development of symbiosis in newly settled, fast-maturing chemosymbiotic mussels in the deep sea. *Mar. Environ. Res.* **112**, 100–112. (doi:10.1016/j.marenvres.2015.07.014)
16. Salerno JL, Macko SA, Hallam SJ, Bright M, Won YJ, McKiness Z, Van Dover CL. 2005 Characterization of symbiont populations in life-history stages of mussels from chemosynthetic environments. *Biol. Bull.* **208**, 145–155. (doi:10.2307/3593123)
17. Gustafson RG, Turner RD, Lutz RA, Vrijenhoek RC. 1998 A new genus and five new species of mussels (Bivalvia, Mytilidae) from deep-sea sulfide/hydrocarbon seeps in the Gulf of Mexico. *Malacologia* **40**, 63–112.
18. Bayne BL. 1971 Some morphological changes that occur at the metamorphosis of the larvae of *Mytilus edulis*. In *The Fourth European Marine Biology Symposium*, pp. 259–280. London, UK: Cambridge University Press.
19. Handschuh S, Baeumler N, Schwaha T, Ruthensteiner B. 2013 A correlative approach for combining microCT light and transmission electron microscopy in a single 3D scenario. *Front. Zool.* **10**, 44. (doi:10.1186/1742-9994-10-44)
20. Stoecker K, Dorninger C, Daims H, Wagner M. 2010 Double labeling of oligonucleotide probes for fluorescence in situ hybridization (DOPE-FISH) improves signal intensity and increases rRNA accessibility. *Appl. Environ. Microbiol.* **76**, 922–926. (doi:10.1128/AEM.02456-09)
21. Wilde F *et al.* 2016 Micro-CT at the imaging beamline P05 at PETRA III. *AIP Conf. Proc.* **1741**, 030035. (doi:10.1063/1.4952858)
22. Geier B *et al.* 2019 Correlative 3D anatomy and spatial chemistry in animal-microbe symbioses: developing sample preparation for phase-contrast synchrotron radiation based micro-computed tomography and mass spectrometry imaging. In *SPIE optical engineering+applications* (eds B Müller, G Wang). San Diego, CA: SPIE.
23. Moosmann J, Ershov A, Weinhardt V, Baumbach T, Prasad MS, LaBonne C, Xiao X, Kashef J, Hofmann R. 2014 Time-lapse X-ray phase-contrast microtomography for *in vivo* imaging and analysis of morphogenesis. *Nat. Protoc.* **9**, 294. (doi:10.1038/nprot.2014.033)
24. van Aarle W, Palenstijn WJ, De Beenhouwer J, Altantzis T, Bals S, Batenburg KJ, Sijbers J. 2015 The ASTRA toolbox: a platform for advanced algorithm development in electron tomography. *Ultramicroscopy* **157**, 35–47. (doi:10.1016/j.ultramic.2015.05.002)
25. van Aarle W, Palenstijn WJ, Cant J, Janssens E, Bleichrodt F, Dabravolski A, De Beenhouwer J, Joost Batenburg K. Sijbers J. 2016 Fast and flexible X-ray tomography using the ASTRA toolbox. *Opt. Exp.* **24**, 25 129–25 147. (doi:10.1364/oe.24.025129)
26. Schindelin J *et al.* 2012 Fiji: an open-source platform for biological-image analysis. *Nat. Methods* **9**, 676–682. (doi:10.1038/nmeth.2019)
27. Cardona A, Saalfeld S, Schindelin J, Arganda-Carreras I, Preibisch S, Longair M, Tomancak P, Hartenstein V, Douglas RJ. 2012 TrakEM2 software for neural circuit reconstruction. *PLoS ONE* **7**, e38011. (doi:10.1371/journal.pone.0038011)
28. Baker P, Mann R. 1997 The postlarval phase of bivalve mollusks: a review of functional ecology and new records of postlarval drifting of Chesapeake Bay bivalves. *Bull. Mar. Sci.* **61**, 409–430.
29. Cannuel R, Beninger PG, Mc Combie H, Boudry P. 2009 Gill development and its functional and evolutionary implications in the blue mussel *Mytilus edulis*. *Biol. Bull.* **217**, 173–188. (doi:10.1086/BBLv217n2p173)
30. Fisher CR, Childress JJ, Oremland RS, Bidigare RR. 1987 The importance of methane and thiosulfate in the metabolism of the bacterial symbionts of two deep-sea mussels. *Mar. Biol.* **96**, 59–71. (doi:10.1007/BF00394838)
31. Wentrup C, Wendeberg A, Schimak M, Borowski C, Dubilier N. 2014 Forever competent: deep-sea bivalves are colonized by their chemosynthetic symbionts throughout their lifetime. *Environ. Microbiol.* **16**, 3699–3713. (doi:10.1111/1462-2920.12597)
32. Fiala-Medioni A, Le Pennec M. 1987 Trophic structural adaptations in relation to the bacterial association of bivalve molluscs from hydrothermal vents and subduction zones. In *Symposium on Marine Symbioses. 1 (1987)*, pp. 63–74. Philadelphia, PA: Balaban.
33. Arellano SM, Young CM. 2009 Spawning, development, and the duration of larval life in a deep-sea cold-seep mussel. *Biol. Bull.* **216**, 149–162. (doi:10.1086/BBLv216n2p149)
34. Martel A, Tremblay R, Toupoint N, Olivier F, Myrand B. 2014 Veliger Size at Metamorphosis and temporal variability in prodissoconch II morphometry in the blue mussel (*Mytilus edulis*): potential impact on recruitment. *J. Shellfish Res.* **33**, 443–455. (doi:10.2983/035.033.0213)
35. Young CM *et al.* 2012 Dispersal of deep-sea larvae from the intra-American seas: simulations of trajectories using ocean models. *Integr. Comp. Biol.* **52**, 483–496. (doi:10.1093/icb/ics090)
36. Bayne BL. 1965 Growth and the delay of metamorphosis of the larvae of *Mytilus edulis* (L). *Ophelia* **2**, 1–47. (doi:10.1080/00785326.1965.10409596)
37. Breusing C *et al.* 2016 Biophysical and population genetic models predict the presence of 'Phantom' stepping stones connecting mid-Atlantic ridge vent ecosystems. *Curr. Biol.* **26**, 2257–2267. (doi:10.1016/j.cub.2016.06.062)
38. Distel DL, Baco AR, Chuang E, Morrill W, Cavanaugh C, Smith CR. 2000 Do mussels take wooden steps to deep-sea vents? *Nature* **403**, 725–726. (doi:10.1038/35001667)
39. Kaper JB, Nataro JP, Mobley HLT. 2004 Pathogenic *Escherichia coli*. *Nat. Rev. Microbiol.* **2**, 123–140. (doi:10.1038/nrmicro818)
40. Quarmby LM. 2004 Cellular deflagellation. *Int. Rev. Cytol.* **233**, 47–91.
41. Tubiash HS, Chanley PE, Leifson E. 1965 Bacillary necrosis, a disease of larval and juvenile bivalve mollusks I. Etiology and epizootiology. *J. Bacteriol.* **90**, 1036. (doi:10.1128/jb.90.4.1036-1044.1965)
42. Eggermont M *et al.* 2020 The blue mussel inside: 3D visualization and description of the vascular-related anatomy of *Mytilus edulis* to unravel hemolymph extraction. *Sci. Rep.* **10**, 6773. (doi:10.1038/s41598-020-62933-9)
43. Karasov WH, Douglas AE. 2013 Comparative digestive physiology. *Comp. Physiol.* **3**, 741–783. (doi:10.1002/cphy.c110054)
44. Thubaut J, Corbari L, Gros O, Duperron S, Couloux A, Samadi S. 2013 Integrative biology of *Idas iwaotakii* (Habe, 1958), a 'model species' associated with sunken organic substrates. *PLoS ONE* **8**, e69680. (doi:10.1371/journal.pone.0069680)
45. Von Cosel R, Marshall BA. 2010 A new genus and species of large mussel (Mollusca: Bivalvia: *Mytilidae*) from the Kermadec Ridge. *Rec. Musuem N. Z. Te Papa* **21**, 15.
46. Page H, Fisher C, Childress J. 1990 Role of filter-feeding in the nutritional biology of a deep-sea mussel with methanotrophic symbionts. *Mar. Biol.* **104**, 251–257. (doi:10.1007/BF01313266)
47. Streams ME, Fisher CR, Fiala-Médioni A. 1997 Methanotrophic symbiont location and fate of carbon incorporated from methne in a hydrocabon seep mussel. *Mar. Biol.* **129**, 465–476. (doi:10.1007/s002270050187)
48. Wentrup C, Wendeberg A, Huang JY, Borowski C, Dubilier N. 2013 Shift from widespread symbiont infection of host tissues to specific colonization of gills in juvenile deep-sea mussels. *ISME J.* **7**, 1244–1247. (doi:10.1038/ismej.2013.5)
49. Desbruyères D, Almeida A, Biscoito M, Comtet T, Khripounoff A, Le Bris N, Sarradin PM, Segonzac M. 2000 A review of the distribution of hydrothermal vent communities along the northern Mid-Atlantic Ridge: dispersal vs. environmental controls. In *Island, ocean and deep-Sea biology* (eds MB Jones, JMN Azevedo, AI Neto, AC Costa, AMF Martins), pp. 201–216. Dordrecht, The Netherlands: Springer Netherlands.
50. Ansorge R, Romano S, Sayavedra L, Porras MÁG, Kupczok A, Tegetmeyer HE, Dubilier N, Petersen J. 2019 Functional diversity enables multiple symbiont strains to coexist in deep-sea mussels. *Nat. Microbiol.* **4**, 2487–2497. (doi:10.1038/s41564-019-0572-9)
51. Romero Picazo D, Dagan T, Ansorge R, Petersen JM, Dubilier N, Kupczok A. 2019 Horizontally transmitted symbiont populations in deep-sea mussels are genetically isolated. *ISME J.* **13**, 2954–2968. (doi:10.1038/s41396-019-0475-z)
52. Franke M, Geier B, Hammel JU, Dubilier N, Leisch N. 2021 Coming together—symbiont acquisition and early development in deep-sea bathymodioline mussels. FigShare.

royalsocietypublishing.org/journal/rspb *Proc. R. Soc. B* **288**: 20211044

Appendix

Supplementary notes

Supplementary Note 1 - Detailed morphological description of the Bathymodiolus and Gigantidas pediveliger

a) Velum and mantle

The velum occupied the anterior half of the mantle cavity and the most anterior point was connected to the mantle via a thin membrane near the anterior adductor muscle (Figure S3 and S6). The posterior-most part of this membrane was fused with the visceral mass close to the base of the foot (Figure S3 and S6). Furthermore, three velar retractor muscles were present. The mantle epithelium consisted of one to two layers of cells (Figure 2 d–f, Figure S6), except for the mantle folds which consisted of multiple cell layers. The folds were located at the most ventral part of the mussels.

b) The foot

The foot occupied 11% of the soft body volume and was anchored to the shell by two pairs of retractor muscles. The posterior pair were anchored to the shell above the posterior adductor muscle and dorsal-ventral at the base of the foot (Figure S6). The anterior retractor muscle pair were located at the base of the foot close to the pedal ganglion and were connected to the shell near the hinge. The surface of the pediveliger foot was either ciliated or covered with microvilli (Figure 2 g and Figure S8). Three glands were present in the foot of *B. puteoserpentis* pediveligers: the white, purple, and byssus glands (Figure S8). The white gland was located at the base of the foot between the pedal ganglion and posterior adductor muscle, and the purple gland was located close to the white gland (Figure S8 a-f). The byssus gland lay on the ventral side of the white gland, and a pair of ciliated ducts merged into the pedal groove at the heel of the foot (Figure S8 b-d).

c) The central nervous system

Pediveliger had three pairs of fully developed ganglia: the cerebral ganglia located dorsally to the oesophagus and close to the apical plate of the velum, the pedal ganglia situated at the base of the foot, and the visceral ganglia located ventrally to the posterior adductor muscle (Figure S6). Each ganglion was fused with its corresponding partner via commissures (Figure S6). The length of the commissures varied between each ganglion pair: longest between the visceral ganglia and shortest between the pedal ganglia. The cerebral, pedal and visceral ganglia were connected via connectives, all of which were fully developed

(Figure S6). The cerebro-visceral and cerebro-pedal connectives left the posterior region of each cerebral ganglion as one entity, which then split near the region of the larval foot. On each side, the cerebro-pedal connectives dove ventrally towards its respective pedal ganglion, while each cerebro-visceral connectives extended posteriorly towards its respective visceral ganglion.

d) The digestive system

The *Bathymodiolus* and *Gigantidas* pediveliger are planktotrophic and any yolk provided from the parents is limited and only sufficient to last until the larvae have developed their own digestive system and feeding apparatus. The pediveliger feeds by collecting particles with the velum and during the filter-feeding planktonic larval stage, energy storages in form of lipid vesicles are built up. These lipid vesicles serve as storage compounds for the highly energy consuming process of metamorphosis. The pediveliger possessed a fully developed digestive system, composed of mouth, oral labial palp, oesophagus, stomach, two digestive glands, the style sac with crystalline style, the gastric shield, an s-shaped looped intestine and a mid-gut. It was located in the most dorsal part of the mussel beneath the hinge and occupied 29.4% of the soft tissue volume. The oral labial palp was located at the posterior end of the velum near the base of the foot. It was connected via a thin membrane to the velum (Figure S5). No primary topography (rafts) was visible in any of the pediveliger oral labial palps, in contrast to the labial palps of adult mussels. The epithelial cells of the oral labial palps were ciliated and had microvilli. The oesophagus began at the posterior edge of the velum and led into the stomach. Most of the oesophagus was located perpendicular to the hinge line beneath the foot (Figure S6). The cells lining the oesophagus were ciliated and had microvilli. In the pediveliger stage, the stomach was the largest organ of the digestive system. It was situated in the middle of the mussel, underneath the base of the foot and the pedal ganglion (Figure S6). The style sac was located at the posterior end of the stomach and had a diameter of 30–40 µm. The cells lining the style sac were densely ciliated and had large vacuoles in their cytoplasm (Figure S6). The crystalline style was observed in pediveliger stages but not in every specimen (probably due to sample preservation). Membrane-bound lipid vesicles were found in the diverticula of the digestive gland and the epithelial cells of the stomach (Figure S6+ S7). These lipid vesicles had a mean diameter of 15.85 µm (± 4.63; 75 lipid vesicles measured in 3 mussels; n = 75 µm). In the earliest pediveliger, these lipid vesicles formed up to 12.8% of the entire soft body volume (Figure S6). The gastric shield was found at the dorsal wall of the stomach (Figure S6) and its cells were densely ciliated. The mid gut left the stomach at the ventral wall anterior to the style sac. It passed backwards and turned dorsally to fuse into the intestine, which then passed towards the anal papilla. The part of the digestive tract containing the mid gut and the

intestine looped in an s-shape dorsally under the stomach (Figure S6). The ciliated anal papilla was located close to the posterior adductor muscle (Figure S6).

e) The gill basket

In the *Bathymodiolus* and *Gigantidas* pediveliger stage, each gill basket consisted of rudimentary gill filaments and the developing budding zone. The budding zone is a meristem-like zone, which in later developmental stages continuously generates new gill filaments at the posterior end of the gill basket. In mytilids, the first three gill filaments are developed almost simultaneously [1] out of the mantle epithelia, and all subsequent filaments are developed by the budding zone. The shortest filaments were found at the most posterior end of the descending lamellae next to the budding zone (Figure 1 a and Figure S6). The pediveliger gill basket had the fewest rudimentary gill filaments in comparison with later developmental stages (3-4 in *B. puteoserpentis* and 5 in *B. azoricus* and *G. childressi*; Figure S3). Furthermore, these gill filaments were the shortest dorso-ventrally from the gill axis to the ciliated ends (mean length 81 µm, SD = 10 µm, *n* = 16 in *B. puteoserpentis*, mean length 97 µm, SD = 18 µm, *n* = 10 in *G. childressi,* and mean length 78 µm, SD = 12 µm, *n* = 10 in *B. azoricus*). The gill axis (dorsal tissue that supports the gill lamellae) was parallel to the hinge line (Figure 1 a). The space between individual gill filaments of one gill basket ranged from 9 µm to 27 µm in the *B. puteoserpentis* pediveliger (Figure S6). Correlative light and electron microscopy showed that the surface of the entire gill filament was densely covered with cilia and microvilli (Figure 2 a) and no symbiotic bacteria were present.

Supplementary Note 2 Morphological changes that occur during the metamorphosis

a) The digestive system

The *Bathymodiolus* and *Gigantidas* pediveliger had a fully developed digestive system with a looped mid gut and intestine (Figure S11 a-e). The rafts of the labial palps were first observed in a plantigrade with a size of 436 µm. During the metamorphosis, the apical plate moved into the oral labial palps, which then split into the upper and lower labial palps (Figure S6, S9 and S10). Instead of being located beneath the foot and parallel to the hinge line, the plantigrade oesophagus had a more perpendicular position (Figure S10). Organs like the stomach, oesophagus, intestine and style sac increased in size but retained their general morphological traits (Figure 1, Figure S6, S9 and S10). During the transition from a post larvae to a juvenile mussel, the complex digestive system got streamlined and the looped intestine straightened. Furthermore, the volume of lipid vesicles decreased from 12.83% of the soft-body volume in pre-metamorphosis mussels (mean diameter 15.85 µm, ± 4.63, *n* = 75) to 3.9% in metamorphosing mussels (mean diameter 16.32 µm, ± 6.74, *n* = 53), to 1.8%

in post-metamorphosis mussels (mean diameter 8.37 µm, 1.74, *n* = 60), and to their complete absence in juveniles (Figure 1, Figure S6, S9 and S10, and Table S6).

b) Gill development and growth

During metamorphosis, the gill filament number increased by one in all species (*B. puteoserpentis,* 5; *B. azoricus,* 6; and *G. childressi,* 6). Furthermore, reorientation of the gill basket in the mantle cavity led to the first gill filament pair (which are attached to the visceral mass along their entire anterior face) being located closer to the mouth and the labial palps. Depending on the specimen, the posterior end of the gill basket was tilted by 20–40° (Figure 1a to c). This reorientation aligned the growth axis of the gill with the length axis of the mussel. In the plantigrade stage, there was an increase in the dorso-ventral filament length (increasing from 68 µm to 159 µm in *B. puteoserpentis,* from 73 µm to 215 µm in *G. childressi* and from 68 µm 110 µm in *B. azoricus*) and the frontal-abfrontal filament depth. Gill filaments of *G. childressi* (mean = 125.49 µm, sd = 33.77 µm, *n* = 52) were larger than *B. puteoserpentis* (mean = 115.21 µm, sd = 24.56 µm, *n* = 40) and *B. azoricus* (mean = 93.58 µm, sd = 18.17 µm, *n* = 10). Additionally, gill filaments separated from each other and the gaps between the filaments increased (up to 120 µm). The gill filament tips disconnected from each other after metamorphosis (Figure 1 c and Figure S9). At the end of metamorphosis, a distinct ciliated and non-ciliated region could be identified (Figure S6). The non-ciliated region was filled with bacteria (Figure 2 c). This symbiont colonization led to the hypertrophic morphology of the epithelial cells. The hypertrophy contributed to a drastic increase of the relative gill volume from 4.6% to 28% after the mussels were colonized (Table S6).

In one 2-mm *B. puteoserpentis* juvenile mussel a well-developed right and left gill could be identified. Each gill consisted of the descending (25 gill filaments) and ascending lamella (9 gill filaments) of the inner demibranch. In one 3-mm mussel the descending lamella (4 gill filaments) of the outer demibranch was in the process of development. Upon reaching 1 cm shell length, the gill was completely developed and consisted of the inner and outer demibranch with the ascending and descending lamellae.

Supplementary Discussion

Although all individuals in this study were collected from mussel beds on the sea floor, the pediveligers were always aposymbiotic. We therefore assume that these late planktonic larval stages were in the process of settling on the sea floor. Mussel larvae can react to cues like current flow, water chemistry and temperature, and substratum characteristics that could play a critical role in detecting vent plumes and inducing settlement [2-4]. At smaller spatial scales, bacteria may also play a role in inducing settlement and metamorphosis in marine invertebrates [5]. It is tempting to speculate that the symbiont-like bacteria we observed on the larval shells, or microorganisms in the mussel beds, including possible free-living forms of the symbionts, play a role in inducing the settlement and metamorphosis of *Bathymodiolus* mussels.

Supplementary Methods

Sampling and fixation

Bathymodioline mussels are not subject to CITES or any other international regulations and sampling in the Gulf of Mexico at the Mid-Atlantic Ridge did not require a permit. Sampling and export permission for *B. azoricus* had been granted by Portuguese authorities through diplomatic notes. When required, import permissions were granted by German authorities. All deep-sea mussels were collected from the sea floor with remotely operated vehicles: *B. puteoserpentis* from the Semenov vent field on the MAR at 2447 m depth with the German Research Vessel (RV) Meteor during cruise M126 in 2016, *B. azoricus* from the Bubbylon vent on the MAR at 1002 m depth during the RV Meteor cruise M82-3 in 2010, and *G. childressi* at the Mississippi Canyon site 853 in the Gulf of Mexico at 1071 m depth with the RV Nautilus (Ocean Exploration Trust) during cruise NA58 in 2015 (detailed information in Table S1). *M. edulis* were collected in the Baltic Sea at a site close to Kiel, Germany at 1.5 m water depth. Upon recovery, specimens were fixed for morphological analysis and FISH in 2% paraformaldehyde (PFA) in phosphate buffer saline (PBS), and for morphological analysis and TEM in 2.5% glutaraldehyde (GA) in PHEM buffer (piperazine-N, N′-bis , 4-(2-hydroxyethyl)-1-piperazineethanesulfonic acid, ethylene glycol-bis(β-aminoethyl ether and $MgCl_2$) [6]. *B. azoricus* samples were fixed using a modified Trumps solution containing 0.05 M sodium cacodylate buffer, 2% glutaraldehyde and 2% paraformaldehyde. After fixation, samples were stored in the corresponding buffers (PFA: ethanol/PBS; GA: PHEM or sodium cacodylate).

Shell measurements

Specimens were photographed with a Nikon SMZ 25 stereomicroscope equipped with a Nikon Ds-Ri2 colour camera and the software NIS-Elements AR. Total shell dimensions were recorded as shown in Figure S1c (Table S2) and shell margin limits were identified by their unique colouration (Figure S1b and d).

Sample preparation for histological analysis and correlative TEM

PFA-fixed samples were decalcified with a 0.5 M ethylenediaminetetraacetic acid (EDTA) solution (for details see Supplementary Methods e). For histological analysis, samples of all three species were post-fixed with 1% osmium tetroxide (OsO4) for 1-2 h at 4°C and washed three times with PHEM. The mussels were dehydrated with an ethanol series of increasing concentration (30% (v/v), 50% (v/v), 70% (v/v), 80% (v/v), 90% (v/v) and 100% (v/v)) at -10 °C, with each step lasting 10 min. The tissue was then transferred into a 50:50 mixture of ethanol and acetone, followed by 100% acetone. Samples were infiltrated with low-viscosity resin (Agar Scientific, UK) step-wise with a 1:3 resin:acetone mixture for 2 h, followed by 2 h

in a 1:1 solution, and overnight in a 3:1 solution. Samples were then transferred twice into pure resin for 2 h. The samples were polymerized at 60–65 °C for 48 h. Sections of 1.5-µm thick sections were cut with a Leica UC7 ultramicrotome (Ultracut UC7 Leica Microsystem, Austria) and stained with 0.5% toluidine blue and 0.5% sodium tetraborate.
For TEM, semi-thin sections were mounted on a freshly trimmed resin block by placing the semi-thin section on applying a drop of Milli Q on the resin block and placing the semi-thin section on the drop of Milli Q. After drying the resin block for 1 h at 40 °C the section was fully adhered to the resin block. Ultra-thin (70 nm) sections were cut on a Leica UC7 ultramicrotome (Ultracut UC7 Leica Microsystem, Austria) and mounted on formvar-coated slot grids (Agar Scientific, United Kingdom) [7]. Sections were contrasted with 0.5% aqueous uranyl acetate (Science Services, Germany) for 20 min and with 2% Reynold's lead citrate for 6 min.

Sample preparation for histological analysis and fluorescence in situ hybridization

PFA-fixed *B. puteoserpentis* were decalcified with a 0.5 M EDTA solution (for details see Supplementary Methods e) and dehydrated by immersing the sample in an increasing ethanol series (30% (v/v), 50% (v/v), 70% (v/v), 80% (v/v), 90% (v/v) and 100% (v/v)) each step lasting 10 min. Samples were embedded in paraffin by incubating the samples in 50:50 Ethanol : RotiHistol (at room temperature), twice in 100% RotiHistol (at room temperature), in 75% RotiHistol and 15% paraffin (at 46°C), in 50% RotiHistol and 50% paraffin (at 46°C), in 15% RotiHistol and 75% paraffin (at 46°C), and in 100% paraffin (at 46°C). Each step lasted 10 min. After the samples were transferred to 100% paraffin this step was repeat four to five times with each step lasting 1h. The paraffin blocks hardened overnight and were sectioned at 5–10 µm thickness on a Leica microtome RM2255. Sections were mounted on Polysine-coated glass slides and baked in a vertical position for 1 h at 60 °C to improve adhesion to the slides. Slides were de-waxed and rehydrated by immersing them three times in 100% (v/v) RotiHistol for 10 min each, followed by a decreasing ethanol series (96% (v/v), 80% (v/v), 70% (v/v) and 50% (v/v), 10 min each). Sections were air dried and encircled with a liquid blocker (PAP-Pen, Science Services).
For *in situ* hybridization, general double labelled probes [8] targeting conserved regions of the 16S rRNA in the domain Bacteria, as well as specific probes for targeting SOX and MOX bacteria were used. As a negative control, an oligonucleotide (non-338) labelled with Atto-550 was used, complementary to the probe EUB I-III, to monitor nonspecific binding (Table S3). Depending on the section size, 20–300 µl of hybridization mixture was applied per section. The 8.4 pmol probe stock solution was diluted 1:10 with the hybridization buffer (Table S9), which contained 30–35% (v/v) of formamide, before the mixture was applied onto the sections. The hybridizations were performed at 46 °C for 3 h in hybridization chambers.

To prevent changes in concentration of the hybridization solution through evaporation, a tissue was saturated with 2 ml of the 30–35% formamide solution and placed in the chamber, thereby assuring equilibrium between the hybridization solution and the surrounding gas phase. After hybridization, samples were washed for 15 min in pre-warmed (48 °C) corresponding washing buffer (Table S10) and then dipped once in ddH_2O. DAPI was applied as a nucleic acid counter-stain. The slides were incubated for 10 min at room temperature, washed twice in ddH_2O and dried.

Decalcification

For decalcification, mussels were re-hydrated with an ethanol series of decreasing concentration (60% (v/v) to 0%, in steps of 10%), with each step lasting 10 min. The samples were washed twice with 1x phosphate-buffered saline (PBS) and transferred into a 0.5 M Ethylenediaminetetraacetic acid (EDTA) PBS solution. Decalcification was performed for 24–240 h depending on the size of the specimens. Samples stored in PHEM-buffer were not treated with EDTA because PHEM-buffer includes EGTA, which decalcifies similarly to EDTA.

Microscopy

LM analyses were performed using a Zeiss Axioplan 2 equipped with an automated stage, two cameras (Axio CAM MRc5) and an Olympus BX61VS slide-scanner equipped with an automated stage and an Olympus XM10 camera

Fluorescence microscopy analyses were performed using an Olympus BX53 compound microscope equipped with a Hamamatsu ORCA Flash 4.0 camera) using a 40x semi-Apochromat and a 100x super-Apochromat oil-immersion objective and the Olympus software cellSens, and a Zeiss LSM 780 confocal laser-scanning microscope equipped with an Airyscan detector using a 100× Plan-Apochromat oil-immersion objective and the Zen-Black software.

Ultra-thin sections were imaged at 20–30 kV with a Quanta FEG 250 scanning electron microscope (FEI Company) equipped with a scanning transmission electron microscope detector using the xT microscope control software ver. 6.2.6.3123.

SRµCT measurements

SRµCT datasets were recorded at the Deutsches Elektronen-Synchrotron (DESY) using the P05 beamline of PETRA III, operated by the Helmholtz-Zentrum Hereon (Geesthacht, Germany [9]). The x-ray microtomography setup at 15–30 keV and 5× to 40× magnification was used to scan resin-embedded, OsO_4-contrasted samples with attenuation contrast and uncontrasted samples in PBS-filled capillaries [10], with propagation-based phase contrast.

Scan parameters are summarized in Table S4. The tomography data were processed with custom scripts implementing a TIE phase-retrieval algorithm and a filtered back projection, implemented in the ASTRA toolbox [11-13]. SRµCT models were used to ground truth the volume calculations from histological section series by measuring sectioning-induced tissue compression, which varied between 1 and 7 % depending on the specimen (n = 3).

µCT measurements

The two adult bathymodiolin mussels, *G. childressi* (H1425-019-J1) and *B. azoricus* (D4MS) were scanned with a laboratory-based µCT at the Zoologische Staatssammlung in Munich, Germany. Both mussels were stained in phosphotungstic acid, immersed in ethanol and scanned in solution [14].

Correlative workflow for SRµCT, light and electron microscopy, and FISH

We screened section series of 32 specimens from the three analysed species (Table 1) using light microscopy and by eye identified individual cells and predicted their symbiont colonisation status based on the presence / absence of the morphological characteristics hypertrophy, loss of microvilli and loss of cilia. The location of the cells and their colonization status was marked using Cell Counter in Fiji [15]. Semi-thin sections of nine specimens were re-sectioned, the same fields of view were recorded with TEM, and LM and TEM data was overlaid (Figure S2). To validate the LM-based predictions, symbionts were identified in TEM images based on their morphology. We performed this workflow on samples imaged with either both SRµCT and section series, or samples only prepared as section series (Video S5). We complemented this approach with FISH on sections of seven additional *B. puteoserpentis* specimens.

Image processing and 3D visualisation

Histograms and white balance of microscopy images were adjusted using Fiji and Adobe Photoshop 2021 and figure panels were composed using Adobe Illustrator 2021. Prior to the 3D reconstructions, LM-images were stitched and aligned in *x*, *y* and *z* direction with the software TrackEM2 [16] in Fiji. Image files were imported using “import sequences as grid”. Stitching and blending of the layers was performed choosing “montage multiple layers”. For the automated alignment, a linear alignment was used, allowing for translation and rotation. Individual misalignments were manually corrected using the “aligning with landmarks” option. Exported LM image stacks were used for 3D surface reconstructions.

3D surface reconstructions were performed in Amira 2020.2 (ThermoFisher Scientific). Semi-automated (via thresholds) and manual segmentation were used to label individual organs. The individual labels for each organ were separated with the *arithmetic tool* function: A == 1 (no. of material) and rendered into a 3D surface model using the following steps: *create*

surface, *reduce faces*, *remesh surface* and *smooth surface*. *Faces* were reduced down to a value of 50,000–100,000. Surfaces were remeshed and the percentage value in the ‘Desired Size’ port was kept at 50%. All surface meshes were visualized with the Direct Normals shading mode under *Surface View*.

Co-registration of SRμCT, LM and TEM data was carried out following [7]. For visualisation, LM and TEM data were displayed simultaneously as orthographic slices in a single AMIRA 3D scenario. For the selection of virtual planes within the data sets, the slice tool was used. Individual TEM images were co-registered based on their corresponding LM image, using Adobe Photoshop CS5 (Adobe Systems Software Ireland Ltd.)

Supplementary tables

Table S1. Overview of samples used for the morphological analyses, SRµCT, µCT, FISH and TEM. GA, glutaraldehyde; PFA, paraformaldehyde. All supplementary material can be excessed and downloaded from figshare (https://figshare.com/projects/Coming_together_symbiont_acquisition_and_early_development_in_deep-sea_bathymodioline_mussels/100751). For specific DOIs of individual specimen see table below.

species	sample identifier	develop-mental stage	shell length (µm)	shell height (µm)	sampling location	latitude	longi-tude	sampling depth (m)	sampling year	analyses	fixation	storage buffer	status of symbiont colonization	DOI
B. puteo-serpentis	Bp-hpf	metamorphosis	372.31	375.66	Semenov-2	13.513 N	44.962 W	-2446.5	2016	histology / TEM	2.5% GA	PHEM	very early colonization	
	1555-30	plantigrade	372.42	353.1	Semenov-2	13.513 N	44.962 W	-2446.5	2016	SRµCT / histology	2.5% GA	PHEM	symbiotic	10.6084/m9.figshare.14838339.v1
	1555-27	metamorphosis	385.47	417.85	Semenov-2	13.513 N	44.962 W	-2446.5	2016	SRµCT / histology	2.5% GA	PHEM	apo-symbiotic	10.6084/m9.figshare.14247488.v1 10.6084/m9.figshare.14838348.v1
	1555-16	pediveliger	399.37	420.37	Semenov-2	13.513 N	44.962 W	-2446.5	2016	histology	2.5% GA	PHEM	apo-symbiotic	10.6084/m9.figshare.14247395
	1555-06	pediveliger	404.99	427.36	Semenov-2	13.513 N	44.962 W	-2446.5	2016	histology / TEM	2.5% GA	PHEM	apo-symbiotic	10.6084/m9.figshare.14247329.v1
	1556-61	pediveliger	407.91	382.31	Semenov-2	13.513 N	44.962 W	-2446.5	2016	Dope-FISH	2% PFA	PBS / ethanol	apo-symbiotic	

	1555-31	pediveliger	409.3	408.16	Semenov-2	13.513 N	44.962 W	-2446.5	2016	histology	2.5% GA	PHEM	apo-symbiotic	10.6084/m9.figshare.14247980.v1
	1555-28	pediveliger	409.34	415.8	Semenov-2	13.513 N	44.962 W	-2446.5	2016	SRμCT / histology	2.5% GA	PHEM	apo-symbiotic	10.6084/m9.figshare.14247698.v1 10.6084/m9.figshare.14838369.v1
	1556-26	metamorphosis	410.38	428.54	Semenov-2	13.513 N	44.962 W	-2446.5	2016	Dope-FISH	2% PFA	PBS / ethanol	only SOX	
	1555-45	metamorphosis	411.13	442.17	Semenov-2	13.513 N	44.962 W	-2446.5	2016	histology	2.5% GA	PHEM	apo-symbiotic	10.6084/m9.figshare.14248103.v1
	1555-04	pediveliger	411.23	402.91	Semenov-2	13.513 N	44.962 W	-2446.5	2016	histology / TEM	2.5% GA	PHEM	apo-symbiotic	10.6084/m9.figshare.12367259
	1556-29	plantigrade	414.18	394.26	Semenov-2	13.513 N	44.962 W	-2446.5	2016	Dope-FISH	2% PFA	PBS / ethanol	only SOX	
	1555-14	plantigrade	414.32	394.93	Semenov-2	13.513 N	44.962 W	-2446.5	2016	SRμCT / histology	2.5% GA	PHEM	symbiotic	10.6084/m9.figshare.14838387.v1
	1555-42	metamorphosis	417.82	413.34	Semenov-2	13.513 N	44.962 W	-2446.5	2016	histology	2.5% GA	PHEM	apo-symbiotic	10.6084/m9.figshare.14248046.v1

1556-05	pediveliger	418.47	463.48	Semenov-2	13.513 N	44.962 W	-2446.5	2016	Dope-FISH	2% PFA	PBS / ethanol	apo-symbiotic	10.6084/m9.figshare.12367247
1555-03	plantigrade	432.29	447.89	Semenov-2	13.513 N	44.962 W	-2446.5	2016	histology / TEM	2.5% GA	PHEM	symbiotic	10.6084/m9.figshare.14247305.v3
1556-62	plantigrade	432.8	433.97	Semenov-2	13.513 N	44.962 W	-2446.5	2016	Dope-FISH	2% PFA	PBS / ethanol	symbiotic	
1556-07	plantigrade	434.02	445.35	Semenov-2	13.513 N	44.962 W	-2446.5	2016	Dope-FISH	2% PFA	PBS / ethanol	symbiotic	
1555-01	plantigrade	435.53	404.12	Semenov-2	13.513 N	44.962 W	-2446.5	2016	histology / TEM	2.5% GA	PHEM	symbiotic	10.6084/m9.figshare.11709399
1555-05	metamorphosis	436.44	390.65	Semenov-2	13.513 N	44.962 W	-2446.5	2016	histology / TEM	2.5% GA	PHEM	start of colonization	10.6084/m9.figshare.12367247.v1
1555-02	plantigrade	439.64	493.34	Semenov-2	13.513 N	44.962 W	-2446.5	2016	histology / TEM	2.5% GA	PHEM	symbiotic	10.6084/m9.figshare.14248436.v1
1556-49	juvenile	2053.09	1451.25	Semenov-2	13.513 N	44.962 W	-2446.5	2016	Dope-FISH	2% PFA	PBS / ethanol	symbiotic	
1555-47	juvenile	2290.09	1508.85	Semenov-2	13.513 N	44.962 W	-2446.5	2016	SRμCT	2.5% GA	PHEM	symbiotic	10.6084/m9.figshare.14248496.v1

	1555-22	juvenile	3072.61	2060.11	Semenov-2	13.513 N	44.962 W	-2446.5	2016	SRμCT / histology	2.5% GA	PHEM	symbiotic	10.6084/m9.figshare.12728075.v1
G. childressi	M102	metamorphosis	383.82	406.78	Mississippi Canyon 853	28.123 N	-89.139 E	-1071.00	2015	histology	2.5% GA	PHEM	start of colonization	10.6084/m9.figshare.14248553.v1
	Gc-hpf-small	metamorphosis	389.94	406.16	Mississippi Canyon 853	28.123 N	-89.139 E	-1071.00	2015	histology	2.5% GA	PHEM	start of colonization	10.6084/m9.figshare.14248670.v1
	Gc-hpf-large	plantigrade	429.08	500.32	Mississippi Canyon 853	28.123 N	-89.139 E	-1071.00	2015	histology	2.5% GA	PHEM	symbiotic	10.6084/m9.figshare.14248643.v1
	M103	plantigrade	433.13	463.17	Mississippi Canyon 853	28.123 N	-89.139 E	-1071.00	2015	histology	2.5% GA	PHEM	symbiotic	10.6084/m9.figshare.14248559.v1
	M101	pediveliger	434.37	447.76	Mississippi Canyon 853	28.123 N	-89.139 E	-1071.00	2015	SRμCT / histology / TEM	2.5% GA	PHEM	apo-symbiotic	10.6084/m9.figshare.14248589.v1 10.6084/m9.figshare.14838432.v1
	H1425-019-J1	adult	56310	31740	Green Canyon 234	27.746 N	-91.222 E	-540.00	2015	μCT	Davidson's fixative	PBS / ethanol	symbiotic	10.6084/m9.figshare

															.54582 40.v1
B. azoricus	1643-03	pediveliger	452.23	483.72	Bubbylon	37.801 N	-31.537 E	-1002.00	2010	histology TEM	2.5% GA	Trump's solution	apo-symbiotic		
	1624-13	pediveliger	465.12	522.93	Bubbylon	37.801 N	-31.537 E	-1002.00	2010	histology	2% PFA	PBS / ethanol	apo-symbiotic	10.608 4/m9.fi gshare .14248 910.v1	
	1643-02	plantigrade	498.16	510.22	Bubbylon	37.801 N	-31.537 E	-1002.00	2010	SRμCT / histology	2.5% GA	Trump's solution	symbiotic	10.608 4/m9.fi gshare .14838 450.v1	
	1624-17	plantigrade	549.1	583.44	Bubbylon	37.801 N	-31.537 E	-1002.00	2010	histology	2% PFA	PBS / ethanol	symbiotic	10.608 4/m9.fi gshare .14249 006	
	1643-01	metamorphosis	566.76	597.38	Bubbylon	37.801 N	-31.537 E	-1002.00	2010	histology	2.5% GA	Trump's solution	start of colonization	10.608 4/m9.fi gshare .14249 021.v1	
	1626-01	juvenile	2170	1430	Bubbylon	37.801 N	-31.537 E	-1002.00	2010	SRμCT	2% PFA	PBS / ethanol	symbiotic		
	1629-124	juvenile	2600	1500	Bubbylon	37.801 N	-31.537 E	-1002.00	2010	SRμCT	2% PFA	PBS / ethanol	symbiotic		
	1624-121	adult	10600	6000	Bubbylon	37.801 N	-31.537 E	-1002.00	2010	SRμCT	2% PFA	PBS / ethanol	symbiotic		
	D4MS	adult	53352	17078	Montsegu r	37.288 N	-32.276 E	-1700.00	2013	μCT	2% PFA	PBS / ethanol	symbiotic	10.608 4/m9.fi	

														gshare .54582 34.v1
M. edulis	252-1	juvenile	2198	1480	Kiel	54.394 N	10.190 E	-1.5	2018	SRµCT	2.5% GA	PHEM	aposymbiotic	10.608 4/m9.fi gshare .14838 807.v1

Table S2. Shell dimensions of *Bathymodiolus* and *Gigantidas* individuals. Individuals are sorted by increasing shell length. *B. azoricus* mussels were sampled at the Bubbylon vent at 1002 m water depth, *B. puteoserpentis* at the Semenov-2 vent at 2446 m water depth and *G. childressi* mussels at the Mississiooi Canyon 853 at 1071 m water depth.

species	identifier	developmental stage	shell length (µm)	shell height (µm)
B. azoricus	1626-12	pediveliger / metamorphosis	392.36	505.18
B. azoricus	1624-45	pediveliger / metamorphosis	438.55	526.14
B. azoricus	1624-41	pediveliger / metamorphosis	448.79	523.95
B. azoricus	1643-03	pediveliger	452.23	483.72
B. azoricus	1626-15	pediveliger / metamorphosis	459.18	501.96
B. azoricus	1624-12	pediveliger / metamorphosis	460.77	516.14
B. azoricus	1626-05	pediveliger / metamorphosis	464.71	466.27
B. azoricus	1624-13	pediveliger	465.12	522.93
B. azoricus	1626-32	pediveliger / metamorphosis	466.08	530.28
B. azoricus	1624-02	pediveliger / metamorphosis	470.00	510.00
B. azoricus	1624-29	pediveliger / metamorphosis	470.86	525.05
B. azoricus	1624-56	plantigrade	472.50	540.31
B. azoricus	1626-21	pediveliger / metamorphosis	474.14	554.33
B. azoricus	1626-33	plantigrade	477.36	514.94
B. azoricus	1626-19	pediveliger / metamorphosis	477.45	509.89
B. azoricus	1624-36	plantigrade	480.93	514.35
B. azoricus	1624-25	plantigrade	480.95	524.56
B. azoricus	1624-38	pediveliger / metamorphosis	481.45	516.30
B. azoricus	1624-06	pediveliger / metamorphosis	482.46	529.78
B. azoricus	1626-30	pediveliger / metamorphosis	485.83	542.96
B. azoricus	1624-24	pediveliger / metamorphosis	486.43	543.35
B. azoricus	1624-28	plantigrade	486.57	522.45
B. azoricus	1626-10	plantigrade	487.00	534.74
B. azoricus	1626-07	pediveliger / metamorphosis	488.52	515.81
B. azoricus	1626-11	pediveliger / metamorphosis	490.03	545.64
B. azoricus	1624-31	plantigrade	490.71	548.67
B. azoricus	1624-03	plantigrade	491.18	549.80
B. azoricus	1626-06	pediveliger / metamorphosis	496.85	538.00
B. azoricus	1626-14	plantigrade	497.18	553.92
B. azoricus	1643-02	plantigrade	498.16	510.22
B. azoricus	1624-04	pediveliger / metamorphosis	502.44	513.91
B. azoricus	1626-08	pediveliger / metamorphosis	502.87	515.49

B. azoricus	1624-33	plantigrade	503.23	545.05
B. azoricus	1624-19	plantigrade	505.57	524.99
B. azoricus	1624-32	pediveliger / metamorphosis	506.68	520.30
B. azoricus	1626-29	pediveliger / metamorphosis	508.28	527.29
B. azoricus	1624-52	plantigrade	508.98	522.91
B. azoricus	1624-50	plantigrade	509.09	526.21
B. azoricus	1624-51	plantigrade	509.93	555.65
B. azoricus	1624-01	plantigrade	510.00	540.00
B. azoricus	1624-05	pediveliger / metamorphosis	511.57	538.75
B. azoricus	1626-13	plantigrade	512.08	557.19
B. azoricus	1626-34	pediveliger / metamorphosis	512.93	496.23
B. azoricus	1624-55	plantigrade	517.08	546.18
B. azoricus	1626-23	pediveliger / metamorphosis	518.94	524.56
B. azoricus	1626-24	pediveliger / metamorphosis	523.11	547.44
B. azoricus	1624-20	plantigrade	523.27	547.95
B. azoricus	1626-16	pediveliger / metamorphosis	525.34	566.51
B. azoricus	1624-61	plantigrade	525.89	549.88
B. azoricus	1624-09	pediveliger / metamorphosis	529.03	556.03
B. azoricus	1624-43	plantigrade	535.11	552.63
B. azoricus	1624-22	plantigrade	538.01	522.93
B. azoricus	1624-10	pediveliger / metamorphosis	539.56	571.65
B. azoricus	1624-62	plantigrade	548.75	578.23
B. azoricus	1624-17	plantigrade	549.10	583.44
B. azoricus	1624-08	plantigrade	549.94	569.43
B. azoricus	1624-23	plantigrade	564.93	552.87
B. azoricus	1624-44	plantigrade	566.20	507.37
B. azoricus	1643-01	metamorphosis	566.76	597.38
B. azoricus	1624-48	plantigrade	575.36	562.86
B. azoricus	1624-47	plantigrade	578.06	581.35
B. azoricus	1624-63	plantigrade	583.08	605.97
B. azoricus	1624-30	plantigrade	584.02	568.64
B. azoricus	1624-54	plantigrade	592.51	530.33
B. azoricus	1624-40	plantigrade	596.56	615.77
B. azoricus	1624-34	plantigrade	599.79	614.15
B. azoricus	1626-28	plantigrade	602.94	559.04
B. azoricus	1624-58	plantigrade	611.63	579.10
B. azoricus	1624-46	plantigrade	613.10	623.03
B. azoricus	1626-26	plantigrade	614.86	542.38
B. azoricus	1624-07	plantigrade	616.61	592.04
B. azoricus	1626-25	plantigrade	624.21	562.41
B. azoricus	1624-26	plantigrade	631.25	550.14
B. azoricus	1626-31	plantigrade	638.35	561.34

B. azoricus	1626-09	plantigrade	640.41	567.16
B. azoricus	1624-49	plantigrade	643.33	606.26
B. azoricus	1624-64	plantigrade	643.73	618.60
B. azoricus	1624-11	plantigrade	658.55	632.35
B. azoricus	1624-35	plantigrade	665.63	620.81
B. azoricus	1624-59	plantigrade	672.76	630.40
B. azoricus	1624-14	plantigrade	690.20	619.74
B. azoricus	1624-18	plantigrade	706.98	681.92
B. azoricus	1624-65	plantigrade	707.07	681.16
B. azoricus	1626-17	plantigrade	717.93	683.47
B. azoricus	1629-122	plantigrade	730.00	661.00
B. azoricus	1624-21	plantigrade	731.39	646.22
B. azoricus	1626-18	plantigrade	740.99	651.74
B. azoricus	1624-60	plantigrade	744.97	588.15
B. azoricus	1626-22	plantigrade	754.09	679.86
B. azoricus	1629-03	plantigrade	757.01	809.73
B. azoricus	1626-20	plantigrade	772.60	644.87
B. azoricus	1626-27	plantigrade	794.91	662.61
B. azoricus	1624-57	plantigrade	816.73	676.32
B. azoricus	1629-02	plantigrade	833.91	854.09
B. azoricus	1624-39	plantigrade	842.26	739.78
B. azoricus	1629-01	plantigrade	948.74	1000.00
B. azoricus	1624-27	plantigrade	1005.83	788.64
B. azoricus	1624-37	plantigrade	1189.33	825.73
B. azoricus	1624-16	plantigrade	1200.26	794.25
B. azoricus	1624-53	plantigrade	1589.38	951.29
B. azoricus	1626-01	juvenile	2170.00	1430.00
B. azoricus	1624-15	juvenile	2287.17	1526.11
B. azoricus	1624-114	juvenile	2500.00	1600.00
B. azoricus	1629-124	juvenile	2600.00	1500.00
B. azoricus	1624-115	juvenile	2700.00	1700.00
B. azoricus	1626-03	juvenile	2730.00	1120.00
B. azoricus	1626-02	juvenile	2860.00	1630.00
B. azoricus	1624-112	juvenile	2900.00	1800.00
B. azoricus	1624-116	juvenile	2900.00	1800.00
B. azoricus	1629-123	juvenile	3000.00	1800.00
B. azoricus	1624-117	juvenile	3100.00	1900.00
B. azoricus	1624-118	juvenile	3100.00	2000.00
B. azoricus	1624-113	juvenile	3200.00	2000.00
B. azoricus	1624-119	juvenile	3200.00	1800.00
B. azoricus	1624-120	juvenile	3200.00	2000.00
B. azoricus	1624-125	juvenile	3200.00	1900.00
B. azoricus	1624-126	juvenile	3600.00	2100.00
B. azoricus	1626-04	juvenile	3630.00	2020.00
B. azoricus	1624-121	adult	10600.00	6000.00
G. childressi	M102	metamorphosis	383.82	406.78
G. childressi	M103	plantigrade	433.13	463.17

G. childressi	M101	pediveliger	434.37	447.76
G. childressi	M099	plantigrade	949.75	713.60
G. childressi	M098	plantigrade	1070.29	671.88
G. childressi	M100	plantigrade	1325.54	1027.59
B. puteoserpentis	1556-11	pediveliger / metamorphosis	366.37	393.70
B. puteoserpentis	1555-30	plantigrade	372.42	353.10
B. puteoserpentis	1555-27	metamorphosis	385.47	417.85
B. puteoserpentis	1556-36	plantigrade	391.74	306.57
B. puteoserpentis	1555-12	pediveliger / metamorphosis	392.69	424.94
B. puteoserpentis	1556-45	pediveliger / metamorphosis	396.58	362.52
B. puteoserpentis	1555-16	pediveliger	399.37	420.37
B. puteoserpentis	1555-15	pediveliger / metamorphosis	403.77	417.71
B. puteoserpentis	1555-06	pediveliger	404.99	427.36
B. puteoserpentis	1556-30	pediveliger / metamorphosis	405.11	433.54
B. puteoserpentis	1555-32	pediveliger / metamorphosis	405.47	410.07
B. puteoserpentis	1556-58	plantigrade	406.57	424.66
B. puteoserpentis	1556-48	pediveliger / metamorphosis	406.90	285.45
B. puteoserpentis	1556-61	pediveliger	407.91	382.31
B. puteoserpentis	1555-31	pediveliger	409.30	408.16
B. puteoserpentis	1555-28	pediveliger	409.34	415.80
B. puteoserpentis	1556-26	metamorphosis	410.38	428.54
B. puteoserpentis	1555-45	metamorphosis	411.13	442.17
B. puteoserpentis	1555-04	pediveliger	411.23	402.91
B. puteoserpentis	1556-38	pediveliger / metamorphosis	413.07	449.15
B. puteoserpentis	1556-29	plantigrade	414.18	394.26
B. puteoserpentis	1555-14	plantigrade	414.32	394.93
B. puteoserpentis	1556-35	pediveliger / metamorphosis	414.35	426.24
B. puteoserpentis	1555-42	metamorphosis	417.82	413.34
B. puteoserpentis	1555-13	pediveliger / metamorphosis	418.29	413.66
B. puteoserpentis	1556-05	pediveliger	418.47	463.48
B. puteoserpentis	1556-23	pediveliger / metamorphosis	420.67	374.87
B. puteoserpentis	1556-21	pediveliger / metamorphosis	420.91	402.18
B. puteoserpentis	1556-41	pediveliger / metamorphosis	421.44	420.46
B. puteoserpentis	1556-42	pediveliger / metamorphosis	427.02	426.17
B. puteoserpentis	1556-31	pediveliger / metamorphosis	429.36	458.44
B. puteoserpentis	1556-08	plantigrade	430.08	416.34
B. puteoserpentis	1555-44	plantigrade	431.15	401.41
B. puteoserpentis	1555-03	plantigrade	432.29	447.89

B. puteoserpentis	1556-12	pediveliger / metamorphosis	432.40	435.28
B. puteoserpentis	1556-62	plantigrade	432.80	433.97
B. puteoserpentis	1556-07	plantigrade	434.02	445.35
B. puteoserpentis	1556-43	pediveliger / metamorphosis	434.19	429.49
B. puteoserpentis	1556-32	pediveliger / metamorphosis	434.36	454.08
B. puteoserpentis	1556-28	pediveliger / metamorphosis	435.47	429.78
B. puteoserpentis	1555-01	plantigrade	435.53	404.12
B. puteoserpentis	1555-05	metamorphosis	436.44	390.65
B. puteoserpentis	1555-02	plantigrade	439.64	493.34
B. puteoserpentis	1556-10	plantigrade	450.10	462.96
B. puteoserpentis	1556-22	plantigrade	453.32	461.34
B. puteoserpentis	1556-40	plantigrade	455.20	402.18
B. puteoserpentis	1556-02	plantigrade	456.18	460.44
B. puteoserpentis	1556-53	plantigrade	466.25	450.42
B. puteoserpentis	1556-06	plantigrade	470.17	445.82
B. puteoserpentis	1556-37	plantigrade	473.58	461.28
B. puteoserpentis	1556-57	plantigrade	473.80	467.54
B. puteoserpentis	1555-18	plantigrade	476.51	440.72
B. puteoserpentis	1556-03	plantigrade	482.94	463.48
B. puteoserpentis	1556-17	plantigrade	484.55	500.04
B. puteoserpentis	1556-44	plantigrade	501.13	453.77
B. puteoserpentis	1556-34	plantigrade	526.99	520.48
B. puteoserpentis	1556-04	plantigrade	529.17	499.98
B. puteoserpentis	1556-33	plantigrade	541.16	475.78
B. puteoserpentis	1556-24	plantigrade	544.27	457.28
B. puteoserpentis	1556-25	plantigrade	549.36	542.46
B. puteoserpentis	1556-09	plantigrade	557.16	524.54
B. puteoserpentis	1556-16	plantigrade	576.86	563.26
B. puteoserpentis	1556-20	plantigrade	592.62	516.92
B. puteoserpentis	1556-15	plantigrade	594.13	448.48
B. puteoserpentis	1555-17	plantigrade	600.99	508.09
B. puteoserpentis	1556-59	plantigrade	601.97	521.19
B. puteoserpentis	1555-25	plantigrade	602.05	466.03
B. puteoserpentis	1555-23	plantigrade	607.31	501.68
B. puteoserpentis	1556-46	plantigrade	613.12	539.58
B. puteoserpentis	1555-33	plantigrade	618.94	509.97
B. puteoserpentis	1555-24	plantigrade	637.08	536.66
B. puteoserpentis	1555-43	plantigrade	711.47	592.00
B. puteoserpentis	1555-10	plantigrade	716.63	586.06
B. puteoserpentis	1556-14	plantigrade	724.06	501.79
B. puteoserpentis	1555-11	plantigrade	759.12	633.82
B. puteoserpentis	1555-35	plantigrade	823.51	546.17
B. puteoserpentis	1556-60	plantigrade	825.96	671.65
B. puteoserpentis	1555-26	plantigrade	879.14	674.50
B. puteoserpentis	1556-19	plantigrade	886.64	718.74

B. puteoserpentis	1555-39	plantigrade	962.04	725.98
B. puteoserpentis	1555-36	plantigrade	997.00	774.75
B. puteoserpentis	1555-38	plantigrade	998.26	841.35
B. puteoserpentis	1556-39	plantigrade	1092.47	788.72
B. puteoserpentis	1555-37	plantigrade	1126.02	889.74
B. puteoserpentis	1556-63	plantigrade	1178.77	656.87
B. puteoserpentis	1555-19	plantigrade	1192.74	910.69
B. puteoserpentis	1556-52	plantigrade	1212.82	878.79
B. puteoserpentis	1555-29	plantigrade	1221.64	938.29
B. puteoserpentis	1555-40	plantigrade	1284.74	943.78
B. puteoserpentis	1556-18	plantigrade	1325.99	903.58
B. puteoserpentis	1556-27	plantigrade	1384.38	905.20
B. puteoserpentis	1556-56	plantigrade	1510.52	718.12
B. puteoserpentis	1556-55	plantigrade	1803.69	1036.59
B. puteoserpentis	1555-20	plantigrade	1859.55	1279.78
B. puteoserpentis	1556-01	plantigrade	1868.40	1277.92
B. puteoserpentis	1555-46	plantigrade	1952.05	1278.18
B. puteoserpentis	1556-54	plantigrade	1962.02	1243.06
B. puteoserpentis	1556-49	juvenile	2053.09	1451.25
B. puteoserpentis	1556-51	juvenile	2065.05	1246.96
B. puteoserpentis	1555-47	juvenile	2290.10	1508.85
B. puteoserpentis	1542-08	juvenile	2451.12	1586.87
B. puteoserpentis	1556-50	juvenile	2457.04	1942.16
B. puteoserpentis	1274-2	juvenile	2524.32	1395.75
B. puteoserpentis	1542-02	juvenile	2690.55	1743.98
B. puteoserpentis	1555-48	juvenile	2924.96	1879.83
B. puteoserpentis	1555-22	juvenile	3072.61	2060.11
B. puteoserpentis	1542-01	juvenile	3264.23	2132.32
B. puteoserpentis	1555-21	juvenile	3269.13	2216.87
B. puteoserpentis	1542-03	juvenile	3349.20	2254.64
B. puteoserpentis	1542-05	juvenile	3367.48	2309.16
B. puteoserpentis	1556-64	juvenile	3462.94	2475.79
B. puteoserpentis	1542-07	juvenile	3489.01	2288.36
B. puteoserpentis	1542-04	juvenile	3665.60	2481.33
B. puteoserpentis	1274-1	juvenile	3676.82	2148.00
B. puteoserpentis	1542-09	juvenile	3702.11	2467.06
B. puteoserpentis	1542-06	juvenile	3735.93	2450.20
B. puteoserpentis	1556-47	juvenile	3952.60	2389.68
B. puteoserpentis	1277-4	juvenile	4143.63	2375.39
B. puteoserpentis	1277-1	juvenile	4510.80	2560.52
B. puteoserpentis	1277-3	juvenile	4992.68	2956.97
B. puteoserpentis	1277-2	adult	5162.75	2404.32
B. puteoserpentis	812-8	adult	5763.25	3051.52
B. puteoserpentis	812-7	adult	6302.81	4049.28
B. puteoserpentis	812-3	adult	6818.49	4433.88
B. puteoserpentis	812-6	adult	7801.08	5092.31
B. puteoserpentis	812-2	adult	8336.78	5192.61

B. puteoserpentis	812-4	adult	8893.70	5159.90
B. puteoserpentis	812-1	adult	10658.47	5525.67
B. puteoserpentis	812-5	adult	10964.82	5942.90

Table S3. FISH probes used in this study. All probes were labelled with the corresponding fluorophore on the 3' and 5' ends.

name	target	fluorophore	sequence (5'–3')	reference
EUB I	bacteria	2x Atto 647 or 2x Atto 550	GCTGCCTCCCGTAGGAGT	Amann *et al.* [17]
EUB II	bacteria	2x Atto 647 or 2x Atto 550	GCAGCCACCCGTAGGTGT	Daims *et al.* [18]
EUB III	bacteria	2x Atto 647 or 2x Atto 550	GCTGCCACCCGTAGGTGT	Daims *et al.* [18]
Non 338	bacteria	2x Atto 550	ACTCCTACGGGAGGCAGC	Wallner *et al.* [19]
BMARt-193	sulphur-oxidizing bacteria	2x Atto 550 or 2xAtto 594	CGAAGGTCCTCCACTTTA	Duperron *et al.* [20]
BMARm-845	methane-oxidizing bacteria	2x Pacific Blue or 2x Atto 647	GCTCCGCCACTAAGCCTA	Duperron *et al.* [20]

Table S4. Experimental parameters of the SRµCT samples. cam, camera; eff. pixel, effective pixel size; FOV, field of view.

	sample parameters						imaging parameters					reconstruction	
species	**sample identifier**	**develop-mental stage**	**shell length (µm)**	**shell height (µm)**	**mag**	**FOV (mm)**	**eff. pixel (µm)**	**cam**	**# projections**	**exposure (ms)**	**energy (keV)**	**binning**	**final pixel size**
B. puteoser-pentis	1555-22	juvenile	3072.61	2060.11	20×	1.8 × 1.8	0.65	CCD	1200	800	16	2x	1.3 µm
	1555-47	juvenile	2290.09	1508.85	20×	1.8 × 1.8	0.65	CCD	1200	800	16	2x	1.3 µm
	1555-14	plantigrade	414.32	394.93	40×	0.9 × 0.9	0.35	CCD	2400	2700	16	2x	0.7 µm
	1555-30	plantigrade	372.42	353.10	40×	0.9 × 0.9	0.35	CCD	2400	2000	16	2x	0.7 µm
	1555-28	pediveliger	409.34	415.80	40×	0.9 × 0.9	0.35	CCD	2400	2000	16	2x	0.7 µm
	1555-27	pediveliger	385.47	417.85	40×	0.9 × 0.9	0.35	CCD	2400	2000	16	2x	0.7 µm
G. childressi	M101	pediveliger	434.37	447.76	40×	0.9 × 0.9	0.35	CCD	1200	1200	16	2x	0.7 µm
B. azoricus	1643-02	plantigrade	498.16	510.22	40×	0.9 × 0.9	0.35	CCD	1200	1200	16	2x	0.7 µm
	1629-124	juvenile	2600	1500	20×	1.8 × 1.8	0.65	CCD	1200	1500	26,1	2x	1.3 µm
	1624-121	adult	10600	6000	5×	6.6 × 4.9	1.3	cmos	2400	50	25,9	4x	5.1 µm
	1626-01	juvenile	2170	1430	10×	3.6 x 3.6	1.2	CCD	1200	570	25	2x	2.4 µm

Table S5. Shell size comparisons of the two *Bathymodiolus* and one *Gigantidas* species. *G. childressi* pediveliger were the smallest and *B. azoricus* the largest. sd, standard deviation.

	B. azoricus					
	shell length			**shell height**		
	mean (µm)	**sd**	***n***	**mean (µm)**	**sd**	***n***
pediveliger / metamorphosis	490.47	39.15	31	527.89	22.36	31
plantigrade	649.98	194.79	67	612.74	103.72	67
juvenile	2735.43	578.02	5	1545.22	326.75	5
	G. childressi					
	shell length			**shell height**		
	mean (µm)	**sd**	***n***	**mean (µm)**	**sd**	***n***
pediveliger / metamorphosis	409.09	35.74	2	427.27	28.98	2
plantigrade	944.67	375.29	4	719.06	233.04	4
juvenile	/	/	/	/	/	/
	B. puteoserpentis					
	shell length			**shell height**		
	mean (µm)	**sd**	***n***	**mean (µm)**	**sd**	***n***
pediveliger / metamorphosis	412.38	17.28	32	413.50	34.73	32
plantigrade	782.08	431.85	65	616.36	238.85	65
juvenile	4556.66	2430.18	32	2786.70	1316.99	32

Table S6. Relative organ sizes of one representative per developmental stage in *B. puteoserpentis*. The gills grow substantially over the course of development and the digestive system shrinks between the plantigrade and juvenile stages.

tissue	pediveliger	metamorphosis	plantigrade	juvenile / adult
	relative volume (%)	relative volume (%)	relative volume (%)	relative volume (%)
soft body	100	100	100	100
gills	4.1	23.0	23.1	56.8
foot	11.5	20.4	25.4	16.3
central nerve system	4.1	9.0	7.3	1.2
lipid vesicles	12.8	3.9	1.5	absent
digestive system	29.4	37.8	35.4	9.0
stomach and digestive gland	1.6	5.0	4.0	7.2
velum	32.2	absent	absent	absent
adductor muscle	15.0	7.5	6.6	6.1
retractor muscle	3.7	2.3	2.2	3.3

Table S7. Bacterial densities are highest in adult mussels. Host and bacterial cell areas were calculated from TEM images and set into relation to estimate bacterial densities.

developmental stage	averaged symbiont area per host cell (%)	minimum symbiont area per host cell (%)	maximum symbiont area per host cell (%)	standard deviation	number of host cells / number of mussels
pediveliger	absent	absent	absent	absent	absent
metamorphosis	13.7	2.0	23.2	6.3	12 / 2
plantigrade	19.4	12.2	29.0	5.0	10 / 2
adults	24.4	15.6	32.1	6.1	6 / 2

Table S8. Degree of digestive system reduction in bivalves living in chemosynthetic systems. =, normally developed; -, reduced morphology; /, total disappearance; n.d., no data. The Reduction of the digestive system in mussels from sulphide-rich habitats was revived in [21].

	B. azoricus [22]	*B. brooksi* [23]	*B. heckerae* [23]	*B. thermophilus* [24]	*Solemya reidi* [25]	*Calyptogena magnifica* [26]
labial palps	=	=	-	-	-	-
intestine	-	-	-	-	/	-
stomach	-	-	-	-	/	-
crystalline style and style sac	=	n.d.	n.d.	-	/	-
digestive tubule	-	-	-	-	/	-
digestive gland secretory cells	=	n.d.	n.d.	=	/	-
digestive system	-	-	-	-	/	-

Table S9 FISH hybridisation buffer

	30% formamide (ml)	35% formamide (ml)
5 M NaCl	1.08	1.08
1 M TrisHCl	0.12	0.12
Formamide	1.80	2.10
H_2O	3.00	2.70
20% SDS	0.003	0.003

Table S10 FISH washing buffer

	30% formamide (ml)	35% formamide (ml)
5 M NaCl	1.02	0.70
1 M TrisHCl	1.00	1.00
0.5 M EDTA	0.50	0.50
H_2O	add to 50 ml	add to 50 ml
20% SDS	0.025	0.025

Supplementary figures

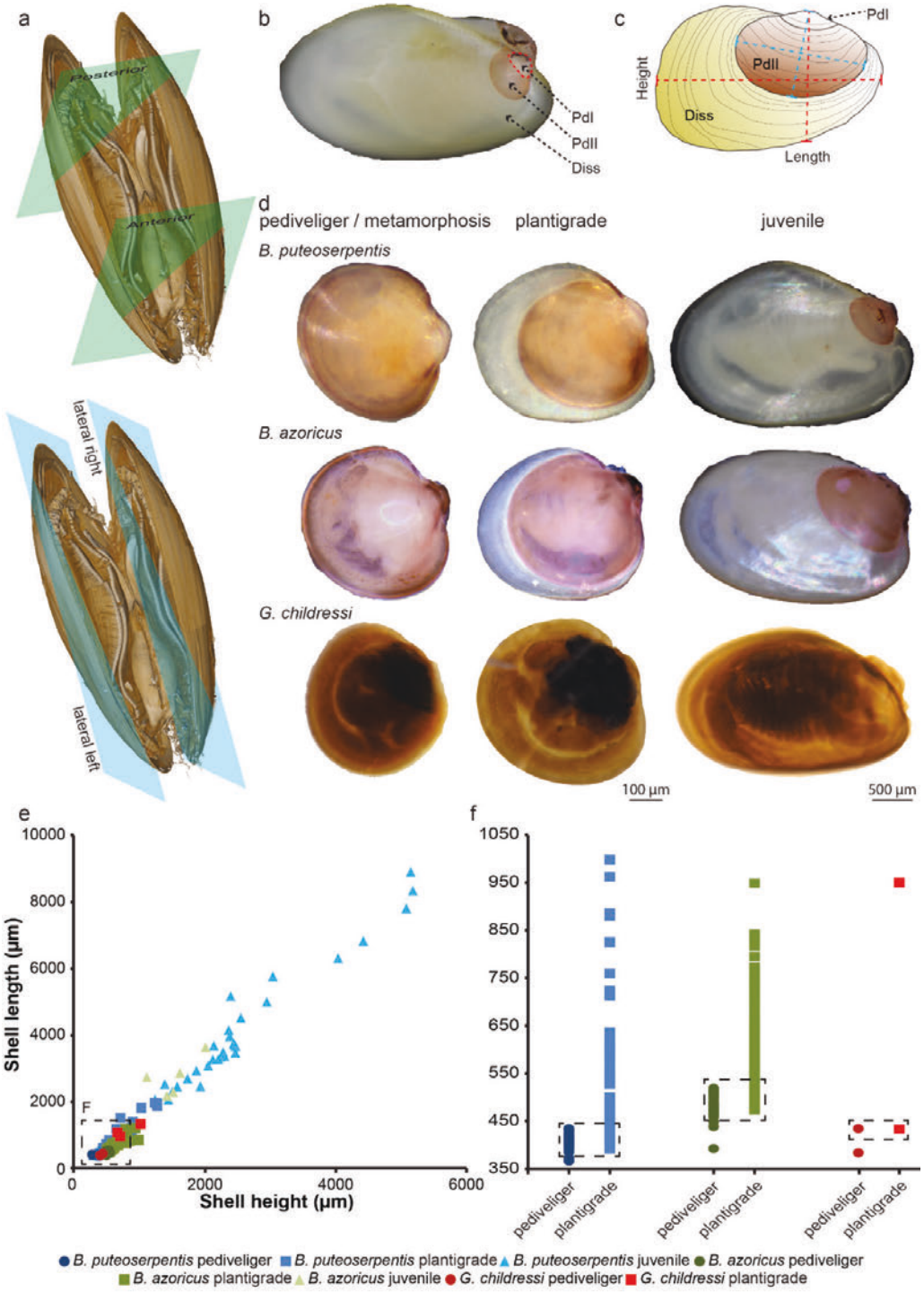

Figure S1. Sample overview and shell dimensions. a) Volume rendering of a *B. azoricus* mussel of 3 cm length showing representations of two different directions of sectioning (anterior to posterior and lateral left to lateral right). **b)** Visualization of the three different shell types of *Bathymodiolus* and *Gigantidas* mussels. **c)** Schematic drawing of the different shell types and the directions of shell measurement. **d)** Examples of the three analysed mussel species at three developmental stages. **e)** Plot of shell length vs. shell height, showing overlap between different developmental stages. **f)** Distribution of shell length for pediveligers and plantigrade. The dashed boxes show the overlap between pediveliger and plantigrade. Pdl, prodissoconch I; PdII, prodissoconch II; dis, dissoconch.

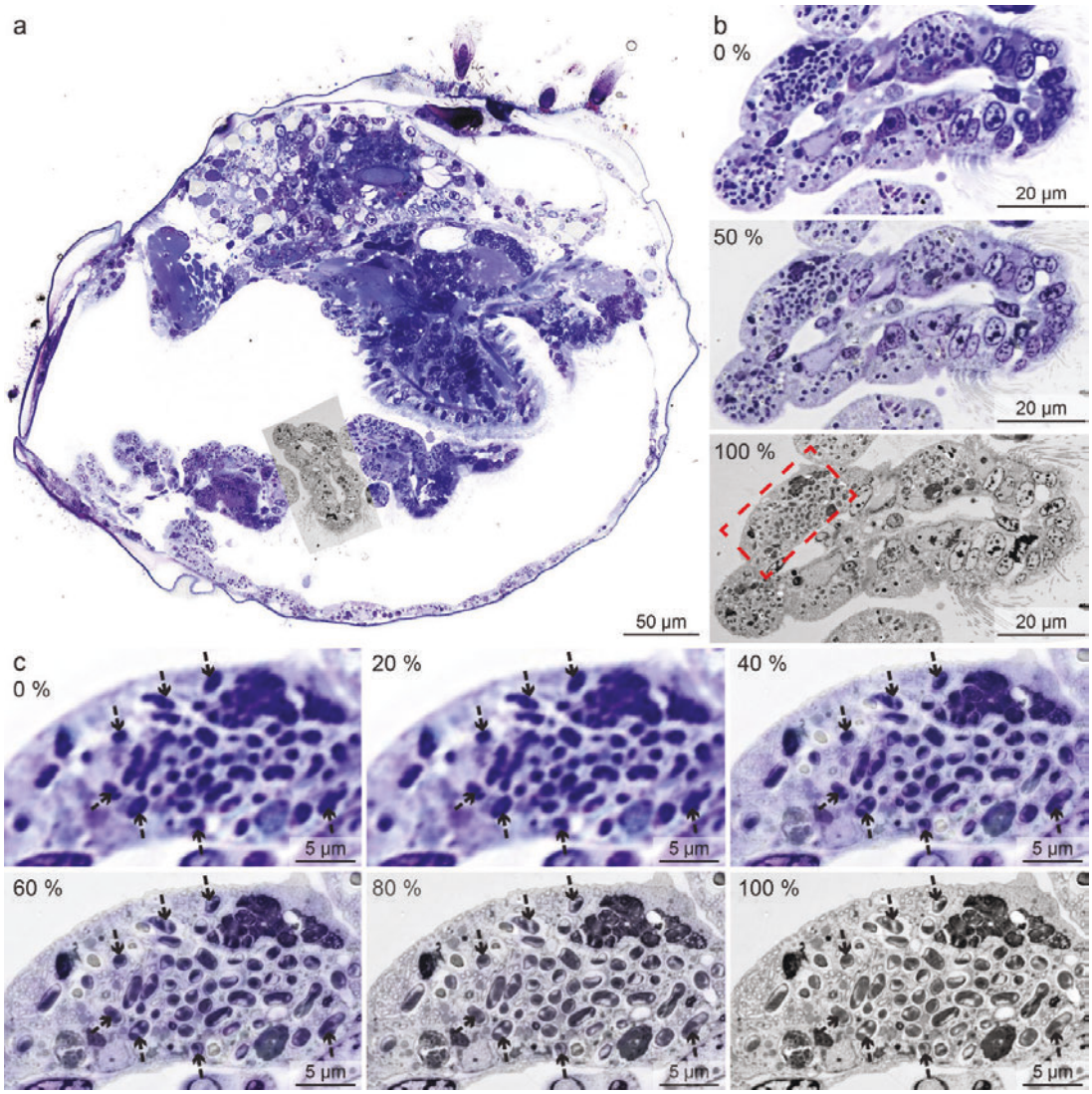

Figure S2. Light microscopic analysis predicts the presence of symbionts, and can be verified with correlative TEM. The overview image (**a**) shows a cross section of a *B. puteoserpentis* mussel during metamorphosis which is already colonized by symbionts. Overlaying LM and TEM data of the same section and area allows identification of MOX symbionts as dark blue dots in the LM data (**b,c**). The percentages are showing value of transparency of the TEM-image. The LM and TEM images were co-registered by using morphological landmarks.

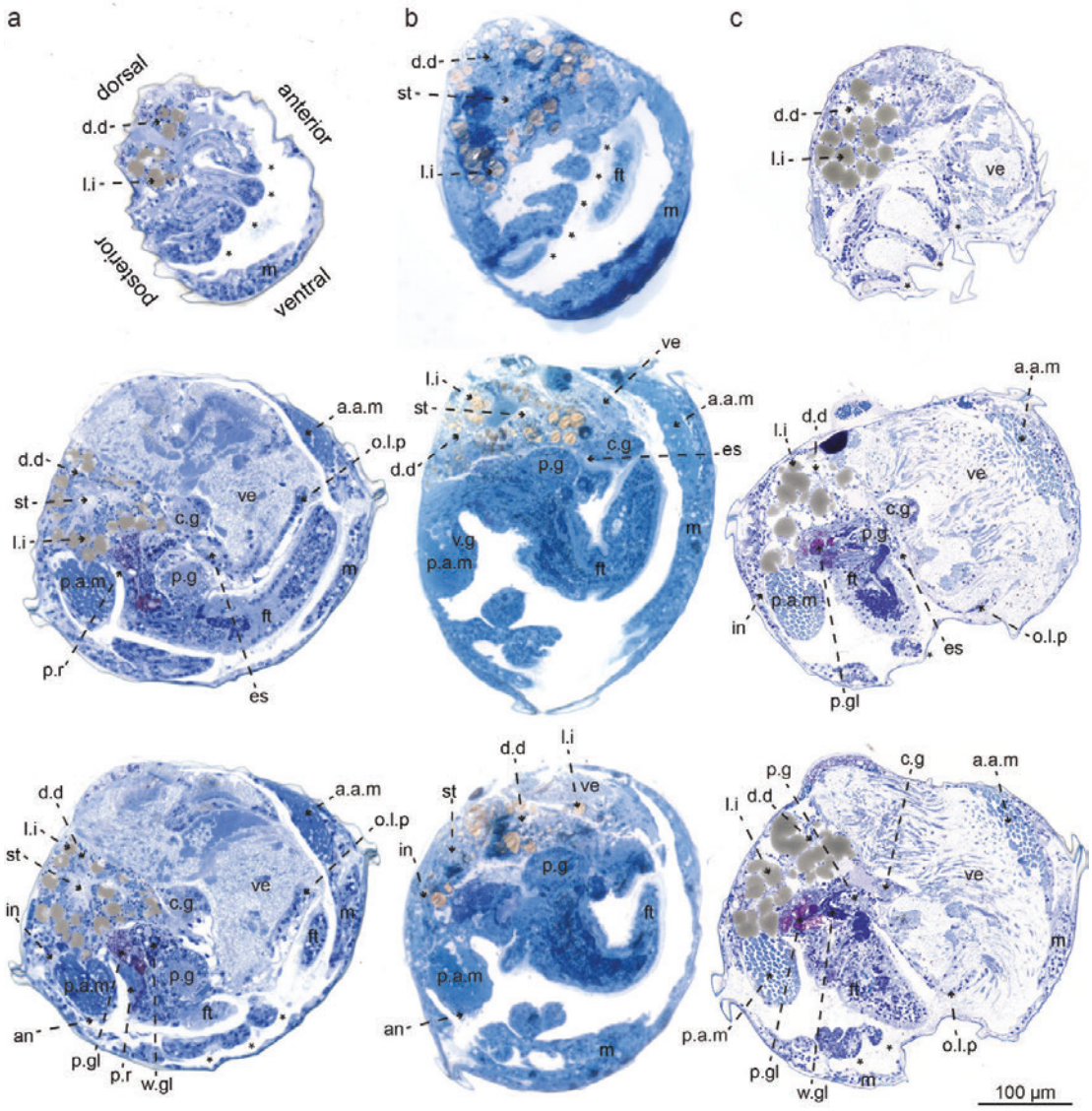

Figure S3. Morphological comparison of *B. puteoserpentis* (a), *G. childressi* (b) and *B. azoricus* (c) pediveliger. From top to bottom, representative micrographs at incremental locations along the lateral–lateral (left–right) axis presenting the detailed morphology of the three analysed species. All major organs, including the foot, gills, velum, digestive system and central nervous system, are similarly developed in the three species. a.a.m, anterior adductor muscle; c.g, cerebral ganglion; d.d, digestive diverticulum; es, esophagus; ft, foot; in, intestine; l.i, lipid vesicles; l.l.p, lower labial palp; m, mantle; o.l.p, oral labial palp; p.a.m, posterior adductor muscle; p.g, pedal ganglia; p.gl, purple gland; r.m, retractor muscle; s.s, style sac; st, stomach; u.l.p, upper labial palp; ve, velum; v.g, visceral ganglion; w.gl, white gland and *, gill filament.

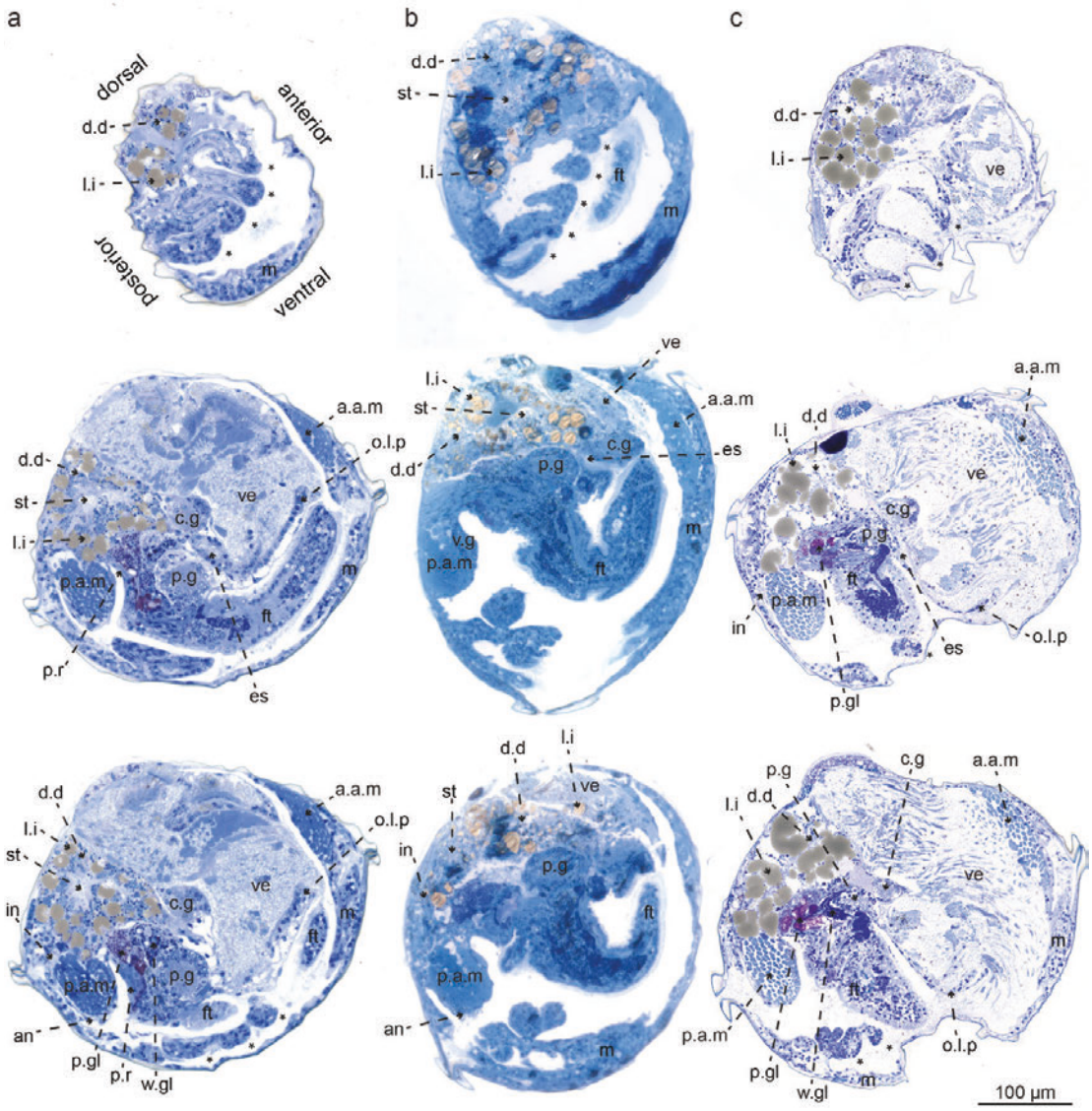

Figure S4. Morphological comparison of *B. puteoserpentis* (a), *G. childressi* (b) and *B. azoricus* (c) plantigrade. From top to bottom, representative micrographs at incremental locations along the lateral–lateral (left–right) axis in plantigrades presenting the detailed morphology of the three analysed species. Only the number of gill filaments differs between the three species. a.a.m, anterior adductor muscle; c.c, cerebral commissure; c.g, cerebral ganglion; d.d, digestive diverticulum; es, esophagus; ft, foot; g.s, gastric shield; in, intestine; l.i, lipid inclusion; l.l.p, lower labial palp; m, mantle; p.a.m, posterior adductor muscle; p.g, pedal ganglia; p.gl, purple gland; r.m, retractor muscle; s.s, style sac; st, stomach; u.l.p, upper labial palp; v.g, visceral ganglion; w.gl, white gland and *, gill filament.

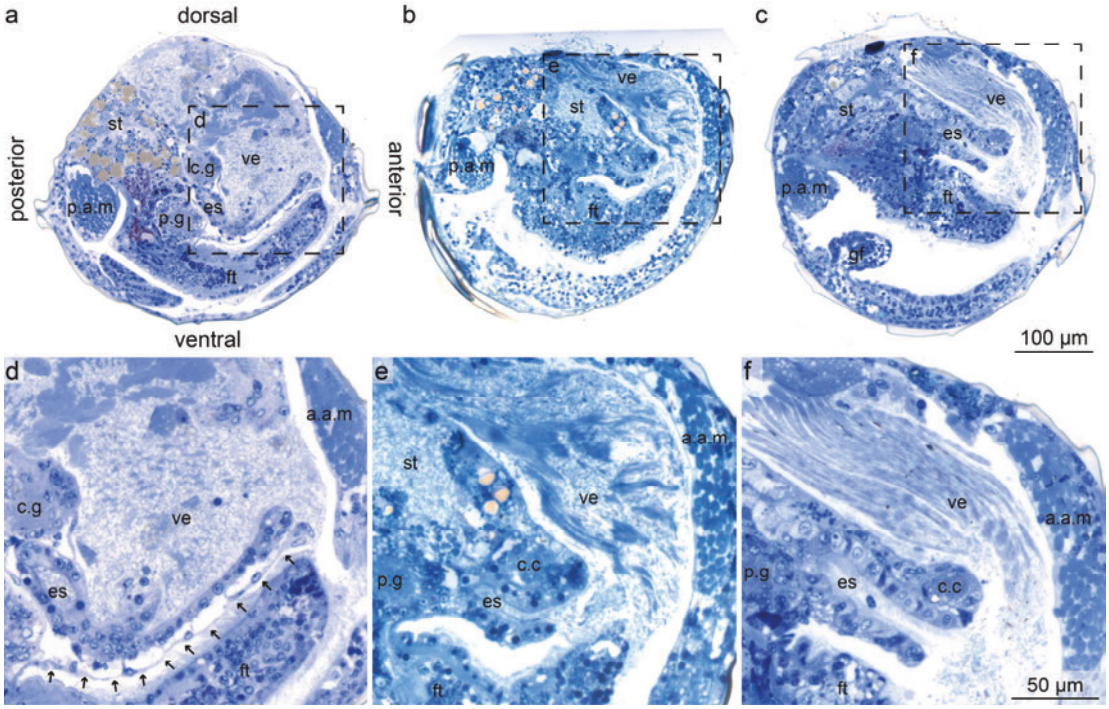

Figure S5. As metamorphosis in *B. puteoserpentis* progresses, velum degradation begins at the most posterior part of the velum. In a first step, the velum membrane (indicated by black arrows in **d**) is degraded, followed by the degradation of the velar tissue (**e,f**). Dashed boxes in a–c are shown magnified in d–f. The same morphological pattern was also observed in *B. azoricus* and *G. childressi.* a.a.m, anterior adductor muscle; c.c, cerebral commissure; c.g, cerebral ganglion; es, esophagus; ft, foot; p.a.m, posterior adductor muscle; p.g, pedal ganglia; st, stomach; ve, velum and *, gill filament.

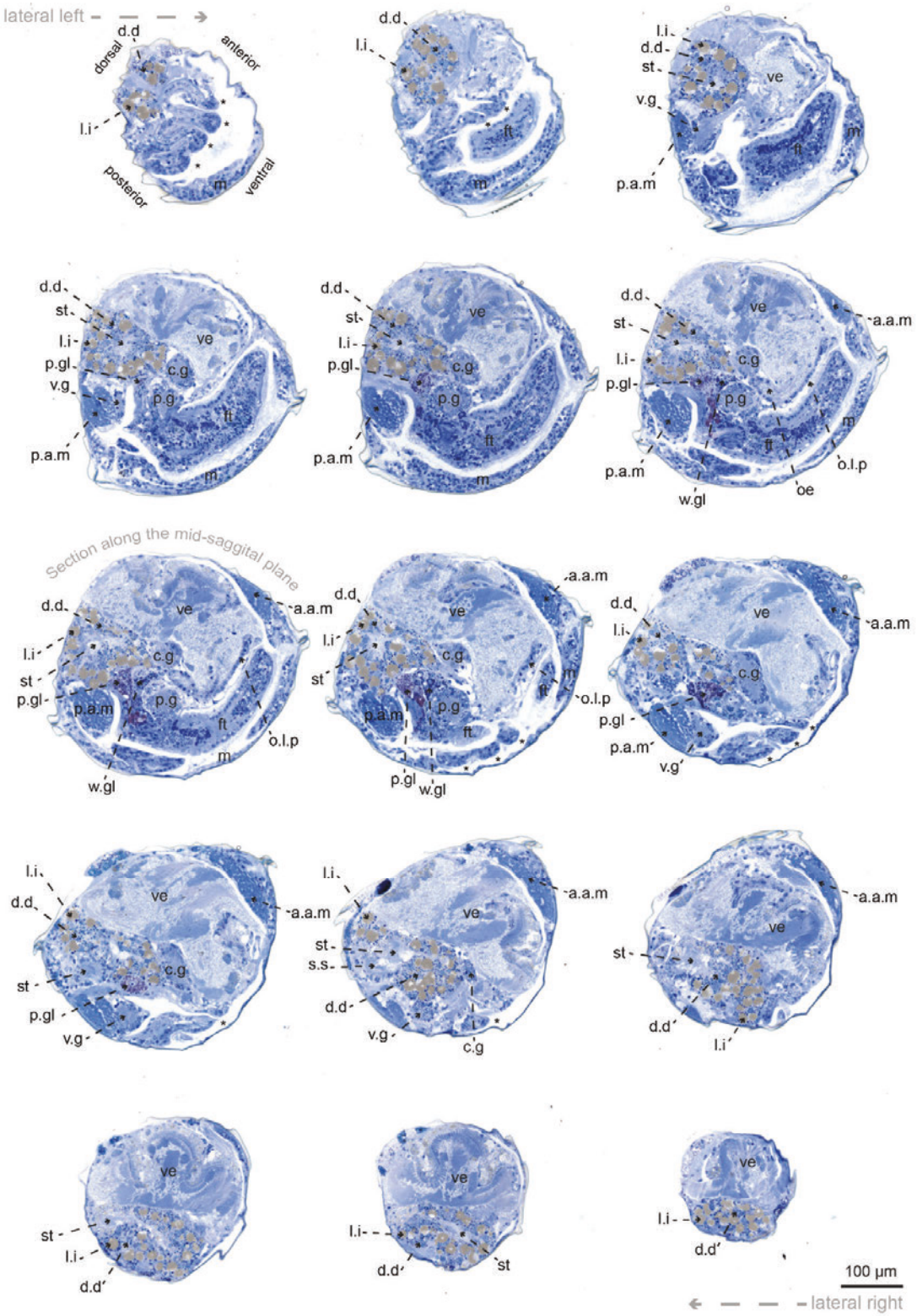

Figure S6. Serial sections of a *B. puteoserpentis* pediveliger. From top left, to bottom right, sections stained with toluidine blue at incremental locations along the sagittal axis. a.a.m, anterior adductor muscle; c.g. cerebral ganglion; d.d, digestive diverticula; ft. foot; l.i, lipid inclusion: m, mantle; o.l.p, oral labial palp; p.a.m, posterior adductor muscle; p.g, pedal ganglia; p.gl, purple gland; st, stomach; ve, velum; v.g, visceral ganglion; w.gl, white gland and *, gill filament.

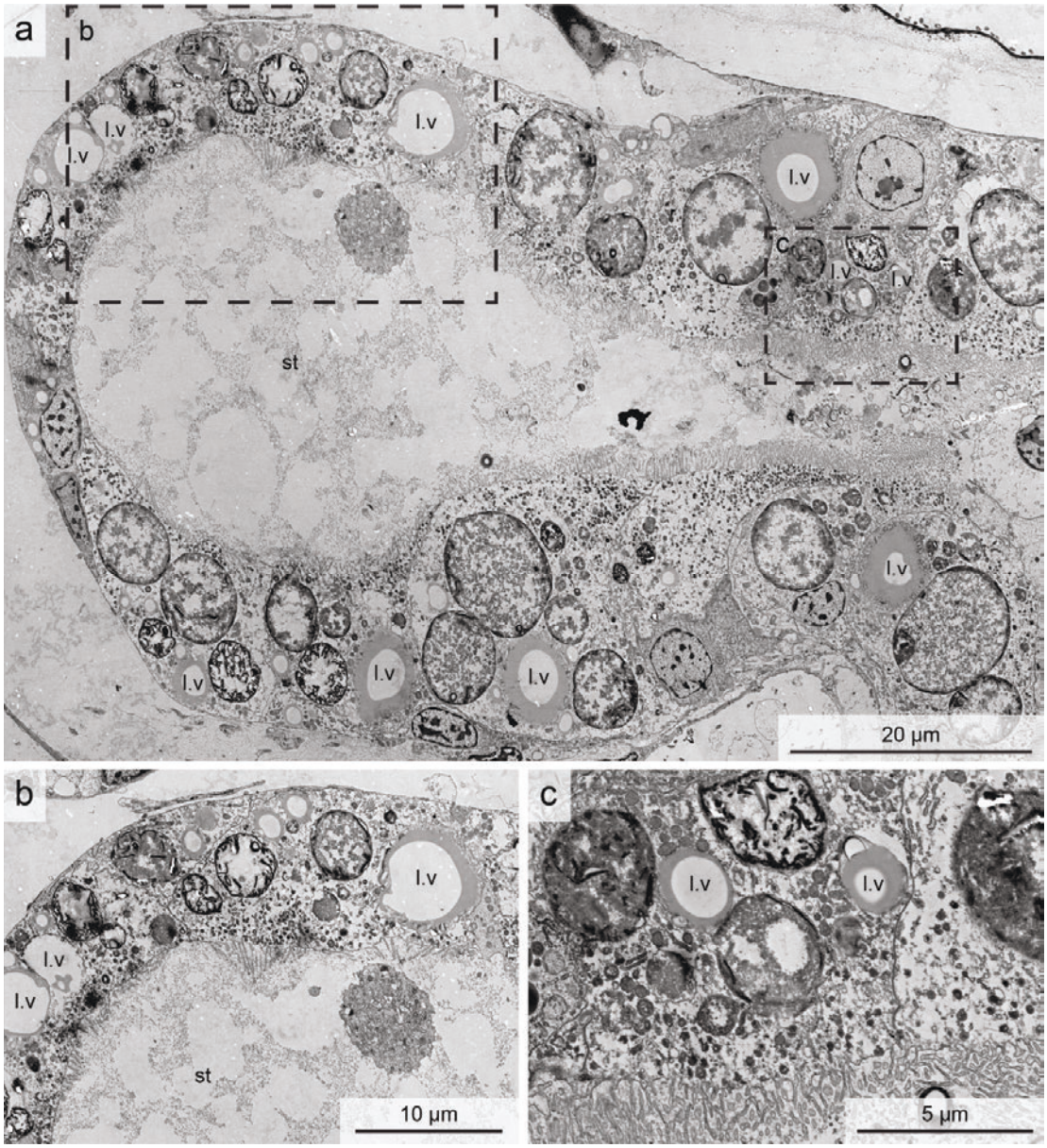

Figure S 7 TEM data of the digestive system of a *B. puteoserpentis* plantigrade shows lipid vesicles in the epithelia cells of the stomach. Lipid vesicles (l.v) are not only located in the digestive diverticula but also in epithelia cells outlining the stomach (st).

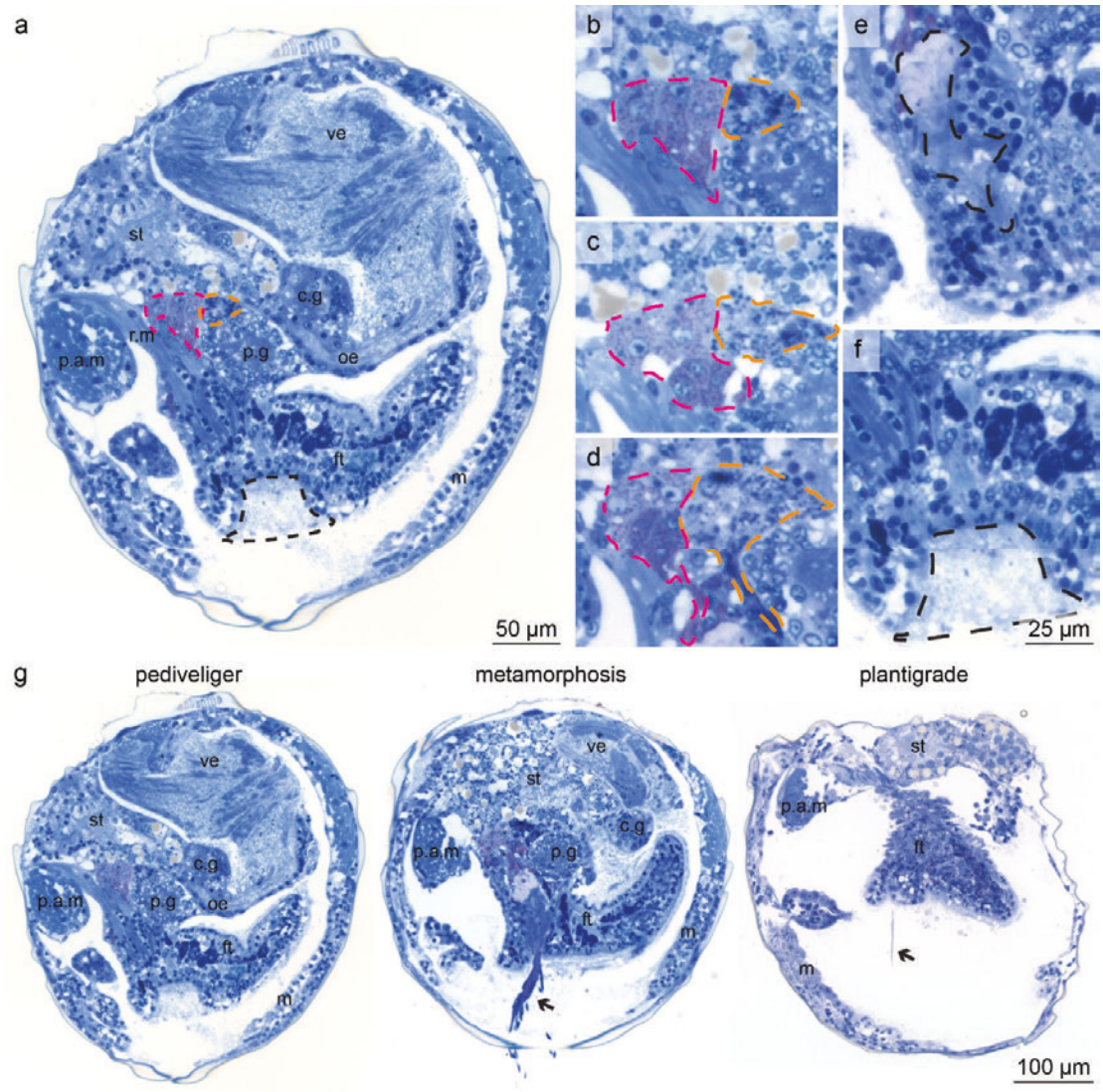

Figure S8. The *B. puteoserpentis* foot is well developed already during the pediveliger stage. In the pediveliger stage, three glands can be identified (**a-f**): the purple gland (outlined in magenta), the white gland (outlined in orange) and the byssus gland and duct (outlined in black). During metamorphosis, the byssus threads (indicated by black arrows; **g**) were produced. c.g, cerebral ganglion; ft, foot; m, mantle; oe, oesophagus; p.a.m, posterior adductor muscle; p.g, pedal ganglion; r.m, retractor muscle; st, stomach and ve, velum.

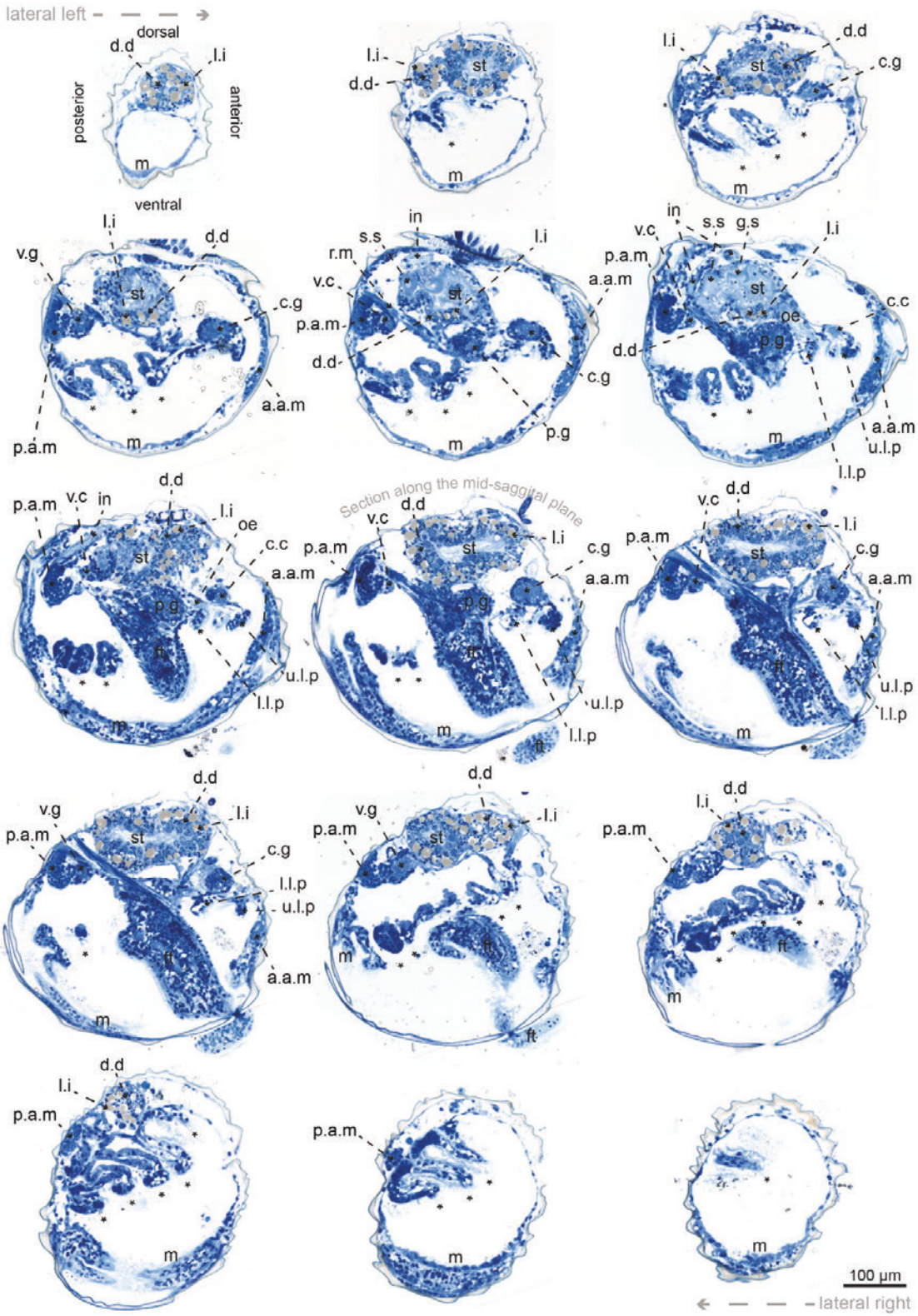

Figure S9. Serial sections of a *B. puteoserpentis* metamorphosing mussel. From top left, to bottom right, micrographs at incremental locations along the sagittal axis. a.a.m, anterior adductor muscle; c.g, cerebral ganglion; d.d, digestive diverticulum; es, esophagus; ft, foot; g.s, gastric shield; in, intestine; l.i, lipid inclusion; l.l.p, lower labial palp; m, mantle; p.a.m, posterior adductor muscle; p.g, pedal ganglia; r.m, retractor muscle; s.s, style sac; st, stomach; u.l.p, upper labial palp; ve, velum; v.g, visceral ganglion and *, gill filament.

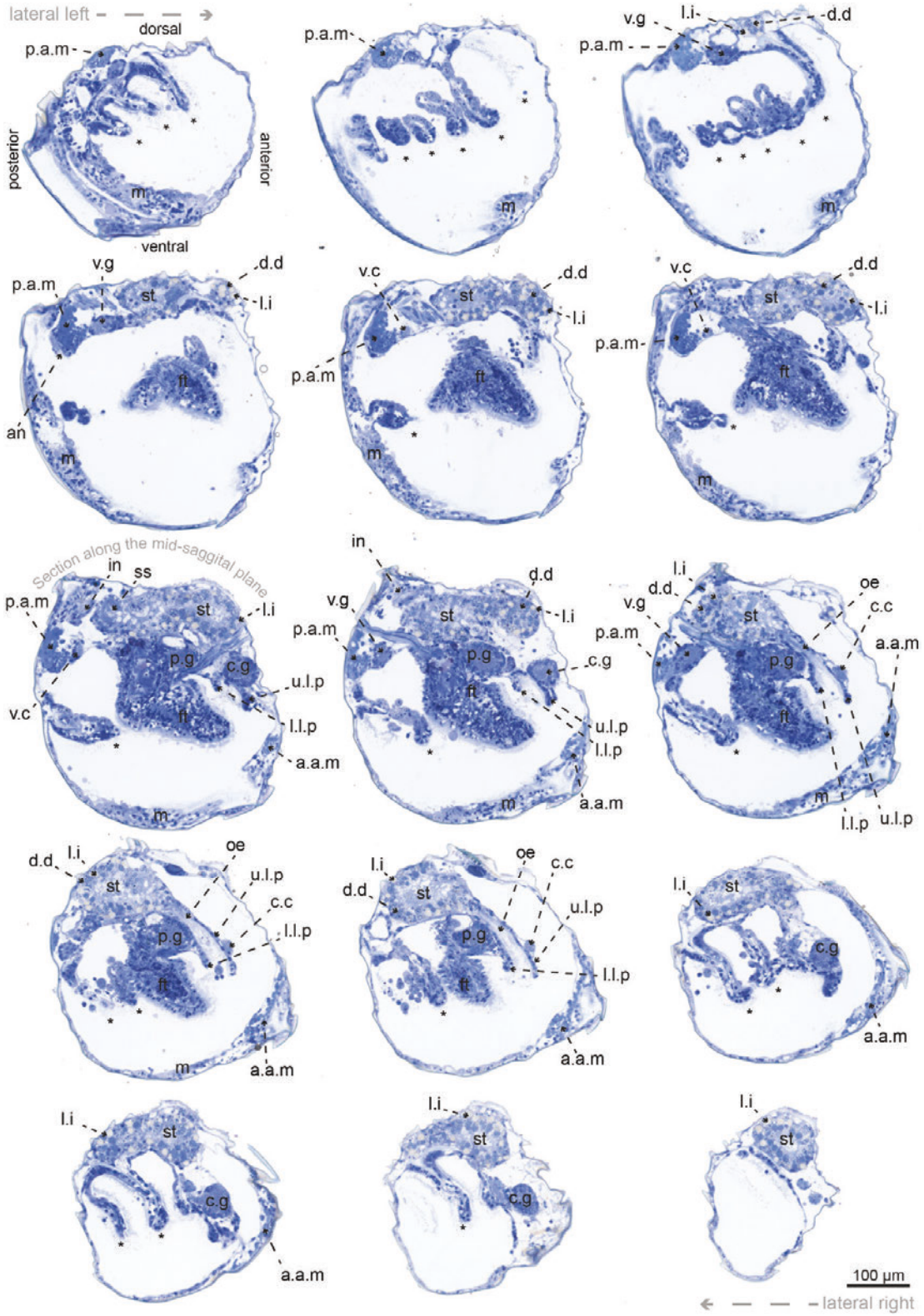

Figure S10. Serial sections of a *B. puteoserpentis* plantigrade. From top left, to bottom right, sections stained with toluidine blue at incremental locations along the sagittal axis. a.a.m, anterior adductor muscle; c.g, cerebral ganglion; d.d, digestive diverticulum; es, esophagus; ft, foot; g.s, gastric shield; in, intestine; l.i, lipid inclusion; l.l.p, lower labial palp; m, mantle; p.a.m, posterior adductor muscle; p.g, pedal ganglia; r.m, retractor muscle; s.s, style sac; st, stomach; u.l.p, upper labial palp; ve, velum; v.g, visceral ganglion and *, gill filament.

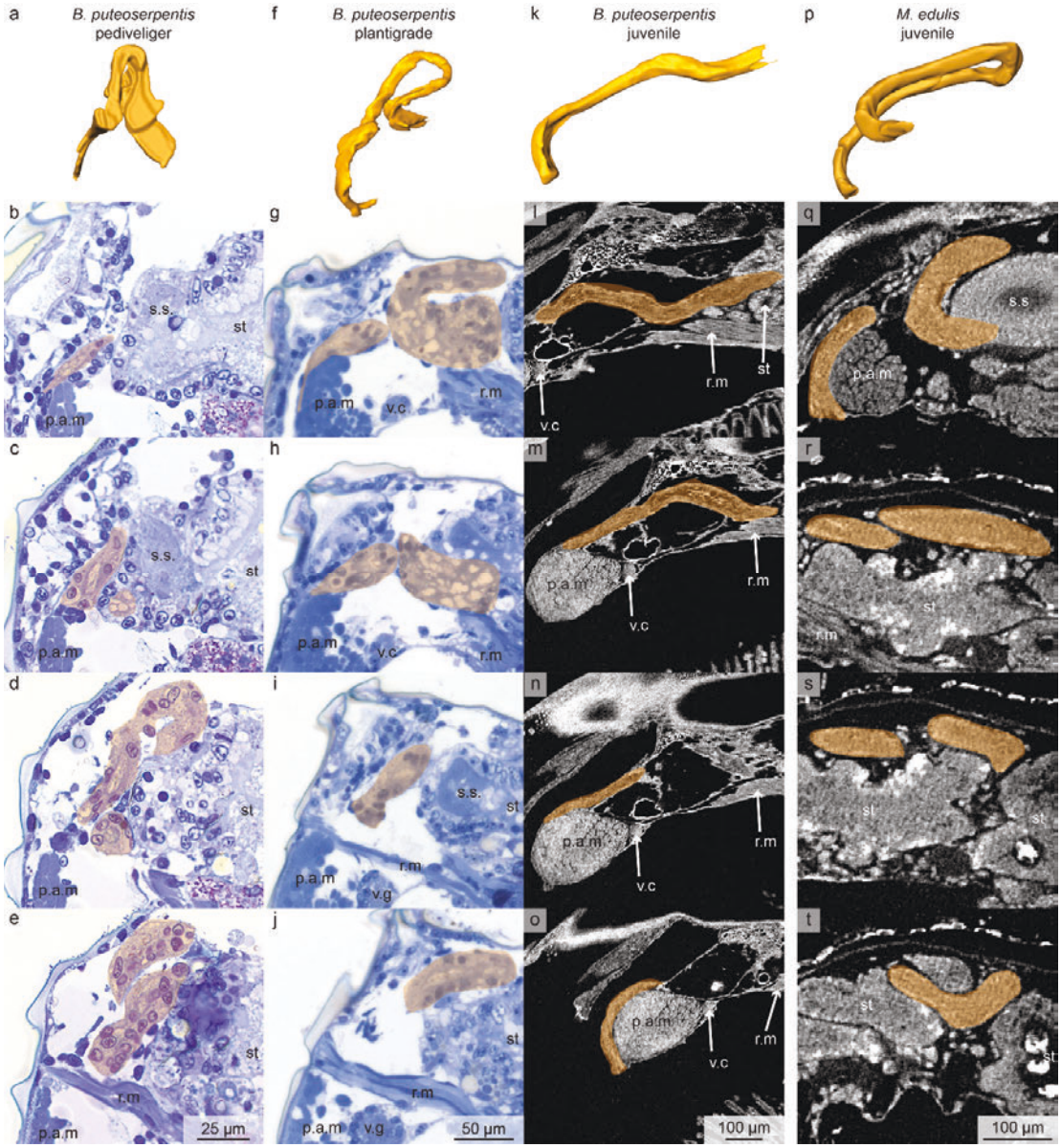

Figure S11. The looped intestine of the *B. puteoserpentis* pediveliger straightens after metamorphosis in comparison to *M. edulis* were it stays looped. 3D reconstructions of the intestine (**a, f** and **k**) show the morphological change over the course of development in *B. puteoserpentis*. Representative serial sections (top to bottom) show a looped intestine in the pediveliger (**b–e**) and plantigrade (**g–j**). The straight intestine is shown by visual slices through SRµCT data from a *B. puteoserpentis* juvenile (**l–o**). In contrast the intestine of a juvenile *M. edulis* mussel stays looped (**p, q–t**). The intestine is indicated by orange coloration in the section series and SRµCT data. Note the different scales for the pediveliger, plantigrade and juvenile mussel. p.a.m, posterior adductor muscle; r.m, retractor muscle; s.s, style sac; st, stomach; v.c, visceral commissure and v.g, visceral ganglion.

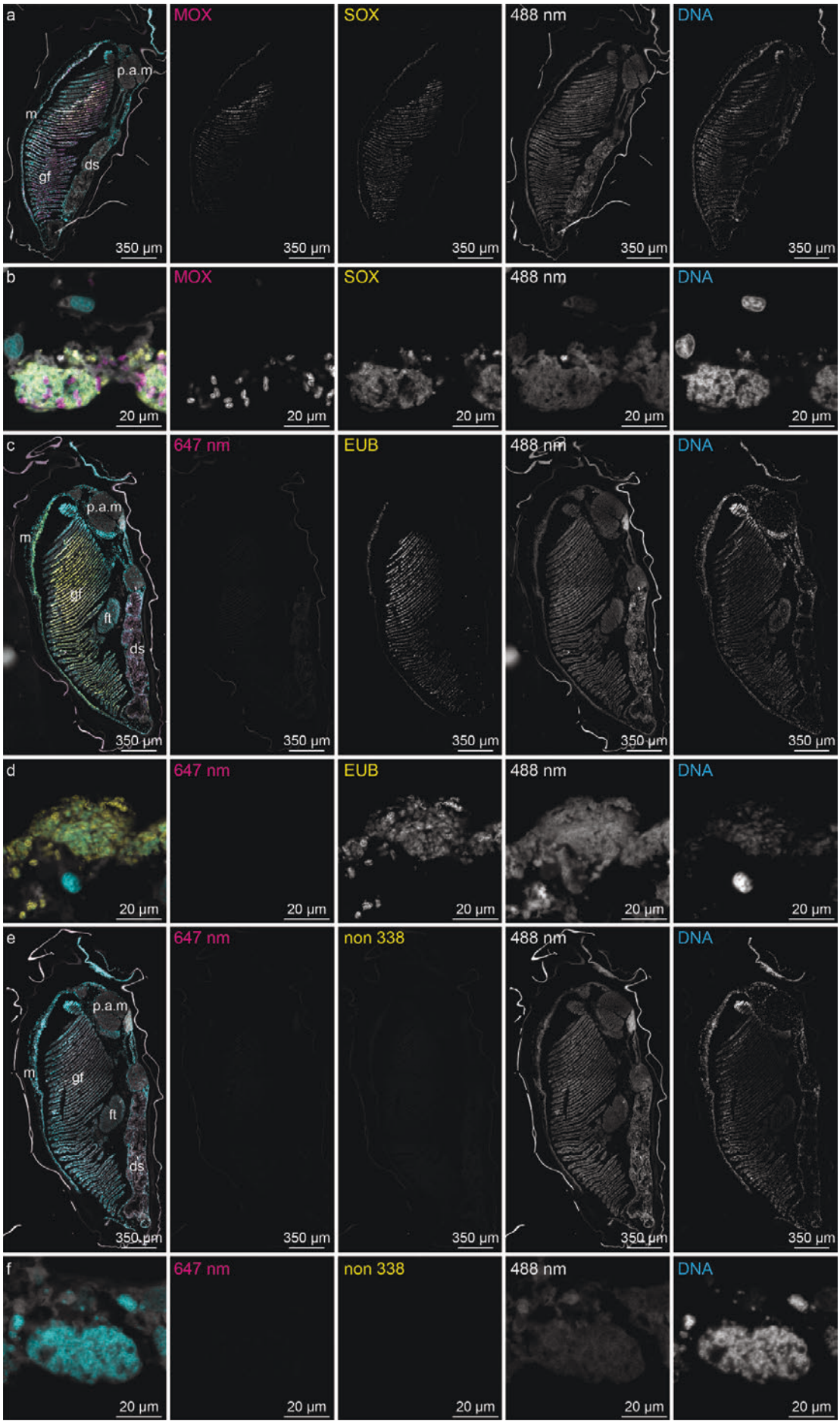
a
MOX
SOX
488 nm
DNA
p.a.m
m
gf
ds
350 µm
b
20 µm
c
647 nm
EUB
ft
d
e
non 338
f

Figure S12. Fluorescence *in situ* hybridization (FISH) of specific symbionts and controls in cross sections of a *B. puteoserpentis* juvenile mussel. Specific oligonucleotides targeting the rRNA of SOX and MOX bacteria show symbiont distributions in the gills and the mantle (**a**). SOX symbionts are represented in yellow and MOX symbionts in magenta. The 488-nm and 647-nm channels were used to detect autofluorescence of the host tissue. DAPI was used as a DNA counterstain (represented in cyan). Both symbiont types colonize the same bacteriocytes (**b**; magnified region of **a**). As a positive control, the EUB I-III probes which stain all eubacteria were used (**c** and **d**; represented in yellow). The EUB I-III signal shows the same symbiont distr bution as seen in **a** and **b.** As a negative control, the NON 338 probe was used (**e** and **f**; represented in yellow), which shows no signal. ds, digestive system; ft, foot: gf, gill filament; m, mantle and p.a.m, posterior adductor muscle.

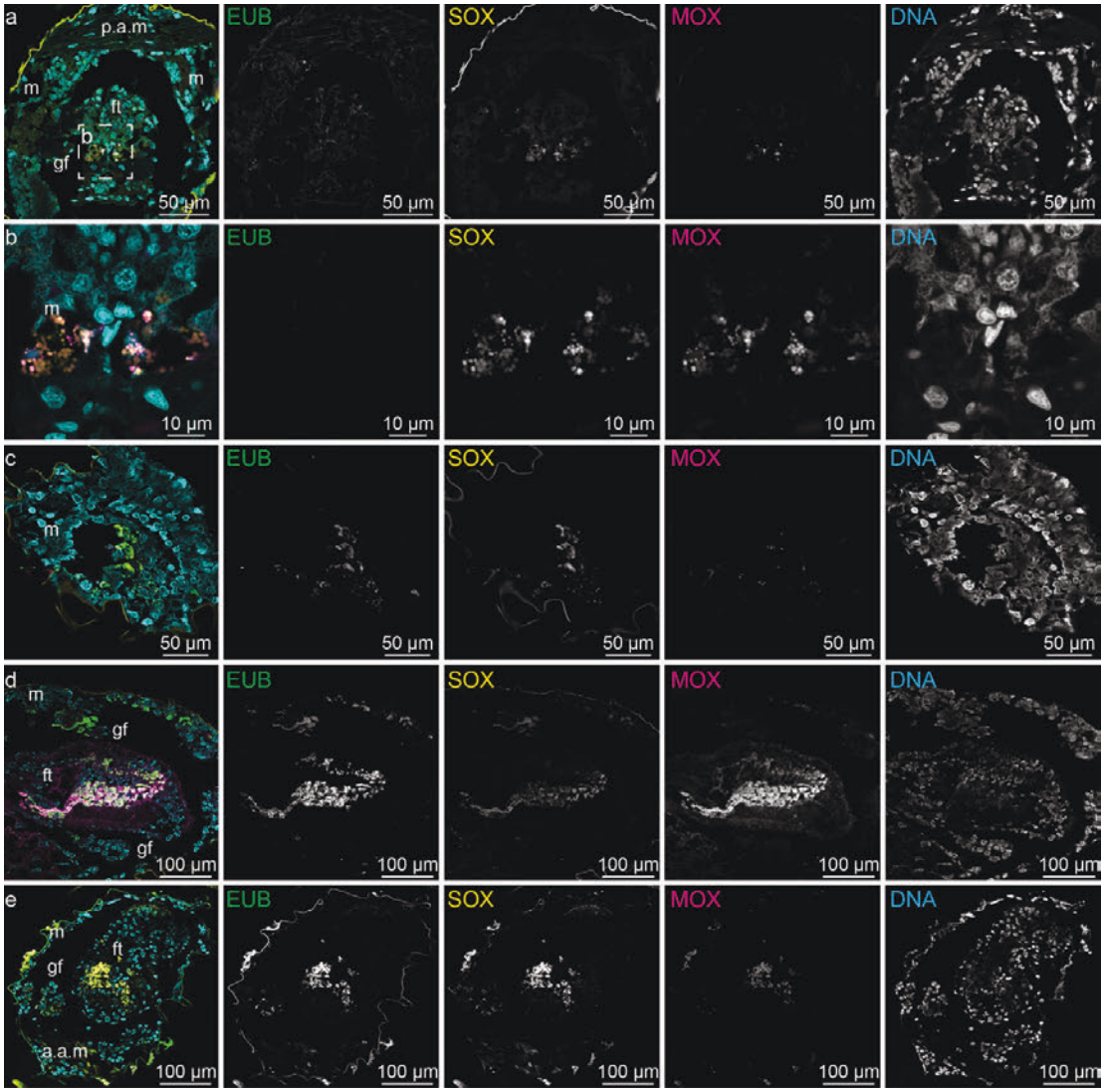

Figure S13. Fluorescence *in situ* hybridization (FISH) of different developmental stages of *B. puteoserpentis* mussels. The *B. puteoserpentis* pediveliger (**a** and **b**) was aposymbiotic. We interpreted the fluorescent signal which can be observed in the foot as autofluorescence, because the EUB channel did not gave any signal in that specific region. Specific oligonucleotides targeting the rRNA of SOX and MOX bacteria show symbiont distributions in the mantle, foot and gills of a *B. puteoserpentis* plantigrade (**c** and **d**). The SOX are represented in yellow and the MOX in magenta. As a positive control, we used the EUB I-III probes (green) to target all bacteria. As a DNA counterstain, DAPI was used (represented in cyan). Both SOX and MOX bacteria were present in all epithelial tissues. The gill filaments of a *B. puteoserpentis* metamorphosing mussel (**e**) was only colonized by SOX, the foot and the mantle by SOX and MOX. a.a.m, anterior adductor muscle; ft, foot; gf, gill filament, m, mantle and p.a.m, posterior adductor muscle.

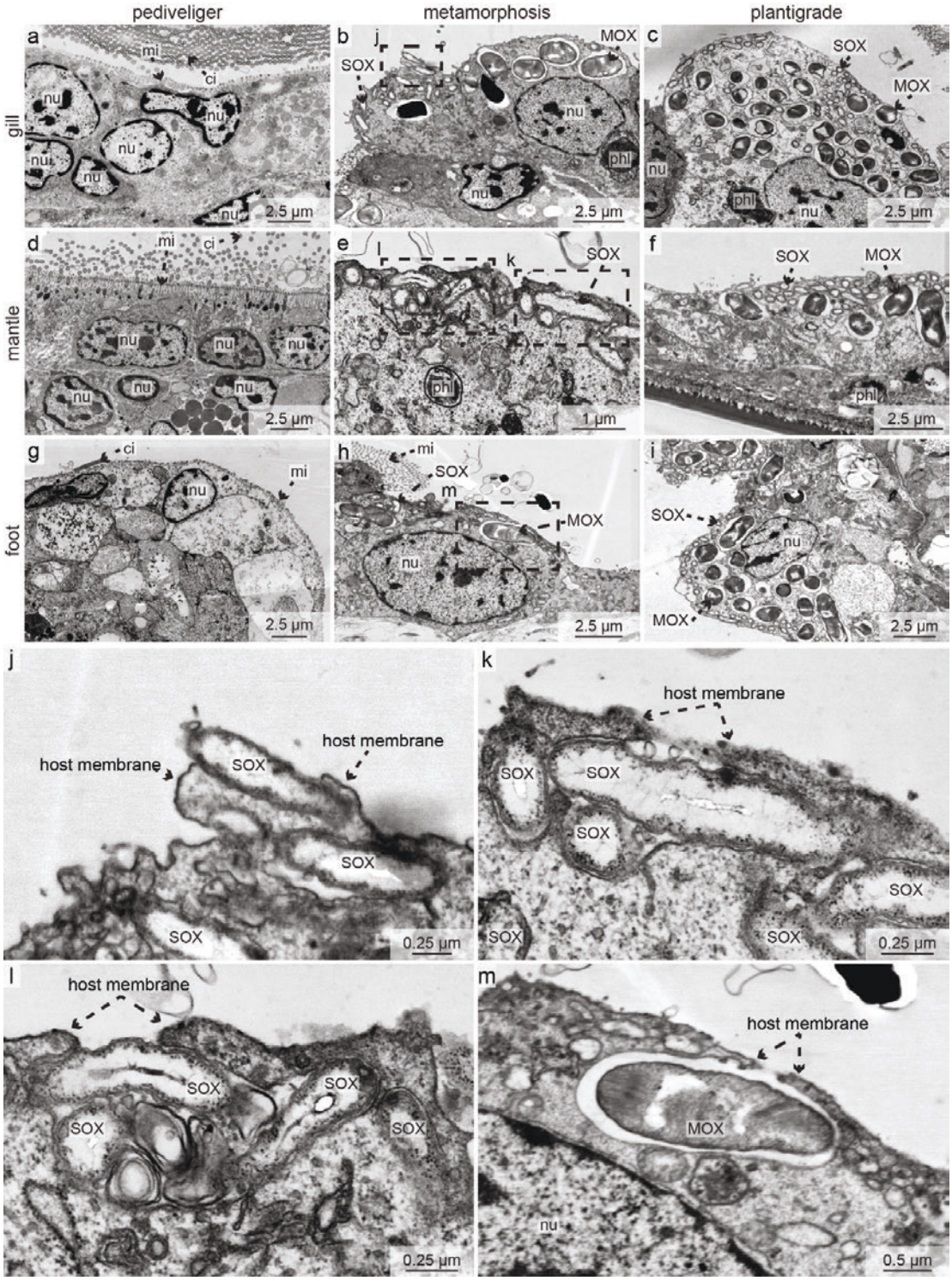

Figure S14. Symbiont colonization starts during the the metamorphosis in *Bathymodiolus puteoserpentis*. TEM micrographs of different epithelial tissues and their state of symbiont colonization: gills (**a–c**), mantle (**d–f**) and foot (**g–i**) of individuals at the pediveliger (**a, d** and **g**), metamorphosis (**b, e** and **h**) and plantigrade stage (**c, f** and **i**). All epithelial tissues of the pediveliger stage are aposymbiotic (**a**, **d** and **g**). During the metamorphosis, the colonization of both symbiont types is still ongoing (**b**, **e** and **h**). In the plantigrade stage, all epithelial tissues are colonized by both symbiont types (**c, f** and **i**). Dashed boxes indicate regions in which symbionts are actively colonizing epithelial tissue (shown magnified in **j – m**). ci, cilia; mi, microvilli; MOX, methane-oxidizing symbiont; nu, nucleus; phl, phagolysosome; SOX, sulphur-oxidizing symbiont.

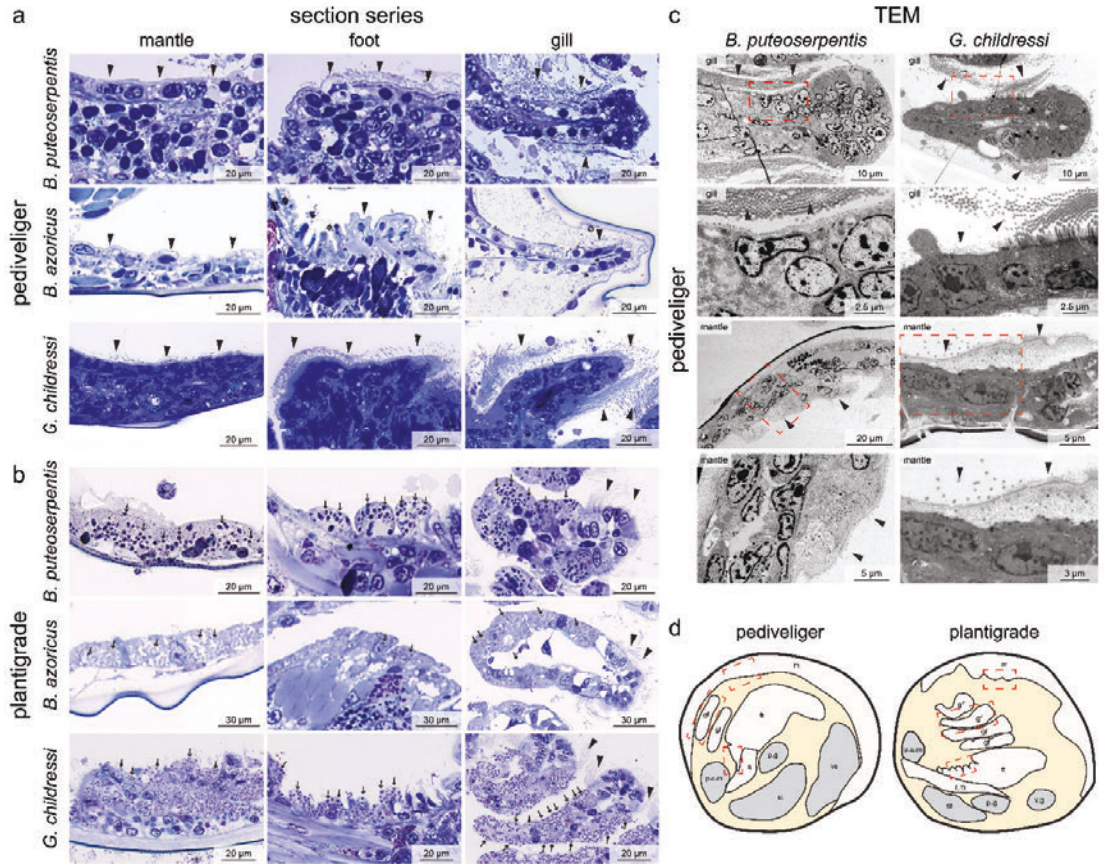

Figure S15 Light and electron microscopy comparison of *B. puteoserpentis, B. azoricus* and *G. childressi*
The light microscopy comparison between pediveliger (**a**) and plantigrades (**b**) shows that the morphological characteristics (hypertrophy, cilia and microvilli loss), which indicate a symbiont colonization, can be observed in all three species. The black arrow heads indicate cilia and microvilli and the black arrows MOX symbionts. **c)** The TEM results of *B. puteoserpentis* and *G. childressi* show that epithelial cells of pediveliger of both species are aposymbiotic and have cilia and/or microvilli (indicated by the black arrow heads). **d)** Schematic drawing of pediveliger and plantigrades showing the analysed regions of **a** and **b .**

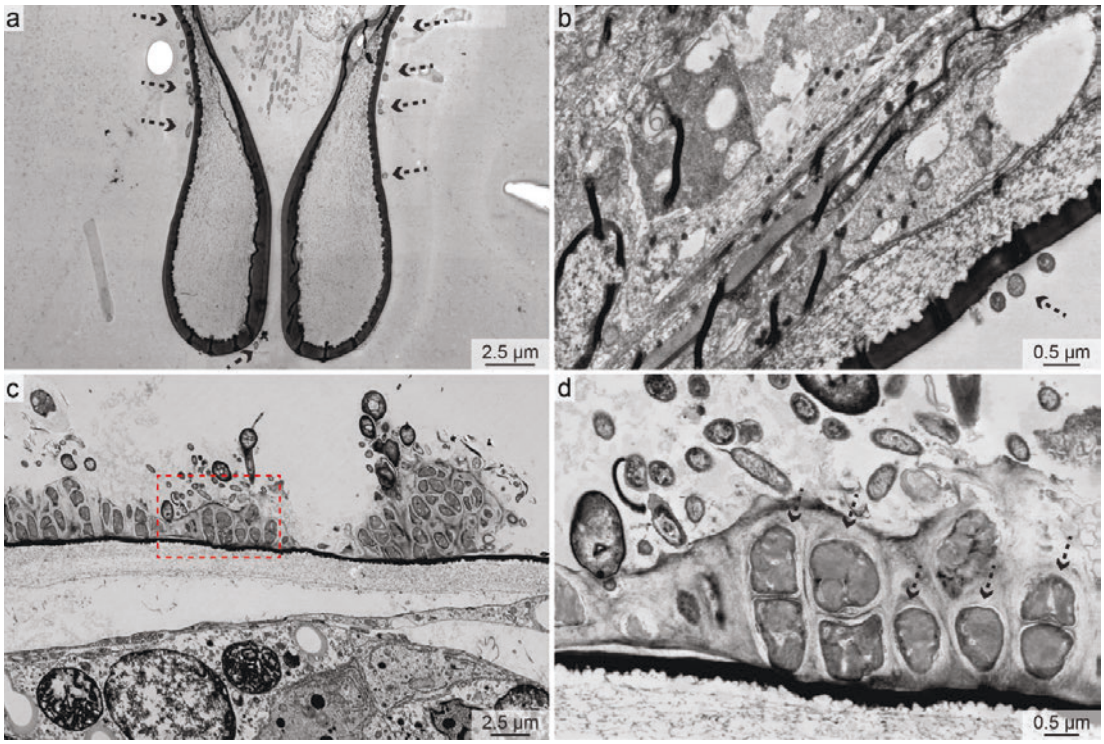

Figure S16. SOX- and MOX-like bacterial morphotypes were identified on the shells of *B. puteoserpentis* pediveliger (a and b) and plantigrade (c and d). TEM data of aposymbiotic pediveliger shows bacteria on the shell that have a similar morphotype to the SOX and MOX symbionts which are indicated by black dashed arrows. FISH analyses of these shell-associated bacteria were not possible because of the strong autofluorescence of the shell.

Supplementary references

[1] Bayne, B.L. 1971 Some morphological changes that occur at the metamorphosis of the larvae of *Mytilus edulis*. In *The Fourth European Marine Biology Symposium* (pp. 259-280.
[2] Manoj Nair, R. & Appukuttan, K.K. 2003 Effect of temperature on the development, growth, survival and settlement of green mussel *Perna viridis* (Linnaeus, 1758). *Aquacult. Res.* **34**, 1037-1045. (doi:10.1046/j.1365-2109.2003.00906.x).
[3] Gribben, P.E., Jeffs, A.G., de Nys, R. & Steinberg, P.D. 2011 Relative importance of natural cues and substrate morphology for settlement of the New Zealand Greenshell™ mussel, *Perna canaliculus*. *Aquaculture* **319**, 240-246. (doi:10.1016/j.aquaculture.2011.06.026).
[4] Dobretsov, S. & Wahl, M. 2008 Larval recruitment of the blue mussel *Mytilus edulis*: The effect of flow and algae. *J. Exp. Mar. Biol. Ecol.* **355**, 137-144. (doi:10.1016/j.jembe.2007.12.018).
[5] Shikuma, N.J., Pilhofer, M., Weiss, G.L., Hadfield, M.G., Jensen, G.J. & Newman, D.K. 2014 Marine Tubeworm Metamorphosis Induced by Arrays of Bacterial Phage Tail–Like Structures. *Science* **343**, 529. (doi:10.1126/science.1246794).
[6] Montanaro, J., Gruber, D. & Leisch, N. 2016 Improved ultrastructure of marine invertebrates using non-toxic buffers. *PeerJ* **4**, e1860. (doi:10.7717/peerj.1860).
[7] Handschuh, S., Baeumler, N., Schwaha, T. & Ruthensteiner, B. 2013 A correlative approach for combining microCT light and transmission electron microscopy in a single 3D scenario. *Front. Zool.* **10**. (doi:10.1186/1742-9994-10-44).
[8] Stoecker, K., Dorninger, C., Daims, H. & Wagner, M. 2010 Double labeling of oligonucleotide probes for fluorescence in situ hybridization (DOPE-FISH) improves signal intensity and increases rRNA accessibility. *Appl. Environ. Microbiol.* **76**, 922-926. (doi:10.1128/AEM.02456-09).
[9] Wilde, F., Ogurreck, M., Greving, I., Hammel, J.U., Beckmann, F., Hipp, A., Lottermoser, L., Khokhriakov, I., Lytaev, P., Dose, T., et al. 2016 Micro-CT at the imaging beamline P05 at PETRA III. *AIP Conference Proceedings* **1741**, 030035. (doi:10.1063/1.4952858).
[10] Geier, B., Franke, M., Ruthensteiner, B., González Porras, M., Gruhl, A., Wörmer, L., Moosmann, J., Hammel, J.U., Dubilier, N., Leisch, N., et al. 2019 Correlative 3D anatomy and spatial chemistry in animal-microbe symbioses: developing sample preparation for phase-contrast synchrotron radiation based micro-computed tomography and mass spectrometry imaging. In *SPIE Optical Engineering + Applications* (eds. B. Müller & G. Wang), SPIE.
[11] Moosmann, J., Ershov, A., Weinhardt, V., Baumbach, T., Prasad, M.S., LaBonne, C., Xiao, X., Kashef, J. & Hofmann, R. 2014 Time-lapse X-ray phase-contrast microtomography for in vivo imaging and analysis of morphogenesis. *Nat. Protoc.* **9**, 294. (doi:10.1038/nprot.2014.033).
[12] van Aarle, W., Palenstijn, W.J., De Beenhouwer, J., Altantzis, T., Bals, S., Batenburg, K.J. & Sijbers, J. 2015 The ASTRA Toolbox: A platform for advanced algorithm development in electron tomography. *Ultramicroscopy* **157**, 35-47. (doi:10.1016/j.ultramic.2015.05.002).
[13] van Aarle, W., Palenstijn, W.J., Cant, J., Janssens, E., Bleichrodt, F., Dabravolski, A., De Beenhouwer, J., Joost Batenburg, K. & Sijbers, J. 2016 Fast and flexible X-ray tomography using the ASTRA toolbox. *Opt.Express* **24**, 25129-25147. (doi:10.1364/oe.24.025129).
[14] Geier, B., Sogin, E.M., Michellod, D., Janda, M., Kompauer, M., Spengler, B., Dubilier, N. & Liebeke, M. 2020 Spatial metabolomics of in situ host–microbe interactions at the micrometre scale. *Nat. Microbiol*. (doi:10.1038/s41564-019-0664-6).
[15] Schindelin, J., Arganda-Carreras, I., Frise, E., Kaynig, V., Longair, M., Pietzsch, T., Preibisch, S., Rueden, C., Saalfeld, S., Schmid, B., et al. 2012 Fiji: an open-source platform for biological-image analysis. *Nat. Methods* **9**, 676-682. (doi:10.1038/nmeth.2019).

[16] Cardona, A., Saalfeld, S., Schindelin, J., Arganda-Carreras, I., Preibisch, S., Longair, M., Tomancak, P., Hartenstein, V. & Douglas, R.J. 2012 TrakEM2 Software for Neural Circuit Reconstruction. *PloS one* **7**, e38011. (doi:10.1371/journal.pone.0038011).
[17] Amann, R.I., Binder, B.J., Olson, R.J., Chisholm, S.W., Devereux, R. & Stahl, D.A. 1990 Combination of 16S rRNA-targeted oligonucleotide probes with flow cytometry for analyzing mixed microbial populations. *Appl. Environ. Microbiol.* **56**, 1919.
[18] Daims, H., Brühl, A., Amann, R., Schleifer, K.-H. & Wagner, M. 1999 The Domain-specific Probe EUB338 is Insufficient for the Detection of all Bacteria: Development and Evaluation of a more Comprehensive Probe Set. *Systematic and Applied Microbiology* **22**, 434-444. (doi:10.1016/S0723-2020(99)80053-8).
[19] Wallner, G., Amann, R. & Beisker, W. 1993 Optimizing fluorescent in situ hybridization with rRNA-targeted oligonucleotide probes for flow cytometric identification of microorganisms. *Cytometry* **14**, 136-143. (doi:10.1002/cyto.990140205).
[20] Duperron, S., Bergin, C., Zielinski, F., Blazejak, A., Pernthaler, A., McKiness, Z.P., DeChaine, E., Cavanaugh, C.M. & Dubilier, N. 2006 A dual symbiosis shared by two mussel species, Bathymodiolus azoricus and Bathymodiolus puteoserpentis (Bivalvia: Mytilidae), from hydrothermal vents along the northern Mid-Atlantic Ridge. *Environmental microbiology* **8**, 1441-1447. (doi:10.1111/j.1462-2920.2006.01038.x).
[21] Le Pennec, M., Benninger, P.G. & Herry, A. 1995 Feeding and digestive adaptations of bivalve molluscs to sulphide-rich habitats. *Comparative Biochemistry and Physiology* **111**, 183-189. (doi:10.1016/0300-9629(94)00211-B).
[22] Von Cosel, R., Comtet, T. & Krylova, E.M. 1999 *Bathymodiolus* (Bivalvia: *Mytilidae*) from Hydrothermal Vents on the Azores Triple Junction and the Logatchev Hydrothermal Field, Mid-Atlantic Ridge. *The Veliger* **42**, 218-248.
[23] Gustafson, R.G., Turner, R.D., Lutz, R.A. & Vrijenhoek, R.C. 1998 A new genus and five new species of mussels (Bivalvia, Mytilidae) from deep-sea sulfide/hydrocarbon seeps in the Gulf of Mexico. *Malacologia* **40**, 63-112.
[24] Kenk, V.C. & Wilson, B.R. 1985 A new mussel (Bivalvia *Mytilidae*) from hydrothermal vents in the galapagos rift zone. *Malacologia* **26**, 19.
[25] Reid, R.G.B. 1980 Aspects of the biology of a gutless species of Solemya (Bivalvia: Protobranchia). *Canadian Journal of Zoology* **58**, 386-393. (doi:10.1139/z80-050).
[26] Morton, B. 1986 The functional morphology of the organs of feeding and digestion of the hydrothermal vent bivalve Calyptogena magnifica (Vesicomyidae). *Journal of Zoology* **208**, 83-98. (doi:10.1111/j.1469-7998.1986.tb04711.x).

Chapter IV

This manuscript is in preparation and has not been reviewed by all authors.

How to make a living without symbionts? The vertical migration of planktotrophic deep-sea mussels

Maximilian Franke[1,2], Merle Ücker[1,2], Nicole Dubilier[1,2*] and Nikolaus Leisch[1*]

[1] Max Planck Institute for Marine Microbiology, Celsiusstr. 1, 28359 Bremen, Germany

[2] MARUM Zentrum für Marine Umweltwissenschaften, University of Bremen, Leobener Str. 2, 28359 Bremen, Germany

*Corresponding authors

Nikolaus Leisch, e-mail: nleisch@mpi-bremen.de

Nicole Dubilier, e-mail: ndubilie@mpi-bremen.de

Max-Planck-Institute for Marine Microbiology

Celsiusstr.1, D-28359 Bremen, Germany

Phone: 0049 (0)421 2028

Fax: 0049 (0)421 2028 760

Abstract

The deep sea is one of the most extreme habitats on earth. With hardly any food sources available for animals, it is a challenging environment for animals to live in. Nevertheless, one finds dense populations of invertebrates, especially at hydrothermal vents, cold seeps, and organic falls. Bathymodioline mussels are one of them and can only survive in these extreme habitats because of their nutritional mutualistic symbiosis with chemosynthetic bacteria. Recent studies on the life cycle of these mussels have highlighted that all larvae stages are symbiont-free. But the question on how these larvae can survive in the deep sea without their symbionts remains unresolved. We used a morphology-based stable isotope approach to investigate feeding strategies of different developmental life stages of three bathymodioline species (*B. azoricus, B. puteoserpentis and G. childressi*). Our analysis revealed that bathymodioline larvae feed on phototrophic food sources during their larvae life whereas mussels in post-metamorphosis developmental stages mostly depend on the energy provided by their symbionts. Given the limited access to phototrophic food sources in the deep sea, we hypothesize that bathymodioline larvae migrate vertically in the water column to feed on phototrophic food sources near the euphotic zone.

Introduction

The coexistence of microorganisms and eukaryotes ranges from parasitic to mutualistic associations and can be observed in almost all animal phyla. In mutualistic associations, both partners benefit from each other and the fitness advantage created by this form of symbiosis can allow both partners to survive in otherwise unfavorable habitats [1]. Interestingly, there are symbiotic associations in which the symbionts are colonizing the

host each generation anew [2]. This horizontal symbiont transmission results in host life stages that are free of symbionts. To study how these aposymbiotic life forms can survive is particularly exciting in extreme habitats, where the host could usually not survive without its symbionts.

One of these extreme habitats are deep-sea chemosynthetic environments at hydrothermal vents, cold seeps, and organic falls. These environments are considered deep-sea "oases" because, unlike the rest of the deep sea, they contain a very high proportion of organic matter [3, 4]. The total organic matter pool at these habitats is not dominated by phototrophic organic matter as in other marine habitats, but rather by chemosynthetic organic matter [3]. Input of phototrophic organic matter sinking into the deep sea in the form of marine snow and other sinking particles is limited [5]. Only 3.6% of the carbon produced at the sea-surface reaches the deep sea at 800 m [6] and even less in deeper water layers. The sinking particles are often recalcitrant and thereby not accessible for many animals because easily degradable compounds are already used up over the sinking process [7]. To overcome this organic matter limitation, many deep-sea animals have formed a nutritional symbiosis with chemosynthetic bacteria. This way, they can take advantage of the high energy supply in form of chemosynthetic energy that reducing habitats such as hydrothermal vents, cold seeps, and organic falls provide [8-10].

Bathymodioline mussels are among the most successful fauna in these extreme habitats. They are distributed worldwide at deep-sea hydrothermal vents, cold seeps, and organic falls [8]. To survive in such extreme habitats, these mussels formed a mutualistic symbiosis with two types of chemosynthetic bacteria: sulfur-oxidizing (SOX)

symbionts, whose main source of energy are reduced sulfur compounds, and methane-oxidizing symbionts (MOX), which gain their energy from oxidizing methane [11, 12]. These oxidations then fuel carbon fixation.

Bathymodioline mussels gain most of their nutrition through intracellular digestion of their symbionts but also direct nutrient transfer from the symbionts to the host might be possible [13, 14].Furthermore it is also known that bathymodioline mussels supplement their nutrition by filter-feeding [15]. From the morphology of their digestive system it was hypothesized that the filter-feeding in adults is not as efficient as the intracellular digestion of symbionts. While in adult mussels, the symbionts are found in specialized gill cells called bacteriocytes, they colonize all epithelial tissues in juveniles and post metamorphosis mussels [16, 17]. Bathymodioline mussels have horizontally transmitted symbionts and their larvae stages are free of symbionts until the onset of metamorphosis [17, 18]. The aposymbiotic larvae live planktotrophic and need to gain their nutrition only through filter-feeding [19, 20]. On a morphological level, their digestive system is capable of filter-feeding and gets reduced as soon as they are fully colonized by symbionts. It has been hypothesized that this reduction is linked to the nutritional change from filter-feeding during larval life to chemosynthetic symbiosis once the mussels are fully colonized [17]. Franke *et al.* [17] also reported that aposymbiotic mussel larvae build up large amounts (13% of the soft body volume) of lipid vesicles that serve as energy storages during the energy consuming process of metamorphosis. The question on which food source bathymodioline larvae feed in the deep sea and how they can build up such large amounts of energy reserves without symbionts remains unresolved.

Many deep-sea species including bathymodioline mussels are geographically widespread, which lead to at least two hypotheses in the past: A first hypothesis suggests that deep-sea larvae are undergoing a demersal development and migrate near the seafloor to colonize new habitats (Figure 1 B; [20, 21]). A second hypothesis on larval development and migration strategies proposes that planktotrophic deep-sea larvae migrate vertically in the water column to reach faster surface currents, which would transport the larvae farther than the deep-sea currents (Figure 1 C; [22]). In addition to the longer distribution distance, the mussels would have access to more abundant food sources in the euphotic zone, which could allow for an even longer larval phase as these larvae are less likely to experience phases of nutrient limitation. A vertical larval migration could explain the global distribution patterns of many deep-sea species, including bathymodioline mussels. It is not surprising that by now, multiple studies have presented first evidence for such migration patterns in various deep-sea species such as decapods, gastropods, tube worms, and echinoids [23-25]. Bathymodioline larvae were first thought to develop near the fertilization site in the deep sea near hydrothermal vents and cold seeps [20, 26], however, Arellano *et al.* [27] have described the sampling of larvae of *G. childressi* in the euphotic zone of the Gulf of Mexico.

In this study, we aimed to investigate if bathymodioline larvae migrated vertically in the water column or if they developed near hydrothermal vents into adult mussels. We analyzed different developmental stages, from pediveliger to adults, of the three bathymodioline species *Bathymodiolus azoricus, B. puteoserpentis* (from hydrothermal vents at the Mid-Atlantic Ridge (MAR)), and *Gigantidas childressi* (originally described

as *"B". childressi* [28], from cold springs in the Gulf of Mexico). The early developmental stages of these mussels were too small to be tracked in the water column which is why we used a different approach. In ecology research, analysis of natural abundances of stable isotopes are an established method to estimate the relationships between food sources and their consumers [29]. In the past it was reported that bathymodioline larvae rely on chemosynthetic food sources similar to adult mussels [30]. Salerno *et al.* [30] measured bulk stable isotope signatures of larvae, which were pooled together in one large sample set. Bulk measurements neglect differences between organs and especially between proteins and lipids. Lipids are depleted by up to 9‰ in $\delta^{13}C$ due to their different synthesis pathways [31]. As Franke *et al.* [17] reported about 13% of the soft body volume of bathymodioline larvae are composed of lipid vesicles. Due to this reason the bulk stable isotope signatures presented by Salerno *et al.* [30] could have been influenced by the depleted lipid vesicles. To overcome this problem we used a morphology-based stable isotope approach by using a secondary ion mass spectrometer (SIMS). This image based technology allowed us to examine not only the averaged stable isotope signatures of individual mussels, but also their organ specific stable isotope signatures. Due to the great spatial resolution of the SIMS we could even resolve the stable isotope signature of the lipid vesicles. By comparing the stable isotope signatures of the lipid vesicles and whole individuals with the published stable isotope data from potential food sources (Table 1), we were able to draw conclusions about bathymodioline larval development and migration. To statistically support our conclusions on migration patterns we performed stable isotope mixing models with different food sources from the deep sea and sea-surface environment.

Methods

Sampling and fixation

Specimens of *B. azoricus, B. puteoserpentis*, and *G. childressi* were collected at the sea floor with remote operated vehicles. *B. azoricus* and *B. puteoserpentis* were sampled at the Mid-Atlantic Ridge during the Meteor cruise M82-3 in 2010 at the Bubbylon vent site (37.801 N, -31.537 W; water depth: 1002 m) and during the Meteor cruise M126 in 2016 at the Semenov vent field (13.513 N, -44.962 W; water depth: 2446.5 m). Mussels of *G. childressi* were sampled in the Gulf of Mexico during the Nautilus cruise NA58 in 2015 at the site Mississippi Canyon 853 (28.123 N, -89.139 W; water depth: 1071 m). Upon recovery, specimens were fixed in 2% paraformaldehyde (PFA) in phosphate buffer saline (PBS). After fixation, samples were stored in the corresponding buffer (ethanol / PBS 60:40) at -20 °C. Sampling details of all samples are listed in Table S1.

Sample preparation for stable isotope analyses

For isotope ratio mass spectrometry (IRMS) analyses, gill, foot and mantle were dissected from frozen and PFA-fixed osmium tetroxide (OsO_4) postfixed adult bathymodioline mussels. For the OsO_4 post fixation the samples were incubated with 1% (v/v) OsO_4 for 1 - 2 h at 4 °C and washed three times with PBS. Afterwards the tissues were dried in glass exetainers at 60°C for at least 72 h. Dried tissue was grinded in aluminum foil and at least 0.5 mg was transferred into tin capsules for later analyses.

As pediveliger, metamorphosing mussels and plantigrades of all three species were too small to be dissected into their individual organs we used a secondary ion mass spectrometry (SIMS) approach to analyze whole mussels and tissue-specific stable isotope ratios. All individuals of the different developmental stages as well as adult

tissue were embedded in paraffin and thin-sectioned. Prior to paraffin embedding, some PFA-fixed samples were post fixed with 1% (v/v) OsO_4 for 1 - 2 h at 4 °C and washed three times with PBS to preserve the lipid vesicles. Mussels were dehydrated with an ethanol series of increasing concentration ((v/v); 30%, 50%, 70%, 80%, 96% and 3 x 100%), with each step lasting 10 min. Afterwards the tissue was transferred into 100% (v/v) RotiHistol and incubated two times for 10 min. Samples were transferred into a solution of RotiHistol and paraffin (50:50) and incubated for 40 min at 60°C. Samples were transferred into pure paraffin and incubated six times for 40 min at 60°C. The last step was an overnight incubation. Paraffin blocks were cut into 3 - 7 µm sections on a Leica microtome RM2255 (Leica, Germany) and sections were mounted on gold-coated glass sample holders. The sample holders were baked in vertical position for one hour at 60 °C to improve adhesion to the glass. Sample holders were de-waxed and rehydrated by immersing them three times in 100% (v/v) RotiHistol for 10 min each, which was followed by a decreasing ethanol row (concentration in (v/v); 96%, 80%, 70% and 50%, 10 min each).

Stable isotope analyses

Isotope ratio mass spectrometry

The natural abundance of ^{13}C and ^{15}N of the internal control samples (adult tissue) were measured at the Center for Stable Isotope Research and Analysis (KOSI) at the University of Goettingen, with an Elemental Analyzer (Eurovector) coupled to an isotope ratio mass spectrometer (Delta Plus XL IRMS, Thermo Finnigan MAT, Bremen, Germany).

Large-geometry secondary ion mass spectrometry

Natural abundance of ^{13}C and ^{15}N of different bathymodioline developmental stages (pediveliger, metamorphosing mussels, plantigrades and adults) was analyzed using secondary ion mass spectrometry (SIMS) on an IMS 1280 (Cameca, Gennevilliers, France) at the Natural History Museum in Stockholm, Sweden. Paraformaldehyde fixed tissue sections were mounted onto gold-coated glass slides and covered with a 5 nm-thick gold layer. Areas of interest (110 x 110 µm) were pre-sputtered with a primary caesium-ion (Cs1) beam (2.5 nA) for 10 sec and then imaged using a 50 pA Cs1 beam with a spatial resolution between 0.5 and 1 µm with an raster size of 100 µm x 100 µm for 60 cycles. Secondary ion images (256 x 256 pixel) were recorded for $^{13}C^{14}N$, $^{12}C^{14}N$ and $^{12}C^{15}N$.

Data processing

Isotope ratio mass spectrometry

$\delta^{13}C$ and $\delta^{15}N$ ratios of the internal control samples were calculated with the following equations:

Equation 1: Calculation of the $\delta^{13}C$ ratios

$$\delta^{13}C\ (‰) = \left(\left(\frac{\frac{^{13}C}{^{12}C}sample}{\frac{^{13}C}{^{12}C}standard}\right) - 1\right) x\ 10^3$$

Equation 2: Calculation of the $\delta^{15}N$ ratios

$$\delta^{15}N\ (‰) = \left(\left(\frac{\frac{^{15}N}{^{14}N}sample}{\frac{^{15}N}{^{14}N}standard}\right) - 1\right) x\ 10^3$$

We used Vienna Pee Dee Belemnite (vPDB) for $\delta^{13}C$ and atmospheric nitrogen for $\delta^{15}N$ as standard ratios. To calculate the isotopic composition of individual organs and

species, we averaged the obtained stable isotope ratios from the individual ROIs by using the weighted average.

Secondary ion mass spectrometry

Image and data processing of the SIMS data was done using the CAMECA WinImage2 software. Regions of interest (ROIs) were defined on the $^{12}C/^{14}N$ images corresponding to tissue sections by using the automated ROI detection mode with 200 – 300 counts as a lower limit. From these ROIs tissue-specific isotope ratios, $^{15}N/^{14}N$ and $^{13}C/^{12}C$ were calculated. Tissue from adult bathymodioline mussels was used as an internal standard and measured with the IRMS as well as SIMS. The SIMS data were corrected for the difference between the SIMS and IRMS measurements of the adult bathymodioline tissue, as the SIMS was not corrected with an internal standard. The corrected stable isotope ratios were fit into equation 1 and 2 to calculate the $\delta^{13}C$ and $\delta^{15}N$ ratios of the analyzed tissues. As a standard we used Vienna Pee Dee Belemnite (vPDB) for $\delta^{13}C$ and atmospheric nitrogen for $\delta^{15}N$.

To calculate the isotopic composition of individual organs or whole mussels, we averaged the obtained stable isotope ratios from the individual ROIs by using the weighted average. The Anova and Tukeys HSD test were used to make assumptions about the statistical variance between whole mussels or individual tissues of different developmental stages.

Stable isotope mixing models

We estimated proportional contributions of different food sources to the diet of different developmental stages of *B. azoricus* and *B. puteoserpentis* by using MixSIAR [32, 33](ver. 3.1). MixSIAR is a Bayesian-based isotope mixing model which estimates the

probability distribution of the contribution of different prey to a mixture and evaluates the uncertainty associated with the isotopic values of the prey and predator stock [32, 33]. The model considers isotopic errors by using all $\delta^{13}C$ and $\delta^{15}N$ values of the different developmental stages of *B. azoricus* and *B. puteoserpentis* mussels as inputs and the mean ± standard deviation (SD) of $\delta^{13}C$ and $\delta^{15}N$ values of the different food sources. We used pre-estimated fractionation factors (carbon: 2‰ and nitrogen: 3.6‰) from shallow water mytilids as discrimination factors [34]. The different food sources were inferred from the known ecology of bathymodioline mussels and their stable isotope data were taken from the literature (Table 1). As pediveliger of bathymodioline species are aposymbiotic [17] and were already sampled in the upper water column [27, 35], we included food sources of the upper water layers as well as the chemosynthetic environment of the deep sea into the mixing models (Table 1). During the setup up of the mixing models, we followed the general guidance to mixing model applications suggested by Phillips *et al.* [36].

Table 1 Stable isotope value of different food sources which were used for the stable isotope mixing models. The stable isotope values were averaged from the different literature resources. The standard deviation is indicated for each food source and stable isotope in the brackets. POM: particulate organic matter.

food sources	mean $\delta^{13}C$ [‰]	mean $\delta^{15}N$ [(‰)]	literature
surface microplankton	-21.61 (± 1.17)	2.05 (± 0.72)	[37-39]
bacteria surface	-13.04 (± 1.13)	-0.44 (± 0.19)	[40]
POM surface	-23.33 (± 1.77)	1.43 (± 2.45)	[41-43]
POM deep sea	-23.29 (± 1.69)	1.90 (± 1.64)	[6, 43-45]
phototrophic food sources	**-21.82 (± 2.98)**	**1.61 (± 1.79)**	
chemosynthetic bacteria	**-32.51 (± 5.33)**	**-1.89 (± 4.14)**	[46-49]
symbiont host mix	**-30.65 (± 0.64)**	**-12.39 (± 0.89)**	this study

To resolve if pediveliger feed on phototrophic food sources, we calculated multiple isotope mixing models: A general model that only included pooled food sources (phototrophic food sources, chemosynthetic food sources, and symbionts), and more specific stable isotope mixing models that included all food resources of Table 1 (Figure S1 – S3). For all models, we used the averaged stable isotope ratios per individual as input data and developmental stages and species as fixed effects. The results of the mixing models were reported as percentages ranging from 0 to 99%, where the minimum and maximum values are used to determine the importance of food sources to the diet of different developmental stages of *B. azoricus* and *B. puteoserpentis* mussels.

Results

Significant trophic change between bathymodioline larvae and adults

We used detailed morphological information on different life stages (pediveligers, mussels during metamorphosis, plantigrades and adults) of three bathymodioline species (*B. azoricus, B. puteoserpentis,* and *G. childressi*) by Franke *et al.* [17], to analyze the stable carbon and nitrogen isotope ratios of individuals along their life cycle (Figure 1). By combining morphological information (light microscopy of sections) with SIMS and IRMS data, we identified a trophic shift from pediveligers to adult mussels in all three species. Furthermore, we were able to apply stable isotope mixing models, which all suggested a phototrophic based diet for the aposymbiotic pediveligers in *B. azoricus* and *B. puteoserpentis*.

To examine the trophic differences among different developmental stages of three bathymodioline species, we compared the averaged stable isotopic composition of adult tissues (gill, foot, and mantle) measured with an IRMS (control) with the averaged stable

isotopic composition measured with a SIMS of multiple tissue sections per individual for pediveligers, mussels during metamorphosis, and plantigrades. Because we used multiple sections per individual, we were able to determine the averaged stable isotopic composition of whole animals as well as individual organs. Thereby, we could show that pediveliger and mussels during the metamorphosis were significantly more positive in $\delta^{13}C$ and $\delta^{15}N$ (Tukey HSD test, p-value < 0.05, Figure 2 and Table S2) compared to later developmental stages like plantigrades and adults. In *B. azoricus*, the mean $\delta^{13}C$ signature per developmental stage ranged from ~ -21‰ in pediveligers to ~ -31‰ in adult mussels. For $\delta^{15}N$, the signatures ranged from ~ 6‰ to ~ -12‰ (Table S3).The isotopic change between developmental stages was more pronounced in *B. azoricus* mussels compared to the other species (Figure 2). The $\delta^{13}C$ ratios of *B. azoricus* plantigrades ranged from ~ -25‰ to ~ -35‰. This large variance can be explained by varying degrees of development and symbiont colonization, which, according to Franke *et al.* [17], begins during the metamorphosis and continues to form during the plantigrade developmental stage. In *B. puteoserpentis*, the $\delta^{13}C$ and $\delta^{15}N$ ratios ranged from ~ -22‰ to ~ -30‰ ($\delta^{13}C$) and from ~ 6‰ to ~ -13 ‰ ($\delta^{15}N$, Table S3).

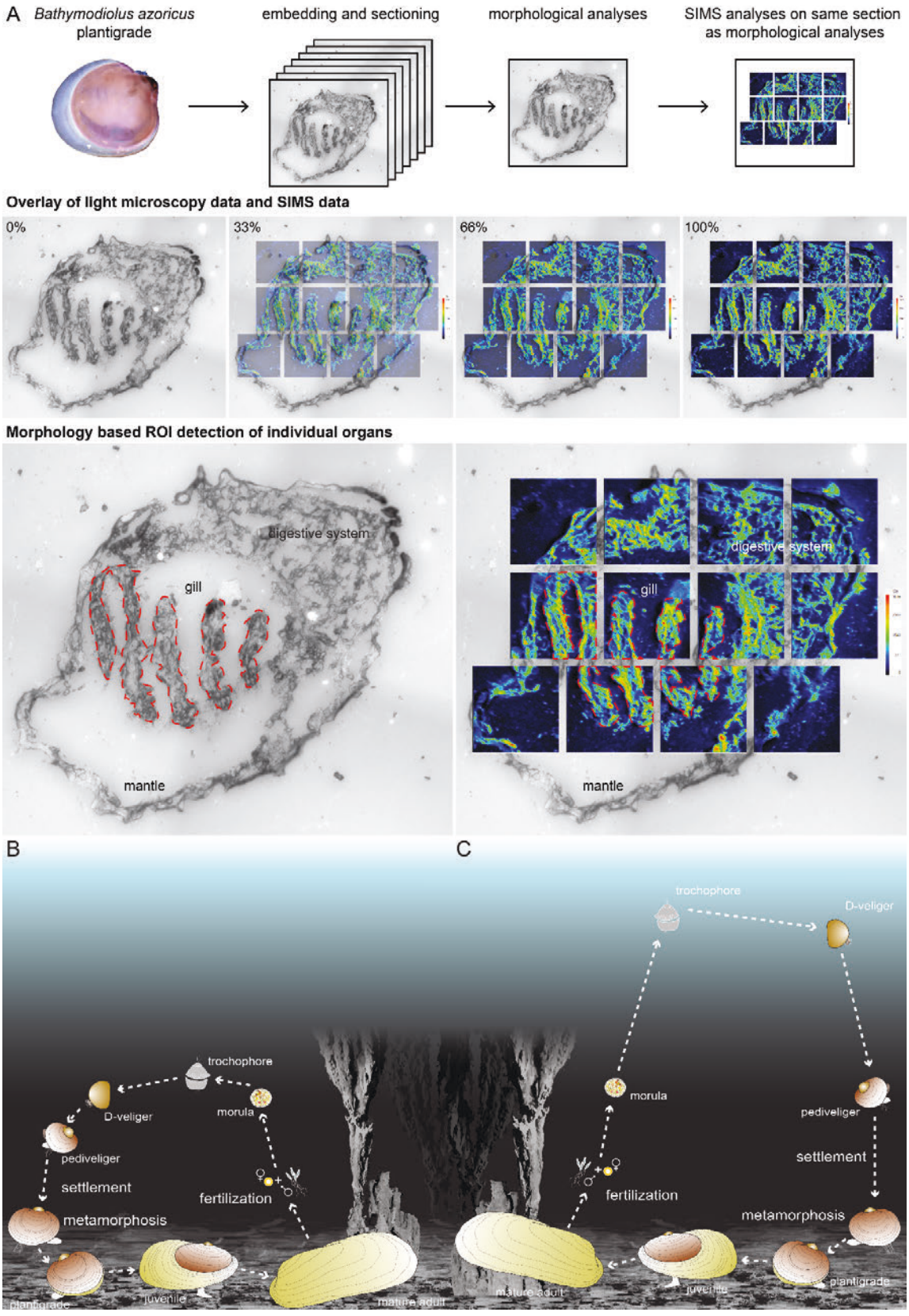
A Bathymodiolus azoricus
plantigrade
embedding and sectioning
morphological analyses
SIMS analyses on same section
as morphological analyses
Overlay of light microscopy data and SIMS data
0%
33%
66%
100%
Morphology based ROI detection of individual organs
digestive system
gill
mantle
digestive system
gill
mantle
B
trochophore
D-veliger
morula
pediveliger
settlement
fertilization
metamorphosis
plantigrade
juvenile
mature adult
C
trochophore
D-veliger
morula
pediveliger
settlement
fertilization
metamorphosis
mature adult
juvenile
plantigrade

Figure 1 A morphologically informed SIMS approach allowed us to analyze the bulk and individual organ stable isotope compositions. A) *Bathymodiolus* mussels of different developmental stages were embedded and sectioned into 3 – 7 µm thin sections. Those sections were analyzed regarding their morphology and the stable isotope composition was determined with a SIMS. Regions of interest (ROI; indicated with the red dashed line) were identified on the light microscopy image and then transferred to the SIMS count images. Thereby, stable isotope signatures of individual organs could be analyzed. **B)** In the past a demersal development has been suggested for bathymodioline mussels. The mussels would develop close to the origin of spawning. **C)** Recently a vertical migration and development was hypothesized for bathymodioline mussels, where larvae reach higher ocean layers for feeding and migration. *Bathymodiolus* life cycles were adapted from Franke *et al.* [17].

The Mid-Atlantic Ridge mussels showed a similar isotopic signature over their development although both mussels originate from different habitats (*B. azoricus:* ~ 1000 m and *B. puteoserpentis*: ~ 2440 m, Table S1). Overall, the stable carbon values of the seep mussel *G. childressi* were more negative compared to the stable carbon values of both hydrothermal vent species *B. azoricus* and *B. puteoserpentis* (Figure 2). Especially the $\delta^{13}C$ values of adult *G. childressi* mussels were depleted by about 30‰ compared to the hydrothermal vent species. Also in earlier developmental stages a difference in the stable carbon isotope was visible. *G. childressi* mussels during the metamorphosis and plantigrades had $\delta^{13}C$ values of ~ -33‰ and -38‰, respectively. This was a difference of about 10‰ to the hydrothermal vent species in each of the two stages (Figure 2 and Table S3). The stable nitrogen values of all three species were relatively similar per developmental stage except for post larvae of *G. childressi,* which were ~ 7‰ enriched compared to the hydrothermal vent species (Figure 2 and Table S3).

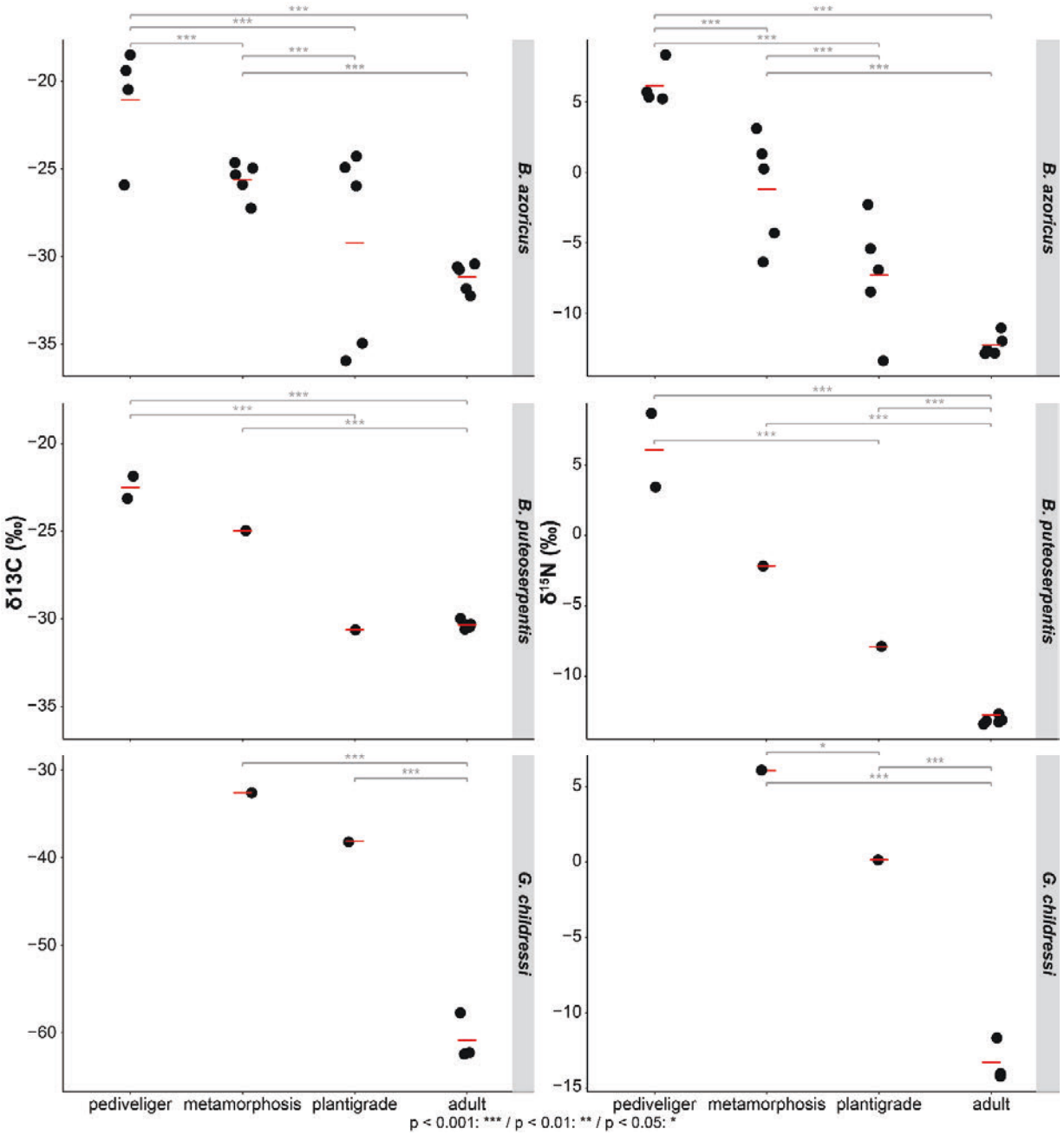

Figure 2 $\delta^{13}C$ and $\delta^{15}N$ ratios indicate a trophic shift between bathymodioline pediveliger and adults. The stable isotope values are displayed on the y-axis and the developmental stages on the x-axis. Each black dot represents the averaged stable isotope ratio of one individual. The red bar indicates the averaged isotopic signature per developmental stage. Significant values are represented by the grey bars and *: *** $p < 0.001$, ** $p < 0.01$ and * $p < 0.05$.

$\delta^{13}C$ and $\delta^{15}N$ values of lipid storages were more negative compared to the rest of the soft body

The morphologically informed SIMS measurements of multiple sections per individual allowed us to estimate individual stable isotope ratios of specific tissues and organs without the need for manual dissection (Figure 1 A). We used light microscopy information to determine ROIs and transferred those to the count images of the SIMS (Figure 1 A). Based on the identified ROIs, we calculated the $\delta^{13}C$ and $\delta^{15}N$ values for the different organs. For this analysis, we only included *B. azoricus* and *B. puteoserpentis* mussels from different developmental stages (pediveliger to adults), as the sample set of *G. childressi* was too small. We only had one *B. puteoserpentis* mussel, which was under ongoing metamorphosis, in our sample set, therefore we only provided the bulk measurements here and did not perform any specific tissue analyses for this developmental stage. Furthermore, we had to remove the lipid analyzes for *B. puteoserpentis* pediveliger as the point measurements resulted in low count rates. Therefore, we only performed the specific stable isotope analyses on the lipid vesicles for *B. azoricus* pediveliger.

The mean stable isotope signatures of the different organs did not differ significantly within one developmental stage and species (Tukey HSD test, p-value < 0.05, Table S 4). All analyzed organs were not significantly different to the overall bulk signatures per developmental stage (Figure 3 and Table S4). One exception are *B. azoricus* plantigrades, where gill and foot stable isotope signatures were slightly more negative compared to the bulk signatures. This shift was significant and could be explained by the ongoing symbiont colonization in this developmental stage. In adult mussels, no

difference between tissues was visible anymore. Between developmental stages, the isotopic differences between individual organs confirmed the differences between the bulk values (Figure 3). Furthermore, all tissues of the *B. azoricus* pediveliger were more positive, when compared to *B. puteoserpentis* pediveligers. This trend was exactly the opposite in mussels during the metamorphosis and plantigrades. No such difference could be observed in adult tissues where the $\delta^{13}C$ and $\delta^{15}N$ ratios were very similar between the two species (Figure 3).

Our analysis revealed that the lipid vesicles were significantly different to all other tissues and organs in *B. azoricus* (Tukey HSD test, p-value > 0.05, Figure 3 and Table S4). From the morphological analyses by Franke *et al.* [17] we know that the lipid vesicles make up ~ 13% of the soft body volume (~ 1.7 million μm^3) during the pediveliger stage. This volume exceeds the averaged egg volume at spawning by 6 to 15 times depending on the species. Eggs can be considered as a sphere, therefore, we used the following formula for the volume calculations: $V = \frac{4}{3}\pi r^3$, as well as the reported egg diameters (*B. azoricus* ~ 80 µm [50], *B. puteoserpentis* ~60 µm [51], and *G. childressi* ~ 70 µm [52]) to calculate the egg volume per species: ~ 268074 μm^3 (*B. azoricus*), ~ 113094 μm^3 (*B. puteoserpentis*) and ~ 179589 μm^3 (*G. childressi*). In *B. azoricus* pediveliger the mean $\delta^{13}C$ signature of the lipid vesicles was ~ -32‰, indicating that the lipid vesicles were ~ 11‰ more depleted in $\delta^{13}C$ than the averaged bulk $\delta^{13}C$ values of *B. azoricus* pediveligers(~ -21‰, Figure 3). The corresponding $\delta^{15}N$ ratio showed a similar trend with the lipid vesicles at ~ -6‰ (~ 12‰ depletion compared to the averaged bulk $\delta^{15}N$ ratio, Figure 3).

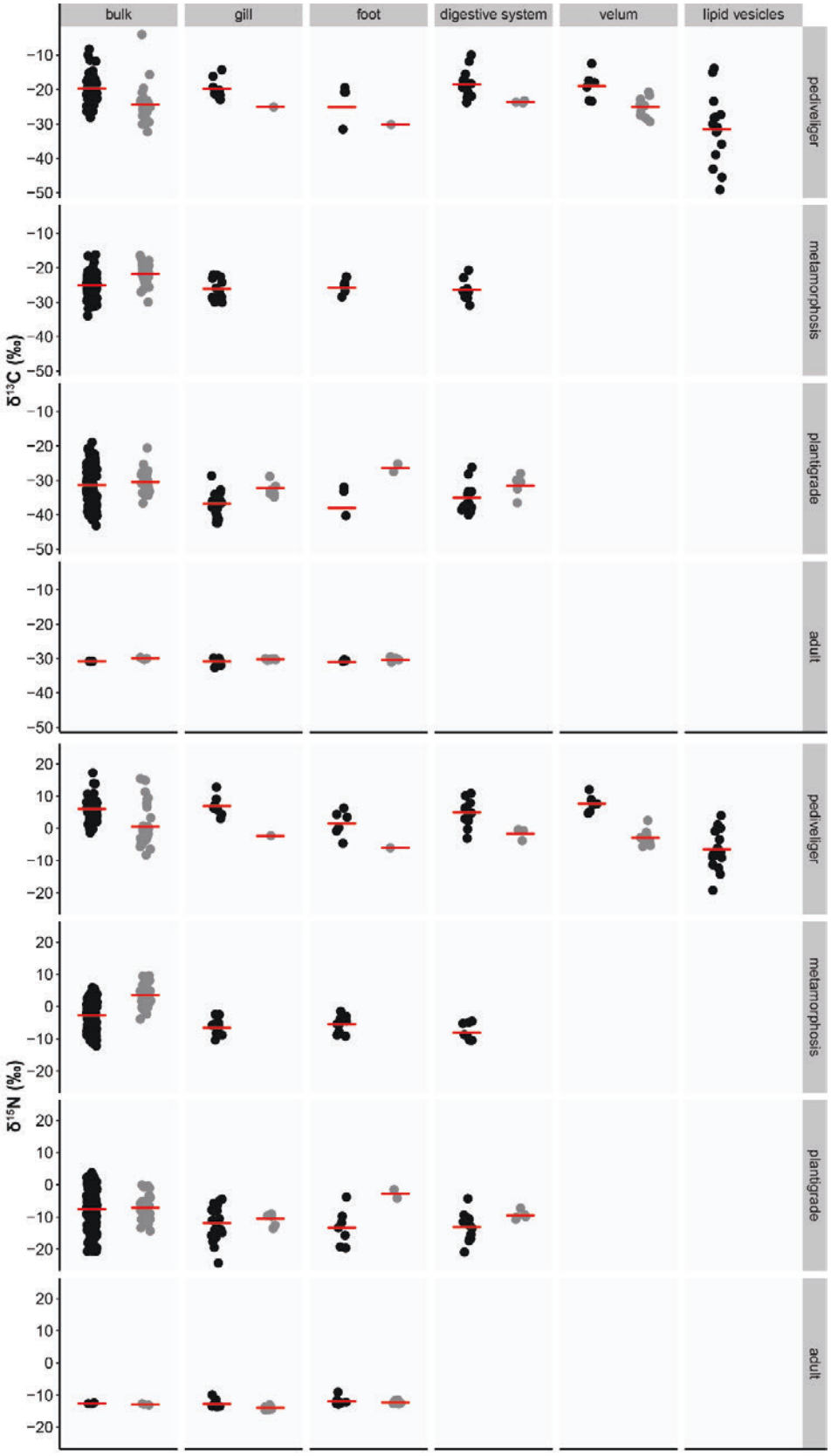
bulk
gill
foot
digestive system
velum
lipid vesicles
pediveliger
metamorphosis
plantigrade
adult
δ13C (‰)
δ15N (‰)

Figure 3 Tissue specific $\delta^{13}C$ and $\delta^{15}N$ ratios indicate that the lipid vesicles are depleted in $\delta^{13}C$ and $\delta^{15}N$ compared to the rest of the tissues. The stable isotope values are displayed on the y-axis. Each dot represents one ROI measurement of the corresponding organ and developmental stage. All samples were pooled per developmental stage and the average $\delta^{13}C$ and $\delta^{15}N$ ratios per tissue and developmental stage is indicated by the red bar. *B. azoricus* is presented in black and *B. puteoserpentis* in grey.

The large volume and the depleted $\delta^{13}C$ and $\delta^{15}N$ ratios of lipid vesicles in pediveligers suggests that these lipid vesicles do not originate from the original yolk pool, which is passed on from the parental organisms, and therefore need to be generated by the larvae during their planktotrophic larvae life.

Bathymodiolus pediveliger feed on phototrophic food sources

We used a Bayesian mixing model for our SIMS and IRMS data of different developmental stages of *B. azoricus* and *B. puteoserpentis* to clarify the potential food sources on which these different developmental stages feed. The stable isotope data of potential food sources was based on literature data (Table 1). To calculate these mixing models, we used pre estimated fractionation factors (carbon: 2‰ and nitrogen: 3.6‰) from shallow water mytilids [34]. First, we applied a general stable isotope mixing model with pooled food sources (phototrophic and chemosynthetic food sources, and the symbiont host mix) and then expanded the analysis to more specific models with individual food sources.

In the first run using pooled food sources (phototrophic and chemosynthetic, and the symbiont host mix), the general mixing model predicted a phototrophic-based diet for *B. azoricus* (72.8%) and *B. puteoserpentis* (72.4%) pediveliger which would be in line with uptake of food entirely via filter-feeding (Figure 4 and Table S5). Over the development, the feeding strategy changed towards a dependency on the energy provided by their chemosynthetic symbionts (*B. azoricus* plantigrades*:* 67.2% and adults: 89.7%, *B.*

puteoserpentis plantigrades: 68.5% and adults: 90.6%; Figure 4 and Table S5). Mussels of both species, which were under ongoing metamorphosis, had a mixed diet. The diet was still dominated by phototrophic food sources (*B. azoricus*: 52.3% and *B. puteoserpentis*: 52.2%), but not as much as during the pediveliger stage. The remaining nutrition was made up of the energy provided by their symbionts (*B. azoricus* 32.6%, *B. puteoserpentis* 34.4%) and only minor amounts of free-living chemosynthetic bacteria (*B. azoricus* 15.1%, *B. puteoserpentis* 13.4%, Figure 4 and Table S5) according to our model.

Also in the second analysis run with more specific stable isotope mixing models including individual food sources, (Figure S1 – S3 and Table 1) a phototrophic based nutrition in *Bathymodiolus* larvae was predicted, which changed to a chemosynthetic dependency in later developmental stages. Depending on the included food sources, the larvae nutrition was either based on deep-sea, surface or both phototrophic food sources. This suggests that the stable isotope values of these food sources were too similar to be differentiated by the mixing model. We weighted all food sources equally as no biological information is available if one of them is preferred over the other. To conclude, all analysis runs of the mixing models showed that *Bathymodiolus* larvae probably rely on phototrophic food sources in a chemosynthetic dominated environment.

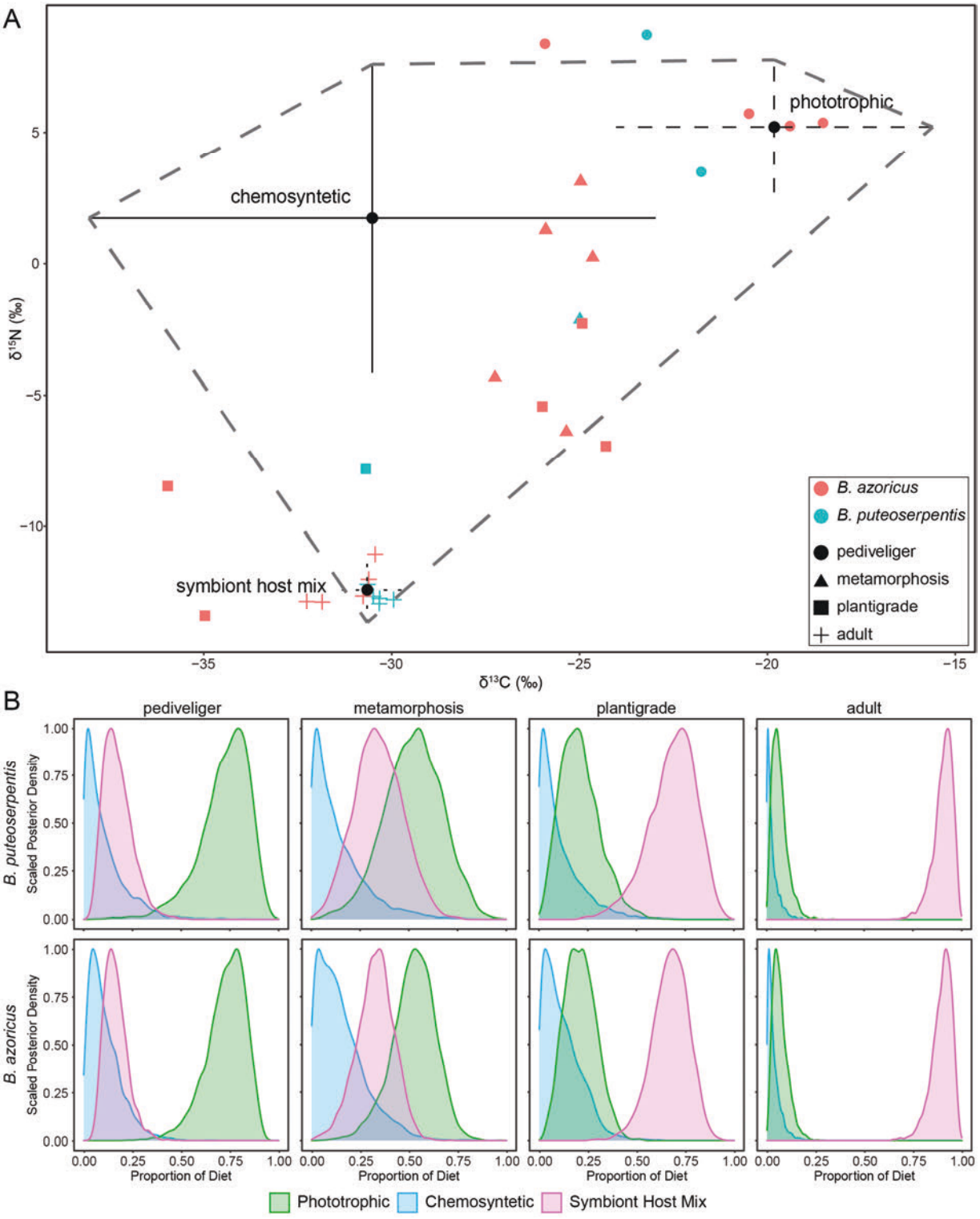

Figure 4 Stable isotope mixing model shows that *Bathymodiolus* pediveliger rely on phototrophic food sources. A) The isospace represents the carbon ($\delta^{13}C$) on the x-axis and nitrogen ($\delta^{15}N$) isotopic ratios on the y-axis of potential food sources. The different developmental stages of *B. azoricus* (red) and

B. puteoserpentis (blue) are indicated as circle: pediveliger, triangle: mussels during metamorphosis, square: plantigrades, and cross: adults. The different food sources of Table 1 were clustered in phototrophic and chemosynthetic food sources and symbiont host mix. The dashed grey line indicates the mixing polygon. **B)** The outcome of the stable isotope mixing model is presented in density plots for each developmental stage and species. On the x-axis the proportion of the different diets to the overall nutrition is listed and on the y-axis the probability how likely this distribution is. Phototrophic food sources are displayed in green, chemosynthetic food sources in blue and the symbiont host mix in magenta. The model indicates a nutritional shift from phototrophic food sources to the energy provided by the symbionts over the development.

The isospace plots of all mixing models showed that with the included food sources not all stable isotope signatures of the different developmental stages of *B. azoricus* and *B. puteoserpentis* could be explained (Figure 4 and Figure S1 – S3). Some adult mussels as well as plantigrades were not included in the mixing polygon which suggests that a food source might be missing. One explanation why these developmental stages were not included into the mixing polygon is that the isotope signatures of the symbionts are no pure signatures. The stable isotope signature of the symbionts included in the mixing models is a mix signature from SOX, MOX and host tissue. This mixed signature could simply be not as negative as it might be when we would include pure SOX, MOX or host fraction signatures. This could shift the boundaries of the mixing polygon in a way that all developmental stages are included. As there is no stable isotope data for pure symbiont fractions we can only work with the mixed values at the moment.

Discussion

The lifestyle of different *Bathymodiolus* developmental stages is reflected by their nutritional status

In a recent morphological study by Franke *et al.* [17], the authors hypothesized that bathymodioline mussels change their feeding strategy over their development based on morphological changes of the digestive system and the presence of symbionts in developmental stages after metamorphosis. They postulated that the aposymbiotic

larvae live from filter-feeding while juvenile and adult mussels changed their feeding strategy to a dependency on the energy provided by their symbionts. Here, we used the detailed morphological information from Franke *et al.* [17] regarding the different developmental stages of bathymodioline mussels and analyzed their averaged as well as tissue specific $\delta^{13}C$ and $\delta^{15}N$ signatures. We could identify a significant trophic shift in the $\delta^{13}C$ and $\delta^{15}N$ signature between larvae and adult mussels in all three analyzed bathymodioline species (*B. azoricus, B. puteoserpentis*, and *G. childressi*). Bathymodioline larvae and metamorphosing mussels of all three species were significantly more positive in $\delta^{13}C$ and $\delta^{15}N$ compared to plantigrades and adult mussels. When putting these stable isotope values into context, it becomes clear that aposymbiotic bathymodioline larvae likely feed on phototrophic food sources (72%) while post-metamorphosis developmental stages rely on the energy provided by their chemosynthetic symbionts.

Recently, it has been reported that bathymodioline larvae build up large energy reservoirs in form of lipid vesicles (they make up ~ 13% of the soft body volume) [17]. Especially these lipid vesicles, which do not undergo tissue turnover, serve as an ideal marker for larvae nutrition as they are built up only once during larvae life. Therefore, the stable isotope signature of those lipids should reflect the stable isotope signature of the larval food source with a fractionation factor of up to 9‰ and 3.6‰ relative to the $\delta^{13}C$ and $\delta^{15}N$ ratios [31, 34]. The measured $\delta^{13}C$ (*B. azoricus*: -32‰) and $\delta^{15}N$ (*B. azoricus*: -6‰) ratios reflect, under consideration of the fractionation factor, a phototrophic diet ($\delta^{13}C$: ~-21‰ and $\delta^{15}N$: 1.61‰, Table 1) during larvae life.

The significant trophic shift in $\delta^{13}C$ and $\delta^{15}N$ signatures over the development and the phototrophic stable isotope signature of the lipid vesicles support the morphological findings of Franke *et al.* [17] and clearly show that bathymodioline mussels change their feeding strategy over their development. Taking the stable isotope and morphological data together [17], we conclude that during the larval life bathymodioline mussels live planktotrophic [19] and filter-feed on phototrophic derived food sources. As soon as the mussels metamorphose and get colonized by their symbionts, their nutritional strategy shifts into a dependency on the energy provided by their symbionts.

How can *Bathymodiolus* larvae survive in the deep sea when feeding only on phototrophic food sources?

Surprisingly, the stable isotope signature of the larvae studied here does not match the habitat they live in. While the stable isotope signature of the larvae reflect a phototrophic nutrition, their habitat is dominated by chemosynthetic derived organic matter [3, 53]. Therefore, the planktotrophic larvae either actively select for phototrophic food sources e.g., marine snow, or they are not feeding at hydrothermal vents and cold seeps but rather in an environment which is dominated by phototrophic food sources (Figure 5).

To discuss possible larvae feeding strategies, we first need to understand the known biology of these mussels as well as their habitat and potential food sources. Adult bathymodioline mussels mostly rely on the energy provided by their symbionts [8, 54-57] but also supplement their nutrition through suspension feeding of particulate organic matter (POM) and uptake of dissolved organic matter (DOM) [15]. They can suspension feed on both hydrothermally derived and phytoplankton-derived organic matter [13, 58-62]. However, most natural stable isotope signatures, as well as phospholipid derived

fatty acid compositions of adult mussel tissues, have suggested that sea surface-derived particles made little contribution to the overall nutrition of *Bathymodiolus* adults [55-57, 63, 64]. As bathymodioline larvae are aposymbiotic [17], they need to rely on different food sources.

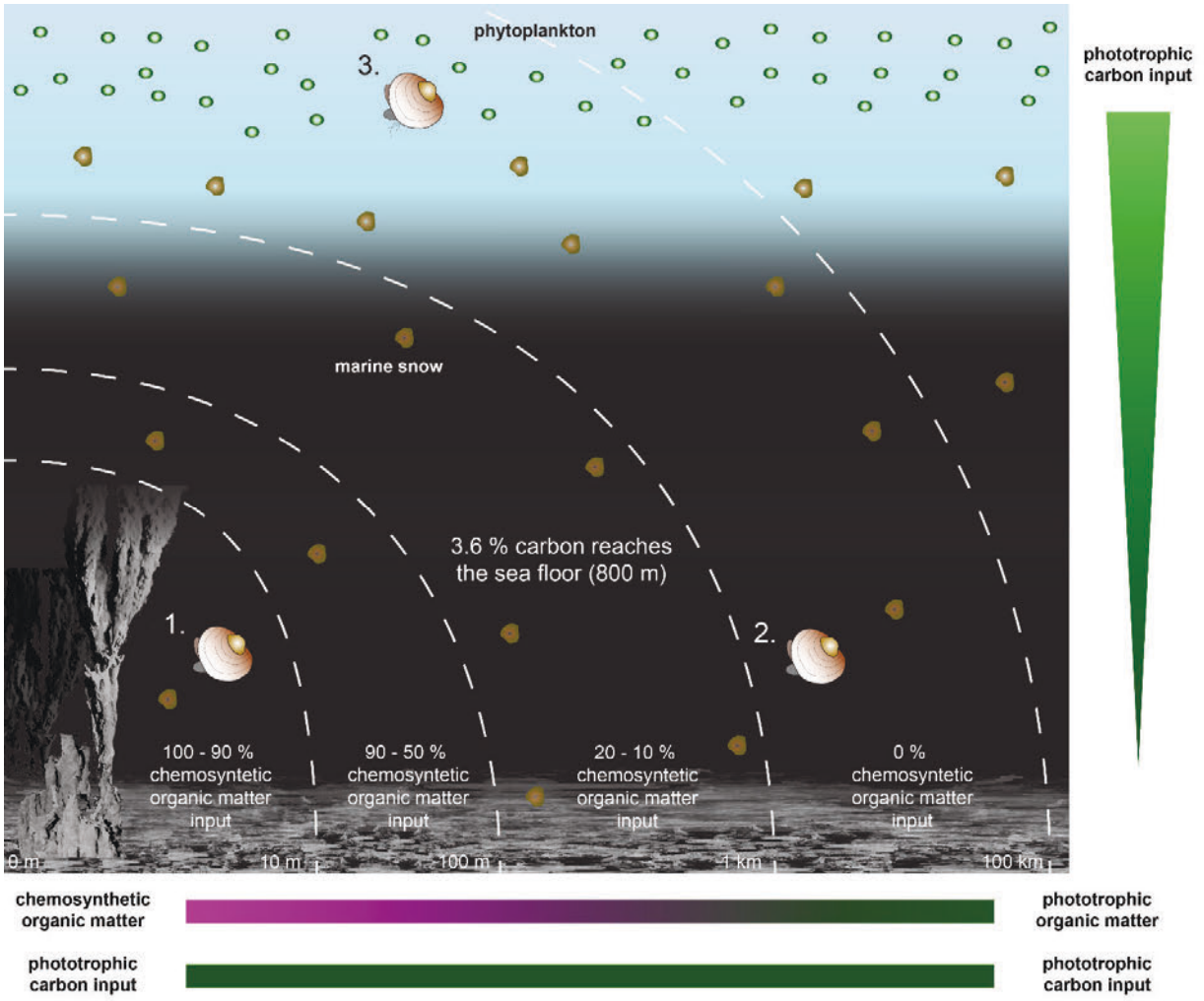

Figure 5 Three migration and developmental strategies can explain the phototrophic stable isotope signatures in bathymodioline larvae. 1) Bathymodioline larvae develop demersal and stay close to the hydrothermal vents. Thereby, they feed selectively only on phototrophic organic matter. **2)** Bathymodioline larvae develop demersal and migrate in the deep sea. As they move away from the hydrothermal vents, they are feeding on the limited phototrophic food sources reaching the sea floor. **3)** Bathymodioline larvae migrate vertically in the water column and thereby get access to “unlimited” phototrophic food sources. Given the low availability of phototrophic food sources in the deep sea and the planktotrophic lifestyle of bathymodioline larvae, a vertical migration is most likely. The figure is adapted after Bell *et al.* [3].

The deep sea at hydrothermal vents is dominated by chemosynthetic derived organic matter. With further distance to hydrothermal vents the chemosynthetic input decreases and the phototrophic organic matter dominates (Figure 5, [3, 53]). As there is no light in the deep sea, phototrophic derived organic matter can only originate from the sea surface. But only about 3.6% of the carbon produced at the sea surface reaches the sea floor at around 800 m water depth [6] and even less reaches deeper water layers. In the past, it has been thought that the rain of organic matter derived from the surface could be of great significance to deep ocean food webs and form a labile food source used for reproductive growth [5]. But the POM fraction, which reaches the sea floor, is mostly comprised of substrates which are recalcitrant and thereby bio-unavailable to most filter-feeding animals [7].

Looking at our stable isotope data and the morphological information from Franke *et al.* [17], three scenarios are plausible. (A) Bathymodioline mussels develop close to hydrothermal vents and selectively feed on phototrophic derived organic matter in a chemosynthetic habitat, (B) bathymodioline mussels live exclusively on integumental feeding of DOM, and (C) bathymodioline mussels migrate in the water column and do not feed close to hydrothermal vents. In the following section, we will discuss these three scenarios and highlight their biological meaning for bathymodioline larvae.

A: Bathymodioline mussels develop close to hydrothermal vents and selectively feed on phototrophic derived organic matter in a chemosynthetic habitat

Our stable isotope data has indicated that bathymodioline larvae live from suspension-feeding of phototrophic derived organic matter. That *B. azoricus* larvae could feed on

phototrophic derived food sources was already postulated by Trask and Van Dover [54], but they did not further discuss which consequences this might have for the larvae. In the past, it has been thought that bathymodioline larvae develop close to hydrothermal vents [20]. As hydrothermal vents and cold seeps are dominated by chemosynthetic organic matter and the POM input from the sea-surface is very limited [3, 6, 53], it is surprising that our stable isotope data suggests that *B. azoricus* and *B. puteoserpentis* larvae live from phototrophic food sources. Both species originate from different water depths (*B. azoricus*: 800 m vs. *B. puteoserpentis:* 2500 m) and therefore should have different access to POM, since the concentration of easily degradable POM decreases with increasing depth [7]. Furthermore, it is questionable if the biomass of the sinking particles is large enough to sustain the non-symbiotic hydrothermal vent fauna together with dense mussel beds and thousands of developing larvae which all compete for the same rare food sources.

Because these larvae actively filter-feed, they would need to exclusively feed on phototrophic derived organic matter to have the observed positive stable isotope signature. Such a selective feeding strategy is not common for planktotrophic larvae [65]. Planktotrophic larvae normally feed on all available food sources to obtain as much energy as possible. This is exactly what has been shown for their shallow water relatives. *M. edulis* can feed on a variety of different food sources, e.g., microplankton, algae, but also heterotrophic bacteria [66-68]. Given the close relationship and conserved development [17] between deep-sea and shallow water species, we assume a similar feeding behavior for bathymodioline larvae. Therefore, it is surprising that our stable isotope data suggest that bathymodioline larvae completely neglect the most

prominent food source at hydrothermal vents and cold seeps, free-floating chemosynthetic bacteria [3, 69, 70] and exclusively feed on limited phototrophic food sources in form of POM while developing in a chemosynthetic dominated habitat (Figure 5).

B: Bathymodioline mussels live exclusively on integumental feeding of DOM

Another scenario would be that bathymodioline mussels gain nutrition through integumental feeding and thereby gain a phototrophic isotopic signature in the deep-sea. *Mytilidae* are known to take up free amino acids from surrounding seawater, which can be used for osmoregulation or as a nutritional supplement [71, 72]. Multiple studies have already reported on the uptake of free amino acids through integumental feeding from ambient seawater in bathymodioline mussels [73-75]. However, it is debatable if bathymodioline mussel can only survive from the DOM pool, as the concentrations of bioavailable molecules like neutral sugars, amino acids, and amino sugars drop to values close to the detection limit in hydrothermal systems [76].

Stubbins and Dittmar [76] showed that bioavailable molecules are present in the deep sea in very low concentrations and Klevenz *et al.* [77] reported that bioavailable dissolved free amino acids have a concentration of 0.143 µmol l^{-1} at vent habitats at the MAR. When considering this concentration, an averaged sized adult *B. azoricus* mussel could assimilate ~ 0.08 µmol C h^{-1}, which is less than 0.3% of the carbon needed for respiration [6]. Bathymodioline pediveliger could sustain ~ 0.1% of their metabolic needs by integumental feeding of dissolved free amino acids when assuming uptake and metabolic rates of their shallow water relatives [78] (for detailed descriptions of the

metabolic calculations see supplementary note 1). Of course, dissolved amino acids are only a small portion of the total DOM pool and not the main food source of bivalves, but they illustrate that a living from only DOM in the deep sea is challenging.

We cannot out rule that *B. azoricus*, *B. puteoserpentis* and *G. childressi* larvae take up DOM and/or POM to supplement their nutrition but based on the bioavailability and concentrations of DOM and POM in the deep sea at hydrothermal vents and cold seeps, it is likely that these food sources contribute only to minor parts to the overall diet of bathymodioline larvae. Therefore, it is surprising that our stable isotope data indicate that bathymodioline larvae selectively feed on phototropic derived organic matter. As these food sources are limited in their habitat, the question arises if bathymodioline larvae stay close to hydrothermal vents or if they migrate to environments with a greater supply of biodegradable phototrophic food sources.

C: Bathymodioline mussels migrate in the water column and do not feed close to hydrothermal vents

Our stable isotope data indicated that *B. azoricus* and *B. puteoserpentis* larvae relied to more than 72% on phototrophic derived organic matter. However, within a radius of 1 km around a hydrothermal vent the deep sea is expected to be dominated by chemosynthetic organic matter (Figure 5) [3]. This indicates that bathymodioline larvae, which we assume are not selectively feeding only on phototrophic POM and cannot survive only from DOM, must have fed further away from hydrothermal vents where phototrophic organic matter is dominating [3]. This could either mean that bathymodioline larvae disperse horizontally in deep-sea currents and feed on the limited phototrophic POM that sinks down from the sea surface into the deep sea, or they

migrate vertically in the water column and thereby reach, with every meter they swim towards the sea-surface, water layers which are more and more dominated by easily degradable phototrophic derived organic matter (Figure 5) [7].

Overall the vertical larval migration mode is a common behavior in shallow water taxa. Since reproductive patterns as well as early life history strategies including developmental mode and larval feeding strategies are phylogenetically constrained characters [19, 79-81], the vertical migration mode may simply be a remnant of evolutionary history for deep-sea species [22, 82]. Therefore, vertical larval migration might be present in a lot of different deep-sea species including bathymodioline mussels.

In several planktotrophic deep-sea larvae, a vertical larvae migration was observed or inferred from stable isotope work, energy content in the eggs, genetic analysis of different populations at different habitats and sampling of deep-sea larvae in the euphotic zone [23, 27, 83, 84]. Especially the wide geographic distribution of many deep-sea species including bathymodioline mussels indicate that a vertical larvae migration might be common in many deep-sea species. A vertical migration mode would allow the larvae to reach faster surface ocean currents, which could disperse the larvae further from their spawning habitat. Larvae that follow a demersal development and migration strategy will remain in slow near bottom currents, which would result in a more limited dispersal [22].

Based on population genetic analyses, bathymodioline mussels with a similar nuclear DNA were found at hydrothermal vents that were over 5600 km apart [85], although the

modeled maximum median dispersal distance was estimated around 150 km for these larvae [86]. A vertical larvae migration was not included in the models by [86], however this migration mode could drastically increase the potential larvae dispersal distances [87-89] and thereby explain the observed pattern from [85]. Young *et al.* [25] and McVeigh *et al.* [90] calculated that *G. childressi* larvae, if migrating into the top 100 m, would be transported horizontally for up to 1000 km. A vertical migration, which would ensure access to more abundant phototrophic food sources, could ensure a prolonged larvae life and thereby, also result in a longer larvae migration. A long-distance dispersal, together with a vertical migration process, can explain the broad biogeographic ranges of most deep-sea taxa and could minimize the risk of mortality of the whole population in these temporally unstable chemosynthetic environments [25, 27, 91, 92].

Taking together the proposed long-distance larvae dispersal by [85], our stable isotope data of the two MAR *Bathymodiolus* species, and the published evidence of vertical migration in *G. childressi* larvae [25, 27, 52], we conclude that a vertical larval migration might be a common behavioral strategy in all bathymodioline larvae. This migration pattern would not only explain the geographic distribution of these mussels but also the phototrophic stable isotope signature of their larvae, as the sea surface layers are dominated by phototrophic food sources.

Challenges and benefits of a vertical larvae migration

Both previously discussed larvae migration and developmental strategies (vertical and demersal development and migration) come with benefits but also disadvantages for developing larvae. The most obvious benefit for a demersal development would be that

developing larvae stay in their desired habitat, which is of benefit for rare environments like hydrothermal vents and cold seeps. But this developmental strategy also comes with challenges like food accessibility in the deep sea, unstable habitats that are even more threatening when larvae migration is limited, the higher possibility of inbreeding, and the limited genetic spread over different habitats [22].

In contrast, vertical larvae migration would solve some of these problems but also comes with its own challenges. Bathymodioline mussels, as well as many other deep-sea species, would not be as vulnerable to external environmental impacts because individual animals could more easily colonize distant habitats and thereby ensure the existence of the entire population. Inbreeding would not be as common when larvae leave their spawning habitat and, most importantly, larvae would benefit from the very abundant (phototrophic) food sources that they could encounter in upper water layers.

The most obvious challenge of the vertical larvae migration mode is that the larvae need to travel for hundreds to thousands of meters through the water column to reach water layers with a higher phototrophic food content. During this migration period, the larvae could encounter predator stress and periods with limited food sources, which mean that the energy for this immense travel period needs to be already present in the egg [22]. However, microorganisms in the mesopelagic zone might provide an important source of food for bathyal larvae. Heterotrophic bacteria are nearly as abundant in the mesopelagic zone as in the euphotic zone [93, 94] and could secure the important energy source that larvae need during their ascent. The obligatory return trip between surface waters and the vent or seep environment might be highly stochastic with a high risk of mortality for many larvae. However, the trade-off between high larval mortality

rates and the benefits of a vertical larval migration appears to be possible, particularly for deep-sea species that produce a large number of offspring in each generation [22, 23, 27, 83, 84], such as bathymodioline mussels.

Summary and Outlook

Our morphology-based stable isotope analyses of different bathymodioline developmental stages revealed a trophic shift between larvae and adults. While bathymodioline larvae had a phototrophic stable isotope signature, the signatures of metamorphosing mussels and all later developmental stages revealed a dependency on energy provided by their chemosynthetic symbionts. Our stable isotope data supports the hypothesize from Franke *et al.* [17] who claimed that these mussels undergo a nutritional shift once colonized by their symbionts based on the morphology of the digestive system. This change in nutrition, which is even reflected in the morphology of these mussels, shows how dependent these mussels are on their symbionts once they have settled on the sea floor.

Our data provides first evidence for a vertical larvae migration in the MAR species *B. azoricus* and *B. puteoserpentis.* These results support the data by Arellano *et al.* [27] who have already suggested a vertical larvae migration for *G. childressi* larvae from the Gulf of Mexico. Next to analyzing the stable isotope composition of different developmental stages, a detailed plankton sampling of different depths and size fractions along the MAR would be beneficial to evaluate if any bathymodioline larvae can be identified in upper water masses. A combined microscopy and sequencing approach like the Tara Ocean sampling campaign would allow for relatively fast analyses of the plankton communities and could shed light on the question if only

bathymodioline mussels migrate vertically in the water column or if other deep-sea taxa do the same. Further stable isotope analyses of more bathymodioline species and other deep-sea taxa can help resolve the question if vertical larvae migration is conserved between many deep-sea taxa with planktotrophic larvae.

Authors' contributions

M.F., N.L. and **N.D.** conceived this study. **M.F.** and **N.L.** wrote the manuscript. **M.Ü.** revised the manuscript and gave valuable input during analyzing the data. **M.F.** performed the sample preparations, the stable isotope analyses, as well as the mixing models.

Funding

Funding was provided by the Max Planck Society, the MARUM Cluster of Excellence 'The Ocean Floor' (Deutsche Forschungsgemeinschaft (German Research Foundation) under Germany's Excellence Strategy - EXC-2077 – 39074603), a Gordon and Betty Moore Foundation Marine Microbial Initiative Investigator Award (grant no. GBMF3811 to N.D.) and a European Research Council Advanced Grant (BathyBiome, Grant 340535 to N.D.).

Acknowledgements

We highly appreciate the work of the captains, crew members, and ROV pilots of the cruises M126, M82-3, and NA58. We are grateful to Christian Borowski and Stéphane Hourdez for their valuable contributions to collecting mussel larvae. We want to thank especially Martin Whitehouse and Heejin Jeon for their technical support during the

measurement time at the NORDSIM lab in Stockholm. Furthermore, we would like to thank Jens Dyckmans for his help with the IRMS measurements done at the Kompetenzzentrum Stabile Isotope Göttingen.

Appendix

Supplementary Note 1 – Available food sources in the deep sea and their availability to bathymodioline mussels

PFA fixation and its influence to stable isotope signatures

To test for stable isotope effects due to PFA fixation, we analyzed the stable isotope composition of frozen tissue and compared it to paraformaldehyde (PFA) fixed tissue as well as PFA fixed $Os0_4$ post-fixed tissue. A pairwise students T-test showed no significant difference on the stable carbon and nitrogen isotope composition of frozen and PFA fixed gill tissue. Furthermore, we also compared the C/N-ratios of frozen and PFA fixed gill tissue. The C/N-ratios of frozen and PFA fixed gill tissue of all three species showed no significant differences. Therefore, we applied no correction factor on the stable isotope composition of the PFA fixed as well as the PFA fixed and $Os0_4$ post-fixed tissues (Table S6).

Stable isotope mixing models

We applied multiple stable isotope mixing models to analyze potential food sources of different developmental stages of *Bathymodiolus* mussels (Figure 4 and Figure S 1-3). Pre-estimated fractionation factors (carbon: 2‰ and nitrogen: 3.6‰) from shallow water mytilids were used as discrimination factors [34]. The different food sources compiled all possible food sources at hydrothermal vents, from phototrophic particulate organic matter, over surface microplankton, to free-living chemosynthetic bacteria and the chemosynthetic symbionts (Table 1). The only possible food source, which was not included into the mixing model was DOM because of the low concentration of easily degradable compounds at hydrothermal vents [77] (for further information see the supplementary section DOM). Since a vertical larvae migration is quite likely for *Bathymodiolus* larvae we also included phototrophic food sources from the euphotic zone (Table 1).

All models showed the same result. Larvae mainly feed on phototrophic food sources while plantigrades and adults mainly feed on the energy provided by their symbionts. Depending on which food sources were included into the individual mixing models the

proportion of the phototrophic diet for larvae varied a bit. But the overall trend was observed in all models (Figure 4 and Figure S 1-3).

To investigate which exact phototrophic food source was the main nutrition of *B. azoricus* and *B. puteoserpentis* pediveliger, we calculated a stable isotope mixing model including multiple phototrophic as well as chemosynthetic food sources (Figure S1). As *Bathymodiolus* larvae live planktotrophic, they potentially migrate vertically in the water column and thereby have access to the upper water layers where phototrophic primary production plays a major role in food webs. Therefore, we included stable isotope values of surface microplankton and surface bacterial communities into the mixing model. The model suggests that pediveliger of *B. azoricus* relied to 31.8% on surface microplankton, to 3.8% on surface bacteria and to 36.8% on deep-sea POM. *B. puteoserpentis* pediveliger relied to 31.6% on surface microplankton, to 3.0% on surface bacteria and to 38.0% on deep-sea POM. The remaining ~ 27% of the diet of *B. azoricus* and *B. puteoserpentis* pediveliger was composed of nutrition from other deep-sea food sources like free-living chemosynthetic bacteria (*B. azoricus* 9.5% and *B. puteoserpentis* 8.5%) and their symbionts (*B. azoricus* 18.1% and *B. puteoserpentis* 18.9%).

As already described by the general stable isotope mixing model (Figure 4), which included only the mean stable isotope values for phototrophic-, chemosynthetic food sources and symbionts, also this isotope mixing model showed the nutritional shift from phototrophic food sources in aposymbiotic larvae to a dependency on the energy provided by the symbionts in post metamorphosis developmental stages (Figure S1). We were not able to identify the exact phototrophic food source of the pediveliger, because the stable isotope values of the different phototrophic food sources were to close together and thereby could not be differentiated by the mixing model. Nevertheless, the model showed that deep-sea as well as surface phototrophic food sources can explain the stable isotope signature of the pediveliger. Given the low abundance and bioavailability of deep-sea POM, which originated from the sea surface, we argue that bathymodioline larvae migrate vertically in the water column.

However, applying a mixing model to such a complex system using natural stable isotope signatures from the literature to infer the contribution of the different food sources to the overall diet of different consumers is difficult and only as meaningful as the data which is put into the model. But it gives an idea of how the system might function. As long as the results are put into biological context, a stable isotope mixing model can be of great value. In the case of the bathymodioline development, the different stable isotope mixing models suggest a phototrophic nutrition in all larvae stages and a shift towards a chemosynthetic dependence on the energy provided by their symbionts in adults. This shift in nutrition is likely linked to the symbiotic state of the different developmental stages. The specific stable isotope mixing model, which included all food sources from the sea surface and sea floor, suggested that bathymodioline larvae feed on surface microplankton as well as deep-sea POM as their main nutrition and thereby might migrate vertically in the water column. Even if the model was not able to differentiate between these two food sources, it still shows that the larvae are not feeding close to hydrothermal vents which are dominated by chemosynthetic organisms.

DOM

Integumental feeding allows *Mytilidae* to take up free amino acids from surrounding seawater which can be used for osmoregulation or as a nutritional supplement [71, 72]. Dissolved free amino acids make up about 3 – 10% of the metabolic needs of *M. edulis* adults [71]. Other studies report rates of ~ 40 – 70% for integumental uptake of dissolved free amino acids in *Mytilus* and other shallow water bivalves [95, 96]. These rates indicate that integumental feeding could be a way for bathymodioline mussels to take up nutrients from the DOM pool. Multiple studies have already reported on the uptake of free amino acids from ambient seawater in *Bathymodiolus* mussels [73-75].

The concentrations of bioavailable molecules like neutral sugars, amino acids and amino sugars drop to values close to the detection limit as they get degraded during the sinking process [76]. The total DOM concentrations at the Mid-Atlantic ridge vent fields Lucky Strike and Menez Gwen varied between 143 to 169 µmol l-1 [97]. Most dissolved organic nitrogen and carbon measurements were done above mussel beds and need to

be interpreted carefully. The measured DOM concentrations can be influenced by mussel excrements and might not be bioavailable for bathymodioline larvae. According to Rossel *et al.* [98], only ~ 17% of the extractable DOM fraction of Menez Gwen fluids was bioavailable.

Riou *et al.* [6] stated that adult *B. azoricus* mussels have a respiration rate of 32.2 µmol C h^{-1}.They assumed that *B. childressi* and *B. azoricus* have similar carbon uptake rates of ~ 7.4 µmol C g^{-1} dry tissue h^{-1} at 10 µmol l^{-1} glycine [73]. Therefore, an averaged sized *B. azoricus* mussel with a shell length of 65.5 mm and a dry weight of 1.56 g could assimilate 347 µmol C h^{-1} with a DOC concentration of 647 µmol l^{-1} [6, 97]. This calculation assumes that the entire DOC concentration of 647 µmol l^{-1} is bioavailable. This high DOC concentration must be interpreted carefully as it was obtained above mussel beds which might have influenced the DOC concentration. The reported concentrations of DOC and dissolved amino acids from hydrothermal vents vary a lot, but Stubbins and Dittmar [76] argued that bioavailable molecules are present in the deep sea in very low concentrations and Klevenz *et al.* [77] reported that bioavailable dissolved free amino acids have a concentration of 0.143 µmol l^{-1} at vent habitats at the MAR. When considering this concentration, an averaged sized adult *B. azoricus* mussel could assimilate 0.08 µmol C h^{-1}. This is less than 0.3% of the carbon needed for respiration.

Pediveligers of the species *Crassostrea gigas* can take up ~2.8% of their metabolic needs through the uptake of dissolved amino acids [78]. Similar ratios were reported for larvae of *M. edulis* [71]. The amino acid concentration used in these experiments was typical for shallow water habitats of ~ 6 µmol l^{-1}. If we apply concentrations of 0.143 µmol l^{-1}, which were reported for MAR vent habitats [77], and assume similar uptake and metabolic rates for bathymodioline pediveliger, they could sustain ~ 0.1% of their metabolic needs by integumental feeding of dissolved free amino acids. Of course dissolved amino acids are only a small portion of the total DOM pool but these small concentrations support the argumentation of Stubbins and Dittmar [76] that bioavailable molecules are present in the deep sea in very low concentrations. Furthermore, the

main food source of bivalve pediveligers are proteins and lipids [99], which are most likely not present in the DOM pool as they were already degraded.

Taken all of this together we cannot rule out that *B. azoricus*, *B. childressi* and *B. puteoserpentis* take up DOM to supplement their nutrition but based on the bioavailable DOM concentrations in the deep sea, it is likely that integumental feeding contributes only to minor parts of the overall diet of bathymodioline larvae to adults.

Supplementary tables

Table S1 Sample overview.

sample	sample no.	developmental stage	sampling location	latitude	longitude	sampling depth [m]	sampling year	analyses	fixation
B. azoricus	1623-10	pediveliger	Bubbylon	37.801 N	-31.537 E	-1002.00	2010	SIMS	PFA + OsO_4
	1623-11	pediveliger	Bubbylon	37.801 N	-31.537 E	-1002.00	2010	SIMS	PFA + OsO_4
	1623-12	pediveliger	Bubbylon	37.801 N	-31.537 E	-1002.00	2010	SIMS	PFA + OsO_4
	1623-15	pediveliger	Bubbylon	37.801 N	-31.537 E	-1002.00	2010	SIMS	PFA
	1623-07	metamorphosis	Bubbylon	37.801 N	-31.537 E	-1002.00	2010	SIMS	PFA
	1623-08	metamorphosis	Bubbylon	37.801 N	-31.537 E	-1002.00	2010	SIMS	PFA
	1623-101	metamorphosis	Bubbylon	37.801 N	-31.537 E	-1002.00	2010	SIMS	PFA
	1623-111	metamorphosis	Bubbylon	37.801 N	-31.537 E	-1002.00	2010	SIMS	PFA
	1623-PI	metamorphosis	Bubbylon	37.801 N	-31.537 E	-1002.00	2010	SIMS	PFA + OsO_4
	1623-121	plantigrade	Bubbylon	37.801 N	-31.537 E	-1002.00	2010	SIMS	PFA
	1623-13	plantigrade	Bubbylon	37.801 N	-31.537 E	-1002.00	2010	SIMS	PFA
	1623-14	plantigrade	Bubbylon	37.801 N	-31.537 E	-1002.00	2010	SIMS	PFA
	1626-28	plantigrade	Bubbylon	37.801 N	-31.537 E	-1002.00	2010	SIMS	PFA + OsO_4
	1626-58	plantigrade	Bubbylon	37.801 N	-31.537 E	-1002.00	2010	SIMS	PFA + OsO_4
	1625-01	adults	Bubbylon	37.801 N	-31.537 E	-1002.00	2010	IRMS & SIMS	PFA
	1625-02	adults	Bubbylon	37.801 N	-31.537 E	-1002.00	2010	IRMS & SIMS	PFA
	1625-03	adults	Bubbylon	37.801 N	-31.537 E	-1002.00	2010	IRMS & SIMS	PFA
	1625-04	adults	Bubbylon	37.801 N	-31.537 E	-1002.00	2010	IRMS & SIMS	PFA
	1625-05	adults	Bubbylon	37.801 N	-31.537 E	-1002.00	2010	IRMS & SIMS	PFA
B. puteoserpentis	1556-21	pediveliger	Semenov-2	13.513 N	44.962 W	-2446.5	2016	SIMS	PFA

	1556-44	pediveliger	Semenov-2	13.513 N	44.962 W	-2446.5	2016	SIMS	PFA
	1556-31	planitgrade	Semenov-2	13.513 N	44.962 W	-2446.5	2016	SIMS	PFA + OsO_4
	1556-59	plantigrade	Semenov-2	13.513 N	44.962 W	-2446.5	2016	SIMS	PFA + OsO_4
	2343-01	adults	Semenov-2	13.513 N	44.962 W	-2446.5	2016	IRMS & SIMS	PFA
	2343-02	adults	Semenov-2	13.513 N	44.962 W	-2446.5	2016	IRMS & SIMS	PFA
	2343-03	adults	Semenov-2	13.513 N	44.962 W	-2446.5	2016	IRMS & SIMS	PFA
	2343-04	adults	Semenov-2	13.513 N	44.962 W	-2446.5	2016	IRMS & SIMS	PFA
	2343-05	adults	Semenov-2	13.513 N	44.962 W	-2446.5	2016	IRMS & SIMS	PFA
G. childressi	H1423-003-04	metamorphosis	Mississippi Canyon 853	28.123 N	-89.139 E	-1071.00	2015	SIMS	PFA
	H1423-003-05	plantigrade	Mississippi Canyon 853	28.123 N	-89.139 E	-1071.00	2015	SIMS	PFA
	H1423-01	adults	Mississippi Canyon 853	28.123 N	-89.139 E	-1071.00	2015	IRMS & SIMS	PFA
	H1423-02	adults	Mississippi Canyon 853	28.123 N	-89.139 E	-1071.00	2015	IRMS & SIMS	PFA
	H1423-03	adults	Mississippi Canyon 853	28.123 N	-89.139 E	-1071.00	2015	IRMS & SIMS	PFA

Table S2 Results of the Tukey-HSD-Test for bulk measurements. The pairwise comparison between different developmental stages of bathymodioline mussel shows that most developmental stages are significantly different. A P-value blow 0.05 is considered as significant.

statistical comparison between stable isotope ratios of different developmental stages	*B. azoricus*		*B. puteoserpentis*		*"B". childressi*	
	$\delta^{13}C$ p value	$\delta^{15}N$ p value	$\delta^{13}C$ p value	$\delta^{15}N$ p value	$\delta^{13}C$ p value	$\delta^{15}N$ p value
metamorphosis vs. pediveliger	0.0000	0.0000	0.0590	0.0877	0.0003	0.6378
plantigrade vs. pediveliger	0.0000	0.0000	0.0000	0.0000	0.0000	0.9999
adult vs. pediveliger	0.0000	0.0000	0.0004	0.0000	0.0000	0.0699
plantigrade vs. metamorphosis	0.0000	0.0000	0.0000	0.0000	0.2154	0.0262
adult vs. metamorphosis	0.0055	0.0000	0.0000	0.0000	0.0000	0.0000
adult vs. plantigrade	0.9936	0.0705	0.9918	0.0009	0.0000	0.0001

Table S3 Stable isotope summary of all samples and developmental stages.

species	sample no.	developmental stage	$\delta^{13}C$	standard deviation	$\delta^{15}N$	standard deviation
B. azoricus	1623-10	pediveliger	-20.49	1.54	5.72	1.48
	1623-11	pediveliger	-19.40	1.42	5.25	1.48
	1623-12	pediveliger	-18.52	1.33	5.37	1.23
	1623-15	pediveliger	-25.92	4.78	8.35	7.21
	average	**pediveliger**	**-21.08**	**3.32**	**6.17**	**1.47**
B. azoricus	1623-07	metamorphosis	-25.90	3.99	1.30	3.00
	1623-08	metamorphosis	-24.97	2.32	3.13	2.91
	1623-101	metamorphosis	-27.25	4.15	-4.31	6.03
	1623-111	metamorphosis	-24.65	3.59	0.26	2.16
	1623-PI	metamorphosis	-25.35	3.32	-6.36	3.12
	average	**metamorphosis**	**-25.62**	**1.02**	**-1.20**	**3.98**
B. azoricus	1623-121	plantigrade	-24.30	0.21	-6.93	1.86

	1623-13	plantigrade	-24.93	6.16	-2.28	4.51
	1623-14	plantigrade	-25.99	2.93	-5.42	2.44
	1626-28	plantigrade	-35.96	4.34	-8.47	3.72
	1626-58	plantigrade	-34.97	4.30	-13.39	5.08
	average	**plantigrade**	**-29.23**	**5.73**	**-7.30**	**4.10**
B. azoricus	1625-01	adults	-30.76	0.08	-12.63	0.46
	1625-02	adults	-30.61	0.47	12.00	0.85
	1625-03	adults	-30.44	0.48	-11.05	1.88
	1625-04	adults	-32.26	0.31	-12.84	0.56
	1625-05	adults	-31.85	0.05	-12.86	0.61
	average	**adults**	**-31.18**	**0.82**	**-12.28**	**0.77**
B. puteoserpentis	1556-21	pediveliger	-23.21	5.57	8.69	5.26
	1556-44	pediveliger	-21.76	3.20	3.47	3.46
	average	**pediveliger**	-22.49	1.03	6.08	3.69
B. puteoserpentis	1556-31	metamorphosis	-24.99	4.40	-2.11	4.04
B. puteoserpentis	1556-59	plantigrade	-30.69	0.48	-7.82	3.77
B. puteoserpentis	2343-01	adults	-30.32	0.48	-12.72	0.96
	2343-02	adults	-29.95	0.64	-12.77	1.42
	2343-03	adults	-30.33	0.14	-12.92	1.22
	2343-04	adults	-30.49	0.52	-12.64	0.79
	2343-05	adults	-30.64	0.57	-12.19	1.03

	average	**adults**	**-30.35**	**0.26**	**-12.65**	**0.28**
B. childressi	H1423-003-04	metamorphosis	-32.58	2.42	6.06	5.54
B. childressi	H1423-003-05	plantigrade	-38.13	7.42	0.13	4.74
B. childressi	H1423-01	adults	-62.53	0.97	-14.02	1.00
	H1423-02	adults	-62.33	1.77	-14.17	0.76
	H1423-03	adults	-57.69	1.74	-11.63	0.24
	average	**adults**	-60.85	2.74	-13.27	1.43

Table S4 Results of the Tukey-HSD-Test for tissue specific measurements. The pairwise comparison between different developmental stages of bathymodioline mussel shows that most developmental stages are significantly different. A P-value blow 0.05 is considered as significant.

statistical comparison between stable isotope ratios of different developmental stages		***B. azoricus***		***B. puteoserpentis***	
		$\delta^{13}C$	**$\delta^{15}N$**	**$\delta^{13}C$**	**$\delta^{15}N$**
		p value	**p value**	**p value**	**p value**
adult	**pediveliger**				
	bulk	0.0118	0	0.3435	0.0057
	digestive system	0.0078	0	0.6182	0.0823
	foot	0.9702	0.0104	1	0.9848
	gill	0.0668	0	0.9959	0.6752
	lipid vesicles	1	0.8981	0.0006	0
	velum	0.0495	0	0.7094	0.0319
	metamorphosis				
	bulk	0.8521	0.0828	0.0127	0.003
bulk	digestive system	0.9972	0.9972	n. d.	n. d.
	foot	0.9859	0.805	n. d.	n. d.
	gill	0.9882	0.9202	n. d.	n. d.
	plantigrade				
	bulk	1	0.9635	1	0.6361
	digestive system	0.9952	1	1	0.9985
	foot	0.7284	1	0.9985	0.3661
	gill	0.8164	1	0.9999	1
	adult				

	mantle	1	1	1	1
	foot	1	1	1	1
	gill	1	1	1	1
foot	**pediveliger**				
	bulk	0	0	0.0069	0
	digestive system	0	0	0.2457	0.0276
	foot	0.7068	0.0002	n. d.	n. d.
	gill	0.0005	0	0.9831	0.6556
	lipid vesicles	1	0.5371	0	0
	velum	0.0006	0	0.1458	0.0014
	metamorphosis				
	bulk	0.0822	0.0001	0.0005	0
	digestive system	0.9108	0.9852	1	0.9984
	foot	0.7442	0.4293	n. d.	n. d.
	gill	0.7202	0.636	n. d.	n. d.
	plantigrade				
	bulk	1	0.6205	1	0.2441
	digestive system	0.9039	1	n. d.	n. d.
	foot	0.2546	1	n. d.	n. d.
	gill	0.1823	1	0.9997	1
	adult				
	mantle	1	1	1	1
	gill	1	1	1	1
gill	**pediveliger**				
	bulk	0	0	0.0047	0
	digestive system	0	0	0.2533	0.0025
	foot	0.7516	0	1	0.8988
	gill	0.0007	0	0.9863	0.3622
	lipid vesicles	1	0.2772	0	0
	velum	0.0008	0	0.1388	0.0015
	metamorphosis				
	bulk	0.1079	0	0.0002	0
	digestive system	0.9345	0.9149	1	0.8518
	foot	0.7909	0.2191	n. d.	n. d.
	gill	0.7719	0.3697	n. d.	n. d.
	plantigrade				
	bulk	1	0.2982	1	0.0082
	digestive system	0.87	1	n. d.	n. d.
	foot	0.2185	1	0.987	0.0662
	gill	0.1469	1	0.9987	0.9587
	adult				
	mantle	1	1	1	0.9994
mantle	**pediveliger**				

	bulk	0	0	0.0014	0
	digestive system	0	0	0.1652	0.0343
	foot	0.6274	0.0002	1	0.9931
	gill	0.0003	0	0.9717	0.706
	lipid vesicles	1	0.623	n. d.	n. d.
	velum	0.0003	0	0.0671	0.0015
	metamorphosis				
	bulk	0.0509	0.0003	0.0004	0
	digestive system	0.8601	0.9926	1	0.9996
	foot	0.6589	0.505	n. d.	n. d.
	gill	0.6269	0.7146	0.9999	1
	plantigrade				
	bulk	1	0.7191	1	0.2955
	digestive system	0.9462	1	n. d.	n. d.
	foot	0.3222	1	0.9638	0.313
	gill	0.2538	1	0	0
plantigrade	**pediveliger**				
	bulk	0	0	0.0002	0.001
	digestive system	0	0	0.0827	0.6999
	foot	0.1582	0.0027	1	1
	gill	0	0	0.9659	0.9983
	lipid vesicles	1	1	0	0
	velum	0	0	0.0048	0.3258
	metamorphosis				
bulk	bulk	0	0	0	0
	digestive system	0.3127	1	n. d.	n. d.
	foot	0.0866	0.9994	n. d.	n. d.
	gill	0.0333	1	n. d.	n. d.
	plantigrade				
	digestive system	0.3898	0.0156	1	0.9984
	foot	0.0297	0.2182	0.9469	0.9864
	gill	0	0.0139	0.9987	0.8482
	pediveliger				
	bulk	0	0	1	0.9987
	digestive system	0	0	0.9999	1
	foot	0.0002	0	n. d.	n. d.
	gill	0	0	1	1
foot	lipid vesicles	0.2036	0.201	0.0082	0.0098
	velum	0	0	1	1
	metamorphosis				
	bulk	0	0	0.8918	0.764
	digestive system	0.0004	0.8367	0.9026	0.8559

	foot	0.0001	0.1572	n. d.	n. d.
	gill	0	0.2751	n. d.	n. d.
	plantigrade				
	digestive system	0.9965	1	n. d.	n. d.
	gill	1	1	0.7383	0.5981
gill	**pediveliger**				
	bulk	0	0	0.0005	0.005
	digestive system	0	0	0.0341	0.1391
	foot	0	0	1	0.9995
	gill	0	0	0.8392	0.877
	lipid vesicles	0.0723	0.0906	n. d.	n. d.
	velum	0	0	n. d.	n. d.
	metamorphosis				
	bulk	0	0	0	0
	digestive system	0	0.9063	1	1
	foot	0	0.1009	n. d.	n. d.
	gill	0	0.1826	n. d.	n. d.
	plantigrade				
	digestive system	0.9997	1	n. d.	n. d.
digestive system	**pediveliger**				
	bulk	0	0	n. d.	n. d.
	digestive system	0	0	n. d.	n. d.
	foot	0.0038	0	1	0.9878
	gill	0	0	n. d.	n. d.
	lipid vesicles	0.8973	0.0436	n. d.	n. d.
	velum	0	0	n. d.	n. d.
	metamorphosis				
	bulk	0	0	0.0006	0.004
	digestive system	0.0082	0.6779	n. d.	n. d.
	foot	0.0014	0.0452	0.9822	0.2669
	gill	0.0005	0.0856	n. d.	n. d.
metamorphosis					
bulk	**pediveliger**				
	bulk	0	0	0.2398	0.375
	digestive system	0.0003	0	0.9999	0.7966
	foot	1	0.8621	0.5365	0.6466
	gill	0.1789	0	0.9998	0.9929
	lipid vesicles	0.0002	0.4072	0.0142	0.0019
	velum	0.1687	0.0002	0.3736	0.0062
	metamorphosis				
	digestive system	1	0.2833	n. d.	n. d.
	foot	1	0.9836	n. d.	n. d.

	gill	1	0.5634	n. d.	n. d.
digestive system	**pediveliger**				
	bulk	0.0229	0	0.0039	0.0026
	digestive system	0.0225	0	0.1225	0.4112
	foot	1	0.0506	1	1
	gill	0.3126	0	0.9294	0.9644
	lipid vesicles	0.5602	1	0	0
	velum	0.248	0	0.0658	0.2356
	metamorphosis				
	foot	1	0.9999	n. d.	n. d.
	gill	1	1	n. d.	n. d.
foot	**pediveliger**				
	bulk	0.0383	0	n. d.	n. d.
	digestive system	0.0378	0.0002	n. d.	n. d.
	foot	1	0.4225	0.9999	1
	gill	0.4338	0.0001	n. d.	n. d.
	lipid vesicles	0.2833	1	n. d.	n. d.
	velum	0.3493	0.0001	n. d.	n. d.
	metamorphosis				
	gill	1	1	n. d.	n. d.
gill	**pediveliger**				
	bulk	0.0042	0	n. d.	n. d.
	digestive system	0.0081	0	n. d.	n. d.
	foot	1	0.1262	n. d.	n. d.
	gill	0.2529	0	n. d.	n. d.
	lipid vesicles	0.2145	1	0	0
	velum	0.2062	0	0.0057	0.0245
pediveliger	**pediveliger**				
bulk	digestive system	1	1	1	0.9999
	foot	0.4051	0.8113	0.9479	0.9672
	gill	1	1	1	1
	lipid vesicles	0	0	0.0001	0.0014
	velum	1	1	1	0.6351
digestive system	**pediveliger**				
	foot	0.2886	0.9951	0.9451	0.9999
	gill	1	1	1	1
	lipid vesicles	0	0	0.0421	0.0046
	velum	1	0.9998	1	1
foot	**pediveliger**				
	gill	0.8203	0.869	0.9993	1
	lipid vesicles	0.3168	0.0998	0.0056	0.0031
	velum	0.7165	0.8049	0.9871	1

gill	**pediveliger**				
	lipid vesicles	0	0	0.2319	0.0421
	velum	1	1	1	1
lipid vesicles	**pediveliger**				
	velum	0	0	0.0002	0.003

Table S5 Results of the general MixSiar Mixing model. SD: standard deviation

species	developmental stage	food source	mean [%]	SD
B. azoricus	pediveligers	phototrophic	72.8	10.2
		chemosynthetic	10.8	8.4
		symbionts	16.3	5.9
	metamorphosis	phototrophic	52.3	11.2
		chemosynthetic	15.1	12.3
		symbionts	32.6	9.6
	metamorphosis	phototrophic	21.0	8.1
		chemosynthetic	11.8	9.5
		symbionts	67.2	9.4
	adults	phototrophic	6.8	3.9
		chemosynthetic	3.5	3.4
		symbionts	89.7	5.2
B. puteoserpentis	pediveligers	phototrophic	72.4	12.5
		chemosynthetic	10.2	10.1
		symbionts	17.4	7.3
	metamorphosis	phototrophic	52.2	14.6
		chemosynthetic	13.4	13.3
		symbionts	34.4	12.3
	plantigrade	phototrophic	21.0	10.0
		chemosynthetic	10.5	10.8
		symbionts	68.5	12.1
	adults	phototrophic	6.6	3.9
		chemosynthetic	2.8	3.0
		symbionts	90.6	4.9

Table S6 Comparison of frozen and PFA fixed adult bathymodioline gill tissue. The C/N ratio is not significantly different compared the frozen and PFA fixed tissue

species	frozen tissue					PFA fixed tissue				
	N (%)	C (%)	C/N	$\delta^{13}C$ (‰)	$\delta^{15}N$ (‰)	N (%)	C (%)	C/N	$\delta^{13}C$ (‰)	$\delta^{15}N$ (‰)
B. azoricus	9.93	42.30	4.26	-30.19	-12.11	11.06	44.86	4.06	-30.90	-12.22
C/N ratio p-value	0.0933									
B. puteoserpentis	9.85	40.35	4.09	-30.24	-12.87	11.21	43.48	3.87	-30.15	-13.70
C/N ratio p-value	0.1389									
B. childrerssi	8.57	41.46	4.84	-67.69	-15.79	10.35	46.44	4.48	-61.52	-14.00
C/N ratio p-value	0.3077									

Supplementary Figures

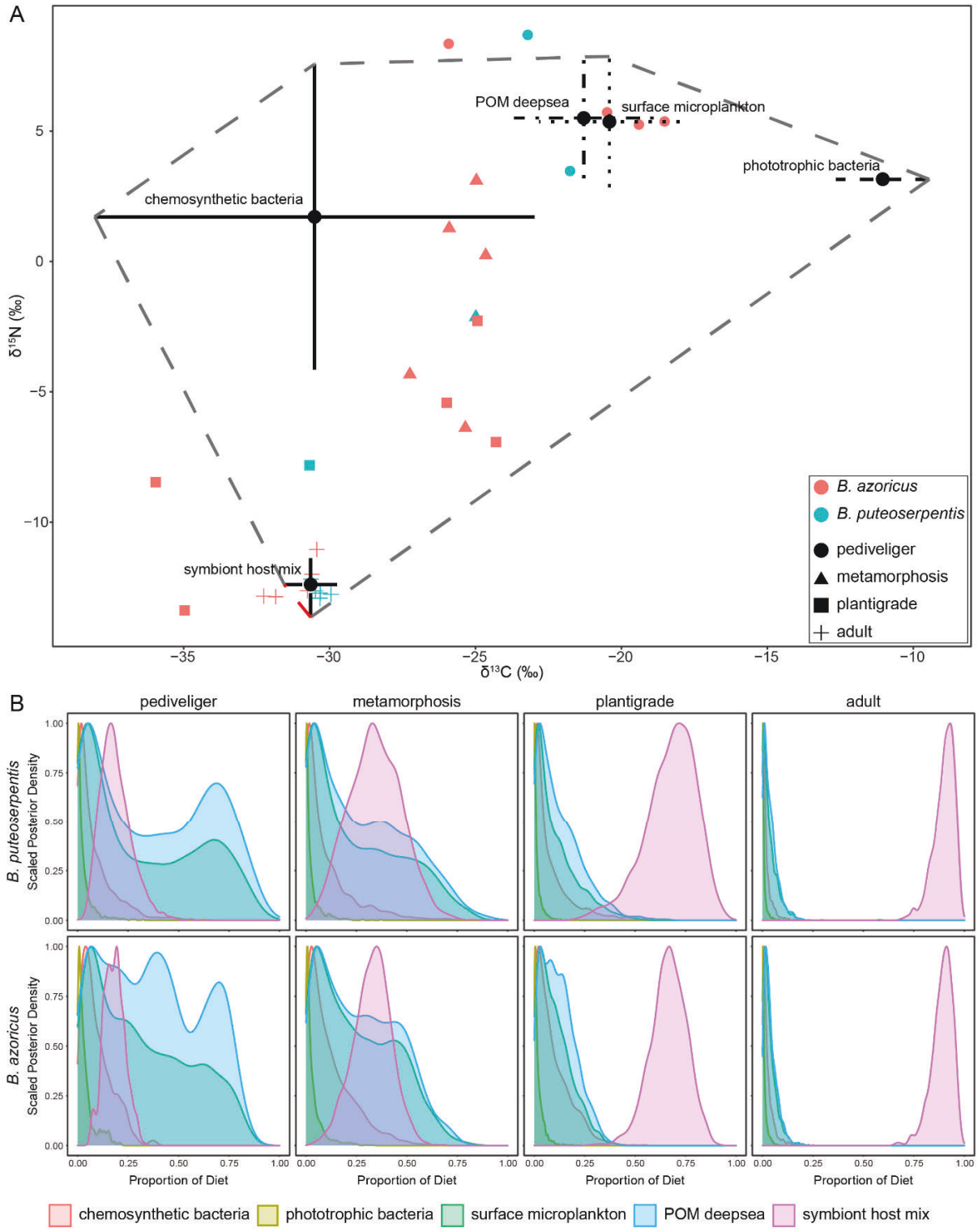

Figure S1 Stable isotope mixing model shows that *Bathymodiolus* pediveliger rely on phototrophic food sources. A) The isospace represents the carbon ($\delta^{13}C$) on the x-axis and nitrogen ($\delta^{15}N$) isotopic ratios on the y-axis of five potential food sources: phototrophic bacteria, surface microplankton, POM deep sea, chemosynthetic bacteria and symbiont host mix. The different developmental stages of *B. azoricus* (red) and *B. puteoserpentis* (blue) are indicated as circle: pediveliger, triangle: mussels during metamorphosis, square: plantigrades and cross: adults. The dashed grey line indicates the mixing polygon. **B)** The outcome of the stable isotope mixing model is presented in density plots for each developmental stage and species. On the x-axis the proportion of the different diets to the overall nutrition is listed and on the y-axis the probability how likely this distribution is. Phototrophic bacteria are displayed in yellow, surface microplankton in green, POM deep-sea in blue, chemosynthetic bacteria in red, and the symbiont host mix in magenta. The model indicates a nutritional shift from phototrophic food sources to the energy provided by the symbionts over the development.

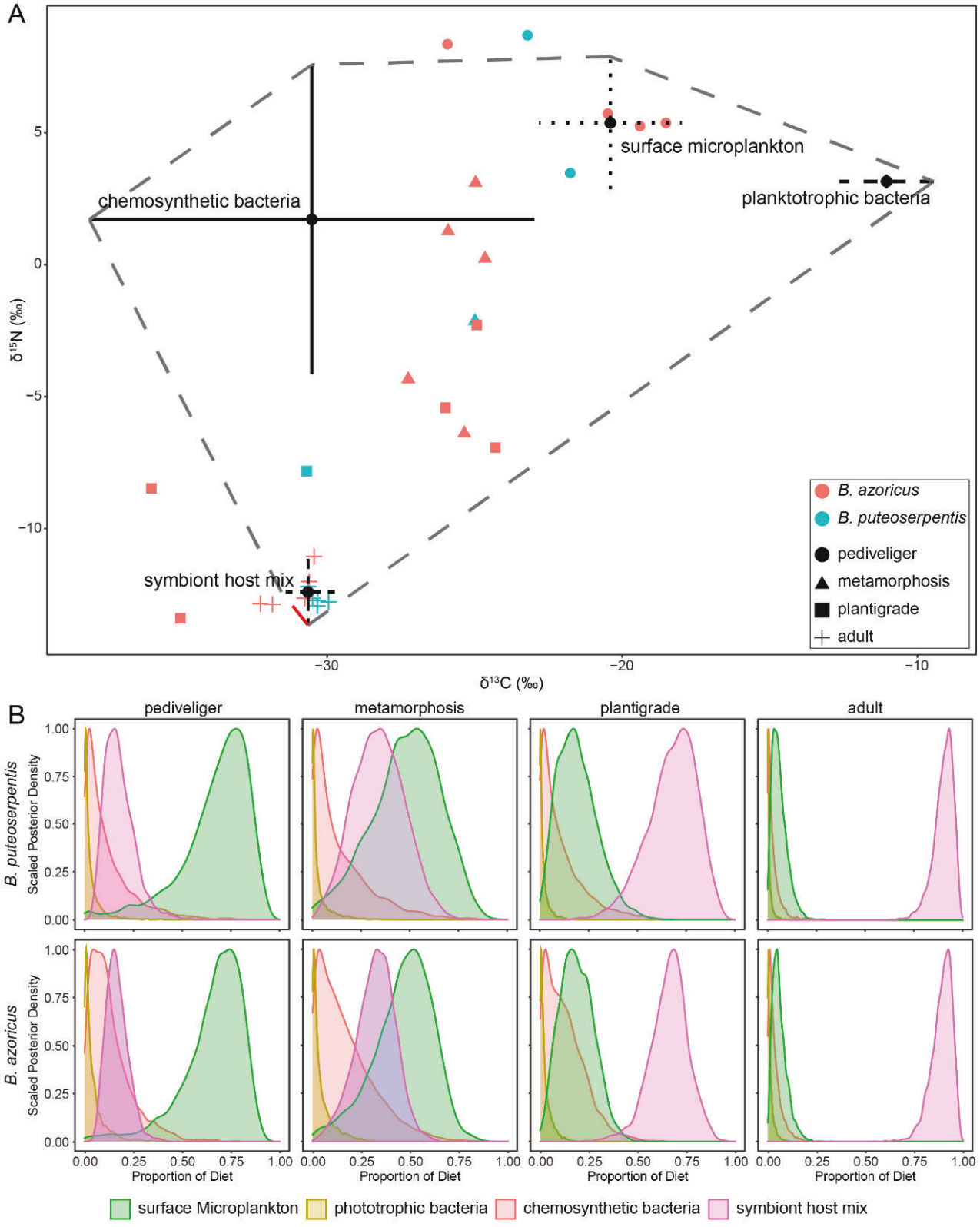
A
surface microplankton
chemosynthetic bacteria
planktotrophic bacteria
symbiont host mix
B. azoricus
B. puteoserpentis
pediveliger
metamorphosis
plantigrade
adult
δ15N (‰)
δ13C (‰)
B
pediveliger
metamorphosis
plantigrade
adult
B. puteoserpentis
B. azoricus
Scaled Posterior Density
Proportion of Diet
surface Microplankton
phototrophic bacteria
chemosynthetic bacteria
symbiont host mix

Figure S2 Stable isotope mixing model shows that *Bathymodiolus* pediveliger rely on phototrophic surace microplankton. A) The isospace represents the carbon ($\delta^{13}C$) on the x-axis and nitrogen ($\delta^{15}N$) isotopic ratios on the y-axis of four potential food sources: phototrophic bacteria, surface microplankton, chemosynthetic bacteria and symbiont host mix. The different developmental stages of *B. azoricus* (red) and *B. puteoserpentis* (blue) are indicated as circle: pediveliger, triangle: mussels during metamorphosis, square: plantigrades and cross: adults. The dashed grey line indicates the mixing polygon. **B)** The outcome of the stable isotope mixing model is presented in density plots for each developmental stage and species. On the x-axis the proportion of the different diets to the overall nutrition is listed and on the y-axis the probability how likely this distribution is. Phototrophic bacteria are displayed in yellow, surface microplankton in green, chemosynthetic bacteria in red, and the symbiont host mix in magenta. The model indicates a nutritional shift from phototrophic food sources to the energy provided by the symbionts over the development.

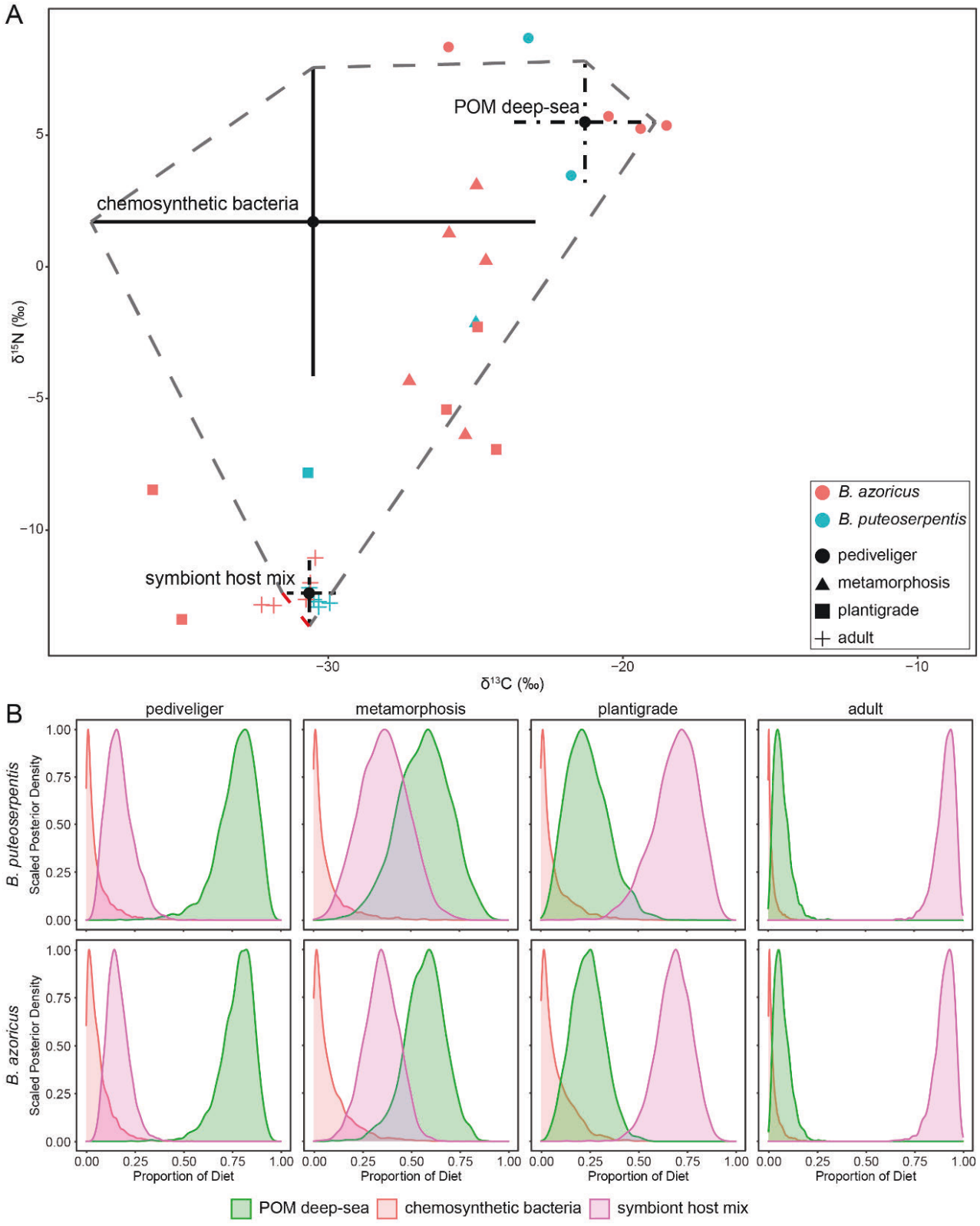
A
POM deep-sea
chemosynthetic bacteria
symbiont host mix
δ15N (‰)
δ13C (‰)
B. azoricus
B. puteoserpentis
pediveliger
metamorphosis
plantigrade
adult
B
pediveliger
metamorphosis
plantigrade
adult
B. puteoserpentis
B. azoricus
Scaled Posterior Density
Proportion of Diet
POM deep-sea
chemosynthetic bacteria
symbiont host mix

Figure S3 Stable isotope mixing model shows that *Bathymodiolus* pediveliger rely on deep-sea POM. A) The isospace represents the carbon ($\delta^{13}C$) on the x-axis and nitrogen ($\delta^{15}N$) isotopic ratios on the y-axis of three potential food sources: POM deep sea, chemosynthetic bacteria and symbiont host mix. The different developmental stages of *B. azoricus* (red) and *B. puteoserpentis* (blue) are indicated as circle: pediveliger, triangle: mussels during metamorphosis, square: plantigrades and cross: adults. The dashed grey line indicates the mixing polygon. **B)** The outcome of the stable isotope mixing model is presented in density plots for each developmental stage and species. On the x-axis the proportion of the different diets to the overall nutrition is listed and on the y-axis the probability how likely this distribution is. Deep-sea POM is displayed in green, chemosynthetic bacteria in red, and the symbiont host mix in magenta. The model indicates a nutritional shift from phototrophic food sources to the energy provided by the symbionts over the development.

References

[1] McFall-Ngai, M., Hadfield, M.G., Bosch, T.C.G., Carey, H.V., Domazet-Lošo, T., Douglas, A.E., Dubilier, N., Eberl, G., Fukami, T., Gilbert, S.F., et al. 2013 Animals in a bacterial world, a new imperative for the life sciences. *Proc. Natl. Acad. Sci. USA* **110**, 3229-3236. (doi:10.1073/pnas.1218525110).
[2] Bright, M. & Bulgheresi, S. 2010 A complex journey: transmission of microbial symbionts. *Nature Reviews Microbiology* **8**, 218-230. (doi:10.1038/nrmicro2262).
[3] Bell, J.B., Woulds, C. & Oevelen, D.v. 2017 Hydrothermal activity, functional diversity and chemoautotrophy are major drivers of seafloor carbon cycling. *Sci. Rep.* **7**, 12025. (doi:10.1038/s41598-017-12291-w).
[4] Hügler, M. & Imhoff, J. 2009 Life at Deep Sea Hydrothermal Vents—Oases Under Water. *The International Journal of Marine and Coastal Law* **24**, 201-208. (doi:10.1163/157180809X421789).
[5] Tyler, P. 1988 Seasonality in the deep sea. *Oceanogr. Mar. Biol. Annu. Rev.* **26**, 227-258.
[6] Riou, V., Colaco, A., Bouillon, S., Khripounoff, A., Dando, P., Mangion, P., Chevalier, E., Korntheuer, M., Santos, R.S. & Dehairs, F. 2010 Mixotrophy in the deep sea: a dual endosymbiotic hydrothermal mytilid assimilates dissolved and particulate organic matter. *Marine Ecology-progress Series* **405**, 187-201. (doi:10.3354/meps08515).
[7] Omand, M.M., Govindarajan, R., He, J. & Mahadevan, A. 2020 Sinking flux of particulate organic matter in the oceans: Sensitivity to particle characteristics. *Sci. Rep.* **10**, 5582. (doi:10.1038/s41598-020-60424-5).
[8] Dubilier, N., Bergin, C. & Lott, C. 2008 Symbiotic diversity in marine animals: the art of harnessing chemosynthesis. *Nature Reviews Microbiology* **6**, 725-740. (doi:10.1038/nrmicro1992).
[9] Sogin, E.M., Kleiner, M., Borowski, C., Gruber-Vodicka, H.R. & Dubilier, N. 2021 Life in the Dark: Phylogenetic and Physiological Diversity of Chemosynthetic Symbioses. *Annu. Rev. Microbiol.* (doi:10.1146/annurev-micro-051021-123130).
[10] Sogin, E.M., Leisch, N. & Dubilier, N. 2020 Chemosynthetic symbioses. *Curr. Biol.* **30**, R1137-R1142. (doi:10.1016/j.cub.2020.07.050).
[11] DeChaine, E. & Cavanaugh, C.M. 2005 Symbioses of methanotrophs and deep-sea mussels (*Mytilidae*: *Bathymodiolinae*). *Prog Mol Subcell Biol.* **41**, 227-249. (doi:10.1007/3-540-28221-1_11).

[12] Distel, D.L., Lee, H.K.-W. & Cavanaugh, C.M. 1995 Intracellular coecistence of methano- and thioautorophic bacteria in a hydrothermal vent mussel. *Microbiology* **92**. (doi:10.1073/pnas.92.21.9598).
[13] Fiala-Médioni, A., Métivier, C., Herry, A. & Le Pennec, M. 1986 Ultrastructure of the gill of the hydrothermal-vent mytilid *Bathymodiolus sp. Mar. Biol.* **92**, 65-72. (doi:10.1007/BF00392747).
[14] Streams, M.E., Fisher, C.R. & Fiala-Médioni, A. 1997 Methanotrophic symbiont location and fate of carbon incorporated from methne in a hydrocabon seep mussel. *Mar. Biol.* **129**, 465-476. (doi:10.1007/s002270050187).
[15] Martins, I., Colaço, A., Dando, P.R., Martins, I., Desbruyères, D., Sarradin, P.-M., Marques, J.C. & Serrão-Santos, R. 2008 Size-dependent variations on the nutritional pathway of *Bathymodiolus azoricus* demonstrated by a C-flux model. *Ecol. Model.* **217**, 59-71. (doi:10.1016/j.ecolmodel.2008.05.008).
[16] Wentrup, C., Wendeberg, A., Huang, J.Y., Borowski, C. & Dubilier, N. 2013 Shift from widespread symbiont infection of host tissues to specific colonization of gills in juvenile deep-sea mussels. *ISME J* **7**, 1244-1247. (doi:10.1038/ismej.2013.5).
[17] Franke, M., Geier, B., Hammel, J.U., Dubilier, N. & Leisch, N. 2021 Coming together - symbiont acquisition and early development in deep-sea bathymodioline mussels. *Proceedings of the Royal Society B: Biological Sciences* **288**, 20211044. (doi:doi:10.1098/rspb.2021.1044).
[18] Laming, S.R., Gaudron, S.M. & Duperron, S. 2018 Lifecycle Ecology of Deep-Sea Chemosymbiotic Mussels: A Review. *Front. Mar. Sci.* **5**. (doi:10.3389/fmars.2018.00282).
[19] Tyler, P.A. & Young, C.M. 1999 Reproduction and dispersal at vents and cold seeps. *J. Mar. Biol. Assoc. U.K.* **79**, 193-208. (doi:10.1017/S0025315499000235).
[20] Lutz, R.A., Jablonski, D., Rhoads, D.C. & Turner, R.D. 1980 Larval dispersal of a deep-sea hydrothermal vent bivalve from the galapagos rift. *Mar. Biol.* **57**, 127-133. (doi:10.1007/BF00387378).
[21] Pearse, J.S. 1969 Slow developing demersal embryos and larvae of the antarctic sea star *Odontaster validus*. *Mar. Biol.* **3**, 110-116. (doi:10.1007/BF00353429).
[22] Young, C.M., Arellano, S.M., Hamel, J.F. & Mercier, A. 2018 Ecology and evolution of larval dispersal in the deep sea. In *Evolutionary ecology of marine invertebrate larvae* (eds. T.J. Carrier, A.M. Reitzel & A. Heyland). Oxford, Oxford University Press.
[23] Van Gaest, A.L. 2006 Ecology and early life history of *Bathynerita naticoidea*: evidence for long-distance larval dispersal of a cold seep gastropod.
[24] Queiroga, H. & Blanton, J. 2004 Interactions Between Behaviour and Physical Forcing in the Control of Horizontal Transport of Decapod Crustacean Larvae. In *Adv. Mar. Biol.* (pp. 107-214, Academic Press.
[25] Young, C.M., He, R., Emlet, R.B., Li, Y., Qian, H., Arellano, S.M., Van Gaest, A., Bennett, K.C., Wolf, M., Smart, T.I., et al. 2012 Dispersal of deep-sea larvae from the intra-American seas: simulations of trajectories using ocean models. *Integr. Comp. Biol.* **52**, 483-496. (doi:10.1093/icb/ics090).
[26] Lutz, R.A., Jablonski, D. & Turner, R.D. 1984 Larval Development and Dispersal at Deep-Sea Hydrothermal Vents. *Science* **226**, 1451. (doi:10.1126/science.226.4681.1451).

[27] Arellano, S.M., Van Gaest, A.L., Johnson, S.B., Vrijenhoek, R.C. & Young, C.M. 2014 Larvae from deep-sea methane seeps disperse in surface waters. *Proc Biol Sci* **281**, 20133276. (doi:10.1098/rspb.2013.3276).
[28] Gustafson, R.G., Turner, R.D., Lutz, R.A. & Vrijenhoek, R.C. 1998 A new genus and five new species of mussels (Bivalvia, Mytilidae) from deep-sea sulfide/hydrocarbon seeps in the Gulf of Mexico. *Malacologia* **40**, 63-112.
[29] Fry, B. 2012 *Stable Isotope Ecology*. New York, Springer-Verlag; 308 p.
[30] Salerno, J.L., Macko, S.A., Hallam, S.J., Bright, M., Won, Y.J., McKiness, Z. & Van Dover, C.L. 2005 Characterization of symbiont populations in life-history stages of mussels from chemosynthetic environments. *Biol. Bull,* **208**, 145-155. (doi:10.2307/3593123).
[31] DeNiro, M.J. & Epstein, S. 1977 Mechanism of carbon isotope fractionation associated with lipid synthesis. *Science* **197**, 261. (doi:10.1126/science.327543).
[32] Stock, B.C., Jackson, A.L., Ward, E.J., Parnell, A.C., Phillips, D.L. & Semmens, B.X. 2018 Analyzing mixing systems using a new generation of Bayesian tracer mixing models. *PeerJ* **6**, e5096. (doi:10.7717/peerj.5096).
[33] Stock, B.C. & Semmens, B.X. 2016 MixSIAR GUI User Manual. Version 3.1. (https://github.com/brianstock/MixSIAR.
[34] Dubois, S., Jean-Louis, B., Bertrand, B. & Lefebvre, S. 2007 Isotope trophic-step fractionation of suspension-feeding species: Implications for food partitioning in coastal ecosystems. *J. Exp. Mar. Biol. Ecol.* **351**, 121-128. (doi:10.1016/j.jembe.2007.06.020).
[35] Arellano, S.M. & Young, C.M. 2009 Spawning, development, and the duration of larval life in a deep-sea cold-seep mussel. *Biol. Bull,* **216**, 149-162. (doi:10.1086/BBLv216n2p149).
[36] Phillips, D.L., Inger, R., Bearhop, S., Jackson, A.L., Moore, J.W., Parnell, A.C., Semmens, B.X. & Ward, E.J. 2014 Best practices for use of stable isotope mixing models in food-web studies. *Canadian Journal of Zoology* **92**, 823-835. (doi:10.1139/cjz-2014-0127).
[37] Mompeán, C., Bode, A., Benítez-Barrios, V.M., Domínguez-Yanes, J.F., Escánez, J. & Fraile-Nuez, E. 2013 Spatial patterns of plankton biomass and stable isotopes reflect the influence of the nitrogen-fixer *Trichodesmium* along the subtropical North Atlantic. *J. Plankton Res.* **35**, 513-525. (doi:10.1093/plankt/fbt011).
[38] Cregeen, S. 2016 Microbiota of dominant Atlantic copepods: *Pleuromamma sp*. as a host to a betaproteobacterial symbiont.
[39] Grall, J., Le Loc'h, F., Guyonnet, B. & Riera, P. 2006 Community structure and food web based on stable isotopes (δ15N and δ13C) analysis of a North Eastern Atlantic Maerl bed. *J. Exp. Mar. Biol. Ecol.* **338**, 1-15. (doi:10.1016/j.jembe.2006.06.013).
[40] Carpenter, E.J., Harvey, H.R., Fry, B. & Capone, D.G. 1997 Biogeochemical tracers of the marine cyanobacterium *Trichodesmium*. *Deep Sea Research Part I: Oceanographic Research Papers* **44**, 27-38. (doi:10.1016/S0967-0637(96)00091-X).
[41] Altabet, M.A. 1990 Organic C, N, and stable isotopic composition of particulate matter collected on glass-fiber and aluminum oxide filters. *Limnol. Oceanogr.* **35**, 902-909. (doi:10.4319/lo.1990.35.4.0902).
[42] Bode, A. & Hernández-León, S. 2018 Trophic Diversity of Plankton in the Epipelagic and Mesopelagic Layers of the Tropical and Equatorial Atlantic Determined with Stable Isotopes. *Diversity* **10**. (doi:10.3390/d10020048).

[43] Denda, A., Stefanowitsch, B. & Christiansen, B. 2017 From the epipelagic zone to the abyss: Trophic structure at two seamounts in the subtropical and tropical Eastern Atlantic - Part II Benthopelagic fishes. *Deep Sea Research Part I: Oceanographic Research Papers* **130**. (doi:10.1016/j.dsr.2017.08.005).
[44] Khripounoff, A., Vangriesheim, A., Crassous, P., Segonzac, M., Colaco, A., Desbruyeres, D., Barthelemy, R., Khripounoff, A., Vangriesheim, A., Crassous, P., et al. 2001 Particle flux in the Rainbow hydrothermal vent field (Mid-Atlantic Ridge): Dynamics, mineral and biological composition. *J. Mar. Res.* **59**, 633-656.
[45] Reid, W.D.K., Wigham, B.D., McGill, R.A.R. & Polunin, N.V.C. 2012 Elucidating trophic pathways in benthic deep-sea assemblages of the Mid-Atlantic Ridge north and south of the Charlie-Gibbs Fracture Zone. *Mar. Ecol. Prog. Ser.* **463**, 89-103. (doi:10.3354/meps09863).
[46] Colaço, A., Dehairs, F. & Desbruyeres, D. 2002 Nutritional relations of deep-sea hydrothermal fields at the Mid-Atlantic Ridge A stable isotope approach. *Deep sea research* **49**, 18. (doi:10.1016/S0967-0637(01)00060-7).
[47] Winkel, M., Pjevac, P., Kleiner, M., Littmann, S., Meyerdierks, A., Amann, R. & Mussmann, M. 2014 Identification and activity of acetate-assimilating bacteria in diffuse fluids venting from two deep-sea hydrothermal systems. *FEMS Microbiol. Ecol.* **90**, 731-746. (doi:10.1111/1574-6941.12429).
[48] Portail, M., Brandily, C., Cathalot, C., Colaço, A., Gélinas, Y., Husson, B., Sarradin, P.-M. & Sarrazin, J. 2018 Food-web complexity across hydrothermal vents on the Azores triple junction. *Deep Sea Research Part I: Oceanographic Research Papers* **131**, 101-120. (doi:10.1016/j.dsr.2017.11.010).
[49] Gebruk, A.V., Southward, E.C., Kennedy, H. & Southward, A.J. 2000 Food sources, behaviour, and distribution of hydrothermal vent shrimps at the Mid-Atlantic Ridge. *J. Mar. Biol. Assoc. U.K.* **80**, 485-499. (doi:10.1017/S0025315400002186).
[50] Colaço, A., Martins, I., Laranjo, M., Pires, L., Leal, C., Prieto, C., Costa, V., Lopes, H., Rosa, D., Dando, P.R., et al. 2006 Annual spawning of the hydrothermal vent mussel, *Bathymodiolus azoricus*, under controlled aquarium, conditions at atmospheric pressure. *J. Exp. Mar. Biol. Ecol.* **333**, 166-171. (doi:10.1016/j.jembe.2005.12.005).
[51] Hessler, R.R., Smithey, W.M., Boudrias, M.A., Keller, C.H., Lutz, R.A. & Childress, J.J. 1988 Temporal change in megafauna at the Rose Garden hydrothermal vent. *Deep-Sea Research* **35**, 1681-1709. (doi:10.1016/0198-0149(88)90044-1).
[52] Arellano, S.M. 2008 Embryology, larval ecology, and recruitment of *Bathymodiolus childressi*, a cold-seep mussel from the gulf of mexico. Oregon, University of Oregon.
[53] Van Dover, C.L. 2000 *The Ecology of Deep-Sea Hydrothermal Vents*. Princeton, Princeton University Press.
[54] Trask, J.L. & Van Dover, C.L. 1999 Site-specific and ontogenetic variations in nutrition of mussels (*Bathymodiolus* sp.) from the Lucky Strike hydrothermal vent field, Mid-Atlantic Ridge. *Limnology Oceanography* **44**, 334-343. (doi:10.4319/lo.1999.44.2.0334).
[55] Van Dover, C.L. & Fry, B. 1989 Stable isotopic compositions of hydrothermal vent organisms. *Mar. Biol.* **102**, 257-263. (doi:10.1007/BF00428287).
[56] Fisher, C.R. 1995 Toward an Appreciation of Hydrothennal-Vent Animals: Their Environment, Physiological Ecology, and Tissue Stable Isotope Values. *Seafloor*

Hydrothermal Systems: Physical, Chemical, Biological, and Geological Interactions, 297-316. (doi:10.1029/GM091p0297).
[57] Becker, E.L., Lee, R.W., Macko, S.A., Faure, B.M. & Fisher, C.R. 2010 Stable carbon and nitrogen isotope compositions of hydrocarbon-seep bivalves on the Gulf of Mexico lower continental slope. *Deep Sea Research Part II: Topical Studies in Oceanography* **57**, 1957-1964. (doi:10.1016/j.dsr2.2010.05.002).
[58] Page, H., Fisher, C. & Childress, J. 1990 Role of filter-feeding in the nutritional biology of a deep-sea mussel with methanotrophic symbionts. *Mar. Biol.* **104**, 251-257. (doi:10.1007/BF01313266).
[59] Page, H.M., Fiala-Medioni, A., Fisher, C.R. & Childress, J.J. 1991 Experimental evidence for filter-feeding by the hydrothermal vent mussel, *Bathymodiolus thermophilus*. *Deep Sea Research Part A. Oceanographic Research Papers* **38**, 1455-1461. (doi:10.1016/0198-0149(91)90084-S).
[60] Le Pennec, M. & Hily, A. 1984 Anatomie, structure et ultrastructure de la branchie d'un Mytilidae des sites hydrothermaux du Pacifique oriental. *Oceanol. Acta* **7**, 517-523.
[61] Le Pennec, M. 1988 Alimentation et reproduction d'un Mytilidae des sources hydrothermales profondes du Pacifique oriental. *Oceanologica Acta, Special issue*.
[62] Le Pennec, M. & Prieur, D. 1984 Observations sur la nutrition d'un mytilidae d'un site hydrothermal actif de la dorsale du Pacifique oriental; Observations on the nutrition of a Mytilidae from an hydrothermal vent of the East Pacifique ride. *Comptes rendus des séances de l'Académie des sciences. Série 3, Sciences de la vie* **298**, 493-498.
[63] Colaco, A., Prieto, C., Martins, A., Figueiredo, M., Lafon, V., Monteiro, M. & Bandarra, N.M. 2009 Seasonal variations in lipid composition of the hydrothermal vent mussel *Bathymodiolus azoricus* from the Menez Gwen vent field. *Mar. Environ. Res.* **67**, 146-152. (doi:10.1016/j.marenvres.2008.12.004).
[64] Colaço, A., Dehairs, F., Desbruyeres, D., Le Bris, N. & Sarradin, P.M. 2002 $\delta^{13}C$ signature of hydrothermal mussels is related with the end-member fluid concentrations of H_2S and CH_4 at the Mid-Atlantic Ridge hydrothermal vent fields *Cah. Biol. Mar.* **43**, 4.
[65] Baldwin, B.S. & Newell, R.I.E. 1991 Omnivorous feeding by planktotrophic larvae of the eastern oyster *Crassostrea virginica*. *Mar. Ecol. Prog. Ser.* **78**, 285-301.
[66] Birkbeck, T.H. & McHenery, J.G. 1982 Degradation of bacteria by *Mytilus edulis*. *Mar. Biol.* **72**, 7-15. (doi:10.1007/BF00393942).
[67] Bayne, B.L., Hawkins, A.J.S. & Navarro, E. 1987 Feeding and digestion by the mussel *Mytilus edulis L.* (Bivalvia: Mollusca) in mixtures of silt and algal cells at low concentrations. *J. Exp. Mar. Biol. Ecol.* **111**, 1-22. (doi:10.1016/0022-0981(87)90017-7).
[68] Prins, T.C., Smaal, A.C. & Pouwer, A.J. 1991 Selective ingestion of phytoplankton by the bivalves *Mytilus edulis L.* and *Cerastoderma edule (L.)*. *Hydrobiological Bulletin* **25**, 93-100. (doi:10.1007/BF02259595).
[69] Bergquist, D.C., Eckner, J.T., Urcuyo, I.A., Cordes, E.E., Hourdez, S., Macko, S.A. & Fisher, C.R. 2007 Using stable isotopes and quantitative community characteristics to determine a local hydrothermal vent food web. *Mar. Ecol. Prog. Ser.* **330**, 49-65. (doi:10.3354/meps330049).
[70] Tunnicliffe, V. 1991 The biology of hydrothermal vents : Ecology and evolution. *Oceanography and Marine Biology* **29**, 319-407.

[71] Ferguson, J.C. 1982 A comparative study of the netmetabolic benefits derived from the uptake and release of free amino acids by marine invertebrates. *The Biological Bulletin* **162**, 1-17. (doi:10.2307/1540965).
[72] Bishop, S.H., Ellis, L.L. & Burcham, J.M. 1983 6 - Amino Acid Metabolism in Molluscs. In *Metabolic Biochemistry and Molecular Biomechanics* (ed. P.W. Hochachka), pp. 243-327, Academic Press.
[73] Lee, R.W., Thuesen, E.V., Childress, J.J. & Fisher, C.R. 1992 Ammonium and free amino acid uptake by a deep-sea mussel (*Bathymodiolus sp.*, undescribed) containing methanotrophic bacterial symbionts. *Mar. Biol.* **113**, 99-106. (doi:10.1007/BF00367643).
[74] Fiala-Médioni, A., Alayse, A.M. & Cahet, G. 1986 Evidence of in situ uptake and incorporation of bicarbonate and amino acids by a hydrothermal vent mussel. *J. Exp. Mar. Biol. Ecol.* **96**, 191-198. (doi:10.1016/0022-0981(86)90242-X).
[75] Lee, R.W. & Childress, J.J. 1995 Assimilation of inorganic nitrogen by seep mytilid Ia, an undescribed deep-sea mussel containing methanotrophic endosymbionts: fate of assimilated nitrogen and the relation between methane and nitrogen assimilation. *Mar. Ecol. Prog. Ser.* **123**, 137-148. (doi:10.3354/meps123137).
[76] Stubbins, A. & Dittmar, T. 2014 Dissolved Organic Matter in Aquatic Systems. (pp. 25-156.
[77] Klevenz, V., Sumoondur, A., Ostertag-Henning, C. & Koschinsky, A. 2010 Concentrations and distributions of dissolved amino acids in fluids from Mid-Atlantic Ridge hydrothermal vents. *GEOCHEMICAL JOURNAL* **44**, 387-397. (doi:10.2343/geochemj.1.0081).
[78] Manahan, D.T. 1983 The uptake and metabolism of dissolves amino acids by bivalve larvae. *The Biological Bulletin* **164**, 236-250. (doi:10.2307/1541142).
[79] Bouchet, P. & Warén, A. 1994 Ontogenetic migration and dispersal of deep-sea gastropod larvae. In *Reproduction, Larval Biology, and Recruitment of the Deep-sea Benthos* (eds. C.M. Young & K.J. Eckelbarger), Columbia University Press.
[80] Eckelbarger, K.J. & Watling, L. 1995 Role of Phylogenetic Constraints in Determining Reproductive Patterns in Deep-Sea Invertebrates. *Invertebr. Biol.* **114**, 256-269. (doi:10.2307/3226880).
[81] Young, C.M. 2003 Reproduction, Development and Life-history traits In *Ecosystems of the Deep Oceans* (ed. P. Tyler), Elsevier.
[82] Dittel, A.I., Perovich, G. & Epifanio, C.E. 2008 *Biology of the Vent Crab Bythograea thermydron: A Brief Review*, SPIE; 15 p.
[83] Yahagi, T., Kayama Watanabe, H., Kojima, S. & Kano, Y. 2017 Do larvae from deep-sea hydrothermal vents disperse in surface waters? *Ecology* **98**, 1524-1534. (doi:10.1002/ecy.1800).
[84] Whitney, J.L., Gove, J.M., McManus, M.A., Smith, K.A., Lecky, J., Neubauer, P., Phipps, J.E., Contreras, E.A., Kobayashi, D.R. & Asner, G.P. 2021 Surface slicks are pelagic nurseries for diverse ocean fauna. *Sci. Rep.* **11**, 3197. (doi:10.1038/s41598-021-81407-0).
[85] Ücker, M. 2021 Metagenomic analyses of a deep-sea mussel symbiosis, Universität Bremen Fachbereich 02: Biologie/Chemie (FB 02).
[86] Breusing, C., Biastoch, A., Drews, A., Metaxas, A., Jollivet, D., Vrijenhoek, Robert C., Bayer, T., Melzner, F., Sayavedra, L., Petersen, Jillian M., et al. 2016 Biophysical and Population Genetic Models Predict the Presence of “Phantom” Stepping

Stones Connecting Mid-Atlantic Ridge Vent Ecosystems. *Curr. Biol.* **26**, 2257-2267. (doi:10.1016/j.cub.2016.06.062).
[87] Hilário, A., Metaxas, A., Gaudron, S.M., Howell, K.L., Mercier, A., Mestre, N.C., Ross, R.E., Thurnherr, A.M. & Young, C.M. 2015 Estimating dispersal distance in the deep sea: challenges and applications to marine reserves. *Front. Mar. Sci.* **2**, 6. (doi:10.3389/fmars.2015.00006).
[88] Cowen, R.K., Paris, C.B. & Srinivasan, A. 2006 Scaling of Connectivity in Marine Populations. *Science* **311**, 522. (doi:10.1126/science.1122039).
[89] Metaxas, A. & Saunders, M. 2009 Quantifying the “Bio-” Components in Biophysical Models of Larval Transport in Marine Benthic Invertebrates: Advances and Pitfalls. *The Biological Bulletin* **216**, 257-272. (doi:10.1086/BBLv216n3p257).
[90] McVeigh, D.M., Eggleston, D.B., Todd, A.C., Young, C.M. & He, R. 2017 The influence of larval migration and dispersal depth on potential larval trajectories of a deep-sea bivalve. *Deep Sea Research Part I: Oceanographic Research Papers*. (doi:10.1016/j.dsr.2017.08.002).
[91] Mitarai, S., Watanabe, H., Nakajima, Y., Shchepetkin, A.F. & McWilliams, J.C. 2016 Quantifying dispersal from hydrothermal vent fields in the western Pacific Ocean. *Proceedings of the National Academy of Sciences* **113**, 2976. (doi:10.1073/pnas.1518395113).
[92] McClain, C.R. & Hardy, S.M. 2010 The dynamics of biogeographic ranges in the deep sea. *Proceedings of the Royal Society B: Biological Sciences* **277**, 3533-3546. (doi:10.1098/rspb.2010.1057).
[93] DeLong, E.F. & Pace, N.R. 2001 Environmental diversity of bacteria and archaea. *Syst. Biol.*
[94] Cho, B.C. & Azam, F. 1988 Major role of bacteria in biogeochemical fluxes in the ocean's interior. *Nature* **332**, 441-443. (doi:10.1038/332441a0).
[95] Langdon, C.J. 1983 Growth Studies with Bacteria-Free Oyster (*Crassostrea gigas*) Larvae Fed on Semi-Defined Artificial Diets. *Biol. Bull,* **164**, 227-235. (doi:10.2307/1541141).
[96] Wright, S.H. & Ahearn, G.A. 2011 Nutrient Absorption in Invertebrates. In *Comprehensive Physiology* (ed. R. Terjung), pp. 1137-1205.
[97] Sarradin, P.M., Caprais, J.-C., Riso, R., Kerouel, R. & Aminot, A. 1999 Chemical environment of the hydrothermal mussel communities in the Lucky Strike and Menez Gwen vent fields, Mid Atlantic Ridge. *Cah. Biol. Mar* **40**, 93-104.
[98] Rossel, P.E., Stubbins, A., Hach, P.F. & Dittmar, T. 2015 Bioavailability and molecular composition of dissolved organic matter from a diffuse hydrothermal system. *Mar. Chem.* **177**, 257-266. (doi:10.1016/j.marchem.2015.07.002).
[99] Holland, D.L. 1978 Lipid reserves and energy metabolism in the larvae of benthic marine invertebrates. *Biochemical and biophysical perspectives in marine biology* **4**, 85-123. (doi:10.1007/s11745-000-0569-z).

Chapter V | Discussion

Chapter V | Discussion, future directions, and concluding remarks

The deep sea is one of the most unexplored and fascinating ecosystems of our planet. Despite its harsh living conditions (absolute darkness, hardly any food sources, high pressure and relatively cold water temperatures), it is the “home” of many marine organisms from vertebrates, over invertebrates to marine bacteria [1]. Especially at hydrothermal vents, cold seeps and organic falls dense populations of animals can be found [2]. Most of these animals, including mussels from the family bathymodiolinae, live in symbiosis with chemosynthetic bacteria [3-5].

In the last 40 years since their discovery, much research has been done on bathymodioline mussels. Especially in the last years, the knowledge gain significantly increased, as many analytical techniques and sampling methods have been improved by technological advances. For example, it has been suggested from phylogenetic work that symbionts are transmitted horizontally [6, 7], that mussels can be associated with up to five different species of symbionts [8-12], and that mussels digest their symbionts intracellularly to obtain energy [13-16]. Therefore, it is astonishing that basic ecological questions of this symbiosis are still not answered and many open questions remain regarding the early development of these animals, when and how the symbioses is initiated, how the aposymbiotic life stages can survive in the deep sea and how the symbionts are associated over the lifetime of these animals. Despite technical improvements in deep-sea sampling, these fundamental questions of symbiosis research are still unanswered in many deep-sea symbioses, or so far only very rudimentarily understood. This is mainly due to the fact that it is almost impossible to collect larval stages of these animals in the deep sea,

as many larvae live planktonically in the water column and are so small that they can hardly be found.

In this thesis I investigated the early development, nutritional strategies in different developmental life stages, symbiont acquisition as well as symbiont-host association in different bathymodioline species (Figure 1). The combination of different imaging techniques, such as µCT, correlative light and electron microscopy and fluorescence in situ hybridization (FISH) revealed that these mussels are colonized by their symbionts during the metamorphosis (chapter III; [17], Figure 1). The morphological informed stable isotope analysis of different developmental stages revealed a nutritional shift from phototrophic derived food sources in larvae to symbiotic energy delivery in adult mussels (Figure 1). From these results I hypothesize that the larvae do not stay and feed at the hydrothermal vents but rather migrate vertically through the water column, most likely towards a shallower feeding ground (chapter IV). Furthermore, by using a 3D ultrastructural imaging approach (FIB-SEM) we could show that different bathymodioline species have a different symbiont-host association form which depends on the symbiont type and not on the habitat as suggested so far (chapter II, Figure 1).

In summary, my thesis answers fundamental questions on the symbiosis between bathymodioline mussels and their chemosynthetic bacterial symbionts. With correlative advanced techniques I was able to show that even in non-model organisms these questions can be answered. I have discussed the results of my thesis already in detail in the individual chapters, therefore I will address in this chapter three questions that have developed as a result of the findings of this thesis.

Furthermore I will highlight why it is worthwhile studying “unusual” systems that have limitations and cannot be treated equally with model systems.

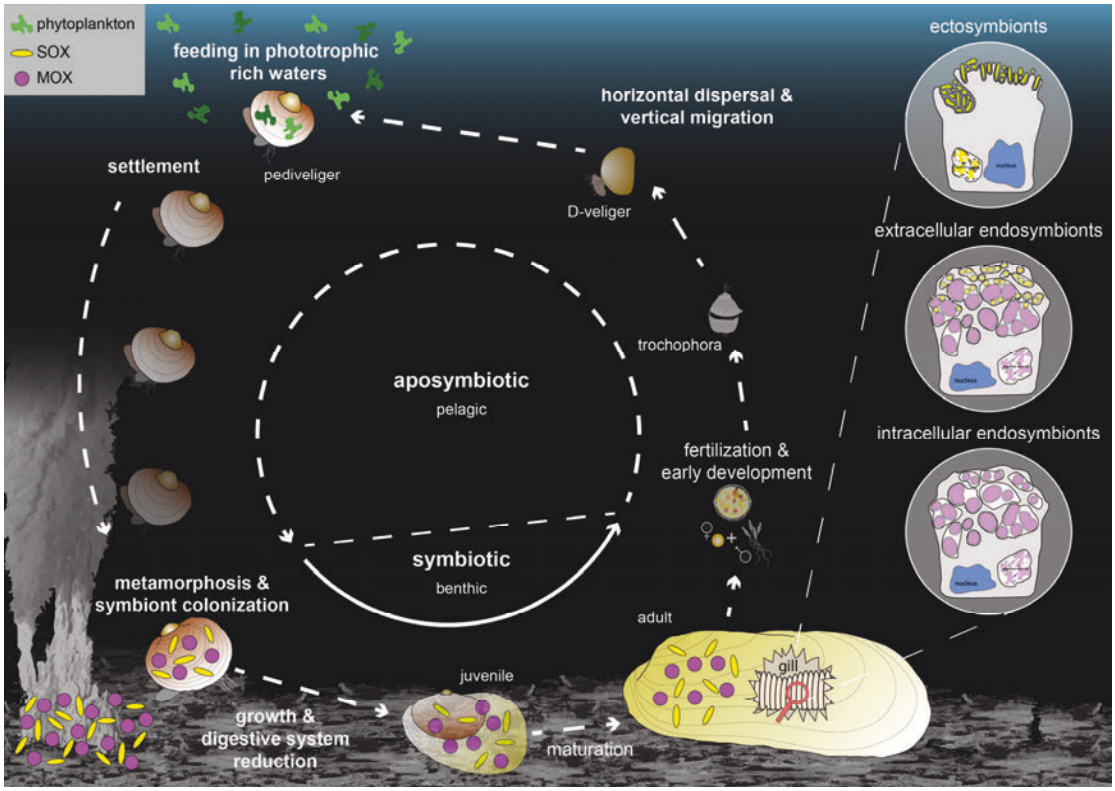

Figure 1 The lifecycle of the bathymodioline symbiosis. The results of this thesis indicate a vertical migration during the larvae life of bathymodioline mussels. This migration would ensure constant supply by phototrophic nutrition. Once the mussels settled at the sea-floor they metamorphose and take up their symbionts. From there on they rely on the energy provided by the symbionts. Different species host their symbionts differently. The symbionts could be associated as ectosymbionts, as extracellular endosymbionts or as intracellular endosymbionts.

5.1 How do bathymodioline larvae sense a potential settling habitat?

For many benthic invertebrates that have planktotrophic larvae, settlement in their desired habitat is a critical process during their life cycle [18]. This process determines not only where the adult will spend its life but determines the survival success of the entire population [18, 19]. Although some benthic animals can still move locally, they do not travel long distances and therefore rarely leave their settlement habitat. If larvae choose a habitat that is not suitable for the benthic adult

animal, the chances of survival tend to be poor, and the population is at risk of extinction [18, 19].

In chapter IV of this thesis, I proposed a vertical larval migration for the aposymbiotic life stages of bathymodioline mussels. The vertical migration results in bathymodioline larvae feeding and building up energy reservoirs in phototrophic rich water layers closer to the sea surface. This means the aposymbiotic larvae leave their safe spawning environments and thus also the access to their horizontally acquired symbionts. Furthermore, they not only move vertically in the water column but also get drifted horizontally with different water currents. Young *et al.* [20] has estimated that these actively vertical swimming larvae can travel distances of about 1000 km from their spawning habitat once reaching faster surface currents. These large larvae migration patterns could explain the geographic distribution of bathymodioline mussels we know today. However, the vertical larvae migration also means that once the planktotrophic larvae initiate their settlement, they have to search for the "oases of the deep sea" [2], which is like looking for a needle in a haystack. How and when bathymodioline larvae initiate settlement and how they sense the chemosynthetic environment in the deep sea is not yet clear. But if we consider the knowledge from shallow water habitats bathymodioline larvae would need to react to different cues, which would initiate different processes such as settlement, finding the final settlement habitat, as well as initiating metamorphosis. The cues responsible for initiating settlement need to be present in shallower depths, as the larvae migrate vertically in the water column and cues responsible for finding a suitable settlement habitat need to be sensed in deeper water layers closer to the settlement habitat, once the larvae sink into deeper layers again [21].

The cues that trigger larval settlement are highly diverse and vary among species. Depending on the taxa, shallow water invertebrate larvae respond to a variety of different signals ranging from chemical, biological, physical, to microbial [18, 22, 23]. It has been shown that in shallow water environments with strong currents, chemical cues can only be detected within a few centimeters by larvae [24]. Therefore, these cues are more likely to direct larvae in certain direction at the final settlement site, but other cues such as currents, noise, temperature, salinity, and pH can influence larval settlement over longer distances [18, 25-27]. These various cues play a major role in larval ecology, determining how populations distribute geographically and where new individuals settle.

Recently, it was shown that the mytilid species *M. galloprovincialis* and *M. coruscus* initiate settlement and metamorphosis as soon as they sense a chemical compound released by a specific biofilm [28-30]. Chang *et al.* [31] presented data that even biofilms of deep-sea bacteria influence the settlement and metamorphosis of developing *M. coruscus* larvae. Not only mussels but also other marine invertebrates such as bryozoans, polychaetes, and barnacles initiate their settlement and metamorphosis as soon as they sense a certain bacterial or diatom biofilm [22, 32-35]. In the case of microbial cues, animals do not respond directly to the microorganisms but to chemical substances released by the bacteria, such as low-molecular-weight metabolites or high-molecular-weight extracellular polymers [23]. As mentioned above the olfactoric sensing is limited to tens of centimeters and therefore determines the settling habitat on a local basis.

In chapter III, I discussed the presence of a bacterial biofilm on the shell of just-settled aposymbiotic pediveligers [17]. Given the response of shallow water mytilids

to biofilms, it is tempting to speculate whether this biofilm may have initiated metamorphosis in bathymodioline bivalves. The morphology on an ultrastructure level of these microorganisms was similar to the known symbionts of bathymodioline mussels. If the free-living symbionts colonize the shells of the mussels first and release chemical compounds that initiate the metamorphosis of the mussels, they would ensure that they could colonize the mussels immediately after the mussels have begun with their metamorphosis. Whether bacterial cues trigger metamorphosis in bathymodioline mussels or whether it was just a coincidence that we observed a biofilm on the shell of these life stages remains unclear. However, it can be assumed that bathymodioline larvae and especially pediveliger are able to react to different cues, as they had all the morphological prerequisites. The pediveliger had a well-developed nervous system as well as a distinctive foot (chapter III; [17]) with which mytilids and oysters sense cues in the water column and on substrata during settlement [36, 37]. It can be concluded that bathymodioline pediveliger need to have a well-developed sensory system to react to different cues to find a suitable settlement habitat and initiate metamorphosis. Furthermore, the initial recognition between the free living symbionts and the pediveliger larvae needs to be controlled in a certain way as well.

In general, data on settlement cues in deep-sea taxa are very limited and it is still an open question how larvae of vent animals find a suitable settlement habitat [21, 38, 39]. Different chemical, physical and biological cues have been hypothesized to impact the metamorphosis and settlement of hydrothermal vent animals [39]. For example hydrogen sulfide content, temperature, turbulence, noise, and suspended microorganisms were suggested to impact the settlement of vent animals [38-41]. The distances over which larvae can detect these cues in the deep-sea have not yet

been determined. However, chemical gradients from the plume of hydrothermal vents could be tracked over greater distances on a basin scale [42]. Nevertheless, it is astonishing how planktotrophic deep-sea larvae find suitable settlement habitats. In particular, organic falls that are temporally limited and randomly distributed in the deep sea are difficult for larvae to find, but are still relatively quickly colonized by chemosynthetic systems [43]. This suggests that there must be cues that can be sensed over long distances and guide the larvae to their desired settlement habitat. Otherwise, these deep-sea taxa would not be as successful in colonizing new habitats, nor would they be geographically as widely distributed.

5.1.1 Future directions

Especially in times of climate change where many of the world's currents are changing [44, 45] and in times of increasing exploitation of the deep ocean through deep-sea mining or deep-sea fishing [46-49], it is important to better understand the relationship between deep-sea habitats and the rest of the world’s oceans. A growing body of data has been presented in the past showing that larvae of deep-sea organisms migrate to the upper ocean layers to feed [21, 50-52]. My data for bathymodioline mussels point in a similar direction (chapter IV). Vertical migration also disperses larvae horizontally over several hundred kilometers before they search for a new settlement habitat. These data suggest that deep-sea organisms do not appear to be as isolated as previously thought, and that their geographic distribution is therefore highly dependent on surface currents. Global climate change has shown that these currents can change, and therefore the distribution of deep-sea organisms could change. In addition, humans are increasingly affecting these habitats, and thus threatening them. To protect these ecosystems in the future, I think it is very important to better understand how they are interconnected with the

rest of the world's oceans and how, for example, deep-sea larvae migrate in the water column and how they colonize new habitats. Since most deep-sea larvae are very small, they cannot be directly tracked during their migration. Therefore, in the following, I propose an experiment to clarify whether deep-sea larvae migrate vertically in the water column and thus depend on surface currents to disperse.

In this thesis I have focused on bathymodioline bivalves and therefore describe the experiment on these animals, but in theory it could be applied to any other deep-sea species as well. To answer this question a sampling campaign would be needed with a similar setup as the Tara Ocean sampling campaign [53], but with a specific adjustments for deep-sea eukaryotic larvae. Samples need to be taken in a size fraction between 200 – 500 µm to include eukaryotic invertebrate larvae. I would include different sampling depths from the deep sea to the surface ocean to evaluate whether the larvae migrate vertically in the water column and to study if they stop at a certain depth or migrate vertically until they reach the euphotic zone. To increase the likelihood of larval sampling, I would focus sampling on a known hydrothermal vent area such as the Mid-Atlantic Ridge and surrounding waters and collect samples at regular intervals several times for at least 9 to 12 months (typical larval life) starting shortly after the known spawning season in December to January [54].

To analyze the different zooplankton fractions of different locations and depths a metagenomics approach similar to the study of de Vargas *et al.* [55] and Pierella Karlusich *et al.* [56] would be needed. However, 18S ribosomal DNA may not provide sufficient resolution because deep-sea larvae are likely underrepresented in surface layers due to abundant phototrophic zooplankton. Therefore, I would suggest to analyze the full length mitochondrial DNA to estimate whether bathymodioline

mussels were present in the surface layers or not. An evolutionary placement algorithm analyzes (for an example see [57]) could ease the data analyzes and resolve if bathymodioline sequences were present in the metagenomics dataset or not.

To find out the specific cues to which bathymodioline larvae react, one would need alive larvae and a way to keep them in aquaria for a longer period of time. These larvae could then be used to conduct laboratory experiments that would bring the larvae into contact with different cues. Starting with factors known to affect shallow-water mytildis and then expanding these experiments to expose larvae to features typical of chemosynthetic habitats, such as higher concentrations of hydrogen sulfide, could clarify the various factors involved in initiating settlement, finding a suitable settlement habitat, and metamorphosis.

In my opinion, it is crucial to understand how the deep-sea habitat is interconnected to the rest of the world's oceans. This also includes understanding how deep-sea larvae disperse and what cues they follow to find their settling habitats. The climate change might influence these distribution patterns by changing the world's surface currents [44, 45]. This could lead to extinctions of deep-sea populations as their larvae might not find suitable settling habitats.

5.2 How do bathymodioline mussels recognize their symbionts and how does the symbiont uptake work?

An important process in any symbiotic system is the transmission of symbionts from one generation to the next [58]. In the case of horizontally transmitted symbionts, it is particularly important that both symbiotic partners have specific recognition mechanisms so that the host can find its symbionts among the multitude of free-living

bacteria [58]. How exactly this recognition between the two partners works and which mechanisms are used to take up the symbionts is not yet clear in most symbiotic systems and only studied in some model organisms [59, 60].

5.2.1 Where do bathymodioline mussels find their symbionts?

How bathymodioline mussels recognize their specific symbionts in the environment and how the symbiont uptake works on a molecular level remains unresolved so far. In the context of this thesis I could show that the symbionts are taken up rapidly during the metamorphosis and I could show that in bathymodioline species that harbor SOX and MOX symbionts the SOX symbiont colonizes first (chapter III; [17]). If the larvae sense the free living symbiotic population via a chemical cue they already need to be in close proximity as chemical cues can only be sensed by larvae within a few centimeters [24]. The rapid symbiont colonization shortly after the larvae settlement in the reducing habitats suggests that free-living symbionts are present in high numbers. However, Ücker [61] showed that this seems to be not the case at least for the SOX symbionts. Only a small fraction (~ 7%) of the total free-living bacterial community at Mid-Atlantic Ridge hydrothermal vents belonged to the order Thiomicrospirales [61], to which the SOX symbionts also belong [62]. Ücker [61] performed an evolutionary placement analysis which indicated that the 16S rRNA sequences of the found Thiomicrospirales were most similar to sequences of various free-living marine bacteria and chemosynthetic symbionts from vent and seep clams and mussels. These results indeed showed that close relatives of the bathymodioline SOX symbionts were present around the mussel beds but in low concentrations.

The question of how bathymodioline mussels find their symbionts cannot be answered with the available data. However, several hypotheses have already been

proposed about the origin of the symbionts taken up by the larvae. The classical assumption is that the larvae take up the symbionts from the environment by filtering the sea-water [63]. Thereby the free-living symbionts enter the mantle cavity of the mussels, come into close contact with the gills and begin to colonize the gill epithelia. In chapter III I could show that the symbiont colonization only started as soon as the velum (the larval swimming and feeding organ) was degraded, as symbionts would directly get transported to the digestive system as long as the velum is still functional [17]. As soon as the gill generated the water flow in the mantle cavity the symbionts started to colonize. However, the free-living SOX symbiont might be present only in minor amounts in the surrounding environment [61], which makes it difficult for the larvae to find the symbionts among all the other free-living bacteria [64, 65]. The free-living bacteria from the environment do not necessarily have to float freely in the water column, but can also be present in biofilms surrounding the mussel beds [66, 67]. That mytilids can be attracted to biofilms has already been shown for some shallow water species [28-31]. Thus, biofilms of free-living symbionts could also be a way for bathymodioline larvae to come into contact with their symbionts in the deep sea.

A second hypothesize was raised recently by Geier [68]. They proposed that bathymodioline mussels feed on their own shed bacteriocytes. Shedding of epithelia cells is a normal process of tissue turnover in mytilids, but feeding on bacteriocytes has the benefit to gain energy from the symbionts. Through an incomplete digestion symbionts could be released into the environment and serve as a free living symbiont pool for newly settled larvae.

A third way bathymodioline larvae could take up symbionts would be as soon as the adult animal dies. In chapter II of this thesis I have proposed a possible "exit" strategy for the symbionts, in mussels that harbor their symbionts extracellularly in a membrane invagination. As soon as the adult mussel dies the symbionts don't need to cross cell membranes to leave the tissue. They could "simply" leave the host again by widen the channel system or detaching from the apical cell membrane. That related intracellular symbionts from other chemosynthetic systems are able to leave host cells after the depth of the host has been shown for the symbionts of tubeworms [69]. This indicates that even the intracellular symbionts of bathymodioline mussels might be able to leave the host tissue again after the host died.

Bathymodioline larvae that settle in an existing mussel bed most likely acquire their symbionts from a mix of all three scenarios described. However, when larvae colonize a new habitat where no adult mussels are present, they must come into contact with the free-living symbionts. These can either be free floating in the water column or in the form of biofilms. However, this requires that the symbionts and larvae have strong recognition mechanisms, so that a small free-living symbiont population is sufficient to initiate the symbiosis.

5.2.2 How does the symbiont recognition and uptake works on a molecular level?

Once the two symbiotic partners have recognized each other in the environment, the 2nd challenge begins: how does the mussel ensure that it only starts a symbiotic association with the specific symbionts? During the initial colonization I found only the specific symbionts (chapter III; [17]), which means that right from the beginning on the symbiosis is very specific. This specificity and the capability to take up new

symbionts is kept throughout the lifetime of these mussels [70]. To establish this specificity between the two partner's specific molecular recognition mechanisms must be involved. To date, data on these regulatory mechanisms are very limited for bathymodioline mussels.

Research on other symbiotic systems have revealed that the different hosts use a variety of different pattern recognition receptors (PRRs) to control the symbiont-host interactions and to recognize their symbionts. These PPRs included leucine rich repeats [71], C-type lectins [72], peptidoglycan recognition proteins (PGRPs) [73], Toll-like receptors (TLRs) and lipopolysaccharide and glucan-binding proteins (LGPBs) [74]. Transcriptomic studies on *Bathymodiolus platifrons* have revealed that some of these PRRs, including TLRs, PGRPs, and C-type lectins, were highly expressed in symbiotic mussels [15, 75, 76]. Especially the receptors TLR13 and the bactericidal/permeability increasing protein (BPI) were under special focus in the study of Wang *et al.* [75]. The TLR13 receptor is an intracellular toll-like receptor that recognizes conserved 23S ribosomal RNA sequences from bacteria only after they have been taken up via phagocytosis [77, 78]. The BPI receptor was highly expressed in symbiotic *B. platifrons* mussels. In the past, it was shown that the mollusk LBP/BPI genes play a crucial role in the establishment of the squid-vibrio symbiosis [79]. Chun *et al.* [80] could show that the messenger RNA expression of this receptor was 9-fold higher in symbiotic squids compared to aposymbiotic squids. Due to its importance in the squid-vibrio symbiosis and the fact that the BPI receptor was highly expressed in symbiotic *B. platifrons* mussels Wang *et al.* [75] suggested that this receptor might also play a crucial role in the recognition of the symbionts in bathymodioline mussels. But further evidence is needed to verify, if these receptors are really involved in symbiont recognition and uptake. Especially because shallow

water mytilids also express immune genes in the gills to a high degree, since the gills are in constant contact with microorganisms that are present in the surrounding seawater [81, 82].

5.2.3 Future directions

So far, mostly transcriptome data are available that provide information on the molecular processes involved in symbiont recognition and uptake in bathymodioline mussels. However, to find out the exact molecular processes involved in symbiont recognition and uptake, further insights are needed. In model organisms, these questions would be addressed with infection studies in aposymbiotic genetically modified hosts. Potential recognition proteins and receptors would be knocked out to evaluate if the symbionts could still be taken up [59, 83, 84]. However, organisms must be culturable for these methods. Both bathymodioline mussels as well as their symbionts cannot be cultured and are very difficult to maintain in the aquarium until now. Therefore, a different approach would be needed to study the recognition and uptake in bathymodioline mussels.

In the following, I describe an experiment that could shed more light on the processes involved in symbiont recognition and uptake. I would suggest to study bathymodioline species which are originating from shallower depths such as *B. azoricus*, *G. childressi* or *V. insolatus*, as these mussels should be easier to maintain in aquaria [85-88]. To look more closely at the initial symbiont recognition and colonization, I would suggest to keep aposymbiotic larvae together with adult mussels in aquaria, since it is assumed that adult mussels release symbionts into the environment [68, 70]. This would be one way that the aposymbiotic larvae could obtain their symbionts in an aquarium setup. In order to understand the molecular

processes in more detail, a combined genomic, transcriptional and imaging approach would be needed. Since live cell imaging is very difficult to realize with these animals, one would have to fix samples for genomic, transcriptomic and imaging analysis at regular intervals over the duration of the metamorphosis, as this is the time period these larvae get colonized by their symbionts (chapter III, [17]). Potential receptor candidates need to be identified by a differential expression analysis of different life stages, expecting higher expression rates in mussels that get colonized vs. low expression rates in aposymbiotic larvae. After identifying potential targets specific antibodies would indicate if the labeled receptors co-localize with the bacteria during colonization. This would provide further evidence, in addition to the transcriptomic and genomic analysis, as to whether certain receptors/proteins play a role in the symbiont recognition and uptake of bathymodioline mussels.

The experiment described above relies on living larvae that can survive in the aquarium for a period of time. Since the collection of these developmental stages is not trivial, one can also work with fixed samples. In this specific case it is important to have a high number of replicates and enough developmental stages to cover the process of metamorphosis and symbiont colonization. The described correlative approach of genomic, transcriptomic and imaging analyses can then be carried out as explained above and has the potential to resolve the molecular processes involved in the initial symbiont host recognition and uptake in bathymodioline mussels.

5.3 How do bathymodioline symbionts leave their host?

In chapter II of this thesis, I demonstrated a third form of symbiont-host association in bathymodiolin mussels, the symbionts were located extracellularly in a complex

membrane invagination connected to the outside by a channel system. The symbionts were not associated intracellularly in vacuoles nor as ectosymbionts on the outside of the apical cell membrane, as recently assumed for bathymodioline species from hydrothermal vents and cold seeps [13, 89, 90]. From these results, I proposed that the extracellular endosymbionts could potentially leave the host more easily than the intracellular endosymbionts (e.g., of *G. childressi*), as they are already in the extracellular medium.

For facultative horizontally transmitted symbionts and pathogens, a crucial step is to leave the host to ensure that there are enough bacteria in the environment to colonize new hosts and to protect bacterial population from extinction should the host die [69, 91-93]. By modifying the host cytoskeleton and proteins involved in the formation of the channels, which are connecting the bacterial compartments with the outside, the extracellular endosymbionts of bathymodioline mussels might be able to escape the host cell. This process could be initiated by the symbionts interacting with the host cytoskeletal proteins that form the channels. Or the symbionts are simply released into the environment as the host cytoskeleton changes during cell depth and thereby removes the channel structure. In plant and animal cells, it has been shown that the cytoskeleton rearranges itself to initiate cell death [94, 95]. This rearrangement could lead to the disintegration of the channel system in bathymodioline mussels and a release of symbionts into the environment. However, shed bacteriocytes still contain bacteria [68], which indicates that the channel system is maintained during the shedding process, but could be remodeled as soon as the host dies. In tubeworms and nodules of *Medicago sativa* it was shown that the intracellular endosymbionts can leave the host as soon as it dies [69, 93]. The host cell membrane disintegrates shortly after the tubeworm died, allowing the symbionts

to leave the host cells [69]. A disruption of the host cell membrane is not necessary for the extracellular endosymbionts of the bathymodiolin mussels, since they are already outside the cell. It would be sufficient if the cytoskeleton is restructured so that the symbionts are released into the environment.

For bathymodioline symbionts leaving the host could be beneficial in various situations: (I) the symbionts could leave the host cell as soon as the host dies, (II) the symbionts could prevent the intracellular digestion by the host and (III) the symbionts would be able to sustain the free living population of symbionts in the environment. How and if the symbionts leave the host remains to be shown. But that symbionts leave the bacteriocytes would fit the hypothesis of Wentrup *et al.* [70] that the mussels infect themselves with symbionts colonizing new cells from already colonized bacteriocytes.

5.3.1 Future direction

Now that I have shown that the extracellular endosymbionts are common in multiple bathymodioline species, the question arises which molecular processes are involved in the formation of this complex structure. In the following, I will discuss an experiment to resolve these processes.

As these mussels cannot be cultured I suggest to do a combined approach of (I) differential gene expression analysis of *B. manusensis* (ectosymbionts), *B. puteoserpentis* (extracellular endosymbionts), and *G. childressi* (intracellular endosymbionts) host and bacterial transcriptomes and (II) a targeted imaging approach visualizing target proteins via a specific antibody staining. By comparing different mussels that exhibit the different symbiont-host association forms, target proteins could be more easily defined. I would first restrict the analyses to proteins of

the host cytoskeleton, since these interfere with the membrane and are responsible for shaping the membrane [96]. Next to the proteins discussed in chapter II, one other potential target protein could be dynamin. Dynamin is responsible for the membrane fission during clathrin-independent endocytosis and phagocytosis [97]. During this process, a phagocytic cup is formed and eventually the membranes fuse and the particle is internalized in a vacuole [97]. The symbiont uptake in bathymodioline mussels might also follow the phagocytotic path but gets modified by the symbionts. The symbionts could suppress the expression of dynamin or prevent dynamin from binding to the phagocytic cup. Thereby, the membranes would not be able to fuse, resulting in the formation of a tubular structure.

As soon as target proteins have been identified during the differential gene expression analysis, specific antibodies would need to be synthesized to visualize the different proteins. By combining the specific antibody labeling with a membrane stain one could verify if the target proteins are responsible for shaping the channel systems. For this super resolution microscopy, such as Stimulated Emission Depletion (STED) microscopy might be necessary to visualize the individual channels and supporting proteins.

Since the morphology of this symbiotic arrangement is not comparable to any known association between bacteria and eukaryotes, resolving the molecular processes is not trivial. Furthermore, most likely a number of different proteins are involved in the formation of this complex morphology, which does not make the underlying molecular processes any easier to resolve. But with the comparison of the different species, different expression rates of cytoskeletal proteins should be detectable and should

give a first idea of which proteins might be involved in shaping this specific symbiont host association.

5.4 Why is it worth studying non-model organisms from extreme environments?

In the past, research in biology was often divided into cellular-molecular-developmental biology and ecology-evolutionary biology [98]. While most evolutionary biologists have focused on studying the diversity of different habitats, cell and evolutionary biologists have worked on model organisms on which they could test their hypotheses and concepts [99]. Many of the today declared model organism were studied because they were relatively easy to culture in the lab and thereby relatively easy to genetically modify [98-100]. The information obtained from these model organisms has led to the development of general concepts in biology. For example infection assays combined with knockout mutants have enabled researchers to investigate the molecular processes involved in pathogens / symbiont host recognition and colonization [59, 83, 84, 101].

The division of biology has resulted in researchers of both directions concentrating on their specific research and often do not interconnect each other [98]. As a result, ecological and evolutionary aspects of many model organisms are still not well understood. Today, it is becoming increasingly clear that many of these model organisms, on which many basic principles of biology have been discovered and described, are not representative of their close relatives [98]. This is mainly due to the fact that established model organisms were determined by whether they are easy to culture and have short life cycles. But this limited field of view with rather "simple" organisms has fundamental consequences. Some of the established model

organisms are "ecological outliers", which rather escape the selection pressure by predators, environment and competitors than to face it [98]. Longer-lived and slow-growing relatives of the species must face this pressure through adaptation. The ability of these model organisms to escape selection pressure has significantly limited the traits that biologist can study in these systems [98].

Therefore, research on non-model organisms has become more and more important over the last years and technological advances, which were mainly developed by studying model organisms, have led to a significant increase in knowledge of these non-model systems [100, 102]. In particular, the development and availability of relatively inexpensive sequencing techniques has led to the study of unknown habitats as well as non-culturable organisms during the last years [103]. However, metagenome studies alone are not sufficient to answer biological questions because evolution only affects the phenotype and thus genes may be present that are not used. Therefore, these methods often need to be supported with metatranscriptome, metaproteome as well as experimental data. The experimental prove of a biological question is exactly the difficulty when working with non-model organisms, as most of these methods, such as CRISPR/Cas9-mediated gene editing [104], still rely on the cultivation of the study-organism. The RNA interference (RNAi) technique enabled researchers in the past to down regulate the expression of specific proteins [105]. This technique was recently also applied to no-model systems [106], which are capable to survive for a longer time periods in the lab. To apply RNAi on any organism, the genetic understanding of the study organism needs to be very high so that target proteins, which are about to be down-regulated, can be identified and specific siRNAs can be produced. Since these properties are not present in all organisms, methods that are independent of cultivation are needed.

Correlative approaches combining multiple techniques, from genomics, over mass-spectrometry and different imaging techniques (Figure 2), on the same sample set have the potential to overcome these problems. In the scope of this thesis, I have shown that by combining different techniques such as µCT, histology, TEM, FISH, light microscopy, IRMS and SIMS on the same set of samples, the gap between cellular biology and ecology can be bridged even in non-model systems.

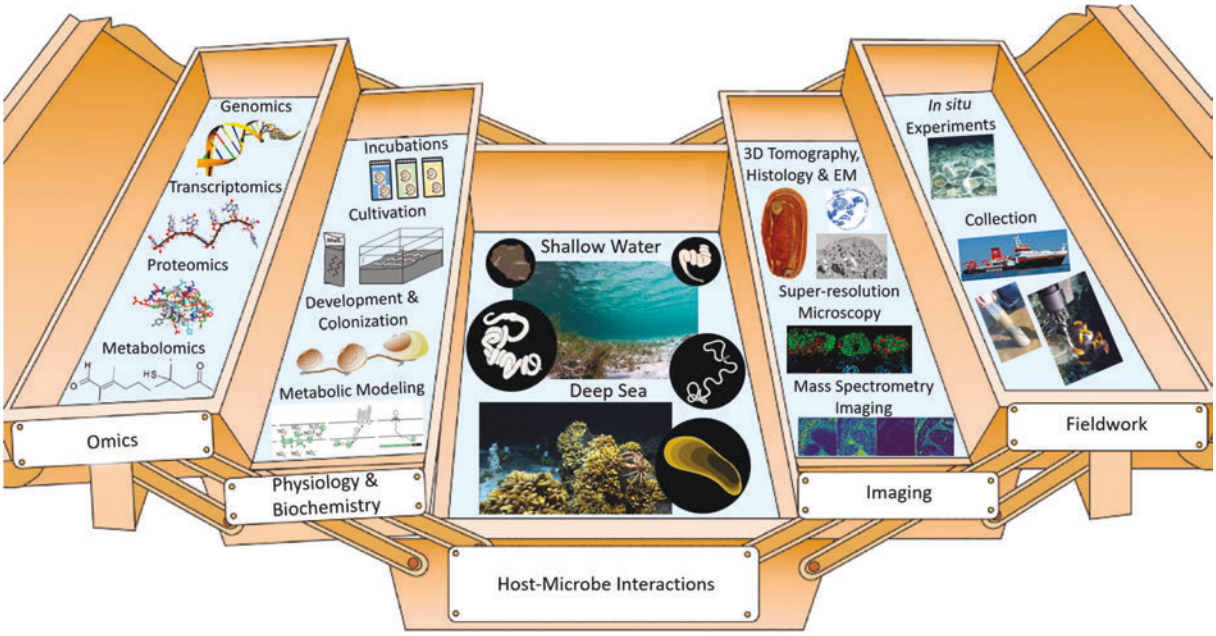

Figure 2 Toolbox of techniques to study non-model organisms and their interaction with their microbial symbionts. This figure was taken from Geier [68] and originally modified after Pohlschroder and Schulze [107]. The use of the figure was licensed under the license 5167531510703.

In my opinion these correlative approaches will become even more important as they offer great potential for understanding molecular processes in non-model systems in the future. In particular, combining genomic and transcriptomic data with targeted imaging techniques, such as the generation of specific antibodies for target genes or a correlative light and electron microscopic approach, would allow basic biological principles described in model organisms to be tested in non-model organisms. The recent study from Vergara *et al.* [108] has shown how such a correlative approach,

combining cell type-specific gene expression data with detailed morphology in a model organism, can clarify fundamental questions, such as understanding how different expression patterns lead to which cellular phenotype. In addition, they have explicitly emphasized that the approach they have developed could be adapted to other systems, and since the techniques they used are culture-independent, it would be interesting to test this approach also on a non-model organisms.

With the technical advances of recent years, it is now possible to test concepts developed in model organisms in a variety of other organisms as well. This makes it possible to understand whether these concepts are conserved between species or whether some species have deviations from the commonly known mechanisms. For example, in the context of this thesis I was able to show that early development in bathymodioline species is comparable to the development of their aposymbiotic shallow-water relatives (chapter III; [17]) and that bathymodioline larvae presumably have a vertical larval migration, which is also common among their shallow-water relatives (chapter IV). It has been shown that despite sharing the same protein machinery, the cell division of some bacteria deviates from the generally accepted concept originally described in *Escherichia coli* [109], as these bacteria divide longitudinally rather than horizontally [110]. These examples show that it is very important to focus on model organisms in order to better and more easily understand molecular processes in biology, but that work on non-model organisms should not be neglected as this is the only way to study the diversity of nature.

5.5 Concluding remarks

The research presented in my thesis provides new insides in how chemosynthetic symbiosis are established and maintained over the lifecycle of the holobiont. My results have shown that larvae of bathymodioline mussels from hydrothermal vents and cold seeps are aposymbiotic and feed on phototrophic food sources. Furthermore, I was able to show when the symbionts colonize the mussels and which morphological changes are associated with the onset of symbiosis, but also with the persistence of the holobiont during its life cycle. These changes have led from the adaptation of single cells (loss of microvilli and cilia / formation of a complex channel system) to the reduction of whole organs, such as the digestive tract. These data highlight that this symbiosis is another example of how eukaryotes adapt their development and morphology to host their bacterial symbionts. In these systems, in which the symbionts are transmitted horizontally, it is astonishing which information needs to be anchored in the developmental plan of the host so that the two symbiotic partners can recognize each other in the next generation and start their coexistence.

To study these interactions in more detail, in my opinion it is important in symbiosis research to focus not only on the symbiotic organ and a developmental stage itself, but rather investigate the whole life cycle of the holobiont. This is the only way to understand: (I) how the free-living stages of both symbiotic partners can survive, (II) which changes in the host are induced by the symbiosis, and (III) how the association is maintained over the development of the host.

Within the scope of this thesis, I was able to solve some fundamental questions regarding cell biology and ecology in the symbiosis between bathymodioline mussels and their chemosynthetic symbionts. However, my results have also raised new

questions about the molecular processes that shape the various symbiont-host associations involved in symbiont recognition and uptake, as well as evolutionary questions about how deep-sea larvae disperse in the world's oceans. Especially, in the context of global climate change, basic research on organisms from extreme habitats is particularly important, as it is one way to understand the interrelationships between the different world's ecosystems. This includes the deep sea, which is more threatened than ever by global climate change and the expansion of deep-sea mining and fishing. Understanding how this habitat is connected to the rest of the world's oceans is, in my opinion, one of the most important challenges facing marine research in the coming years.

References

[1] Schiaparelli, S., Rowden, A.A. & Clark, M.R. 2016 Deep-Sea Fauna. In *Biological Sampling in the Deep Sea* (eds. M.R. Clark, M. Consalvey & A.A. Rowden), pp. 16-35, John Wiley & Sons,.
[2] Hügler, M. & Imhoff, J. 2009 Life at Deep Sea Hydrothermal Vents — Oases Under Water. *The International Journal of Marine and Coastal Law* **24**, 201-208. (doi:10.1163/157180809X421789).
[3] Dubilier, N., Bergin, C. & Lott, C. 2008 Symbiotic diversity in marine animals: the art of harnessing chemosynthesis. *Nature Reviews Microbiology* **6**, 725-740. (doi:10.1038/nrmicro1992).
[4] Sogin, E.M., Kleiner, M., Borowski, C., Gruber-Vodicka, H.R. & Dubilier, N. 2021 Life in the Dark: Phylogenetic and Physiological Diversity of Chemosynthetic Symbioses. *Annu. Rev. Microbiol.* (doi:10.1146/annurev-micro-051021-123130).
[5] Jannasch, H.W. 1985 Review Lecture - The chemosynthetic support of life and the microbial diversity at deep-sea hydrothermal vents. *Proceedings of the Royal Society of London. Series B. Biological Sciences* **225**, 277-297. (doi:10.1098/rspb.1985.0062).
[6] Won, Y.J., Jones, W.J. & Vrijenhoek, R.C. 2008 Absence of cospeciation between deep-sea mytilids and their thiotrophic endosymbionts. *J. Shellfish Res.* **27**, 129-138. (doi:10.2983/0730-8000(2008)27[129:AOCBDM]2.0.CO;2).
[7] Won, Y.J., Hallam, S.J., O'Mullan, G.D., Pan, I.L., Buck, K.R. & Vrijenhoek, R.C. 2003 Environmental Acquisition of Thiotrophic Endosymbionts by Deep-Sea Mussels of the Genus *Bathymodiolus*. *Appl. Environ. Microbiol.* **69**, 6785-6792. (doi:10.1128/aem.69.11.6785-6792.2003).
[8] Zielinski, F.U., Pernthaler, A., Duperron, S., Raggi, L., Giere, O., Borowski, C. & Dubilier, N. 2009 Widespread occurrence of an intranuclear bacterial parasite in vent and seep bathymodiolin mussels. *Environ. Microbiol.* **11**, 1150-1167. (doi:10.1111/j.1462-2920.2008.01847.x).
[9] Assié, A., Borowski, C., van der Heijden, K., Raggi, L., Geier, B., Leisch, N., Schimak, M.P., Dubilier, N. & Petersen, J.M. 2016 A specific and widespread association between

deep-sea *Bathymodiolus* mussels and a novel family of Epsilonproteobacteria. *Environmental Microbiology Reports* **8**, 805-813. (doi:10.1111/1758-2229.12442).
[10] Rubin-Blum, M., Antony, C.P., Borowski, C., Sayavedra, L., Pape, T., Sahling, H., Bohrmann, G., Kleiner, M., Redmond, M.C., Valentine, D.L., et al. 2017 Short-chain alkanes fuel mussel and sponge *Cycloclasticus* symbionts from deep-sea gas and oil seeps. *Nat Microbiol* **2**, 17093. (doi:10.1038/nmicrobiol.2017.93).
[11] Duperron, S., Bergin, C., Zielinski, F.U., Blazejak, A., Pernthaler, A., McKiness, Z.P., DeChaine, E., Cavanaugh, C.M. & Dubilier, N. 2006 A dual symbiosis shared by two mussel species, *Bathymodiolus azoricus* and *Bathymodiolus puteoserpentis* (Bivalvia: Mytilidae), from hydrothermal vents along the northern Mid-Atlantic Ridge. *Environ. Microbiol.* **8**, 1441-1447. (doi:10.1111/j.1462-2920.2006.01038.x).
[12] Duperron, S., Nadalig, T., Caprais, J.-C., Sibuet, M., Fiala-Médioni, A., Amann, R. & Dubilier, N. 2005 Dual Symbiosis in a *Bathymodiolus* sp. Mussel from a Methane Seep on the Gabon Continental Margin (Southeast Atlantic): 16S rRNA Phylogeny and Distribution of the Symbionts in Gills. *Appl. Environ. Microbiol.* **71**, 1694-1700. (doi:10.1128/aem.71.4.1694-1700.2005).
[13] Fiala-Médioni, A., Métivier, C., Herry, A. & Le Pennec, M. 1986 Ultrastructure of the gill of the hydrothermal-vent mytilid *Bathymodiolus sp. Mar. Biol.* **92**, 65-72. (doi:10.1007/BF00392747).
[14] Fiala-Medioni, A. & Le Pennec, M. 1987 Trophic structural adaptations in relation to the bacterial association of bivalve molluscs from hydrothermal vents and subduction zones. In *Symposium on marine symbioses. 1 (1987)* (pp. 63-74, Balaban, Philadelphia, .
[15] Zheng, P., Wang, M., Li, C., Sun, X., Wang, X., Sun, Y. & Sun, S. 2017 Insights into deep-sea adaptations and host-symbiont interactions: a comparative transcriptome study on *Bathymodiolus* mussels and their coastal relatives. *Mol. Ecol.* (doi:10.1111/mec.14160).
[16] Kádár, E., Davis, S.A. & Lobo-da-Cunha, A. 2008 Cytoenzymatic investigation of intracellular digestion in the symbiont-bearing hydrothermal bivalve *Bathymodiolus azoricus*. *Mar. Biol.* **153**, 995-1004. (doi:10.1007/s00227-007-0872-0).
[17] Franke, M., Geier, B., Hammel, J.U., Dubilier, N. & Leisch, N. 2021 Coming together - symbiont acquisition and early development in deep-sea bathymodioline mussels. *Proceedings of the Royal Society B: Biological Sciences* **288**, 20211044. (doi:doi:10.1098/rspb.2021.1044).
[18] Hodin, J., Ferner, M.C., Heyland, A. & Gaylord, B. 2017 I feel that! Fluid dynamics and sensory aspects of larval settlement across scales. In *Evolutionary ecology of marine invertebrate larvae* (eds. T.J. Carrier, A.M. Reitzel & A. Heyland), Oxford University Press.
[19] Pineda, J., Hare, J.A. & Sponaugle, S. 2007 Larval transport and dispersal in the coastal ocean and consequences for population connectivity. *Oceanography* **20**, 22-39. (doi:10.5670/oceanog.2007.27).
[20] Young, C.M., He, R., Emlet, R.B., Li, Y., Qian, H., Arellano, S.M., Van Gaest, A., Bennett, K.C., Wolf, M., Smart, T.I., et al. 2012 Dispersal of deep-sea larvae from the intra-American seas: simulations of trajectories using ocean models. *Integr. Comp. Biol.* **52**, 483-496. (doi:10.1093/icb/ics090).
[21] Yahagi, T., Kayama Watanabe, H., Kojima, S. & Kano, Y. 2017 Do larvae from deep-sea hydrothermal vents disperse in surface waters? *Ecology* **98**, 1524-1534. (doi:10.1002/ecy.1800).
[22] Hadfield, M.G. 2011 Biofilms and Marine Invertebrate Larvae: What Bacteria Produce That Larvae Use to Choose Settlement Sites. *Annual Review of Marine Science* **3**, 453-470. (doi:10.1146/annurev-marine-120709-142753).
[23] Qian, P.-Y., Lau, S.C., Dahms, H.-U., Dobretsov, S. & Harder, T. 2007 Marine biofilms as mediators of colonization by marine macroorganisms: implications for antifouling and aquaculture. *Mar. Biotechnol.* **9**, 399-410. (doi:10.1007/s10126-007-9001-9).
[24] Koehl, M.A.R., Strother, J.A., Reidenbach, M.A., Koseff, J.R. & Hadfield, M.G. 2007 Individual-based model of larval transport to coral reefs in turbulent, wave-driven flow:

behavioral responses to dissolved settlement inducer. *Mar. Ecol. Prog. Ser.* **335**, 1-18. (doi:10.3354/meps335001).
[25] Morello, S.L. & Yund, P.O. 2016 Response of competent blue mussel (*Mytilus edulis*) larvae to positive and negative settlement cues. *J. Exp. Mar. Biol. Ecol.* **480**, 8-16. (doi:10.1016/j.jembe.2016.03.019).
[26] Dixson, D.L., Abrego, D. & Hay, M.E. 2014 Reef ecology. Chemically mediated behavior of recruiting corals and fishes: a tipping point that may limit reef recovery. *Science* **345**, 892-897. (doi:10.1126/science.1255057).
[27] von der Meden, C., Porri, F., McQuaid, C.D., Faulkner, K. & Robey, J. 2010 Fine-scale ontogenetic shifts in settlement behaviour of mussels: Changing responses to biofilm and conspecific settler presence in *Mytilus galloprovincialis* and *Perna perna*. *Marine Ecology-progress Series - MAR ECOL-PROGR SER* **411**, 161-171. (doi:10.3354/meps08642).
[28] Bao, W.-Y., Satuito, C.G., Yang, J.-L. & Kitamura, H. 2007 Larval settlement and metamorphosis of the mussel *Mytilus galloprovincialis* in response to biofilms. *Mar. Biol.* **150**, 565-574. (doi:10.1007/s00227-006-0383-4).
[29] Wang, C., Bao, W.Y., Gu, Z.Q., Li, Y.F., Liang, X., Ling, Y., Cai, S., Shen, H. & Yang, J. 2012 Larval settlement and metamorphosis of the mussel *Mytilus coruscus* in response to natural biofilms. *Biofouling* **28**, 249-256. (doi:10.1080/08927014.2012.671303).
[30] Yang, J.-L., Shen, P.-J., Liang, X., Li, Y.-F., Bao, W.-Y. & Li, J.-L. 2013 Larval settlement and metamorphosis of the mussel *Mytilus coruscus* in response to monospecific bacterial biofilms. *Biofouling* **29**, 247-259. (doi:10.1080/08927014.2013.764412).
[31] Chang, R.-H., Yang, L.-T., Luo, M., Fang, Y., Peng, L.-H., Wei, Y., Fang, J., Yang, J.-L. & Liang, X. 2021 Deep-sea bacteria trigger settlement and metamorphosis of the mussel *Mytilus coruscus* larvae. *Sci. Rep.* **11**, 919. (doi:10.1038/s41598-020-79832-8).
[32] Dahms, H.-U., Dobretsov, S. & Qian, P.-Y. 2004 The effect of bacterial and diatom biofilms on the settlement of the bryozoan *Bugula neritina*. *J. Exp. Mar. Biol. Ecol.* **313**, 191-209. (doi: 10.1016/j.jembe.2004.08.005).
[33] O'Connor, N.J. & Richardson, D.L. 1998 Attachment of barnacle (*Balanus amphitrite Darwin*) larvae: responses to bacterial films and extracellular materials. *J. Exp. Mar. Biol. Ecol.* **226**, 115-129.
[34] Dobretsov, S. & Rittschof, D. 2020 Love at First Taste: Induction of Larval Settlement by Marine Microbes. *Int J Mol Sci* **21**, 731. (doi:10.3390/ijms21030731).
[35] Harder, T., Lam, C. & Qian, P. 2002 Induction of larval settlement in the polychaete *Hydroides elegans* by marine biofilms: an investigation of monospecific diatom films as settlement cues. *Mar. Ecol. Prog. Ser.* **229**, 105-112. (doi:10.3354/meps229105).
[36] Bayne, B.L. 1971 Some morphological changes that occur at the metamorphosis of the larvae of *Mytilus edulis*. In *The Fourth European Marine Biology Symposium* (pp. 259-280.
[37] Cranfield, H.J. 1973 Observations on the Function of the Glands of the Foot of the Pediveliger of *Ostrea edulis* during Settlement *Mar. Biol.* **22**, 13. (doi:10.1007/BF00389175).
[38] Adams, D.K., Arellano, S.M. & Govenar, B. 2012 Larval Dispersal: Vent Life in the Water Column. *Oceanography* **25**, 256-268. (doi:10.5670/oceanog.2012.24).
[39] Mullineaux, L.S. 2014 Deep-sea hydrothermal vent communities. In *Marine community ecology and conservation* (pp. 383-400.
[40] Chen, C., Lin, T.-H., Watanabe, H.K., Akamatsu, T. & Kawagucci, S. 2021 Baseline soundscapes of deep-sea habitats reveal heterogeneity among ecosystems and sensitivity to anthropogenic impacts. *Limnol. Oceanogr.* **n/a**. (doi:10.1002/lno.11911).
[41] Lin, T.-H., Chen, C., Watanabe, H.K., Kawagucci, S., Yamamoto, H. & Akamatsu, T. 2019 Using soundscapes to assess deep-sea benthic ecosystems. *Trends Ecol. Evol.* **34**, 1066-1069. (doi:10.1016/j.tree.2019.09.006).
[42] Resing, J.A., Sedwick, P.N., German, C.R., Jenkins, W.J., Moffett, J.W., Sohst, B.M. & Tagliabue, A. 2015 Basin-scale transport of hydrothermal dissolved metals across the South Pacific Ocean. *Nature* **523**, 200-203. (doi:10.1038/nature14577).
[43] Cunha, M.R., Matos, F.L., Génio, L., Hilário, A., Moura, C.J., Ravara, A. & Rodrigues, C.F. 2013 Are Organic Falls Bridging Reduced Environments in the Deep Sea? - Results

from Colonization Experiments in the Gulf of Cádiz. *PLOS ONE* **8**, e76688. (doi:10.1371/journal.pone.0076688).
[44] Trossman, D. & Palter, J. 2021 Changing Ocean Currents. In *From Hurricanes to Epidemics: The Ocean's Evolving Impact on Human Health - Perspectives from the U.S.* (ed. K. Conrad), pp. 11-26. Cham, Springer International Publishing.
[45] Voosen, P. 2020 Climate change spurs global speedup of ocean currents. *Science* **367**, 612-613. (doi:10.1126/science.367.6478.612).
[46] Clark, M.R., Durden, J.M. & Christiansen, S. 2020 Environmental Impact Assessments for deep-sea mining: Can we improve their future effectiveness? *Mar. Policy* **114**. (doi:10.1016/j.marpol.2018.11.026).
[47] Clark, M.R., Althaus, F., Schlacher, T.A., Williams, A., Bowden, D.A. & Rowden, A.A. 2016 The impacts of deep-sea fisheries on benthic communities: a review. *ICES J. Mar. Sci.* **73**, i51-i69. (doi:10.1093/icesjms/fsv123).
[48] Ramirez-Llodra, E., Tyler, P.A., Baker, M.C., Bergstad, O.A., Clark, M.R., Escobar, E., Levin, L.A., Menot, L., Rowden, A.A., Smith, C.R., et al. 2011 Man and the Last Great Wilderness: Human Impact on the Deep Sea. *PLOS ONE* **6**, e22588. (doi:10.1371/journal.pone.0022588).
[49] Koschinsky, A., Heinrich, L., Boehnke, K., Cohrs, J.C., Markus, T., Shani, M., Singh, P., Smith Stegen, K. & Werner, W. 2018 Deep-sea mining: Interdisciplinary research on potential environmental, legal, economic, and societal implications. *Integr. Environ. Assess. Manage.* **14**, 672-691. (doi:10.1002/ieam.4071).
[50] Van Gaest, A.L. 2006 Ecology and early life history of *Bathynerita naticoidea*: evidence for long-distance larval dispersal of a cold seep gastropod.
[51] Arellano, S.M., Van Gaest, A.L., Johnson, S.B., Vrijenhoek, R.C. & Young, C.M. 2014 Larvae from deep-sea methane seeps disperse in surface waters. *Proc Biol Sci* **281**, 20133276. (doi:10.1098/rspb.2013.3276).
[52] Whitney, J.L., Gove, J.M., McManus, M.A., Smith, K.A., Lecky, J., Neubauer, P., Phipps, J.E., Contreras, E.A., Kobayashi, D.R. & Asner, G.P. 2021 Surface slicks are pelagic nurseries for diverse ocean fauna. *Sci. Rep.* **11**, 3197. (doi:10.1038/s41598-021-81407-0).
[53] Sunagawa, S., Acinas, S.G., Bork, P., Bowler, C., Acinas, S.G., Babin, M., Bork, P., Boss, E., Bowler, C., Cochrane, G., et al. 2020 Tara Oceans: towards global ocean ecosystems biology. *Nature Reviews Microbiology* **18**, 428-445. (doi:10.1038/s41579-020-0364-5).
[54] Dixon, D., Lowe, D., Miller, P., Villemin, G., Colaço, A., Serrao-Santos, R. & Dixon, L. 2006 Evidence of seasonal reproduction in the Atlantic vent mussel *Bathymodiolus azoricus*, and an apparent link with the timing of photosynthetic primary production. *J. Mar. Biol. Assoc. U.K.* **86**, 1363-1371. (doi:10.1017/S0025315406014391).
[55] de Vargas, C., Audic, S., Henry, N., Decelle, J., Mahé, F., Logares, R., Lara, E., Berney, C., Le Bescot, N., Probert, I., et al. 2015 Eukaryotic plankton diversity in the sunlit ocean. *Science* **348**, 1261605. (doi:10.1126/science.1261605).
[56] Pierella Karlusich, J.J., Ibarbalz, F.M. & Bowler, C. 2020 Phytoplankton in the Tara Ocean. *Annual Review of Marine Science* **12**, 233-265. (doi:10.1146/annurev-marine-010419-010706).
[57] Gruber-Vodicka, H.R., Leisch, N., Kleiner, M., Hinzke, T., Liebeke, M., McFall-Ngai, M., Hadfield, M.G. & Dubilier, N. 2019 Two intracellular and cell type-specific bacterial symbionts in the placozoan *Trichoplax H2*. *Nat Microbiol* **4**, 1465-1474. (doi:10.1038/s41564-019-0475-9).
[58] Bright, M. & Bulgheresi, S. 2010 A complex journey: transmission of microbial symbionts. *Nature Reviews Microbiology* **8**, 218-230. (doi:10.1038/nrmicro2262).
[59] Wolfowicz, I., Baumgarten, S., Voss, P.A., Hambleton, E.A., Voolstra, C.R., Hatta, M. & Guse, A. 2016 *Aiptasia sp.* larvae as a model to reveal mechanisms of symbiont selection in cnidarians. *Sci. Rep.* **6**, 32366. (doi:10.1038/srep32366).

[60] McFall-Ngai, M.J. 2014 The importance of microbes in animal development: lessons from the squid-vibrio symbiosis. *Annu. Rev. Microbiol.* **68**, 177-194. (doi:10.1146/annurev-micro-091313-103654).
[61] Ücker, M. 2021 Metagenomic analyses of a deep-sea mussel symbiosis, Universität Bremen Fachbereich 02: Biologie/Chemie (FB 02).
[62] Lalish, K.M. 2015 Elucidating the metabolic activities of SUP05, an abundant group of marine sulfur oxidizing gamma-proteobacteria.
[63] Page, H., Fisher, C. & Childress, J. 1990 Role of filter-feeding in the nutritional biology of a deep-sea mussel with methanotrophic symbionts. *Mar. Biol.* **104**, 251-257. (doi:10.1007/BF01313266).
[64] Meier, D.V., Bach, W., Girguis, P.R., Gruber-Vodicka, H.R., Reeves, E.P., Richter, M., Vidoudez, C., Amann, R. & Meyerdierks, A. 2016 Heterotrophic Proteobacteria in the vicinity of diffuse hydrothermal venting. *Environ. Microbiol.* **18**, 4348-4368. (doi:10.1111/1462-2920.13304).
[65] Sogin, M.L., Morrison, H.G., Huber, J.A., Mark Welch, D., Huse, S.M., Neal, P.R., Arrieta, J.M. & Herndl, G.J. 2006 Microbial diversity in the deep sea and the underexplored "rare biosphere". *Proc Natl Acad Sci U S A* **103**, 12115-12120. (doi:10.1073/pnas.0605127103).
[66] Fontanez, K.M. & Cavanaugh, C.M. 2014 Evidence for horizontal transmission from multilocus phylogeny of deep-sea mussel (*Mytilidae*) symbionts. *Environ. Microbiol.* **16**, 3608-3621. (doi:10.1111/1462-2920.12379).
[67] Crépeau, V., Cambon-Bonavita, M.-A., Lesongeur, F., Randrianalivelo, H., Pierre-marie, S., Sarrazin, J. & Godfroy, A. 2011 Diversity and function in microbial mats from the Lucky Strike hydrothermal vent field. *FEMS Microbiol. Ecol.* **76**, 524-540. (doi:10.1111/j.1574-6941.2011.01070.x).
[68] Geier, B. 2020 Correlative mass spectrometry imaging of animal–microbe symbioses, Universität Bremen FB02 Biologie/Chemie.
[69] Klose, J., Polz, M.F., Wagner, M., Schimak, M.P., Gollner, S. & Bright, M. 2015 Endosymbionts escape dead hydrothermal vent tubeworms to enrich the free-living population. *Proceedings of the National Academy of Sciences* **112**, 11300. (doi:10.1073/pnas.1501160112).
[70] Wentrup, C., Wendeberg, A., Schimak, M., Borowski, C. & Dubilier, N. 2014 Forever competent: deep-sea bivalves are colonized by their chemosynthetic symbionts throughout their lifetime. *Environ. Microbiol.* **16**, 3699-3713. (doi:10.1111/1462-2920.12597).
[71] Chu, H. & Mazmanian, S.K. 2013 Innate immune recognition of the microbiota promotes host-microbial symbiosis. *Nat. Immunol.* **14**, 668-675. (doi:10.1038/ni.2635).
[72] Bulgheresi, S., Schabussova, I., Chen, T., Mullin Nicholas, P., Maizels Rick, M. & Ott Jörg, A. 2006 A New C-Type Lectin Similar to the Human Immunoreceptor DC-SIGN Mediates Symbiont Acquisition by a Marine Nematode. *Appl. Environ. Microbiol.* **72**, 2950-2956. (doi:10.1128/AEM.72.4.2950-2956.2006).
[73] Troll, J.V., Adin, D.M., Wier, A.M., Paquette, N., Silverman, N., Goldman, W.E., Stadermann, F.J., Stabb, E.V. & McFall-Ngai, M.J. 2009 Peptidoglycan induces loss of a nuclear peptidoglycan recognition protein during host tissue development in a beneficial animal-bacterial symbiosis. *Cell. Microbiol.* **11**, 1114-1127. (doi:10.1111/j.1462-5822.2009.01315.x).
[74] McFall-Ngai, M., Nyholm, S.V. & Castillo, M.G. 2010 The role of the immune system in the initiation and persistence of the *Euprymna scolopes*--*Vibrio fischeri* symbiosis. *Semin. Immunol.* **22**, 48-53. (doi:10.1016/j.smim.2009.11.003).
[75] Wang, H., Zhang, H., Wang, M., Chen, H., Lian, C. & Li, C. 2019 Comparative transcriptomic analysis illuminates the host-symbiont interactions in the deep-sea mussel *Bathymodiolus platifrons*. *Deep Sea Research Part I: Oceanographic Research Papers* **151**, 103082. (doi:10.1016/j.dsr.2019.103082).

[76] Wong, Y.H., Sun, J., He, L.S., Chen, L.G., Qiu, J.-W. & Qian, P.-Y. 2015 High-throughput transcriptome sequencing of the cold seep mussel *Bathymodiolus platifrons*. *Sci. Rep.* **5**, 16597-16611. (doi:10.1038/srep16597).
[77] Oldenburg, M., Krüger, A., Ferstl, R., Kaufmann, A., Nees, G., Sigmund, A., Bathke, B., Lauterbach, H., Suter, M., Dreher, S., et al. 2012 TLR13 Recognizes Bacterial 23S rRNA Devoid of Erythromycin Resistance–Forming Modification. *Science* **337**, 1111-1115. (doi:10.1126/science.1220363).
[78] Ren, Y., Ding, D., Pan, B. & Bu, W. 2017 The TLR13-MyD88-NF-κB signalling pathway of *Cyclina sinensis* plays vital roles in innate immune responses. *Fish Shellfish Immunol.* **70**, 720-730. (doi:10.1016/j.fsi.2017.09.060).
[79] Beamer, L.J., Carroll, S.F. & Eisenberg, D. 1998 The BPI/LBP family of proteins: A structural analysis of conserved regions. *Protein Sci.* **7**, 906-914. (doi:10.1002/pro.5560070408).
[80] Chun, C.K., Troll, J.V., Koroleva, I., Brown, B., Manzella, L., Snir, E., Almabrazi, H., Scheetz, T.E., Bonaldo Mde, F., Casavant, T.L., et al. 2008 Effects of colonization, luminescence, and autoinducer on host transcription during development of the squid-vibrio association. *Proc Natl Acad Sci U S A* **105**, 11323-11328. (doi:10.1073/pnas.0802369105).
[81] Philipp, E.E.R., Kraemer, L., Melzner, F., Poustka, A.J., Thieme, S., Findeisen, U., Schreiber, S. & Rosenstiel, P. 2012 Massively Parallel RNA Sequencing Identifies a Complex Immune Gene Repertoire in the lophotrochozoan *Mytilus edulis*. *PLOS ONE* **7**, e33091. (doi:10.1371/journal.pone.0033091).
[82] Zhang, L., Li, L., Guo, X., Litman, G.W., Dishaw, L.J. & Zhang, G. 2015 Massive expansion and functional divergence of innate immune genes in a protostome. *Sci. Rep.* **5**, 8693. (doi:10.1038/srep08693).
[83] Kehl, A., Göser, V., Reuter, T., Liss, V., Franke, M., John, C., Richter, C.P., Deiwick, J. & Hensel, M. 2020 A trafficome-wide RNAi screen reveals deployment of early and late secretory host proteins and the entire late endo-/lysosomal vesicle fusion machinery by intracellular *Salmonella*. *PLoS Path.* **16**, e1008220. (doi:10.1371/journal.ppat.1008220).
[84] Dunn, S.R., Phillips, W.S., Green, D.R. & Weis, V.M. 2007 Knockdown of Actin and Caspase Gene Expression by RNA Interference in the Symbiotic Anemone *Aiptasia pallida*. *The Biological Bulletin* **212**, 250-258. (doi:10.2307/25066607).
[85] Colaco, A., Bettencourt, R., Costa, V., Lino, S., Lopes, H., Martins, I., Pires, L., Prieto, C. & Serrao Santos, R. 2010 LabHorta: a controlled aquarium system for monitoring physiological characteristics of the hydrothermal vent mussel *Bathymodiolus azoricus*. *ICES J. Mar. Sci.* **68**, 349-356. (doi:10.1093/icesjms/fsq120).
[86] Tietjen, M. 2020 Physiology and ecology of deep-sea *Bathymodiolus* symbioses, Universität Bremen.
[87] Von Cosel, R. & Marshall, B.A. 2010 A new genus and species of large mussel (Mollusca: Bivalvia: *Mytilidae*) from the Kermadec Ridge. *Records of the Musuem of New Zealand Te Papa* **21**, 15.
[88] Gustafson, R.G., Turner, R.D., Lutz, R.A. & Vrijenhoek, R.C. 1998 A new genus and five new species of mussels (Bivalvia, Mytilidae) from deep-sea sulfide/hydrocarbon seeps in the Gulf of Mexico. *Malacologia* **40**, 63-112.
[89] Fiala-Médioni, A., McKiness, Z., Dando, P., Boulegue, J., Mariotti, A., Alayse-Danet, A., Robinson, J. & Cavanaugh, C. 2002 Ultrastructural, biochemical, and immunological characterization of two populations of the mytilid mussel *Bathymodiolus azoricus* from the Mid-Atlantic Ridge evidence for a dual symbiosis. *Mar. Biol.* **141**, 1035-1043. (doi:10.1007/s00227-002-0903-9).
[90] Thubaut, J., Corbari, L., Gros, O., Duperron, S., Couloux, A. & Samadi, S. 2013 Integrative Biology of *Idas iwaotakii* (Habe, 1958), a 'Model Species' Associated with Sunken Organic Substrates. *PLOS ONE* **8**, e69680. (doi:10.1371/journal.pone.0069680).
[91] Anttila, J., Ruokolainen, L., Kaitala, V. & Laakso, J. 2013 Loss of Competition in the Outside Host Environment Generates Outbreaks of Environmental Opportunist Pathogens. *PLOS ONE* **8**, e71621. (doi:10.1371/journal.pone.0071621).

[92] Sundberg, L.-R., Kunttu, H.M.T. & Valtonen, E.T. 2014 Starvation can diversify the population structure and virulence strategies of an environmentally transmitting fish pathogen. *BMC Microbiol.* **14**, 67. (doi:10.1186/1471-2180-14-67).
[93] Vance, C.P., Johnson, L.E.B., Halvorsen, A.M., Heichel, G.H. & Barnes, D.K. 1980 Histological and ultrastructural observations of Medicago sativa root nodule senescence after foliage removal. *Canadian Journal of Botany* **58**, 295-309. (doi:10.1139/b80-030).
[94] Smertenko, A. & Franklin-Tong, V.E. 2011 Organisation and regulation of the cytoskeleton in plant programmed cell death. *Cell Death & Differentiation* **18**, 1263-1270. (doi:10.1038/cdd.2011.39).
[95] Franklin-Tong, Vernonica E. & Gourlay, Campbell W. 2008 A role for actin in regulating apoptosis/programmed cell death: evidence spanning yeast, plants and animals. *Biochem. J.* **413**, 389-404. (doi:10.1042/BJ20080320).
[96] McMahon, H.T. & Boucrot, E. 2015 Membrane curvature at a glance. *J. Cell Sci.* **128**, 1065-1070. (doi:10.1242/jcs.114454).
[97] Antonny, B., Burd, C., De Camilli, P., Chen, E., Daumke, O., Faelber, K., Ford, M., Frolov, V.A., Frost, A., Hinshaw, J.E., et al. 2016 Membrane fission by dynamin: what we know and what we need to know. *EMBO J.* **35**, 2270-2284. (doi:10.15252/embj.201694613).
[98] Alfred, J. & Baldwin, I.T. 2015 New opportunities at the wild frontier. *eLife* **4**, e06956. (doi:10.7554/eLife.06956).
[99] Fields, S. & Johnston, M. 2005 Whither Model Organism Research? *Science* **307**, 1885-1886. (doi:doi:10.1126/science.1108872).
[100] Gladfelter, A.S. 2015 How nontraditional model systems can save us. *Molecular biology of the cell* **26**, 3687-3689. (doi:10.1091/mbc.E15-06-0429).
[101] Man, S.M., Ekpenyong, A., Tourlomousis, P., Achouri, S., Cammarota, E., Hughes, K., Rizzo, A., Ng, G., Wright, J.A., Cicuta, P., et al. 2014 Actin polymerization as a key innate immune effector mechanism to control *Salmonella* infection. *Proceedings of the National Academy of Sciences* **111**, 17588. (doi:10.1073/pnas.1419925111).
[102] Russell, J.J., Theriot, J.A., Sood, P., Marshall, W.F., Landweber, L.F., Fritz-Laylin, L., Polka, J.K., Oliferenko, S., Gerbich, T., Gladfelter, A., et al. 2017 Non-model model organisms. *BMC Biol.* **15**, 55. (doi:10.1186/s12915-017-0391-5).
[103] da Fonseca, R.R., Albrechtsen, A., Themudo, G.E., Ramos-Madrigal, J., Sibbesen, J.A., Maretty, L., Zepeda-Mendoza, M.L., Campos, P.F., Heller, R. & Pereira, R.J. 2016 Next-generation biology: Sequencing and data analysis approaches for non-model organisms. *Marine Genomics* **30**, 3-13. (doi:10.1016/j.margen.2016.04.012).
[104] Ishino, Y., Krupovic, M., Forterre, P. & Margolin, W. 2018 History of CRISPR-Cas from Encounter with a Mysterious Repeated Sequence to Genome Editing Technology. *J. Bacteriol.* **200**, e00580-00517. (doi:10.1128/JB.00580-17).
[105] Shan, G. 2010 RNA interference as a gene knockdown technique. *The International Journal of Biochemistry & Cell Biology* **42**, 1243-1251. (doi:10.1016/j.biocel.2009.04.023).
[106] Seybold, A.C., Wharton, D.A., Thorne, M.A.S. & Marshall, C.J. 2016 Establishing RNAi in a Non-Model Organism: The Antarctic Nematode *Panagrolaimus sp. DAW1*. *PLOS ONE* **11**, e0166228. (doi:10.1371/journal.pone.0166228).
[107] Pohlschroder, M. & Schulze, S. 2019 *Haloferax volcanii*. *Trends Microbiol.* **27**, 86-87. (doi:10.1016/j.tim.2018.10.004).
[108] Vergara, H.M., Pape, C., Meechan, K.I., Zinchenko, V., Genoud, C., Wanner, A.A., Mutemi, K.N., Titze, B., Templin, R.M., Bertucci, P.Y., et al. 2021 Whole-body integration of gene expression and single-cell morphology. *Cell* **184**, 4819-4837.e4822. (doi:10.1016/j.cell.2021.07.017).
[109] Lutkenhaus, J. 1993 FtsZ ring in bacterial cytokinesis. *Mol. Microbiol.* **9**, 403-409. (doi:10.1111/j.1365-2958.1993.tb01701.x).
[110] Leisch, N., Verheul, J., Heindl, N.R., Gruber-Vodicka, H.R., Pende, N., den Blaauwen, T. & Bulgheresi, S. 2012 Growth in width and FtsZ ring longitudinal positioning in a gammaproteobacterial symbiont. *Curr. Biol.* **22**, R831-R832. (doi:10.1016/j.cub.2012.08.033).

Personal contribution to each manuscript

Manuscript 1 | Chapter II

How to live with, on and in eukaryotic cells? The different forms of symbiont-host associations in bathymodioline mussels

Conceptual design	60 %
Data acquisition and experiments	75 %
Analysis and interpretation of results	85 %
Preparation of figures and tables	100 %
Writing the manuscript	95 %

Manuscript 2 | Chapter III

Coming together—symbiont acquisition and early development in deep-sea bathymodioline mussels

Conceptual design	65 %
Data acquisition and experiments	80 %
Analysis and interpretation of results	90 %
Preparation of figures and tables	100 %
Writing the manuscript	90 %

Manuscript 3 | Chapter IV

How to make a living without symbionts? The vertical migration of planktotrophic deep-sea mussels

Conceptual design	60 %

Data acquisition and experiments	90 %
Analysis and interpretation of results	90 %
Preparation of figures and tables	100 %
Writing the manuscript	90 %

Acknowledgements

This thesis would not have been possible with the support of several colleagues, collaborators, friends, and family.

First of all, I want to thank **Prof. Dr. Nicole Dubilier** for giving me the chance to do my thesis in her department at the Max Planck Institute of Marine Biology in Bremen. I really appreciate all your support and scientific advice over the last years.

Dr. Nikolaus Leisch, Niko, I can't tell you how grateful I am for your great supervision, support and mentorship from the beginning of my master thesis in 2017 until today! I really appreciate how you have supported me over the past years both as a supervisor and as a friend!

I also want to thank **Prof. Dr. Peter R. Girguis** for the examination of my thesis and taking your time to join the committee of my thesis defense.

Furthermore, I want to thank **Prof. Dr. Tilmann Harder, Prof. Dr. Marcel Kuypers**, and **Carlotta Kueck** for taking your time joining the committee of my thesis defense.

I want to thank all my collaborators for their support during measurement time and data analyses at their facilities: **Dr. Jörg U. Hammel** (DESY Hamburg), **Dr. Heejin Jeon** and **Prof. Dr. Martin Whitehouse** (NordSim laboratory Stockholm), **Julian Hennies**, **Dr. Nicole Schieber**, and **Dr. Yannik Schwab** (EMBL Heidelberg).

Special thanks also go to all colleagues at the MPI in Bremen, who helped and supported me a lot during my time in Bremen: Especially **Dr. Christiane Glöckner**, **Bernd Stickfort**, **Andreas Ellrott,** and **Tomas Wilkop**.

I would like to thank **every member** of the Symbiosis Department for a special time at the MPI. I always enjoyed the nice atmosphere in our department, the great science, as well as all the private gatherings and BBQs. I would like to say thank you to all the TAs for their great support in the laboratory, especially **Wiebke Ruschmeier** and **Miriam Sadowski**. Without your support in the laboratory the science I did during the last years would not have been possible.

Bene, where do I start, I would like to thank you for the last years. We had so much fun together, from our time at the DESY in Hamburg to our trip to Patagonia and Antarctica. I couldn't have asked for a better colleague/friend. Also thank you again for proofreading parts of this thesis.

Thank you **Miguel** especially in the beginning of my Master and PhD time to support me whenever I needed help!

Dolma, thank you for being such a great office-mate. I enjoyed the time in our office as well as privately a lot. I would also like to thank you again for proofreading parts of this thesis.

Jan, it's a pity that you joined us in the department only last year. I always enjoyed the time with you at work and in private. I would also like to thank you for proofreading parts of this thesis. I wish you and your family a good future!

Anna, I would like to thank you for the time we had together in the department. We started together with our master projects and have now completed our PhD almost simultaneously. I still remember how we trained together for our first halve marathon. I would also like to thank you for proofreading parts of this thesis.

Merle, thank you for proofreading parts of this thesis. I really enjoyed discussing with you about the bathymodioline symbiosis.

Tina, **Oli**, and **Målin**, thank you for the time we had together in the symbiosis department.

Alex, **Harald**, **Manuel**, and **Christian**, thank you for all your support, advice and help during the last years.

I want to thank my friends **René** und **Sophie** for always being there when I needed some company and support during the last years! **René** thank you for proof reading parts of this thesis!

Ich möchte mich auch bei meinen **Eltern** bedanken! Ohne Eure Unterstützung von Tag eins an wäre dies alles nicht möglich gewesen. Ihr wart immer für mich da und habt mich auf diesem nicht immer einfachen Weg begleitet und unterstützt. Ich

konnte mich immer auf Euren Rat verlassen und wusste, dass ihr, egal was passiert, für mich da sein werdet.

Marie, ich weiß gar nicht, was ich sagen soll. Tausend Dank, dass Du an meiner Seite bist und mich in allem unterstützt! In der letzten Zeit warst Du immer da, wenn ich Dich brauchte, auch wenn die Situationen nicht immer einfach waren. Ich freue mich auf unsere gemeinsame Zukunft und lass uns die Zeit in Weimar/Jena genießen!

Universität Bremen

Bremen, 15.10.2021

Versicherung an Eides Statt

Ich, **Maximilian Alexander Franke**, [redacted]
Matrikelnummer: [redacted]

versichere an Eides Statt durch meine Unterschrift, dass ich die vorstehende Arbeit selbständig und ohne fremde Hilfe angefertigt und alle Stellen, die ich wörtlich dem Sinne nach aus Veröffentlichungen entnommen habe, als solche kenntlich gemacht habe, mich auch keiner anderen als der angegebenen Literatur oder sonstiger Hilfsmittel bedient habe.

Ich versichere an Eides Statt, dass ich die vorgenannten Angaben nach bestem Wissen und Gewissen gemacht habe und dass die Angaben der Wahrheit entsprechen und ich nichts verschwiegen habe.

Die Strafbarkeit einer falschen eidesstattlichen Versicherung ist mir bekannt, namentlich die Strafandrohung gemäß § 156 StGB bis zu drei Jahren Freiheitsstrafe oder Geldstrafe bei vorsätzlicher Begehung der Tat bzw. gemäß § 161 Abs. 1 StGB bis zu einem Jahr Freiheitsstrafe oder Geldstrafe bei fahrlässiger Begehung.

Des Weiteren bestätige ich hiermit gemäß §7, Abs. 7, Punkt 4, dass die zu Prüfungszwecken beigelegte elektronische Version meiner Dissertation identisch ist mit der abgegebenen gedruckten Version. Ich bin mit der Überprüfung meiner Dissertation gemäß §6 Abs. 2, Punkt 5 mit qualifizierter Software im Rahmen der Untersuchung von Plagiatsvorwürfen einverstanden.

Bremen, 15.10.2021, [redacted]

Ort, Datum, Unterschrift